DOE/PC/90045--T14

FINAL REPORT

Report Period

September 1, 1990 to January 31, 1994

for

CATALYST AND PROCESS DEVELOPMENT FOR SYNTHESIS GAS CONVERSION TO ISOBUTYLENE

Submitted to

United States Department of Energy
Pittsburgh Energy Technology Center

May 6, 1994

by

Rayford G. Anthony and Aydin Akgerman
Co-Principal Investigators

Project Team

Dr. C.V. Philip, Associate Research Scientist
Dr. Can Erkey, Research Associate
Mr. Zhentao (Jeffrey) Feng, Research Assistant and Ph.D. Student
Mr. Walter S. Postula, Research Assistant and Ph.D. Student
Mr. Jianhua Wang, Research Assistant and Ph.D. Student

Kinetics, Catalysis, and Reaction Engineering Laboratory
Department of Chemical Engineering
Texas A&M University
College Station, TX 77843-3122

UNDER DOE CONTRACT NO. DE-AC22-90PC90045

(Texas A&M Research Foundation Project No. 6722)

DISCLAIMER

EXECUTIVE SUMMARY

Project Motivation and Objectives

Recent amendments to the Clean Air Act will, once again, require reformulation of gasoline. The Environmental Protection Agency has set new standards for fuel vapor pressure, volatile organic compounds (VOCs), aromatic content, and oxygen content (*1*). The vapor pressure limit (summer 1992) was set at 9 psi while VOCs are to be reduced by 15% by 1995 (compared to 1990). Total aromatics in the gasoline pool are limited to 25 vol% with benzene limited to 1 vol%. Oxygen content will be a minimum of 2-2.7 wt% depending on the area in which the gasoline is used. The purpose of these stricter guidelines is to limit exhaust and evaporative emissions. Carbon monoxide (CO), unburned hydrocarbons (HC), and nitrogen oxides (NO_x) are the three primary sources of exhaust pollution from today's gasoline, combined with low molecular weight hydrocarbons and aromatics (VOCs) as evaporative sources (*2*).

Methyl-tertiary-butyl ether (MTBE) is an additive that has received increased attention because of its potential to solve some of the problems associated with current gasoline blends. Addition of MTBE to gasoline can reduce exhaust emissions of CO, HC, and NO_x and evaporative emissions by replacing VOCs while maintaining the octane rating at an acceptable level. The demand for MTBE is currently the fastest growing of any petrochemical and is likely to continue increasing at a high rate (*3*). The supply of MTBE is directly linked to the supply of isobutylene, a key reactant. The demand for reformulated gasoline could result in a shortage of isobutylene on a worldwide basis (*4*). Isomerization of 1-butene and dehydrogenation of isobutane are two current processes that could supplement the isobutylene pool. These two processes are expensive and are limited by the supply of C_4 feedstocks (*2-6*). Catalytic cracking can also be utilized to produce a stream with 10-15% isobutylene, but this process is very energy intensive. A process that would take advantage of an ample supply of feed gas is direct conversion of coal derived synthesis gas into isobutylene. Synthesis gas refers to a mixture of carbon monoxide and hydrogen. The reaction for producing synthesis gas from coal is

$$C_{(s)} + H_2O_{(g)} \xrightarrow{1273\ K} CO_{(g)} + H_{2\,(g)}$$

A process producing isobutylene from synthesis gas could be combined with a methanol synthesis unit and a MTBE synthesis unit since the technology already exists for these two operations.

Previous work on isosynthesis (conversion of synthesis gas to isobutane and isobutylene) was performed at very low conversions or extreme process conditions. No model existed for the prediction of carbon monoxide conversion or product distribution. Such a model would be useful in scale-up to an industrial sized reactor.

The objectives of this research were (1) determine the optimum process conditions for isosynthesis; (2) determine the optimum catalyst preparation method and catalyst composition/properties for isosynthesis; (3) determine the kinetics for the best catalyst; (4) develop reactor models for trickle bed, slurry, and fixed bed reactors; and (5) simulate the performance of fixed bed trickle flow reactors, slurry flow reactors, and fixed bed gas phase reactors for isosynthesis.

Results and Conclusions

More improvement in catalyst activity and selectivity is needed before isosynthesis can become a commercially feasible (stand-alone) process. With the current catalysts, isosynthesis may be used in conjunction with a coal burning power plant. The synthesis gas produced could be used to produce higher value (C_2-C_8 hydrocarbons) products. The methane produced from the isosynthesis can be used to generate power.

Catalysts prepared by the precipitation method show the most promise for future development as compared with those prepared hydrothermally, by calcining zirconyl nitrate, or by a modified sol-gel method. Precipitation is a comparatively simple procedure in which dopants can easily be added to the zirconia. For current catalysts the high temperatures (>673 K) required for activity also cause the production of methane (because of thermodynamics). A catalyst with higher activity at lower temperatures would magnify the unique selectivity of zirconia for isobutylene. Perhaps with a more active catalyst and acidification, oxygenate production could be limited at lower temperatures. Pressures above 50 atm cause an undesirable shift in product distribution toward heavier hydrocarbons.

Carbon deposition on the catalyst occurs fairly quickly (~ 2 hours) and does not alter the surface area compared with the deposition of heavier hydrocarbons. These hydrocarbons can be characterized as "soft coke" and are easily removed. A constant activity is reached within 4 hours after bringing a fresh catalyst on stream. Product distribution is more sensitive to changes in process conditions, especially temperature cycling.

Co-feeding hydrogen sulfide and presulfiding has the beneficial effect of decreasing C_2 and C_3 production while doubling or tripling C_5 production, especially 3-methyl-1-butene. Isobutylene fraction among the C_4's also showed an increase. These changes in selectivity were accompanied by no loss in activity in the case of co-feeding and only a slight loss in the case of presulfiding. The resistance of zirconia to sulfur poisoning means that the sulfur in the synthesis gas (initially in the coal) need not be removed. The C_5 branched alkenes can be used to produce TAME which is also an additive currently being used in gasoline. The 3-methyl-1-butene can easily be isomerized into 2-methyl 2-(or 1-) butene since the branch needs to be located next to the double bond for TAME production. More study into the interaction between sulfur and zirconia would yield a better understanding of the selectivity change and possibly of the isosynthesis mechanism.

Oxygen vacancies are required for an active catalyst and may be responsible for the unique selectivity of isosynthesis catalysts. A catalyst doped with 1.72% Mg (wt) was the most active singly-doped zirconia with a CO conversion of 29% (32 wt% C_1, 29 wt% C_4, 26 wt% C_5+) at 673 K, 50 atm, 1/1 CO/H_2 ratio, and 90 second space time. A dopant that introduced the most oxygen vacancies per cation and was close in size to zirconium gave a more active catalyst. A multicomponent doped (Y-Ba-Cu) zirconia was more active but produced more methane. Multiple dopings of zirconia may be the course needed to produce active catalysts at lower temperatures.

Catalyst characteristics have a strong impact on the stability and reactivity of the intermediates. Basic sites catalyze the CO insertions and acidic sites stabilize the methoxide species on the surface and promote condensation reactions. Both CO insertion and condensation reactions contribute to chain propagation in isosynthesis. A balance of acidity-basicity is important for an active isosynthesis catalyst. A deficiency of acidic sites or basic sites reduced the activity. However, strong acidity was not desirable since methane was produced from the excessive methoxide on the surface. Characterization of catalysts by

temperature programmed desorption showed that acid-base properties were modified by preparation procedures. Zirconias prepared by the modified sol-gel method showed increased basicity as compared with those prepared by calcination of zirconyl salts.

A model was developed that can predict carbon monoxide conversion and product distribution. The rate equation for carbon monoxide conversion contains only a rate constant and an adsorption equilibrium constant. The product distribution was predicted using a simple ratio of the rate of CO conversion. No equations for predicting conversion or product distribution existed before this study. Additionally, the hydrocarbon distribution of isosynthesis were generated by a semi-empirical kinetic model with two adjustable parameters α and κ. The model was developed by adding an additional chain propagation step for C_2 intermediate to account for the contribution to chain growth by condensation reactions. The parameter α was defined as the probability of chain growth by CO insertion and κ was related to the ratio of condensation to CO insertion. Furthermore, desorption of β-C_3 intermediates was assumed negligible.

The form of the carbon monoxide rate equation can be obtained from three simplified mechanisms in which CO is either molecularly adsorbed or reacts from the gas phase, H_2 is dissociatively adsorbed, and CO_2 is the most strongly adsorbed/most abundant surface specie. Discrimination between these mechanisms was not possible. The values obtained by parameter estimation for activation energy and CO_2 heat of adsorption are reasonable. Analysis of the parameters obtained for modeling of the product distribution shows that the catalysts are most efficient in converting carbon from carbon monoxide into C_4 hydrocarbons. The model can be used for scale-up in the event isosynthesis becomes a more viable commercial process.

Report Format

This report is divided into Introduction, Experimental, and Results and Discussion sections. The Tables and Figures for each section follow the last page of text in that section. Appendix C contains a listing of publications and presentations based on this work.

TABLE OF CONTENTS

TABLE OF CONTENTS (Continued)

Page

LIST OF TABLES

LIST OF TABLES (Continued)

LIST OF TABLES (Continued)

LIST OF FIGURES

LIST OF FIGURES (Continued)

LIST OF FIGURES (Continued)

FIGURE Page

LIST OF FIGURES (Continued)

LIST OF FIGURES (Continued)

FIGURE Page

LIST OF FIGURES (Continued)

FIGURE Page

CHAPTER I

INTRODUCTION

Isobutylene Synthesis

Pichler and Ziesecke (*7*) were the first to study (and name) the isosynthesis reaction. Isosynthesis refers to the synthesis of *iso*-C_4 hydrocarbons from carbon monoxide and hydrogen. In their study, several single component and multicomponent oxide catalysts were tested for activity toward isosynthesis. Thorium dioxide (ThO_2) and zirconium dioxide (ZrO_2) were found to be the most active single component catalysts. Overall, a 20% Al_2O_3/ThO_2 catalyst was found to be the most active. Pichler and Ziesecke (*7*) performed experiments at high temperatures (648-773 K) and high pressures (150-1000 atm) (1 atm = 1.01325×10^5 N/m^2). Although high conversions were obtained, in most cases the isobutylene yield was low. However, isobutylene was the primary C_4 product with ZrO_2 catalyst. Additionally, operation at lower pressures would be desirable because of the cost associated with high pressure equipment.

More recent investigations on the activity and selectivity of zirconium dioxide have been performed (*8-14*). Kieffer *et al.* (*8*) investigated CO hydrogenation over rare earth metal oxides (La_2O_3 and Dy_2O_3) at 400 atm and 683-748 K. They observed ~25% C_4's with 80% selectivity to *iso*-C_4's at about 20-25% total carbon monoxide conversion. Both hydrocarbons and methanol were formed. Addition of palladium to these oxides resulted in an increase in methane formation. A two step mechanism in which methanol formed first and then transformed into the hydrocarbons was suggested.

Maehashi *et al.* (*9*) performed isosynthesis using a glass vacuum reactor system with a gas recirculating pump at temperatures from 523-673 K. Also, several tests at 21 atm were conducted in a flow reactor system. They reported a very high selectivity to isobutylene (~80%) among all hydrocarbons at 623 K and 0.68 atm. Conversion for low pressure runs was less than 5%. Carbon monoxide conversion was surprisingly high for the flow system; however, ~80% of the product was carbon dioxide.

Maruya *et al.* (*10,11*) investigated the effects of various metal promoters. They found that sodium increased the selectivity to C_4's while decreasing overall activity. Cerium was found to increase activity while maintaining high C_4 selectivity (~75%). Catalysts doped with niobium were less active and did not give the typical isosynthesis distribution. Instead, the Schulz-Flory plot resembled that of Fischer-Tropsch synthesis. The electronegativity of the dopant oxide was thought to play an important role in selectivity toward C_4's, especially isobutylene. An increase in catalyst acidity promoted methane formation and retarded the formation of C_4 hydrocarbons. They concluded that the formation of C_2 species from C_1 species was the rate determining step of the reaction. This work was also performed at very low conversions.

Tseng *et al.* (*12*) examined the mechanism by the incorporation of ^{13}C labeled oxygenated compounds into the products. These studies were performed at 623-698 K, 35 atm, and 1/1 CO/H_2 ratio. Methane and methanol were the dominant products even though conversions were low. Two chain growth steps were proposed. One involved CO insertion into a bound aldehyde or ketone and the other involved condensation between methoxide and a surface bound enolate. Maruya *et al.* (*11*) also found evidence to support this mechanism.

Jackson and Ekerdt (*13*) doped zirconia with calcium and yttrium oxides in varying concentrations to investigate the effect of oxygen vacancies and acidity on the isosynthesis reaction carried out at conditions similar to Tseng *et al.* (*12*). The most active catalysts were those in which ionic conductivity was a maximum, suggesting that vacancies in the crystal lattice play an important role in the reaction. Jackson and Ekerdt (*14*) also studied the effect of catalyst acidity on C_3 intermediates. They found that more acidic catalysts stabilized the branched C_3 intermediates which led to more C_4 products, but not necessarily the highest branched to linear [C_4's and C_5's] ratio. A balance of acidic and basic sites on the surface was believed necessary for maximum isobutylene production.

Reaction Mechanism

Though there is still controversy regarding the detailed mechanisms, it may be generally agreed that C_4 hydrocarbons are formed by the following steps (*12,15*):
1. *Chain initiation:* An adsorbed H reacts with carbon monoxide to form an adsorbed formate species for chain initiation.

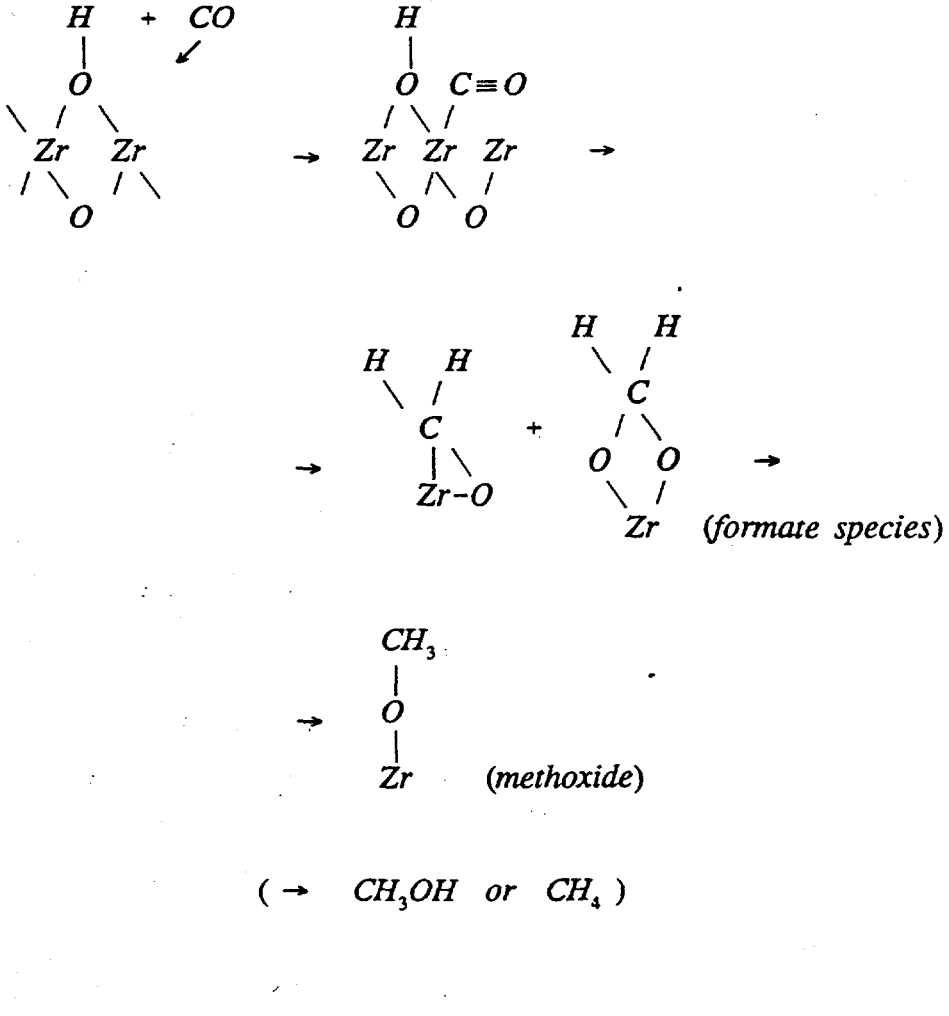

2. Other adsorbed intermediates are formed via *chain propagation by CO insertion.* This reaction is equivalent to the chain growth in F-T synthesis. As can be seen, linear intermediates are formed on the surface. CO attacks the carbon-metal bond.

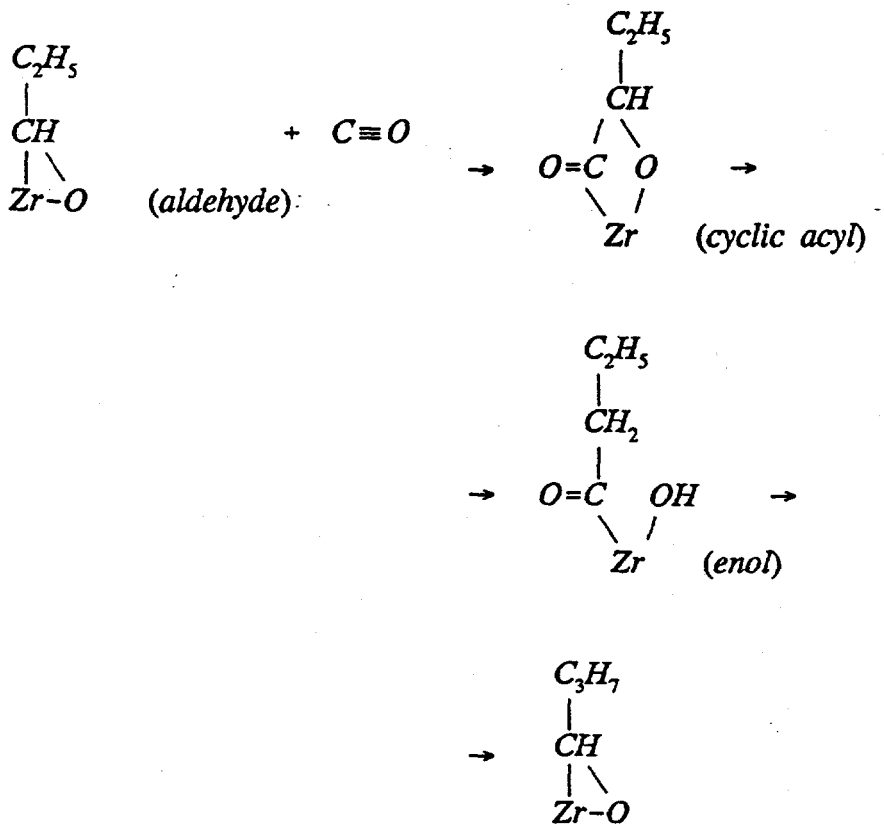

3. A unique reaction for isosynthesis is the *chain propagation by condensation* of an intermediate with the adsorbed formate. Branched intermediates are formed on the surface and react with an alkoxide. Though condensation reactions are slow compared with CO insertion, they are kinetically significant because of the large surface concentration of adsorbed formate groups on the catalyst.

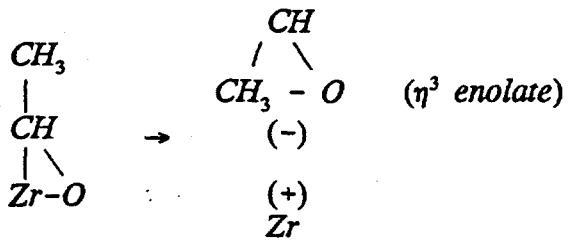

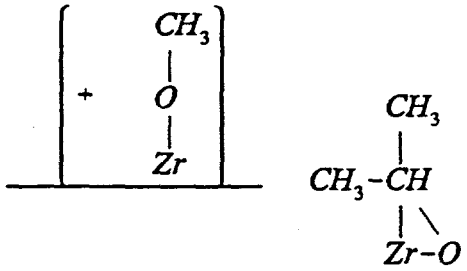

4. In addition to propagating, intermediates may *terminate* by desorbing into hydrocarbons

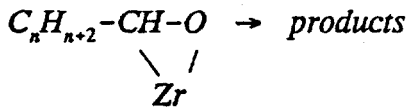

Condensation reactions contribute to the deviations in hydrocarbon distribution of isosynthesis from that of a Anderson-Schulz-Flory polymerization scheme, which results in a large amount iso-C_4 hydrocarbons in the product. Zirconia is one of the active metal oxides for catalyzing condensation reactions (*15*), and consequently, a large amount of isobutane and isobutene is produced over the catalysts.

An excellent review of isosynthesis has been written by Sofianos (*4*) and contains more detailed information on proposed mechanisms.

Zirconia Synthesis by Precipitation

Nearly all work on isobutylene synthesis has been performed using zirconia prepared by co-precipitation. Studies done on the crystal phase (*16-20*) obtained from precipitation indicate that both *p*H and the presence of other metal dopant ions play a role in determining the final crystal phase.

Zirconia gels were precipitated from zirconyl nitrate or zirconyl chloride solutions with ammonium hydroxide or sodium hydroxide depending on *p*H (*16-18*). When these gels were calcined at 873 K the predominant crystal phase was either monoclinic or tetragonal. Gels precipitated in the 6.5-10.4 *p*H range resulted in monoclinic zirconia while those

precipitated at higher or lower *p*H resulted in tetragonal zirconia. It was observed that the presence of sodium did not stabilize the tetragonal phase when the *p*H was in the range of 6.5 to 10.4.

Benedetti *et al.* (*19,20*) observed that sodium (3-4 weight %) could stabilize the cubic phase of zirconia up to calcination temperatures of 853 K. The zirconia gel was precipitated from zirconyl chloride solutions using either ammonium hydroxide or sodium hydroxide. Samples precipitated at high *p*H and washed to leave 0.5% sodium were found to give mainly tetragonal phase upon calcination. A sample precipitated at *p*H=8 resulted in a mixture of monoclinic and tetragonal phases. The crystal phase formed was attributed to the presence or absence of sodium, not *p*H.

The three polymorphs of zirconium dioxide mentioned above have been studied extensively. The structure of monoclinic zirconia (*21*) is the most complicated because it is the least symmetrical. Monoclinic zirconia is the stable phase at room temperature when calcined at high temperature. Tetragonal (*22*) and cubic (*23*) zirconia normally exist at higher temperatures, but can be stabilized at lower temperatures by doping the zirconia with other metal cations. The phase transitions of zirconia with temperature at atmospheric pressure are shown below.

$$\text{Monoclinic} \underset{\sim 1223\ \text{K}}{\overset{1443\ \text{K}}{<\!\text{---}\!>}} \text{Tetragonal} \overset{2643\ \text{K}}{<\!\text{---}\!>} \text{Cubic} \overset{2979\ \text{K}}{<\!\text{---}\!>} \text{Melt}$$

Kinetics and Thermodynamics

Isobutane and isobutene are not the only products from the hydrogenation of carbon monoxide under the conditions of this work. As the broad product distribution places severe limitations on the attractiveness of isosynthesis as a commercial operation, the various underlying constraints associated with the synthesis, with respect to the selective formation of isobutane and isobutene, are discussed in detail.

Formation of hydrocarbons

The reactions of carbon monoxide and hydrogen form a variety of products, including alcohols, ethers, alkanes, alkenes, water, carbon dioxide, and carbon as follows:

$$CO + 2\,H_2 \rightarrow CH_3OH \quad \textit{methanol}$$

$$CO + H_2 \rightarrow \frac{1}{3}\,CH_3OCH_3 + \frac{1}{3}\,CO_2 \quad \textit{dimethyl ether}$$

$$CO + \frac{n+1}{2n}\,H_2 \rightarrow \frac{1}{2n}\,C_nH_{2n+2} + \frac{1}{2}\,CO_2 \quad \textit{alkanes}$$

$$CO + \frac{1}{2}\,H_2 \rightarrow \frac{1}{2n}\,C_nH_{2n} + \frac{1}{2}\,CO_2 \quad \textit{alkenes}$$

$$CO_2 + H_2 \rightarrow CO + H_2O \quad \textit{reverse water-gas shift}$$

$$CO \rightarrow \frac{1}{2}\,C + \frac{1}{2}\,CO_2 \quad \textit{Boudouart reaction}$$

Figure 1.1 shows the equilibrium constants for some of these reactions as a function of temperature. The thermodynamic properties are obtained from Stull *et al.* (*24*). Of all the hydrogenation reaction to form hydrocarbons, methanation is thermodynamically the most favorable. At equilibria, only methane, carbon dioxide, carbon, and water are found in the products (Table 1.1).

Furthermore, the formation of saturated hydrocarbons is more favorable than that of unsaturated hydrocarbons. For example, consider the following reactions to form isobutane and isobutene:

$$CO + \frac{5}{8}\,H_2 \rightarrow \frac{1}{8}\,i\text{-}C_4H_{10} + \frac{1}{2}\,CO_2 \quad \textit{isobutane}$$

$$CO + \frac{1}{2}\,H_2 \rightarrow \frac{1}{8}\,i\text{-}C_4H_8 + \frac{1}{2}\,CO_2 \quad \textit{isobutene}$$

At 700 K and 70 atm with 1/1 CO/H_2 in the feed, the weight ratio of isobutane to isobutene in the equilibrium mixture is about 3500 to 1.

Distribution of isomers

The Gibbs free energies of formation determine the equilibrium distribution of isomers. At 700 K, the distribution of butenes is 49.22% isobutene, 24.16% *trans*-2-butene, 15.74% *cis*-2-butene and 10.88% 1-butene, and the distribution of butanes is 59.93% *n*-butane and 40.07% isobutane. Therefore, the formation of linear butane and butenes are quite favorable at thermodynamic equilibrium.

Formation of alkenes

Formation of heavy hydrocarbons (carbon number > 5) is favorable at conditions of

the isosynthesis reaction. To illustrate this, consider the following reactions to form C_2 to C_6 alkenes at 700 K:

	$\Delta G°$ *(kcal/mol)*
$4\ CO + 2\ H_2 \rightarrow C_2H_4 + 2\ CO_2$	-0.2
$C_2H_4 + 2\ CO + H_2 \rightarrow C_3H_6 + CO_2$	-3.52
$C_3H_6 + 2\ CO + H_2 \rightarrow C_4H_8 + CO_2$	-1.57
$C_4H_8 + 2\ CO + H_2 \rightarrow i\text{-}C_5H_{10}$ (2-methyl-2-butene) $+ CO_2$	-1.44
$i\text{-}C_5H_{10} + 2\ CO + H_2 \rightarrow i\text{-}C_6H_{12}$ (3-methyl-2-pentene) $+ CO_2$	-1.11

Isobutene is not a very favorable product and a large amount of pentene and hexene is formed at equilibrium (Figure 1.2) (It should be pointed out that the distribution is calculated in the absence of alkanes). The limitation on the formation of alkenes caused by the formation of alkanes is more severe for strong hydrogenation catalysts, as reported by Fajula *et al.* (*25*) and Gadalla *et al.* (*26*).

Kinetic constraints

CO hydrogenation to form hydrocarbons is seen as starting from a single carbon unit whose size is gradually increased by the repeated addition of other single carbon units, as follows (*27-29*):

$$CO + H_2 \rightarrow [Y_1] \xrightarrow{k_{p_1}} [Y_2] \xrightarrow{k_{p_2}} [Y_3] \xrightarrow{k_{p_3}} [Y_4] \xrightarrow{k_{p_4}} [Y_5] \ldots$$
$$\downarrow k_{t_1} \qquad \downarrow k_{t_2} \qquad \downarrow k_{t_3} \qquad \downarrow k_{t_4} \qquad \downarrow k_{t_5}$$
$$P_1 \qquad P_2 \qquad P_3 \qquad P_4 \qquad P_5$$

where $[Y_i]$ and P_i denote intermediates and hydrocarbons with carbon number of i. Further, assume:

1. Starting from initial chain Y_1, any chain Y_n can be formed by n-1 propagation steps.
2. The chance for any intermediate chain to propagate rather than terminate is given by

$$\alpha = \frac{k_p}{k_p + k_t}$$

where k_p is the rate constant for propagation from $[Y_n]$ to $[Y_{n+1}]$ and k_t is the rate constant for termination of $[Y_n]$ to product P_{n+1}.

3. α is independent of n, i.e., probabilities of termination and propagation are independent of the length of the carbon chain attached to the surface.

Then, we have:

$$\frac{d[Y_{n+1}]}{dt} = k_p[Y_n] - (k_p + k_t)[Y_{n+1}] = 0$$

$$\frac{\dfrac{d[P_{n+1}]}{dt}}{\dfrac{d[P_n]}{dt}} = \frac{k_t[Y_{n+1}]}{k_t[Y_n]} = \frac{k_p}{k_p + k_t}$$

$$\frac{[P_{n+1}]}{[P_n]} = \frac{k_p}{k_p + k_t} = \alpha$$

and we obtain a Schulz-Flory-Anderson distribution typical of polymerization reactions:

$$[P_1] = [P_0]\alpha,\ [P_2] = [P_1]\alpha = [P_0]\alpha^2,\ \ldots,\ [P_n] = [P_0]\alpha^n.$$

In general,

$$C_n = \alpha^n ln^2\alpha, \text{ or } lnC_n = 2ln(ln\alpha) + nln\alpha$$

where C_n is the mole fraction of product P_n, and $ln^2\alpha$ is obtained from normalizing the distribution by summation over all products. A straight line is obtained by plotting lnC_n vs n.

Even though the above Schulz-Flory-Anderson distribution is obtained for Fischer-Tropsch synthesis, it is not obtained for isosynthesis. Figure 1.3 compares the hydrocarbon distribution for isosynthesis with that for the F-T reaction. A discontinuity at C_4 is observed for isosynthesis. This deviation from the standard polymerization distribution in the F-T synthesis is unique in the forming of C_4 hydrocarbons (*15*), and cannot be explained by the assumption of equal-reactivity of polymer chains (i.e., α is independent of carbon chain).

Constraints on selectivity

Kinetic constraints also affects product selectivity. Consider the following reactions:

$CO + H_2 \rightarrow [C_1] \rightarrow C_1$	k_0
$CO + H_2 + [C_1] \rightarrow [C_2] \rightarrow C_2$	k_1
$CO + H_2 + [C_2] \rightarrow [C_3] \rightarrow C_3$	k_2
$CO + H_2 + [C_3] \rightarrow [C_4] \rightarrow C_4$	k_3
$CO + H_2 + [C_4] \rightarrow [C_5] \rightarrow C_5$	k_4
$CO + H_2 + [C_5] \rightarrow [C_6] \rightarrow C_6$	k_5
$CO + H_2 + [C_6] \rightarrow [C_7] \rightarrow C_7$	k_6
$CO + H_2 + [C_7] \rightarrow [C_8] \rightarrow C_8$	k_7

By arbitrarily assuming $k_1 = k_2 = 0.25k_3 = k_4 = k_5 = k_6 = k_7 = 0.5k_0$, a selectivity versus space time plot is obtained (Figure 1.4) by applying the procedure presented by Aris (*31*) and Holland and Anthony (*32*). The effect of the chain growth mechanism on the selectivity is apparent since the plot indicates that C_4 hydrocarbons cannot be produced with

a selectivity higher than a certain limit which is determined by the ratios of the reaction rate constants. Figure 1.4 also indicates that only C_1 can be produced with a selectivity close to 100%, which places a very severe constraint on the selective production of lower alkenes.

Constraints caused by methanation and Boudouart reaction

The formations of methane by methanation and carbon by the Boudouart reaction are thermodynamically more favorable than the isosynthesis reaction, and hence restrict the selective production of lower alkenes (*30*). Methanation can be slightly suppressed by the use of short contact time and low temperatures. Another factor that affects methanation is the hydrogenation strength of the catalyst. For example, catalysts such as nickel and platinum are well known for their strong hydrogenation activity and produce mainly methane. Carbon deposition further causes methanation, since some types of carbon are readily hydrogenated to methane (*33*). The deposition of carbon in itself causes major problems: it may lead to excessive methane formation, catalyst deactivation, destruction of catalyst pellets, and increased attrition and physical plugging of the reactor (*30*).

Modeling

Very few attempts have been made in modeling the conversion or product distribution of the isosynthesis reaction. Such models would be useful in designing an industrial size reactor. Part of the reason for the lack of work on modeling may be the low conversion usually obtained.

Maruya *et al.* (*10*) calculated activation energies of 79, 84, and 96 kJ/mol for C_2, C_3, and linear C_4 hydrocarbon formation over the temperature range 523-723 K and 210 kJ/mol for branched C_4 hydrocarbons (523-623 K). The rate of C_4 hydrocarbon formation at 673 K was found to be first order in hydrogen and second order in carbon monoxide. Those for C_1, C_2, and C_3 hydrocarbons were written as functions having maximums with carbon monoxide pressure.

Karles and Ekerdt (*34*) used the mechanism for isosynthesis over zirconia proposed by Tseng *et al.* (*12*) and Jackson and Ekerdt (*13*) to model the product distribution using six fitted rate constants. The model utilized several assumptions about the surface species and predicted the wt% distribution among the hydrocarbons through C_7's. No C_6+ hydrocarbons were detected in their effluent stream however, and no mention was made of the carbon monoxide conversion levels.

TABLE 1.1. Conversions and product distributions[a] of CO/H_2 reactions at equilibrium

Pressure (atm)	50		70	
Temperature (K)	653	723	653	723
CO	0.000339	0.001660	0.000295	0.001401
H_2	0.000886	0.001936	0.000750	0.001639
CO_2	0.338798	0.360891	0.338427	0.360205
H_2O	0.331568	0.312950	0.331927	0.313742
C	0.223619	0.214070	0.223464	0.213770
CH_4	0.104789	0.108471	0.105138	0.109227
C_2H_6	0	0.000016	0.000016	0.000016
CO conversion	0.999636	0.998214	0.999732	0.998675
H_2 conversion	0.986799	0.97117	0.990141	0.97848

[a] Distributions are on a weight basis, 1/1 CO/H_2 in the feed.

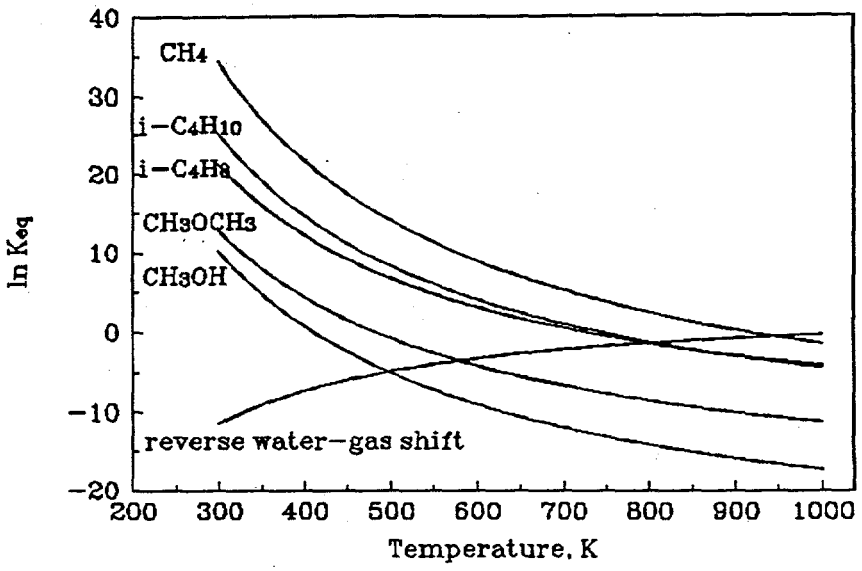

Figure 1.1. Temperature dependence of equilibrium constants. Hydrogenation of CO is exothermic.

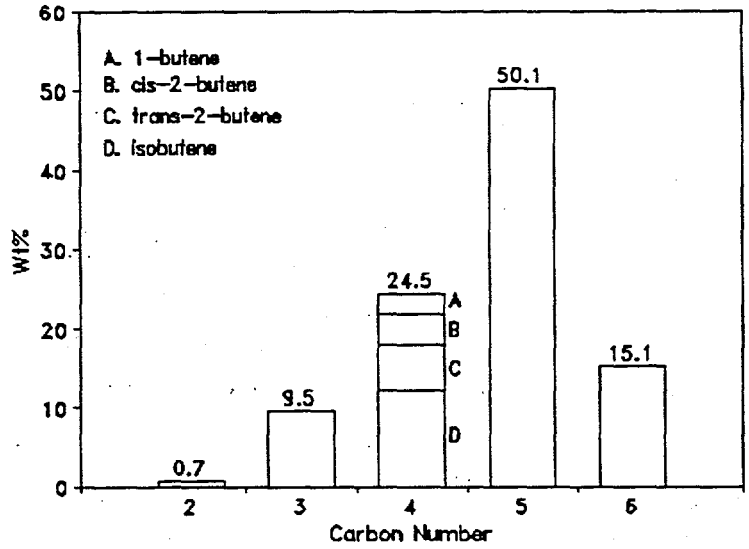

Figure 1.2. Equilibrium distributions of alkenes from hydrogenation of CO at 700 K, 70 atm, and 1/1 CO/H_2 ratio.

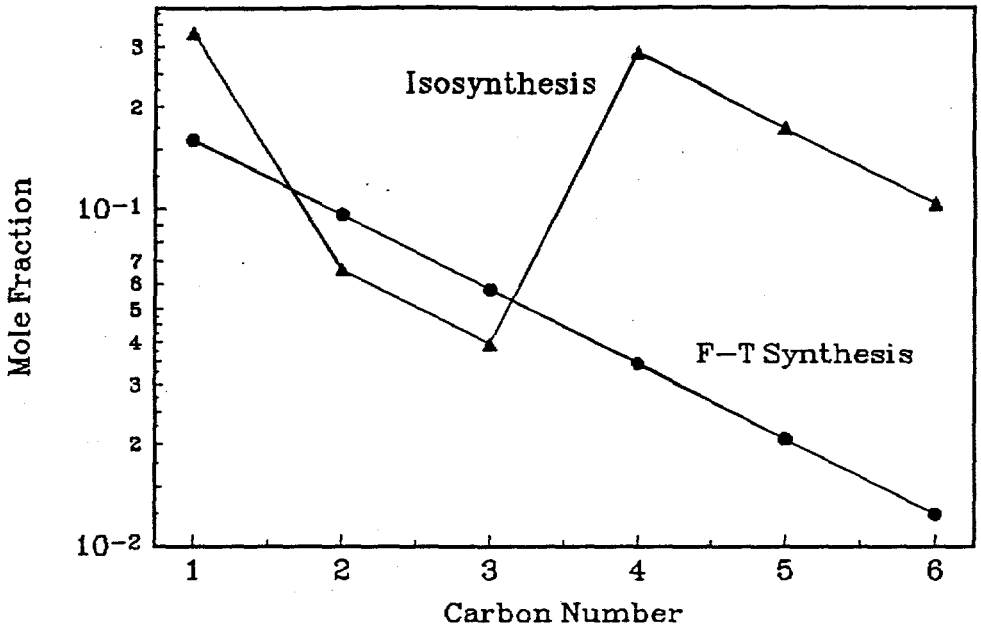

Figure 1.3. The Schulz-Flory-Anderson plots for the distributions of hydrocarbons. ▲: Isosynthesis (*4*); ●: F-T synthesis (*28*).

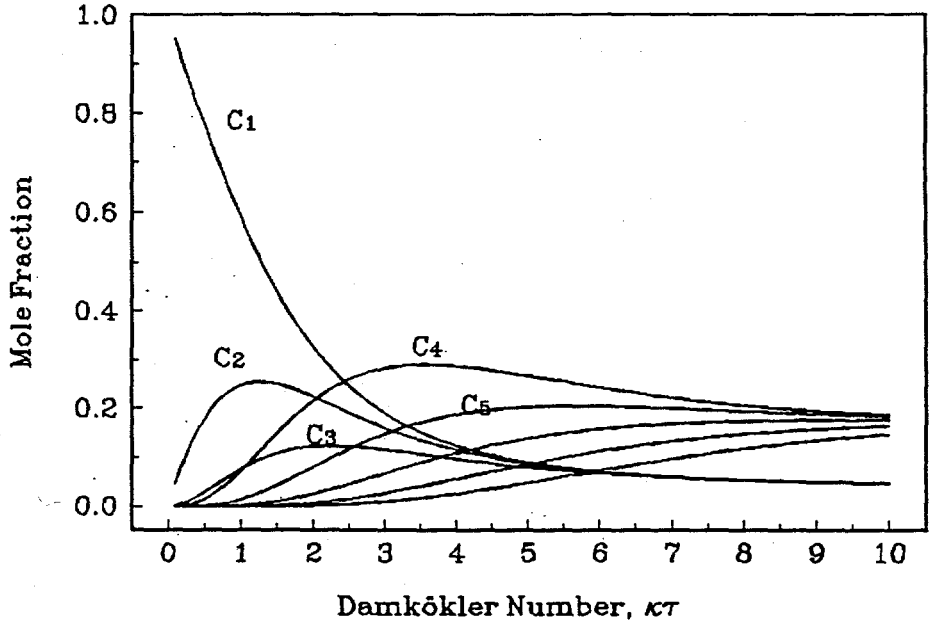

Figure 1.4. Distribution of C_1 to C_8 hydrocarbons as a function of space time.

CHAPTER II

EXPERIMENTAL

Catalyst Preparation

In this research catalysts doped with a single component were predominantly used. However, several multicomponent doped zirconias were prepared by both the precipitation and hydrothermal methods. The details of each preparation method are discussed in its respective section.

Zirconia prepared by precipitation (ppt.)

Single component catalysts included those doped with oxides of lithium, magnesium, manganese, aluminum, cerium, dysprosium, and tantalum. Multicomponent doped catalysts included a sodium-titanium-thorium zirconia and a yttrium-barium-copper zirconia. The following procedure was used in preparing the majority of catalysts. About 41 grams of zirconyl nitrate plus the weight of the source compound required to give the desired molar ratio of dopant to zirconium were dissolved in water (deionized and distilled) in the ratio of 20 ml of water per gram of solid. A 1.5 wt% ammonium hydroxide solution was prepared using 1.3333 ml of ammonium hydroxide stock solution (28-30 wt%) per gram of solid. The gel was precipitated by slowly pouring the metal salts solution into the ammonium hydroxide solution while stirring. Before filtering, the *p*H of the gel solution was adjusted with nitric acid to 7.00 and allowed to stand for 24 hours. Usually after precipitation the *p*H of the solution with gel was between 9.5 and 10.5. About 700 ml was poured off the top of each batch before filtering began. The gel was filtered and washed twice with ~1000 ml of water each time. After filtering and washing the gel was dried at 383 K for 24 hours. Final dehydration was accomplished by calcining at 723 K for 2½ hours. The calcined samples were ground and sieved to <250 μm before bulk density was measured. Sodium was included in the zirconia by precipitating with both NaOH and NH_4OH.

Zirconia prepared hydrothermally (HT)

Two doped zirconias were prepared by a hydrothermal method. One contained sodium and titanium while the other contained sodium, titanium, and thorium. In the first sample, the molar ratios of Zr/Ti and Na/Ti were 3 and 0.5 and in the second sample the molar ratios of Zr/Ti, Na/Ti, and Th/Ti were 18, 0.6, and 0.2. The first step in this synthesis was preparing two mixtures. In both preparations, mix A contained 25 wt% tetramethylammoniumhydroxide in methanol, 18 wt% NaOH in water, and tetrabutylammoniumbromide. In one case, mix B contained 70 wt% zirconium(IV) propoxide in 1-propanol and 97% titanium(IV) isopropoxide. In the other case mix B also contained thorium nitrate. Mix B was added to mix A while stirring. The gel formed was transferred to a 550 ml stainless steel reactor. Water was added during the washing of the plastic containers used for the two mixtures. The reactor was then sealed and heated in an oven at 443 K. The first preparation was heated for 116 hours while the second was heated for 24 hours. After removal from the reactor the zirconia was filtered, washed with acetone, and

then calcined at 773 K for 2½ hours.

Zirconia prepared by calcining zirconyl nitrate (CAL)

Two zirconias were prepared by this method. The first was a smaller batch to determine the calcination period necessary before no more weight loss occurred in the catalyst. In both cases the zirconyl nitrate was held at 373 K for 2 hours then ramped to 773 K in 1 hour and 20 minutes. The first batch was removed and weighed after 4 hours at 773 K and then again after 7 hours. It was found that no further weight loss had occurred. The second batch was held at 773 K for 4 hours. A similar procedure was used by Evans *et al.* (*35*) in preparing tetragonal zirconia.

Zirconia prepared by a conventional sol gel method (CSG)

A sol gel method was used to prepare zirconia-alumina. To distinguished between this method and the modified sol gel method discussed later, this method is referred to a conventional sol gel method. Zirconium isopropoxide (0.18 moles) was mixed with aluminum butoxide (0.01 moles), and then the mixture of alkoxides was hydrolyzed by adding 190 ml water dropwise. The precipitate was collected by filtering and drying, and was then calcined (773 K for 3 hours). Each batch yielded about 5 grams of material, and is referred to as Al_2O_3-ZrO_2 (CSG).

Zirconia prepared by a modified sol gel method (MSG)

Zirconium oxides were synthesized using a modified sol gel method proposed by Dosch *et al.* (*36*) of Sandia National Laboratories. Some modifications of the initial procedure were made in this study, including varying the type of base and using acetone instead of acetone-water for drying and rinsing. The procedure of synthesis is summarized as follows:

$$\underset{\text{(metal alkoxide)}}{M(OC_nH_{2n+1})_m} + \underset{\text{(base)}}{OH^-} \xrightarrow{\text{methanol}} \text{a soluble intermediate}$$

$$\text{soluble intermediate} \xrightarrow[\text{hydrolysis}]{\text{acetone}} HMO_x$$

$$HMO_x \xrightarrow{\text{calcination}} MO_{m/2} \quad (M=Zr,\ Si \text{ or } Al).$$

Metal alkoxide was slowly added to a methanol solution of a base (inorganic or organic) to form a soluble intermediate. The intermediate was rapidly added to a 1:10 by volume water and acetone solution. The slurry was continuously stirred until the particles were suspended in the solution. Finally, the precipitate was collected by filtering and drying in a vacuum at 353 K overnight. After calcination (773 K for 3 hours), the catalyst was ground and sieved to 250 μm particles.

To synthesize catalysts with different properties, both inorganic (sodium hydroxide) and organic (tetramethylammonium hydroxide) bases were used in the preparation. Mixed

alkoxides were also used in some preparations. Alkali metals, alkaline earth metals, and some transition metals were also added to the catalysts by dissolving the corresponding hydroxides or nitrates in the methanol solution in the first step. The volumes of water, methanol and acetone in the synthesis were 16, 48 and 160 ml, respectively. Two batches of calcium-zirconias, Ca-ZrO_2 (MSG) (0.5 wt% Ca) and Ca(2%)-ZrO_2 (MSG) were prepared with different loadings of calcium.

All the catalysts were prepared by using an organic base (tetramethylammonium hydroxide) except for SiO_2-ZrO_2-NaOH (MSG) which was prepared by using an inorganic base (sodium hydroxide). After the preparation and before calcination, SiO_2-ZrO_2-NaOH was treated with HCl at a *p*H of 4 four times to remove over 99.99 wt% of the sodium from the catalyst.

Catalyst Characterization

The surface area of each catalyst and pore volume/pore diameter of several samples were measured using the BET method and a fully automated Micromeritics® Digisorb 2600 apparatus. The catalyst sample is placed in a sample bulb and degassed at 473 K under high vacuum (1.3×10^{-8} atm) overnight, then the sample bulb is removed and placed in the measurement section of the instrument. The manufacturer's operation manual contains detailed descriptions of the equipment and procedures. The X-ray diffraction (XRD) patterns were obtained using a Scintag XDS-2000 X-ray diffractometer with a Cu anode and a continuous scan of 4° (2θ) per minute.

A Varian atomic absorption spectrometer, model Spectra AA-30, was used to measure the metal composition of some of the catalysts. Hydrofluoric acid was added when necessary to dissolve the catalyst.

The acid-base properties of the modified sol gel catalysts were measured by a temperature programmed desorption (TPD) of ammonia and carbon dioxide. Ammonia and carbon dioxide were stored in gas cylinders. TPD experiments were conducted at atmospheric pressure. Figure 2.1 is the schematic diagram of the TPD apparatus. Typically, a 200 mg sample was loaded in a quartz reactor and activated in a helium stream by heating to 933 K at a rate of 5 K/min and maintaining that temperature for 10 minutes. After the sample was cooled to 343 K, carbon dioxide or ammonia was adsorbed for 30 minutes. The sample was then flushed with helium at a temperature of 343 K and a flowrate of 20 cm^3/min for 2 hours to remove physisorbed adsorbent. The effluent was monitored by a thermal conductivity detector and an integrator. The detector was calibrated by injecting a known volume of carbon dioxide or ammonia into the injection port.

Materials

Table 2.1 shows the source compounds and their purities for the oxides prepared by the precipitation, hydrothermal, and calcination methods. The majority of starting materials were purchased from Aldrich. The thorium nitrate was purchased from Alfa Products while NH_4OH (A.C.S. Reagent) and HNO_3 (70.7%) were purchased from Fisher and Mallinckrodt respectively.

Table 2.2 lists the chemicals used in the synthesis of modified sol gel catalysts. Standard solutions for the atomic absorption experiments were purchased from Fisher Scientific and Aldrich Chemical. The water used in all preparations was distilled and

deionized.

Carbon monoxide (C.P. grade, 99.5%) in an aluminum cylinder and 1.06±0.02% hydrogen sulfide in hydrogen were purchased from Matheson Gas Products. Carbon monoxide (C.P. grade, 99.5%) in an iron cylinder, hydrogen and nitrogen (reactor purge) gas cylinders were acquired from Bob Smith Corporation. Air (3776 ppm), methane (18 ppm), and water (<5 ppm) were the main impurities in the carbon monoxide. There was also <1 ppm each of carbon dioxide, ethylene, ethane, and propane present. Helium, nitrogen, hydrogen and air cylinders needed to operate the gas chromatographs (GC) were also purchased from Bob Smith.

Apparatus and Procedure

Fixed bed reactor 1

A schematic of the reactor system is shown in Figure 2.2. Carbon monoxide, hydrogen, and nitrogen were passed through molecular sieve (5A) filters to remove water. When the hydrogen sulfide/hydrogen mixture was used it was not passed through a molecular sieve as the hydrogen sulfide would be removed. An aluminum cylinder was used instead of iron in some cases in order to eliminate the formation of iron carbonyls in the cylinder that could poison the catalyst. When the iron carbon monoxide cylinder was used the gas was also passed through an activated charcoal bed and in some cases also a commercial zirconia guard bed to remove any carbonyls.

The purified reactant gases were fed to the reactor through 15 micron filters and Brooks 5850E mass flow meters controlled by 5896 controllers also from Brooks. The carbon monoxide and hydrogen flow meters were rated at 0-28 and 0-30 standard liters per hour respectively. The flow meters were calibrated by measuring the volumetric flow rate with the soap bubble meters for various controller settings. There was no significant difference in pressure drop between flowing through the reactor or through the bypass. Before the reactor, the reactants were mixed in a 75 cm^3, 304 stainless steel container filled with glass beads. The reactor was made from 304 or 316 stainless steel with an overall length of 29 cm and an internal diameter of 0.493 cm. The reactor was heated in a gas chromatograph oven using a coil-type resistance heater. Air was circulated by a fan located inside the oven. The thermocouple measuring reaction temperature was placed outside the reactor about halfway down the length of the catalyst bed and about 2 cm from the reactor wall. Three to fifteen grams of catalyst were loaded into the reactor depending on the bulk density. All other tubing was 0.318 cm or 0.159 cm 316 stainless steel. The reactor pressure was maintained using a Grove S-91W back pressure regulator. Temperature control was accomplished using an Omega 6100 controller. The lines from the 15 micron filter at the reactor exit up to and including the sampling valve (N) were wrapped with heating tape and held at ~400 K to eliminate product condensation in the lines before the liquid trap.

The reactor effluent could be injected into two on-line GCs. An SRI model 8610-30 GC equipped with both thermal conductivity (TCD) and flame ionization (FID) detectors and a 0.318 cm × 1.83 m Porapak Q 80/100 column was used to monitor oxygenate production and give a partial separation of the C_5 hydrocarbon fraction. However, the C_6+ fraction could not be quantified on this GC. To inject on this GC the sample valve (N) was turned so the sample loop was in-line with the flowing product stream. Thirty seconds were allowed before the sample valve was switched back to inject the sample into the column.

Integration was performed by the Peaksimple® II software (from SRI) on an IBM PC.

Separation of CO, H_2, CO_2, and all the C_1-C_4 hydrocarbons was accomplished using a Carle series S TCD GC controlled by a Hewlett Packard 3385A automation system. This system controlled the valve switching of three different sampling valves contained within the GC. This GC used five separate columns and a palladium hydrogen transfer system. The injection procedure for this GC consisted of turning valve V8 to direct flow to the GC instead of to the vent. Two minutes were allowed to flush the sample loop before the sample was taken. Additionally, a gas tight syringe was used to inject a sample of the reactor effluent into a similar Carle series S TCD/FID GC. Valve V7 was closed to direct flow through the sample port (M) and into the syringe. The syringe was filled in this manner to minimize the amount of air that might contaminate the sample. The syringe was filled and injected into the sample loop three or four times to ensure that the sample loop was completely flushed. The C_5+ hydrocarbon fraction was given in the column back-flush.

The reactor was filled with catalyst by first plugging one end with glass wool (~½ inch) and then funneling the powder in from the other end. Any volume inside the reactor not filled with catalyst was packed with glass wool. After the reactor was installed a leak test was performed. First, the back pressure regulator was set to a pressure ~5 atm larger than would be used in the experiment. Then nitrogen was passed through the system at this pressure. Leaks were detected using a soap solution. The three-way valves on either side of the mass flow meters were used to bring the pressure up on both sides of the meter without flowing gas through them. This allowed a faster build-up to the desired pressure without the problem of sticking the mass flow meter closed because of a large pressure drop. Nitrogen could be accurately controlled with the carbon monoxide flow meter because the correction factor between these two gases is approximately one.

During heat-up of the reactor, the system was pressurized to 35 atm and nitrogen was passed over the catalyst at 100 sccm. Heat-up of the reactor from room temperature to 673 K required about 17 minutes.

The catalyst was pretreated at 673 K and 35 atm in flowing nitrogen for 18 hours. After pretreatment the pressure was adjusted to the desired reaction pressure, the reactor was bypassed using valves V3 and V4, and the CO and H_2 or (H_2+H_2S) flows were started. Once the composition and flowrate of the feed was measured the reactor was brought on-line. Between experiments, nitrogen was passed over the catalyst (at reaction temperature) at 100 sccm.

A minimum of 2 hours (17 hours for most runs) were allowed for the reaction to come to steady state before effluent analysis began. An experiment consisted of four injections to each of the GC's over a 4-5 hour period. The effluent flow rate was measured at both the beginning and end of this period while noting room temperature and pressure. The GC output was used to determine carbon monoxide and hydrogen conversions as well as product distributions and mass balances.

Fixed bed reactor 2

The CDS 900 reactor system (Figure 2.3) was designed and manufactured by Chemical Data Systems, a subsidiary of Autoclave Engineering. It was a complete gas/liquid phase reaction system designed to facilitate studies of catalytic and non-catalytic processes. The system's modular design permitted a degree of flexibility in both design and operation. It was comprised of three basic modules: Reactor System, Control System, and Analytical

System.

The reactor system was designed to be entirely housed within a temperature-controlled oven. Reactant preparation consisted of receiving, metering, and selectively mixing up to four gases or a combination of two gases and two liquids. In this study, four gas inlets were used for hydrogen, carbon monoxide, nitrogen, and a standard gas mixture (containing nitrogen with roughly 1 vol% of C_1 to C_4 hydrocarbons, carbon dioxide and carbon monoxide: for GC calibration). After the mixer/vaporizer, the mixture passed through a reactor status valve. The setting of this valve determined the inlet stream to the reactor. Either reactants or a failsafe purge gas (nitrogen) was flowing into the system depending on the position of the valve. When the reactor status valve was "on", the reactants entered a 1.27 cm ID stainless steel reactor.

The reactor was heated by a three-zone stainless steel annular heater. The temperature of each heating zone was controlled individually and simultaneously. The pressure inside the reactor was controlled by an automatic back pressure regulator located at the outlet of the reactor. Both the inlet and outlet pressures of the reactor were monitored by pressure transducers and gauges. Two rupture disks were connected to the inlet and outlet of the reactor to ensure safety.

After the back pressure regulator, the product stream, now at atmospheric pressure, exited the reactor module cabinet through a heated transfer line and entered the analytical system. The analytical system consisted of a gas chromatograph equipped with parallel FID and TCD systems. The TCD system included two Porapak Q columns, a Molecular Sieve 5A column, and a palladium hydrogen transfer tube, while the FID system was equipped with a 50 meter BP-1 capillary column. The component separation was complete, except for 1-butene and isobutene, which were separated by the previously described off-line Carle TCD/FID GC. The exhaust stream from the GC was vented to a fume hood.

Molecular sieve (5A) beds were installed in both carbon monoxide and hydrogen feed lines to remove residual moisture. Additionally, a zirconium oxide filter and an activated charcoal filter were installed in the carbon monoxide line to remove carbonyls.

Carbon monoxide and hydrogen were stored in gas cylinders located in a ventilation hood. Roughly 20 grams of catalysts were charged to the reactor. The reactor was pressured to reaction condition at room temperature by flowing nitrogen, and then heated to reaction temperature at a rate of 5 K/min and maintained at that temperature for four hours before reactants were continuously fed into the system and nitrogen feed was discontinued.

Trickle bed reactor

A schematic diagram of the trickle bed reactor system in shown in Figure 2.4. The feed gases are purified by flow through a guard bed consisting of activated carbon and molecular sieves with particle size of 0.16 cm. Hydrogen and carbon monoxide flowrates are controlled with Brooks model 5850E mass flow meters which have flow ranges of 0-2 and 0-1.5 standard liters per hour, respectively. The flow meters were calibrated by checking the controller set point versus the volumetric flowrate determined by the bubble meter.

The feed gas streams are combined at a predetermined CO/H_2 ratio. To enhance mixing, the gases are passed through a bed of glass beads prior to the reactor. Decalin was fed to the unit using a Milton Roy pump. A relief valve, which is set at 106 atm, was placed before the reactor to prevent uncontrolled pressure rises in the system. The reactor

is a 316 stainless steel tube, 25 cm long, 0.96 cm ID, and 1.2 cm OD. It was mounted vertically in a bed of aluminum pellets. The reactor is divided into three sections. Prior to and after the 7 cm catalyst bed are 6 and 12 cm supporting sections filled with 0.2 cm diameter glass beads. The reactor was heated by the heating block and controlled by a Omega model 6100 temperature controller. A thermocouple inserted through the middle of the catalyst bed was used to measure the temperature of the bed. The reactor pressure was maintained with a Grove model 91W back pressure regulator. The reactor effluent passed through the back pressure regulator where the pressure was reduced to atmospheric pressure prior to the gas oil separator. The decalin collected at the bottom of the separator was recycled to the reactor. After the gas oil separator a sampling port was used to take gas samples for analysis. The effluent gas was passed through a soap bubble meter to measure the volumetric flow rate before it was vented to a fume hood. The decalin used in this study was obtained from Sigma Chemical and exists as *cis* and *trans* isomers of decahydronaphthalene with a minimum purity of 98% as determined by gas chromatography.

Slurry reactor

A schematic diagram of the slurry reactor system is given in Figure 2.5. The apparatus before and after the reactor is the same as that described for the trickle bed. Decalin was also used as the oil for the slurry experiments.

The reactor was a stirred 100 cm^3 Autoclave model EZ seal with six ports and one thermowell. The feed was introduced to the bottom of the reactor through a dip tube. A 50 micron porous metal filter was connected to the effluent port to prevent the entrainment of catalyst particles. A baffle bar and impeller were connected to the stainless steel reactor cover. The impeller was driven by a Magnadrive II stirrer. Cooling water was passed through the Magnadrive assembly to keep the temperature of the assembly in the permissible range. The reactor was heated using a furnace supplied by the manufacturer which was controlled by a Thermolyne Furnatrol I furnace controller.

TABLE 2.1. Chemicals utilized in precipitated, hydrothermal, and calcination catalyst preparation

Compound	Purity	Main impurities (ppm)
$ZrO(NO_3)_2 \cdot 5H_2O$	tech	Hf-3700, Fe-400, Si-250
NaOH	97%	Na_2CO_3-10000, K-2000
$LiNO_3$	99.99%	Cs-16, Ca-7, K-1, Na-0.8
$Ba(NO_3)_2$	99.98%	Sr-100, Si-25, Ni-10
$Cu(NO_3)_2 \cdot 3H_2O$	99.999%	None detected
$Mg(NO_3)_2 \cdot 6H_2O$	99.995+%	Na-9, Mn-1, Zn-1
$Mn(NO_3)_2 \cdot 6H_2O$	98%	No analysis
$Al(NO_3)_3 \cdot 9H_2O$	99.997%	Si-2, Na-1
$Ce(NO_3)_3 \cdot 6H_2O$	99%	La-2000, Ca-65, Si-25
$Dy(NO_3)_3 \cdot 5H_2O$	99.9%	Si-100, Er-35, Ca-4
$TiCl_3$	99%	No analysis
$Y(NO_3)_3 \cdot 5H_2O$	99.9%	Si-25, La-10, Ca,Mg < 0.2
$Th(NO_3)_4 \cdot 4H_2O$	98%	La < 2000, Ti-100, Fe-20
TaF_5	98%	No analysis
$(CH_3)_4NOH$ (25 wt% in MeOH)		No analysis
$(C_4H_9)_4NBr$	99%	No analysis
$Ti(i\text{-}OC_3H_7)_4$	97%	No analysis
$Zr(OC_3H_7)_4$ (70 wt% in $1\text{-}C_3H_7OH$)		No analysis

TABLE 2.2. Chemicals used in modified sol gel catalyst preparation

Chemical	Formula	Manufacturer	Purity and State
Tetraisopropyl titanate	$Ti(OC_3H_7)_4$	Aldrich	97%, liquid
Tetraorthoethyl silicate	$Si(OC_2H_5)_4$	Aldrich	97%, liquid
Zirconium isopropoxide	$Zr(OC_3H_7)_4$	Aldrich	70% in C_3H_7OH
Aluminum *tri sec* butoxide	$Al(C_4H_9O)_3$	Aldrich	97%, liquid
Zirconyl chloride	$ZrOCl_2 \cdot 8H_2O$	Aldrich	98%, solid
Sodium hydroxide	NaOH	Aldrich	97%, solid
Potassium hydroxide	KOH	Aldrich	87.1%, solid
Methanol	CH_3OH	Mallinckrodt	99.9%, liquid
Acetone	CH_3COCH_3	Mallinckrodt	99.8%, liquid
Hydrochloric acid	HCl	Baker	37.3%, liquid
Sulfuric acid	H_2SO_4	Baker	95.9%, liquid
Nitric acid	HNO_3	Mallinckrodt	70.3%, liquid
Ammonium hydroxide	NH_4OH	Baker	30%, liquid
Tetramethylammonium hydroxide	$(CH_3)_4NOH$	Aldrich	25% in MeOH
Rubidium hydroxide	RbOH	Aldrich	50% in H_2O
Lithium hydroxide	LiOH	Aldrich	98%, solid
Cesium hydroxide	CsOH	Aldrich	50% in H_2O
Barium hydroxide	$Ba(OH)_2$	Aldrich	98%, solid
Calcium nitrate	$Ca(NO_3)_2 \cdot xH_2O$	Aldrich	83.5%, solid
Magnesium nitrate	$Mg(NO_3)_2 \cdot 6H_2O$	Aldrich	99%, solid

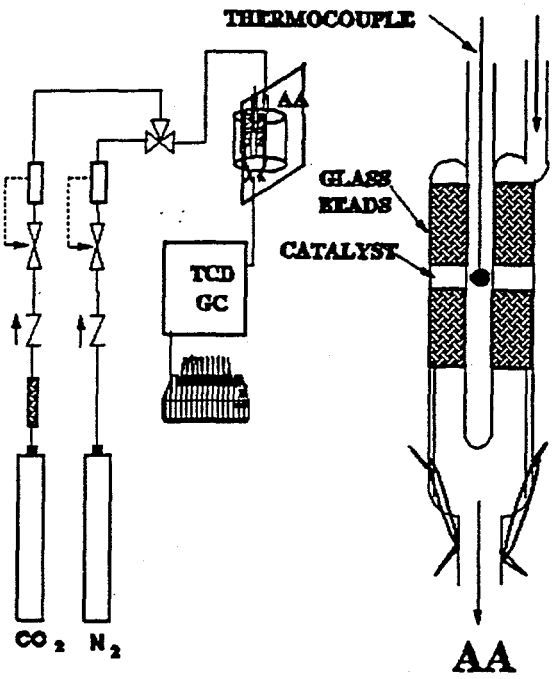

Figure 2.1. Schematic diagram of TPD apparatus.

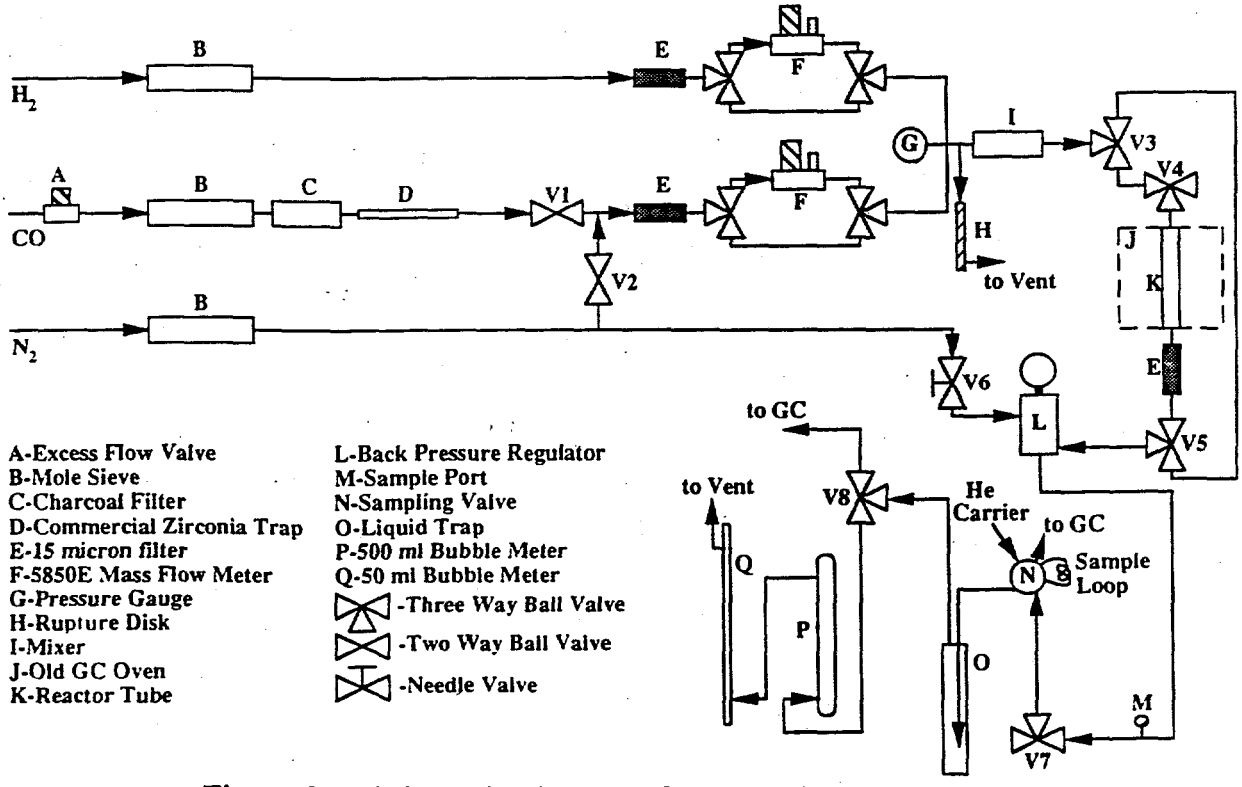

Figure 2.2. Schematic diagram of fixed bed reactor system 1.

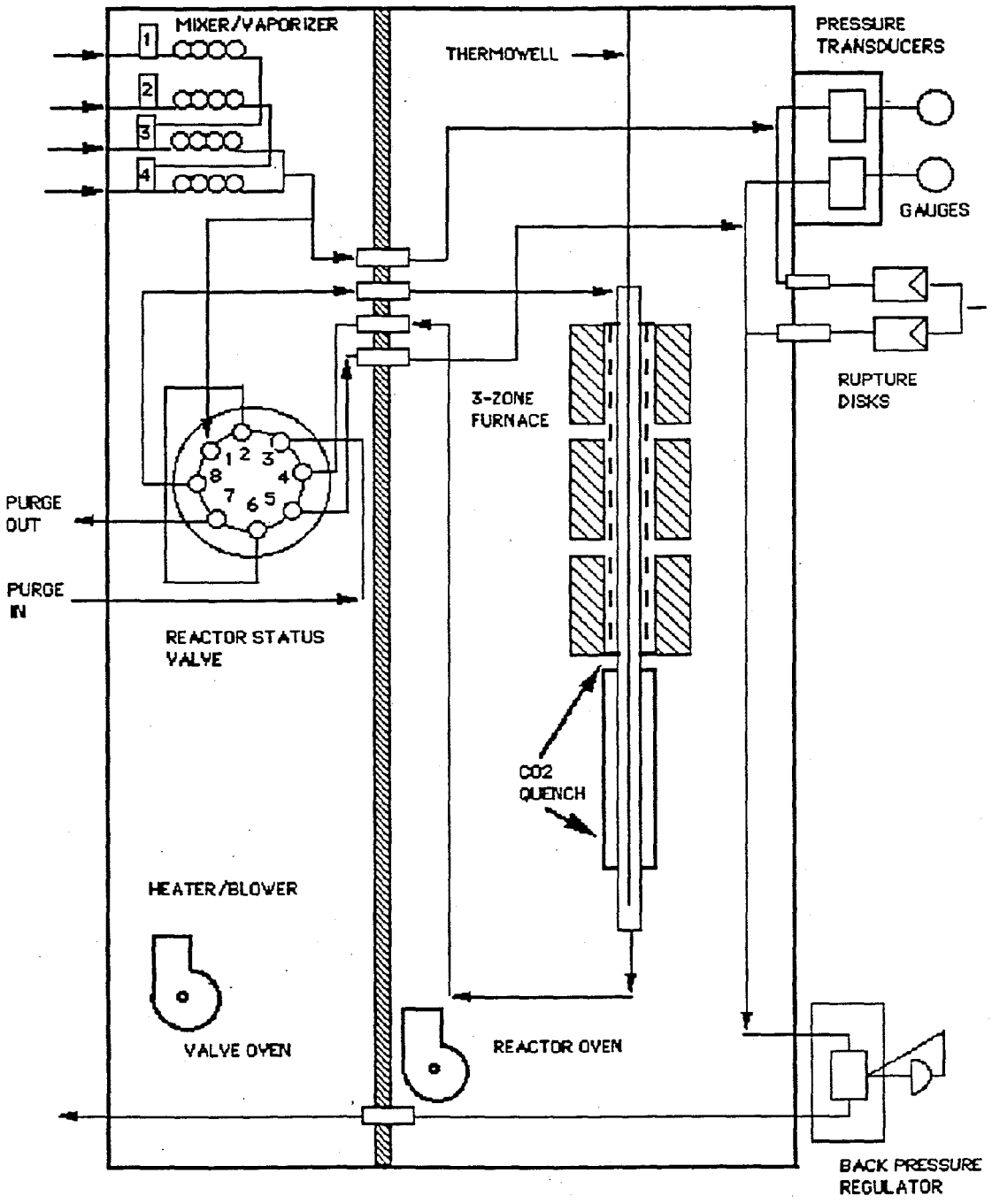

Figure 2.3. CDS 900 Micro-scale bench-top reaction system (Fixed bed reactor 2).

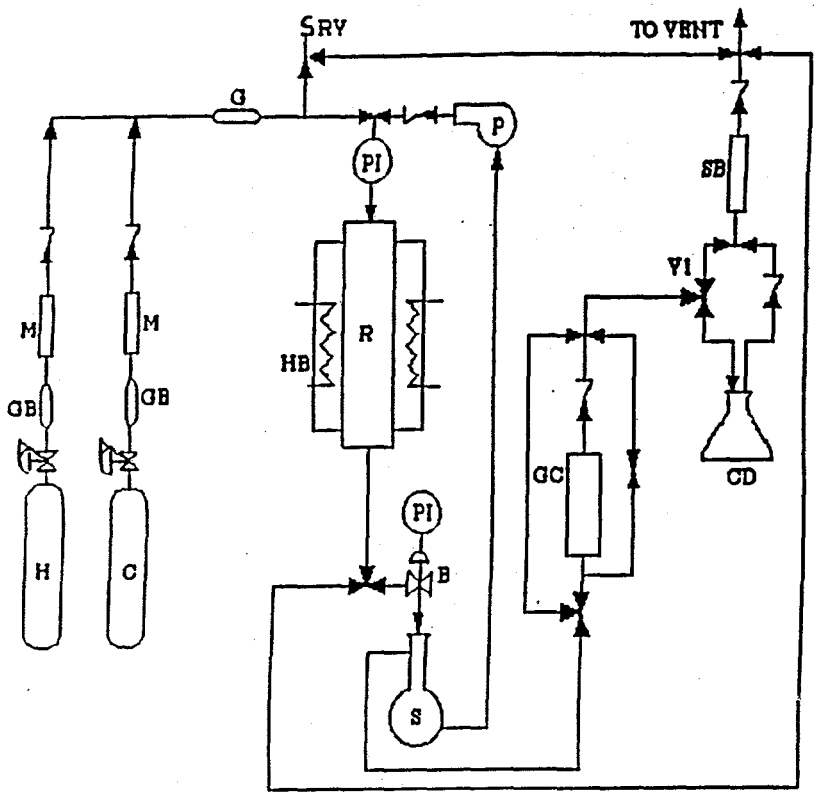

B. Back Pressure Regulator
C. Carbon Oxides Mixture
CD. Condenser
G. Glass Bead Bed
GB. Guard Bed
H. Hydrogen
HB. Heating Block
M. Mass Flow Controller
P. Pump
PI. Pressure Indicator
R. Reactor
RV. Relieve Valve
S. Separator
SB. Soap Bubble Meter
VI. Three Way Valve

Figure 2.4. Schematic diagram of trickle bed reactor system.

1. hydrogen cylinder
2. CO cylinder
3. activated carbon trap
4. activated carbon trap
5. mass flow controller
6. mass flow controller
7. glass beads mixer
8. autoclave reactor
9. recirculation pump
10. back pressure regulator
11. gas-oil separator
12. soap bubble meter

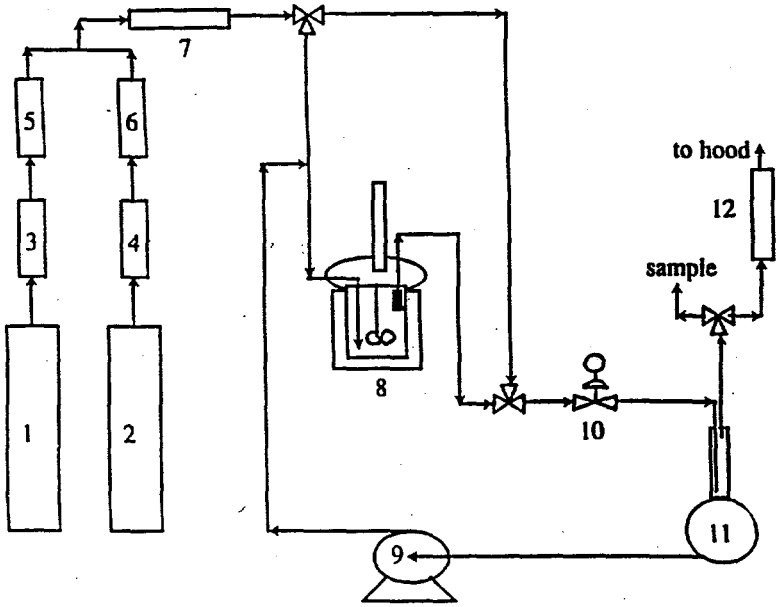

Figure 2.5. Schematic diagram of slurry reactor system.

CHAPTER III

RESULTS AND DISCUSSION

Catalyst Characterization

The results for all methods of preparation are given in this section. The effect of calcination time, temperature, and method of preparation on catalyst properties will be discussed first. A separate sub-section discussing the catalysts prepared for the oxygen vacancy experiments is included because these catalysts should be compared in context with each other.

Effect of calcination time, temperature, and method of preparation

A batch of precipitated zirconia was prepared to examine the effect of calcination time on the surface area and structure. This batch was divided into smaller samples after the drying step. Each sample was placed in the muffle furnace after the temperature had reached 773 K. Table 3.1 shows the changes in surface area and XRD pattern with time.

The distinction between crystal phases was made based on the interlayer spacing (d spacing) and relative intensities found in XRD analysis. The d spacing and relative intensities for each of the polymorphs of zirconia are shown in Table 3.2.

The XRD patterns for the samples in Table 3.1 are shown in Figures 3.1, 3.2, and 3.3 respectively. In all XRD patterns the bottom axis is the diffraction angle (2θ) in degrees, the top axis is d spacing (Å), and the left axis is intensity. The numbers printed by the major peaks are d spacing and intensity for that peak. With increasing calcination time at 773 K, more of the sample is converted from the cubic phase to the monoclinic phase. When an equal mixture of samples calcined for 5, 30, and 180 minutes were recalcined for 3½ hours (again with furnace hot) a mixture of monoclinic and cubic zirconia resulted with a surface area of 48 m^2/g. The sample was recalcined again for 3 hours and no change in XRD pattern was observed and the surface area decreased slightly to 47 m^2/g.

A larger batch of precipitated zirconia was also prepared to observe how surface area and structure changed with higher calcination temperatures. The entire batch was subjected to drying at 383 K for 24 hours. After this, the batch was divided into three samples. These results are shown in Table 3.3.

The XRD patterns for these samples are shown in Figures 3.4, 3.5, and 3.6 respectively. The sample calcined at 1273 K resulted in a completely monoclinic zirconia. Calcination at 723 K gave a mixture of cubic and monoclinic phases. Calcining at 773 K gave predominantly monoclinic zirconia when the normal calcination procedure was followed, while calcining at 723 K resulted in predominantly cubic. The samples that were calcined at 773 K also did not spend as much time in the mother liquor (as gel) before they were filtered and washed. This may also contribute to the stabilization of the cubic phase. Figure 3.7 shows a predominantly monoclinic zirconia obtained by calcining at 773 K, while Figure 3.5 shows the result at 723 K. Normally, the cubic phase is not stable at room temperature, but this is only after high temperature (> 1000 K) calcination. These high temperatures are used to sinter the zirconia for use as a structural ceramic. In this study, 723 K calcination was used in the majority of precipitated samples. This temperature gave

higher surface areas than those obtained at 773 K and was greater than or equal to the maximum reaction temperature. Fully stabilized cubic zirconia could be prepared by the addition of dopant cations of larger size or lower charge than zirconium. More explanation of this stabilization is given in the section on oxygen vacancy catalysts. Figure 3.8 shows the XRD pattern of a fully stabilized cubic zirconia doped with cerium.

The first hydrothermal preparation resulted in the cubic phase while the second resulted in a mixture of cubic and monoclinic. The XRD pattern for the first preparation is shown in Figure 3.9. The decreased cooking time and lesser amount of stabilizing cations in the second sample may be the reason the cubic phase was not fully stabilized. Both of these samples were calcined at 773 K.

Preparation of zirconia by calcining zirconyl nitrate resulted in a mixture of the cubic and monoclinic phases as seen in Figure 3.10. A drawback to this preparation method is that dopants cannot be added to the zirconia without calcining at much higher temperatures.

Preparation by the modified sol gel method resulted in mainly tetragonal zirconia as shown in Figure 3.11. The commercial zirconia catalyst (Harshaw H-0304) was monoclinic. Doping the catalyst with alkali or alkaline earth metals usually stabilized the cubic phase depending on the level of doping. More discussion on this subject will be given in the section on oxygen vacancy catalysts.

The pore volume, pore diameter, and bulk density varied with preparation method. Typical values obtained for these quantities using the different preparation methods are shown in Table 3.4. The pore size distribution of both precipitated and hydrothermal catalysts is unimodal. Precipitated catalysts had pore diameters of 30-40 Å while the hydrothermal catalysts had pore diameters of 150-200 Å. Calcining zirconyl nitrate resulted in a zirconia with properties of both the precipitated and hydrothermal samples. The pore size distribution was bimodal with pores in both the 30-40 Å and 150-200 Å ranges. The bulk density of these catalysts increased in the order hydrothermal < calcining < precipitated while pore volumes decreased in the same order.

The results of preparations for all catalysts, including those for oxygen vacancy experiments, used for isobutylene synthesis are presented in Table 3.5.

Modification of acid-base properties

The impact of acid-base properties on isosynthesis activity has been suggested in the previous studies (*14,15,38*). By definition, an acid is a proton donor (Brönsted acid) or electron acceptor (Lewis acid), and a base is a proton acceptor (Brönsted base) or electron donor (Lewis base). Zirconia is bifunctional with both acid and base properties:

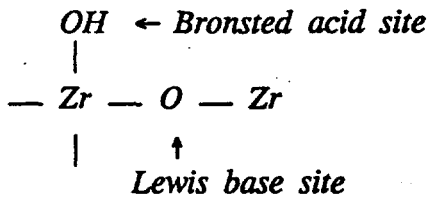

Changes in the preparation procedure often results in a final material with different acidity and basicity (*38*). The acid-base properties can also be modified by adding other metal oxides with cations of varying size and valence (*15*). This section discusses the modification of the acid-base properties of zirconia by changing preparation method (commercial vs.

modified sol gel) and by doping the zirconia with other metal oxides. In the discussion on doping, catalysts doped with alumina and silica will be presented first, followed by those doped with oxides of alkali and alkaline earth metals. These catalysts were prepared by the modified sol gel method.

The commercial zirconia (obtained from Harshaw) was prepared by calcination of zirconyl salts at temperatures over 873 K (*39,40*). It is referred to as ZrO_2 (H-0304). This commercial zirconia has been used previously for isosynthesis (*41*). Zirconia prepared by the modified sol gel method using an organic base $(CH_3)_4NOH$ is referred to as ZrO_2 (MSG). Figure 3.12 compares the basicity of ZrO_2 (MSG) and ZrO_2 (H-0304) as measured by temperature programmed desorption of CO_2. Surface area is not a contributing factor in these measurements since the difference in surface areas is less than 10%. Both catalysts show multiple adsorption sites with similar distribution of weak and strong sites, but ZrO_2 (MSG) has a larger number of basic sites than ZrO_2 (H-0304). The distributions of acidic sites, on the other hand, are fairly close over the two catalysts (Figure 3.13).

Both the total number and the distribution of sites are changed when aluminum or silicon are added to zirconium oxide (Figures 3.14 and 3.15). When aluminum is present with zirconia, stronger acidic sites are formed on the surface:

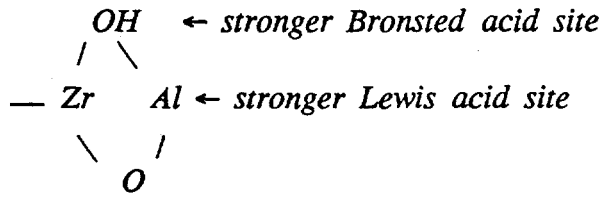

Basicity is also enhanced since electrons are donated by aluminum and are attracted to the electronegative surface oxygen ions making the oxygen ions more basic (*42*). On the other hand, when silicon is added to zirconia, basicity decreases whereas acidity increases, as also shown in Figures 3.14 and 3.15. The mole ratio of Al to Zr is 0.28 on the surface as measure by XPS, whereas the ratio is 0.17 in the bulk as measured by AA.

The effect of adding alkali metal (lithium, sodium, potassium, rubidium and cesium) on modified sol gel isosynthesis catalyst was studied. Doping with alkali metal modifies the acid-base properties, as shown in Figures 3.16 and 3.17. The distribution of metal in catalyst is not the same for all the alkali-promoted zirconias. The mole ratio of Na to Zr on the surface is about 0.20, whereas the ratio in the bulk is 0.042. One the other hand, the mole ratio of K to Zr is 0.045 on the surface and 0.017 in the bulk.

The effect of adding alkaline earth metals (magnesium, calcium and barium) on isosynthesis catalyst was also studied. Doping alkaline metal modifies the acid-base properties, as shown in Figures 3.18 and 3.19.

Catalysts used in oxygen vacancy experiments

Table 3.6 gives the ionic radii (*43*) of the dopants used in this study as well as those of some other cations used in ionic conductivity studies.

Lithium, magnesium, dysprosium, and tantalum were chosen as the +1, +2, +3, and +5 dopants respectively because their ionic radii were fairly close to that of zirconium (−15% different). Additionally, dysprosia was shown to be active for isosynthesis by Kieffer *et al.* (*8*). Aluminum was also used as a dopant even though cubic zirconia can only

dissolve ≈1 mol% of α-Al_2O_3 (*44*) (may be slightly higher for precipitation method) because Rajendran *et al.* (*45,46*) reported that addition of alumina to cubic stabilized zirconia reduces the grain boundary resistivity and increases the overall ionic conductivity. Also, the amount of aluminum that was incorporated into the lattice could be used to test the smaller ion → higher conductivity theory. The yttrium-barium-copper doped zirconia was synthesized because the compound $YBa_2Cu_3O_{7-x}$ (also called the '123' superconductor) was the first high temperature superconductor and is known to have oxygen vacancies. Since the superconductivity is associated with oxygen vacancies, the possibility of increased vacancy mobility (and thus catalyst activity) while maintaining the isosynthesis product distribution motivated the investigation of this catalyst. The equation for this series of dopants (shown below) is similar to the others except that two of the cations are +2 and one is +3.

$$Y_2O_3 + 4BaO + 6CuO \xrightarrow{12ZrO_2} 2Y_{Zr}' + 4Ba_{Zr}'' + 6Cu_{Zr}'' + 13O_O + 11V_O^{\bullet\bullet}$$

The results of the catalyst preparations (batch numbers 9-22 and 24) are shown in Table 3.5. Silver *et al.* (*47*) have shown that bulk (by atomic absorption) and surface (by X-ray photoelectron spectroscopy) dopant concentrations of precipitated zirconia are nearly identical. The XRD patterns of both the lithium and magnesium doped zirconias all showed some trace of the monoclinic phase. The trace was slightly stronger in the case of magnesium. The cubic phase is stabilized both by larger cations (as compared to zirconium) and oxygen vacancies. Doping with lithium and magnesium introduces oxygen vacancies because of their lower valences. However, as shown in Table 3.6, the ionic radii of lithium and magnesium cations are smaller than that of zirconium. The cubic zirconia is stabilized by the vacancies and destabilized by the smaller cation. The monoclinic fraction of the magnesium doped zirconias may have been slightly larger because the magnesium cation is slightly smaller than the lithium cation and more oxygen vacancies are introduced per lithium cation than for magnesium. The aluminum doped zirconias were fully stabilized in the cubic form. This is a result of the creation of oxygen vacancies and smaller grain (crystal) size (*45,46*). A comparison between the XRD patterns of two alumina doped catalysts showed that the more heavily doped zirconia had broader, less intense peaks. This is also characteristic of a finer grain (crystal) size, which is a result of adding alumina (*45,46*). No α-Al_2O_3 could be detected in either pattern. The dysprosium doped catalysts had the XRD patterns of fully stabilized cubic zirconia. This was expected because the dysprosium cation introduces oxygen vacancies and is larger than the zirconium cation. The XRD pattern for the Ta/Zr=0.04 catalyst showed the catalyst had more monoclinic character than the pure zirconia sample. This is a result of oxygen vacancies being eliminated (zirconium vacancies being created). When oxygen vacancies are eliminated the zirconium cation cannot support eightfold coordination with oxygen ions. Thus it becomes 7 coordinated and the monoclinic phase forms. A second compound was not detected in this pattern. The monoclinic peaks were predominant (more zirconium vacancies created) in the Ta/Zr=0.24 catalyst. Also, the primary peak for Ta_2O_5 was present. The '123' catalyst was cubic for the same reasons as the dysprosium catalyst.

The surface areas were all fairly high (85-130 m^2/g) except for the tantalum doped catalyst. This may be the result of more of the monoclinic phase being present in these samples. The higher surface areas of the alumina doped catalyst was most likely the result of small quantities of a separate high surface area alumina phase being formed. As mentioned previously, cubic zirconia can only dissolve ≈1 mol% of α-Al_2O_3. The loss in

surface area after reaction will be discussed in the next section. All catalysts used in the oxygen vacancy experiments were subjected to reaction conditions for ~26 hours.

The bulk densities for the pure, lithium doped, and magnesium doped zirconias were statistically the same ($\approx$2.16 g/cm^3). This is expected even though the molecular weights of lithium and magnesium are small compared to zirconium because the dopant is present in low concentrations. The aluminum doped catalysts had slightly lower bulk densities. This is probably the result of the less dense α-Al_2O_3 phase being present. A higher level of alumina doping led to a further decrease in bulk density. The dysprosium samples had higher densities because the much heavier dysprosium ion was substituted for zirconium. The tantalum catalysts had lower bulk densities because more of the less dense monoclinic phase was present and zirconium was being rejected from the lattice. The '123' zirconia had a slightly higher bulk density because of the incorporated barium.

Table 3.7 shows the number and type of defects introduced into the zirconia lattice for each dopant. Catalysts were prepared in order to test activity at constant vacancy to zirconium ratio (=6/100 Zr), activity at constant metal to zirconium ratio (=4/100 Zr), and to examine the effect of varying dopant level (lithium and magnesium) on activity. A larger number of dopant atoms is required to attain the same level of oxygen vacancies as the valence of the dopant changes from +1 to +3.

Catalyst stability

The catalysts used for isobutylene synthesis showed no change in crystal structure under reaction conditions. Figures 3.20 through 3.23 show XRD patterns for catalysts after reaction. The maximum reaction temperature was always less than or equal to the calcination temperature. Therefore, changes in the phase before and after reaction were not expected.

Most catalyst samples were black when removed from the reactor. This color change occurred even for samples held at reaction conditions for the shortest time (~26 hours). When recalcined for one hour at 723 K (put in furnace hot) the catalysts returned to their original color. The black color was the result of both carbon and heavier hydrocarbon (coke) deposition. The carbon layer deposition will be discussed further in the *Catalyst Activity and Selectivity* section. The surface area is reduced by both coke deposition and thermal sintering. The relative importance of these two effects is indicated in Table 3.5. Comparison between the before reaction (B.R.), after reaction (A.R.), and recalcined (R.C.) columns of Table 3.5 shows that the precipitated catalysts experience a much larger decrease in surface area as a result of coke deposition.

As mentioned earlier, this loss of surface area was fairly consistent regardless of the time spent under reaction conditions. This indicates that a steady state is reached between coke deposition and coke reaction (cracking). The numbers in Table 3.8 are representative of nearly all catalysts (0.04-0.07 g_{coke}/g_{cat}). The second hydrothermal preparation had only ~0.009 g_{coke}/g_{cat}. This may have been the result of its reduced activity and shorter time on stream. This could also be the explanation for the lower value obtained with the calcination catalyst. Thermal sintering occurs at any temperature above absolute zero. The amount of sintering increases with both time and temperature. Platero and Mentruit (*48*) found that significant reduction in surface area of precipitated zirconia occurred at temperatures as low as 700 K. Since 700 K is only slightly above the reaction temperature used in the majority of this study, some loss in surface area because of sintering is expected. The recalcined

surface areas were generally 5-20% lower than the initial surface area (before reaction). The majority of surface area loss was caused by the coke deposition.

Surface areas of catalysts prepared by the hydrothermal and calcining methods were only slightly reduced after reaction. Recalcining these samples resulted in no change in the surface area. The difference in pore size between these catalysts and those prepared by the precipitated method may be the reason that coke deposition does not significantly affect surface area. Also, the reduced activity of these catalysts might contribute to surface area stability.

Catalyst Activity and Selectivity

The intralab reproducibility between the two fixed bed units was shown in the 1992 Contractors' Review Meeting Report. Because the two units yielded the same results for the same catalyst no reference is made in this report as to which unit was used to collect the data.

The experiments can be grouped into eight basic categories: (1) those that were performed to determine the optimal process conditions and catalyst, (2) those using modified sol gel catalysts with modified acid-base properties, (3) those involving hydrogen sulfide, (4) those using the oxygen vacancy theory catalysts, (5) the effect of gel *p*H, (6) the effect of temperature cycling, (7) those using the trickle bed reactor, and (8) those using the slurry reactor. Each of these groups will be discussed in a separate section. All hydrocarbon distributions in the following Tables are given in wt%. Appendix A gives the relationship between wt% and carbon conversion to each of the hydrocarbons. These numbers are essentially equivalent for the conversions achieved in this study.

Blank run

A blank run was conducted at 673 K, 50 atm, 1/1 CO/H_2 ratio, and a 90 second space time in a reactor packed with glass wool. The reactor was pretreated under flowing nitrogen for 18 hours. No reaction was detected under these conditions.

Experiments to determine optimum process conditions and catalyst preparation

Initial activity tests involved catalysts prepared by all methods. The results of initial activity tests for isobutylene synthesis over precipitated, hydrothermal, and calcination catalysts are shown in Figure 3.24. The manganese doped catalyst was almost completely inactive (cannot be shown on same scale with others). A report on the effect of manganese in reducing methane production in Fischer-Tropsch synthesis (*30*) motivated its investigation. Conversion was far below any of the other catalysts and the major product was methane. A possible explanation for the reduced activity and lack of typical isosynthesis product distribution may be that oxygen vacancy availability and mobility was reduced. Further discussion on this subject will be given in the section on oxygen vacancy catalysts. Catalyst activity according to preparation method can be ranked as follows: (ppt.) > (CAL) > (HT). The catalysts prepared by the modified sol gel method were less active than the precipitated catalysts. However, increasing reaction temperature did not have as adverse effect on product distribution. The modified sol gel catalysts were run at a higher temperature. A comparison between precipitated, commercial, and modified sol gel catalysts will be made

at the end of this section. The results for isobutylene synthesis over the modified sol gel catalysts are given in the section on acid-base property modification. The 7% Ce-ZrO_2 was the most active and would be used in further activity/selectivity studies.

The effect of pressure on conversion at the same space time was minimal above 50 atm, but increasing pressure shifted the product distribution toward heavier hydrocarbons. These effects are illustrated in Figures 3.25 and 3.26. Pichler and Ziesecke (*7*) reported a similar trend with increasing pressure. They attributed the increase in conversion at higher pressures to the pressure itself, rather than the increased contact time associated with increasing pressure (same end gas flow rate). In this work, the benefit of increased conversion at higher pressures was offset by the shift in hydrocarbon distribution toward the undesired C_5+ products. A pressure of 50 atm was chosen as the standard because the product distribution was favorable and space times as long as 150 seconds could be attained. As mentioned previously, Pichler and Ziesecke (*7*) obtained high CO conversions (50-90%), but their yield of isobutylene was low. The *iso*-C_4 fraction obtained by Pichler and Ziesecke was predominantly isobutane and a large percentage of the product was heavier hydrocarbons (46% at 723 K and 150 atm). These two observations can be explained by the high pressure of the reaction. Higher pressure would favor production of alkanes and C_5+ products because the number of moles of reactant gases consumed per mole of product formed is greater than for alkenes and lighter hydrocarbons. Also Pichler and Ziesecke produced oxygenates (5%), even at 723 K. This can be attributed to thoria being a more basic oxide, since this study has found that the oxygenate to hydrocarbon ratio produced over acidified zirconia (*p*H of gel adjusted with HNO_3) is generally less than 0.05 (wt basis) at only 673 K. The most significant difference between this work and that of Pichler and Ziesecke is the decrease in undesired products (C_5+ hydrocarbons and oxygenates) while increasing isobutylene selectivity (up to 70% of C_4's) and maintaining a relatively high conversion.

Increasing temperature increased conversion, as expected, but also increased methane and isobutane formation. These effects are illustrated in Figures 3.27, 3.28, and 3.29. A CO conversion of 51% was achieved at 723 K, 50 atm, and 1/1 CO/H_2 over the cerium catalyst. The product, however, contained 60 wt% methane. The equilibrium constants for various reactions that can occur under isosynthesis conditions were given in Figure 1.1. Methane is the thermodynamically favored product at all temperatures while saturated hydrocarbons are slightly favored over unsaturated hydrocarbons. Oxygenates are favored at lower temperatures as found by the methanol synthesis experiments. Thermodynamics can explain the increase in methane and isobutane formation with increasing temperature. The tradeoff between increased oxygenate production and increased methane production appeared to balance at 673 K. This temperature was chosen for most of the remaining activity/selectivity studies over the precipitated catalysts. A temperature of 723 K was used in the majority of activity studies over the modified sol gel catalysts because of their reduced activity (discussed later). As mentioned earlier, the increase in temperature did not have as dramatic effect on methane production for modified sol gel catalysts.

Conversion was also found to be a function of CO/H_2 feed ratio with 1/3 > 1/1 > 2/1 (see Figure 3.30). In this work, interest was focused on hydrogen lean synthesis gas and 1/1 CO/H_2 was adopted as the standard.

Sodium, thorium, and cerium increased catalyst activity over undoped zirconia. It was reported (*10*) that cerium increased activity while retaining the selectivity of pure zirconia and sodium decreased activity while increasing C_4 selectivity. Addition of thorium is expected to increase activity because pure thoria was found to be the most active

isosynthesis catalyst (*7*). More discussion as to why these catalysts increased activity will be given in the section on oxygen vacancy catalyst results. The amount of titanium was decreased and thorium was added to the second hydrothermal preparation with the hope of increasing activity while retaining the same selectivity to *iso*-C_4 hydrocarbons.

Selectivity data for all initial catalysts are shown in Table 3.9. These comparisons are made at almost equal conversions ($\sim$12%) to eliminate the effect of conversion on hydrocarbon distribution. Both pure zirconia and sodium doped zirconia produce mainly a C_5+ fraction. These two catalysts were not acidified in order to limit oxygenate production and the analysis did not account for oxygenates. Therefore, a significant portion of the C_5+ fraction could be dimethyl ether. Both dimethyl ether and methanol were injected independently and they both eluted in the column backflush (C_5+). In other cases dimethyl ether was the only oxygenate produced in detectable quantities and the dimethyl ether/hydrocarbon weight ratio was 0-4%.

Titanium was added to the precipitated zirconia with the hope of achieving the same *iso*-C_4 selectivity as in the hydrothermal case. However, the *i*-$C_4/\Sigma C_4$ ratio remained at about 70-75% for this catalyst. There was a shift in the hydrocarbon distribution for the two catalysts that were acidified. Both showed an increase in C_1-C_4 fraction and a decrease in C_5+ fraction. The *i*-$C_4/\Sigma C_4$ ratio for the 7% Ce-ZrO_2 was slightly lower because the higher activity of this catalyst resulted in production of more linear C_4's. In all cases greater than 90% of the *i*-C_4 fraction was isobutylene.

The catalyst prepared by the calcination method gave a hydrocarbon distribution similar to that of the precipitated catalysts that were acidified. The overall activity of this catalyst was about one-half (space time twice as long to get same conversion) that of the precipitated catalysts. The isobutylene fraction among *i*-C_4's was greater than 90% in this case also.

Both hydrothermally prepared catalysts gave $\sim$100% selectivity to the *iso*-C_4 compounds among C_4's produced (39% and 64% isobutylene respectively). The promotion of the *iso*-C_4 compounds over hydrothermally prepared catalysts could be related to the surface characteristics of the catalysts. Jackson and Ekerdt (*13*) suggested that branched C_4 hydrocarbons are formed by two independent paths. One involves condensation of a η^3-enolate (CH_3-$CH^{(-)}$-CH-O) with an adsorbed methoxide species and the other involves CO insertion in an η^3-enolate. Though both routes lead to the formation of branched C_4's, different surface characteristics are required. The first is catalyzed by strong Lewis acid sites while the second is catalyzed by strong basic sites. The hydrothermal catalysts are more likely to have strong basic sites, since strong bases (sodium hydroxide and tetramethylammoniumhydroxide) were used in their preparation and they were not treated with acid. The hydrocarbon distribution was similar to that of precipitated catalysts. The C_5+ fraction increased when thorium was added in an attempt to increase activity. The overall activity of the hydrothermal catalysts was about one-third (space time three times as long to get same conversion) that of the precipitated catalysts. The unique selectivity to *iso*-C_4's may be a result of the larger pore size of the hydrothermal catalysts as compared with the precipitated catalysts.

Several characteristics were common to all catalysts. As space time increased the amount of methane increased and the ratio of isobutylene to isobutane decreased. The same trends were noted as temperature increased. All of these observations can be explained in terms of thermodynamics. Catalysts showed a slight shift toward production of lighter hydrocarbons with time on stream although conversion remained constant. The modified sol

gel catalysts showed the same trends with regard to pressure, temperature, and CO/H_2 ratio as described above.

A comparison of the precipitated zirconia with zirconia prepared by the modified sol gel (MSG) method and the commercial zirconia (H-0304) is shown in Table 3.10. The commercial and sol gel zirconias were evaluated at higher temperature and longer space times. The precipitated catalyst is much more active than either the commercial or modified sol gel catalysts (almost the same conversion at 50 K lower temperature and $\sim$½ the space time) and produces a larger C_4 fraction. The sol gel catalyst gave a higher selectivity to the *iso*-C_4 compounds.

Time on stream

The changes of catalyst performance with time on stream were studied over a thoria-zirconia catalyst. The catalyst was synthesized by a hydrothermal method. The procedure of experiments is shown in Figure 3.31. In the first 20 hours, the experiment condition was maintained at 723 K, 70 atm and 40 second space time, and two sets of data were taken at time on stream of 4 hours and 20 hours (*A* and *B* in Figure 3.31). Then a series of experiments were conducted at different space times, but still maintaining 723 K. At time on stream of 51 hours, the space time was again set to 40 seconds, and after 4 hours, a set of data was taken (*C* in Figure 3.31). Finally, after a series of experiments at different temperatures, reaction conditions were again set to 723 K, 70 atm and 40 s space time at 84 hours of time on stream, and after four hours, a set of data was taken (*D* in Figure 3.31).

Table 3.11 compares CO conversions and ratios of CH_4/iso-C_4's at different time on stream. Not much change in catalyst performance is observed for the first twenty hours when reaction condition was maintained constant (*A* to *B*). Even after fifty-five hours at the same temperature but different space times (*A* to *C*), the differences in CO conversion and weight ratio of CH_4 to iso-C_4's are within 10% of the first set of data. However, if temperatures were changed between the two set of experiments (*C* and *D*), the fraction of methane increased significantly. More discussion on the effects of temperature cycling on activity and selectivity will be presented later. However, our studies have shown that if a catalyst is held at the same reaction conditions the same level of activity and selectivity can be expected regardless of time on stream. Catalyst performance between catalyst batches synthesized in the same manner is also very reproducible.

Effect of CO cylinder

These experiments were performed in order to eliminate possible poisoning of the catalyst by iron carbonyls $\{Fe(CO)_5\}$ formed in the iron carbon monoxide cylinder. As described in the experimental section, the CO from the iron cylinder was passed though an activated charcoal bed and in some cases a commercial zirconia trap. However, use of the aluminum cylinder would eliminate the possibility of carbonyl formation in the cylinder. The tests were carried out over a fresh portion of the 7% cerium zirconia because it was the most active of the catalysts tested to that point. A comparison of results obtained using the iron and aluminum cylinders is shown in Table 3.12. Conversion is increased by about 10% (3 percentage points) when using the aluminum cylinder. This increase was realized in methane production with a corresponding decrease in C_4 production. The remainder of the hydrocarbon distribution (and C_4 distribution) was not significantly affected by using the

aluminum CO cylinder. If the catalyst was being poisoned by iron carbonyls it was beneficial because the poison acted to reduce the amount of methane formed. However, qualitative analysis of several batches of catalyst for iron after reaction using the indicator thioglycolic acid showed no evidence that iron was being deposited on the catalyst.

Deposition of carbon layer on catalyst

Again, a 7% Ce-ZrO_2 was used (batch number 28) because it was the most active of the initial catalysts tested. This experiment was performed to quantify how much carbon was being laid down on the catalyst by the reaction $2CO \rightleftarrows C + CO_2$. This reaction is exothermic but is still highly favorable (K_{eq}=15700) at 673 K. The two observations that led to the question of whether this reaction was significant were (1) the black color of the catalyst after reaction and (2) during the first two hours after the reactor was brought on-line, the amount of CO_2 in the effluent could not be accounted for simply by the amount of hydrocarbons detected in the reactor effluent.

The catalyst was pretreated under flowing nitrogen (100 sccm) for 17 hours at 673 K and 35 atm. After pretreatment the reactor was bypassed and the carbon monoxide flow was started to flush the lines of nitrogen and obtain a flowrate and baseline area count for 100% CO from the GC. When these measurements were taken the reactor was brought back on-line. The experimental conditions were 673 K, 25 atm, and 90 second space time. A pressure of 25 atm was use to duplicate the partial pressure of CO under normal reaction ($CO + H_2$) conditions. Figure 3.32 shows the breakthrough curve for carbon monoxide. The sampling rate was one every 8 minutes. The effluent was composed primarily of carbon monoxide and carbon dioxide; however, there were also traces of hydrocarbons present. Methane was present in decreasing amounts throughout the experiment (at most 0.005 mol%). The C_2 hydrocarbons were present through the first 4 hours and there were some C_3's present for about an hour. Hydroxyl groups on the catalyst might be the source of hydrogen for the hydrocarbons being produced. Carbon dioxide was still being produced after 12 hours but was less than 0.005 mole fraction. The majority of CO_2 was produced in the first 2 hours. When this catalyst was removed from the reactor it had turned dark brown, not completely black like catalysts subjected to $CO + H_2$ reactions.

The surface area after carbon deposition was 85 m^2/g (initially 88 m^2/g) which is much higher than that normally obtained for catalysts after reaction. When recalcined at 723 K for 1 hour some weight loss occurred and the catalyst returned to its original color. Approximately 0.0018 g_{carbon}/g_{cat} catalyst was lost. This is an order of magnitude less than that for catalysts where both CO and H_2 was fed (given earlier as between 0.04-0.07 g_{coke}/g_{cat}). The surface area after recalcining remained at 85 m^2/g, which showed that the surface area loss was the result of sintering and not carbon deposition. The volume of a monolayer of nitrogen as found by the BET method was 20.2281 cm^3/g for this catalyst. This corresponds to 5.44×10^{20} molecules of nitrogen per gram of catalyst. The number of carbon atoms per gram of catalyst calculated from the weight of carbon lost upon recalcination is 9.03×10^{19}. The van der Waals radius, defined as the closest approach between two atoms without forming a bond, for carbon is 1.85 Å (*43*). The area covered by one carbon atom (assuming spherical geometry) is 10.8 $Å^2$. The area of a nitrogen molecule assumed in the BET calculation is 16.2 $Å^2$. Thus, the number of carbon atoms deposited on the surface as determined from experiment is approximately 11% of that required to have monolayer coverage.

This experiment showed that carbon deposition occurred fairly quickly (~2 hours) and is not significant in reducing catalyst surface area compared with the accumulation of heavier hydrocarbons.

Modification of the acid-base properties

Method of preparation: The effect of method of preparation was examined by comparing zirconia prepared by the modified sol gel method to a commercial zirconia catalyst. ZrO_2 (MSG) is more active than ZrO_2 (H-0304), as shown in Figure 3.33. Since ZrO_2 (MSG) and ZrO_2 (H-0304) have about the same concentration of acidic sites on the surface, and differ only in the concentration of basic sites, the higher activity of ZrO_2 (MSG) is attributed to the increased amount of basic sites available for reaction. Figure 3.34 compares the CO reaction rates over the two catalysts. Each data point corresponds to a different space velocity. A linear regression gives a slope of 1.56. The concentration of basic sites are 0.00616 and 0.00333 mmoles per m^2 for ZrO_2 (MSG) and ZrO_2 (H-0304), respectively, and the ratio is 1.85, which is reasonably close to the slope of the line. The possible relation between the ratio of activities and the ratio of numbers of basic sites suggests that accessible basic sites are one of the requirements for an active isosynthesis catalyst.

The distribution of hydrocarbons is fairly close over ZrO_2 (MSG) and ZrO_2 (H-0304), except that the weight percent of heavy hydrocarbons is slightly higher over ZrO_2 (MSG) (Figure 3.35). The deviation from the Anderson-Schulz-Flory distribution for a standard polymerization reaction is apparent for isosynthesis when the distributions are plotted as Wt%/*n* *vs* n on a semi-log scale (Figure 3.36). For a standard polymerization reaction such as F-T synthesis, a straight line is obtained in the plot, whereas for isosynthesis, a discontinuity is observed at *n* of four. Another characteristic of isosynthesis is the large amount of branched products from the reaction (Figure 3.37). Both ZrO_2 (MSG) and ZrO_2 (H-0304) are selective for isobutene and isobutane, and iso-C_4 weight percent is slightly higher over ZrO_2 (MSG).

The comparison between ZrO_2 (MSG) and ZrO_2 (H-0304) indicates that the modified sol gel method can be used to synthesize zirconium oxide with a larger amount of basic sites on the surface, and consequently, higher isosynthesis activity. One of the keys in the modified sol gel preparation is the type of base used in making the soluble intermediate. Based on the experiments of this work, an organic base such as $(CH_3)_4NOH$ is preferred to an inorganic base such as NaOH to synthesize zirconia for isosynthesis.

Silica and Alumina: Figures 3.38 and 3.39 compare the isosynthesis activity of the three catalysts. Because of its lack of basic sites on the surface, SiO_2-ZrO_2 (MSG) is not active for isosynthesis. Previous work by Pichler and Ziesecke (*7*) also showed that silica is not an active isosynthesis catalyst. One might expect that Al_2O_3-ZrO_2 (MSG) is more active than ZrO_2 (MSG) because of the increased basicity, but in fact, the two catalysts have about the same activity. A possible explanation is the large concentration of aluminum on the surface. Since Al_2O_3 itself is not active for isosynthesis (*4,7*), the increase of activity by enhanced basicity is probably offset by the decrease of surface zirconia available for reaction.

Pichler and Ziesecke (*7*) compared the isosynthesis activity of precipitated thoria and coprecipitated alumina-thoria, and concluded that the presence of alumina in the catalyst increased formation of methane and C_4 hydrocarbons and reduce formation of liquid

hydrocarbons, but had no appreciable effect on carbon monoxide conversion. The same phenomena were observed in this work.

Alkali metals: The impact on methane and C_4 weight percent in hydrocarbons is not the same for all alkali metals (Figure 3.40): decreased methane production is observed over K-ZrO_2 (MSG), and increased C_4 production is observed for K-ZrO_2 (MSG) and Cs-ZrO_2 (MSG). In general, adding alkali metal promotes the production of heavy hydrocarbons ($C_{n>4}$), which is consistent with the observations in previous research (*4,7,15*). Except for Li-ZrO_2 (MSG) and Cs-ZrO_2 (MSG), alkali-promoted catalysts show higher selectivity to iso-C_4 hydrocarbons than for the unpromoted zirconia (Figure 3.41). The low activity of Na-ZrO_2 (MSG) is probably related to the high concentration of sodium on the surface.

Alkaline earth metals: The alkaline earth metals investigated improved the overall selectivity to iso-C_4 hydrocarbons (Figures 3.42 and 3.43). The distribution of C_4 hydrocarbons is not changed significantly (Figure 3.43), but C_4's consist of a larger portion of the total hydrocarbons than for the unpromoted zirconia (Figure 3.42). The majority of modified sol gel catalysts retained a significant level of activity after doping.

Level of dopant: The impact of promoter also depends on the level of loading. Figure 3.44 compares the hydrocarbon distributions for three catalysts with different calcium content. ZrO_2 (MSG) does not contain calcium, Ca-ZrO_2 (MSG), which has been discussed previously in this report, contains about 0.5 wt% calcium, and Ca(2%)-ZrO_2 (MSG) contains about 1.8 wt% calcium. Both Ca(2%)-ZrO_2 (MSG) and Ca-ZrO_2 (MSG) show improvement on hydrocarbon distribution (i.e, higher C_4 wt%) over ZrO_2 (MSG). Methane weight percent is the lowest for a high calcium loading (i.e., 2 wt%), and C_4 weight percent is the highest for a low calcium loading (i.e., 0.5 wt%). The distribution of C_4 hydrocarbons, however, remains fairly constant regardless of the calcium loading, as shown in Figure 3.45. More discussion on doping with lower valence cations and level of doping is given in the section on oxygen vacancy catalysts.

Effect of co-feeding hydrogen sulfide and presulfiding

The motivation for using hydrogen sulfide was the possible reduction in methane formation that might occur because of selective poisoning by sulfur. The 7% cerium zirconia was utilized for these experiments as well. Batch number 6 was used in the non hydrogen sulfide cases while batch number 8 was used when hydrogen sulfide was co-fed. Additionally, a hydrogen sulfide free run was performed over batch 8 as an activity check. Batch number 28 was used for the presulfiding experiment.

The effect of hydrogen sulfide on methane, total C_4, and C_5+ production rates are shown in Figure 3.46. The decrease in methane production rate is a result of an increase in C_5+ production rate, while total C_4 production is slightly increased. The CO conversions at 60 second space time are statistically the same (first two columns under 'without H_2S' heading, Table 3.13) between the two batches.

The product distribution is shifted slightly toward methane and C_5+ with C_4's reduced for the first batch (second column). Possible explanations for the difference in product distribution (more methane and less oxygenates) could be that batch 6 experienced a slightly lower *p*H or slightly higher calcination or reaction temperature. However, the performance for hydrogen sulfide free runs between batches is similar enough to allow meaningful comparison between hydrogen sulfide free and hydrogen sulfide runs ignoring the slight difference in selectivity between catalyst batches. ZrO_2 is apparently unaffected

by hydrogen sulfide as found for ThO_2 by Pichler and Ziesecke (*7*).

The most striking effect of co-feeding hydrogen sulfide is the drastic increase in C_5 production, particularly 3-methyl-1-butene (Tables 3.13 and 3.14). In Table 3.14, the C_5 hydrocarbons are divided into three groups: (1) 3-methyl-1-butene, (2) 2-methyl butane, 1-pentene, 2-methyl-1-butene, and (3) *n*-pentane, *trans*-2-pentene, *cis*-2-pentene, 2-methyl-2-butene. This grouping is based on boiling points and the separation capability of the Porapak Q column in the on-line SRI GC. These groupings are consistent with GC results for injection of standards. Analysis of the C_5 fraction is not possible on the other two gas chromatographs. Thermodynamics show that 3-methyl-1-butene is the least favorable of the branched C_5 alkenes (*24*). Table 3.15 gives the Gibbs free energy of formation for the C_5 alkanes and alkenes.

Overall, 1-pentene is the least favorable C_5 compound but has a very similar ΔG_f° to 3-methyl-1-butene. The 2-methyl alkenes and *cis*- and *trans*-2-pentenes are the major C_5 products for isosynthesis over zirconia just as isobutylene and *cis*- and *trans*-2-butene are the major C_4 products (see Table 3.13). Thus, the second and third groups dominate the C_5 distribution and only a slight amount of the thermodynamically unfavorable 3-methyl-1-butene is formed. When hydrogen sulfide is included, 3-methyl-1-butene composes almost 75% of the C_5 product (Table 3.14). The other two C_5 groups are formed in the same ratio as for the hydrogen sulfide free case. The dramatic increase in C_5 production with hydrogen sulfide could be a result of suppression of chain growth to heavier (C_{10}+) hydrocarbons as was speculated by Nakajo *et al.* (*49*) for acetic acid selectivity, a suppression of C_5 cracking to C_2's and C_3's since a noticeable drop in C_2 and C_3 production occurred, or a decrease in adsorption strength between the catalyst and 3-methyl-1-butene (possibly initial product) that allows it to desorb from the surface before it can react further to the more thermodynamically favored 2-methyl butenes. In this case suppression of chain growth does not mean that the C_6+ fraction cannot increase (as shown in Table 3.13). It is suggested that more of the C_5-C_9 hydrocarbons were formed at the expense of C_{10}+'s when hydrogen sulfide was co-fed.

The effect of increasing space time at constant temperature and pressure under hydrogen sulfide is shown in Table 3.13. The selectivity change is the same as that for the hydrogen sulfide free case. Methane increases (as dictated by thermodynamics) and C_5+ decreases. The C_4's also show a slight increase, but this is because more isobutane is being produced (also expected from thermodynamics). The only oxygenates produced were dimethyl ether and methanol and their production was fairly constant with increasing space time.

Table 3.16 shows the activity and selectivity changes that occur with hydrogen sulfide with changing temperature. It should be noted that the order these experiments were performed is not that of increasing temperature. The base case at 673 K was run first, followed by runs at 698 K, 723 K, and finally 648 K. This is the reason the conversion is lower and more methane and isobutane were produced at 648 K than would be expected from examining data at 673 K, 698 K, and 723 K. It is also the reason the base temperature was not revisited after each excursion. An experiment at the base temperature was performed after those at 698 K, 723 K, and 648 K. The carbon monoxide conversion, methane wt%, and isobutane wt% among C_4's were 18.33 %, 38.03, and 30.77 respectively. These numbers can be compared to those in the first column of Table 3.13 to support the previous observation.

As temperature is increased, methane and C_4 alkane selectivity increase, as expected

from thermodynamics. Throughout these experiments the mass balance on sulfur (as hydrogen sulfide) was always much less than 100%. The sulfur balance (mass sulfur out/mass sulfur in) was 0.015 (~98.5% of sulfur fed was not seen as hydrogen sulfide in the product stream), 0.032, 0.158, and 0.468 for 648 K, 673 K, 698 K, and 723 K respectively. As detailed in the experimental section, the feed composition is checked before each experiment by bypassing the reactor. The area count for hydrogen sulfide on the GC was comparable to that obtained by injecting the mixture directly into the GC with a syringe. Sufficient time was allowed for the area count to reach a steady value indicating that the system has been conditioned to hydrogen sulfide. Therefore, the poor closure on sulfur was the result of reactions with the catalyst and not with the system components (i.e. tubing and fittings). The amount of hydrogen sulfide (and other products) in the effluent was steady over the course of the experiment. One possibility for this lack of closure is the formation of liquid compounds containing sulfur. Even though no new peaks were observed on the SRI GC, which is before the liquid trap, the sulfur containing compound would be present in such a small quantity (mass of sulfur fed <1.5% of total mass fed) that it would be undetectable or masked by another product peak. The fact that the sulfur balance improves with increasing temperature shows that less hydrogen sulfide is being adsorbed at higher temperatures (as expected). This is also reflected in the decrease in C_5+ fraction with increasing temperature and the decrease in 3-methyl-1-butene selectivity. At 648 K, 3-methyl-1-butene composes over 94% of the C_5 product. As temperature increases, thermodynamics and the reduced amount of sulfur adsorbed combine to shift the C_5 product distribution to 2-methyl butane (lowest $\Delta G_f°$). Still, even at 723 K, 3-methyl-1-butene production is much higher than the hydrogen sulfide free case at 673 K which shows that adsorbed sulfur is continuing to affect the selectivity. This is also evident in the relative amounts of C_2+C_3 and C_5+ produced. In a hydrogen sulfide free case the wt% among hydrocarbons for these two fractions was 14.7 and 10.3, while with hydrogen sulfide they are 9.0 and 14.6 respectively at 723 K.

For the presulfiding experiment the catalyst was pretreated in the usual way. The presulfiding procedure was similar to that for the carbon deposition experiment (673 K, 25 atm, 90 second space time) except that the 1.06% H_2S in H_2 mixture was used. The breakthrough curve for H_2S is shown in Figure 3.47. Hydrogen sulfide was adsorbed for about 21 hours. Extrapolating this curve to C/C_o=1.0 would give ~48 hours for saturation. The flow rate of H_2S during presulfiding was 9.766×10^{-4} mol/hr and the area above the breakthrough curve is 339.33 minutes. This gives the total moles of H_2S adsorbed as 5.523×10^{-3}, or 3.326×10^{21} molecules. The total weight of catalyst was 11.0892 grams. Thus, there was 3.00×10^{20} molecules of H_2S per gram of catalyst. This corresponds to ~55% of monolayer coverage if the area covered by an H_2S molecule is assumed to be the same as that covered by a nitrogen molecule.

After 21 hours of presulfiding the reactor was brought off-line and the carbon monoxide flow was started. The feed flow rate and composition [CO and (H_2+H_2S)] were checked and then the reactor was brought back on-line. Analysis began 22 hours later. The results are shown in Table 3.17. It should be noted that the runs without presulfiding were done using the aluminum CO cylinder while the run with presulfiding was not. This would cause the conversion difference between the two runs to decrease by ~3 percentage points. Even with this correction the conversion with presulfiding is lower at equal (90 second) space times. The 60 second space time run without presulfiding is included to allow comparison at equal conversions. The C_5, isobutylene, and 3-methyl-1-butene fractions are

higher for the presulfided catalyst. This catalyst was black after reaction as well. When recalcined at 723 K for one hour a weight loss of 0.0147 g_{coke}/g_{cat} occurred. This is 3-5 times less than the weight loss normally experienced by other catalysts. Batch number 8 in Table 3.8 was the catalyst used in non presulfiding experiments. It appears that presulfiding reduces the amount of coke deposition on the catalyst possibly by reducing adsorption strength between the catalyst and products. The increase in isobutylene and 3-methyl-1-butene could also be explained by reduced interactions between the catalyst less favorable alkene products.

An injection 1 hour after bringing the reactor on-line showed that more H_2S was in the effluent than was being fed. This indicated that some of the previously adsorbed H_2S was being desorbed by CO (and H_2). After the reaction had reached steady state the amount of sulfur in the effluent (as H_2S) was ~5% of that being fed. This is similar to the non presulfiding run in which this number was ~3%. Again, it is most likely that the sulfur is being incorporated into a liquid compound or that the compound is present in very small amounts.

Sulfur analysis of batch number 8 (co-feeding H_2S) after reaction and after recalcination indicated ~0.9 mg sulfur per gram of catalyst. This equates to 1.69×10^{19} molecules of sulfur per gram of catalyst. Based on equal area covered as compared with nitrogen this represents ~3% of monolayer coverage. This shows that a majority of sulfur adsorbed during presulfiding is desorbed under reaction conditions, but this small amount of sulfur still has a significant effect on the product distribution.

Effect of oxygen vacancies

The results of all activity tests are shown in Table 3.18. The description for each run indicates the dopant and amount of dopant used (e.g. LiZ04 refers to catalyst with Li/Zr ratio of 0.04). The catalysts used (batch numbers 9-22, and 24) in the vacancy study can be divided into three groups: (1) single dopant - zirconium vacancies, (2) single dopant - oxygen vacancies, and (3) multiple dopants - oxygen vacancies. The tantalum doped zirconias belong to the first group. As seen in Table 3.18, the two tantalum doped catalysts are relatively inactive compared to the others. The more heavily doped sample is almost completely inactive. A much lower ionic conductivity was noted for zirconia doped with Ta_2O_5 (*50*) and was attributed to the Ta^{+5} cations acting as vacancy suppressors. What this really means is that the tantalum doped zirconias contain zirconium vacancies instead of oxygen vacancies. Since conduction occurs by vacancy migration, both the availability and mobility of the vacancies influence the ionic conductivity. Geometric considerations may explain the decrease in conductivity for zirconias doped with higher valence cations. For anion migration the gaps between the cations are 90% as large as the anions themselves while for cation migration the gaps are only 56% of the cation size (*50*). The ease of anion mobility compared with cation mobility is also evident in calculations performed by Mackrodt and Woodrow (*44*) in which the activation energy for a free anion vacancy jump was found to be ~63 kJ/mol while that for a free cation vacancy jump was ~826 kJ/mol. The fact that the activity decreased significantly as oxygen vacancies disappeared supports the theory that oxygen vacancies are the active catalytic sites (*13,47,51*). Also, the decreased selectivity to C_4's suggests that oxygen vacancies play a vital role in the selectivity of the isosynthesis reaction. The reduced selectivity to C_4's is not a conversion effect.

All of the single component doped catalysts (that created oxygen vacancies) were

active toward isosynthesis. Figure 3.48 shows the comparison between undoped zirconia and those doped with lithium, magnesium, aluminum, and dysprosium. Some of the catalysts are more active than the pure zirconia while some of them are less active as found by Jackson and Ekerdt (*13*). The lithium doped catalyst shows higher activity at lower dopant concentration and levels off at higher dopant concentrations. Since lithium introduces the highest number of oxygen vacancies per lithium atom incorporated into the lattice and has the highest negative charge (-3) of any of the lower valence ions there is increased interaction between the oxygen vacancy and the lithium cation as lithium concentration increases. This could lead to a decrease in the overall vacancy mobility and thus to a decrease in activity. Activity reaches a steady value because the benefit of increased numbers of oxygen vacancies at higher dopant levels is counteracted by increased binding of the vacancies to the dopant cations. The largest activity for lithium doped catalysts may lie in the 0 to 4 Li/100 Zr dopant range.

The magnesium doped catalysts show a maximum in activity around 9 to 10 Mg/100 Zr ($\approx$9 mol% MgO). A maximum in isosynthesis profile also occurs in this same concentration range. This is consistent with results of Jackson and Ekerdt (*13*) for isosynthesis and Etsell and Flengas (*50*) for ionic conductivity. The maximum in C_4's which also occurs at this dopant level lend support to the conclusion that the selectivity of the isosynthesis catalysts are directly related to the oxygen vacancy availability and mobility as well. A maximum occurs because of the tradeoff between the increasing number of oxygen vacancies present and increasing hindrance of vacancy mobility.

The samples doped with +3 cations show somewhat lower activity than the lithium- and magnesium-doped catalysts. Since only two batches of aluminum and dysprosium doped catalysts were tested it is not clear where the maximum in activity occurs, but it appears to lie in the 6 to 10 M/100 Zr range for both dopants. The lower activity of the aluminum doped zirconia might be attributed to all of the alumina not dissolving in the zirconia phase. However, since the XRD patterns did not indicate a second phase and the alumina mole percent was relatively low (2-6%), the reduced activity was more likely the result of stronger interactions between the oxygen vacancies and the small aluminum cation. The reduction of activity in the dysprosium samples may be attributed to a steric blocking effect of vacancy migration by the larger dysprosium cation.

Figure 3.49 shows the effect of dopant ionic radius on activity at a constant level of oxygen vacancies. An apparent maximum near the radius of zirconium (0.814 Å) lends support to findings that the highest ionic conduction would be obtained with dopant similar in size to zirconium (*52-57*). Figures 3.50 and 3.51 show the relationship between activity and the dopant charge to ionic radius ratio at constant oxygen vacancies and constant dopant to zirconium ratio respectively. Both of these show activity to increase with decreasing charge to radius ratio. One might expect a +1 dopant to be less active because of the increased attraction between an oxygen vacancy (+2) and the -3 charge of the dopant in the zirconium lattice site. However, recall that the +1 dopant introduces the most oxygen vacancies per dopant atom (Table 3.7) so a lower concentration of dopant is required for the same level of oxygen vacancies as +2 and +3 dopants. The lower concentration would actually reduce the amount of interaction between oxygen vacancies and dopant cations leading to an increase in activity (conductivity). Low concentrations of a lower valence cation with radius similar to that of zirconium may be the optimum design for single component doped zirconia catalysts.

The product distribution was not significantly affected by any of the lower valence

dopants (see Table 3.18). This is particularly interesting in that for most reactions the properties of the additives usually have a noticeable effect on product distributions. In the case of isosynthesis it seems that the vacancies are more important than the dopant. Slightly more methane and less C_5+ was produced over the doped zirconias as compared to the pure zirconia. This may be attributed to an increase in catalyst acidity because of the introduction of electron accepting oxygen vacancies. Also, the +3 dopants produced more oxygenates (methanol and dimethyl ether) than the +1 or +2 dopants. For dysprosium, the explanation may be that Dy_2O_3 is a more basic oxide than ZrO_2. However, since alumina is more acidic the reason for increased oxygenate production over aluminum doped catalysts is unclear.

The final group consists of the yttrium, barium, copper '123' doped zirconia. As mentioned, the motivation for studying this catalyst was the possibility of increasing activity because of increased oxygen vacancy mobility. Table 3.18 gives the results for the two runs performed over this catalyst. Run YBCZ was done with the standard CO/H_2 feed while run YBCZS was performed using a feed of CO and the 1.06% H_2S in H_2 mixture.

A 43% increase in CO conversion over that obtained with the pure zirconia catalyst was achieved for run YBCZ. This increase in conversion was realized as an increase in methane production. Also, the *iso*-C_4 distribution favored isobutane over isobutylene. The increase in methane production could be attributed to the copper which is a component of low temperature methanol synthesis catalysts. The formation of isobutane instead of isobutylene is the result of a more acidic catalyst caused by the increase in oxygen vacancy availability and mobility. The large increase in conversion strengthens the theory that active catalysts have a high degree of oxygen vacancy availability and mobility.

Hydrogen sulfide was added to the feed because of its previously found effect on product distribution. A 33% increase in CO conversion over the non-H_2S case (90% increase over the pure zirconia catalyst) was achieved while co-feeding H_2S. This increase in conversion was not expected since the previous studies had shown that H_2S did not affect activity. Hydrogen sulfide may have caused an increase in oxygen vacancy mobility possibly by incorporation of S^{-2} into the zirconia lattice. No change in the XRD pattern was observed that might indicate the formation of another phase. Again, this increase was realized in methane production ($\sim$74 wt% of hydrocarbon product). The fraction of isobutane in the C_4's was even larger than for the non-H_2S case. This implies that the acidity of the catalyst was enhanced by the addition of H_2S. The C_5 fraction did increase with the addition of H_2S and 3-methyl-1-butene selectivity went from $\sim$0 to 50 wt% (among C_5's). However, this slight increase in C_5 fraction was dwarfed by the huge increase in methane. The small amount of oxygenates produced when pure hydrogen was used and complete disappearance with hydrogen sulfide supports the conclusion that the '123' zirconia was more acidic than pure zirconia and that this acidity was enhanced by the addition of H_2S.

Effect of gel pH

These experiments used batches 9 and 25-27 (see Table 3.5). These gels were adjusted to *p*Hs of 7.0, 10.0, 8.5, and 5.5 respectively. Catalytic activity was slightly affected by *p*H. The conversion over zirconia at *p*H 5.5 and 10.0 was statistically the same. The conversion over zirconia at *p*H 7.0 was slightly lower, while that at *p*H 8.5 was $\sim$15% higher. The amount of oxygenates produced was expected to increase with increasing *p*H. The largest amount of oxygenates were produced over the zirconia adjusted to *p*H 10.0, but no clear trend in oxygenate production with *p*H was evident. Figures 3.52 and 3.53 show

that the isobutylene to isobutane ratio, isosynthesis profile [$C_4/(C_2+C_3)$], isobutylene fraction among C_4's, and isobutylene to methane ratio increased with increasing *p*H (basicity).

Jackson and Ekerdt (*13*) found that high isosynthesis profiles were associated with more acidic catalysts. One possible explanation for the conflict is that Jackson and Ekerdt's data are at very low conversions (<2%). It is well known that conversion can have a significant effect on product distribution. Jackson and Ekerdt also found that the amount of C_1 produced was larger for catalysts with lower isosynthesis profiles. The same trend is observed here, the wt% of methane decreases with increasing isosynthesis profile (basicity). The isobutylene to methane ratio increased with *p*H because the isobutylene fraction increased and methane decreased. The isobutylene to isobutane ratio increased with increasing *p*H possibly because hydrogenation was reduced with decreasing acidity. Isobutylene and isobutane were the only C_4 components to show a significant change in amount produced with *p*H.

Effect of temperature cycling

As mentioned earlier, the catalytic activity decreased and the hydrocarbon distribution shifted toward the more thermodynamically stable products with any temperature cycling. These effects for the 7% Ce-ZrO_2 catalyst are shown in Table 3.19. The first column (Fresh) in Table 3.19 is for a batch of catalyst loaded into the reactor and subjected to normal pretreatment procedures. Both 60 and 90 second space times are shown for the fresh catalyst for comparison with the cycled and reheated catalyst. The second column is the result for the same catalyst after the temperature cycle 673 K → 698 K → 723 K → 673 K. These experiments (Fresh and Cycled) were performed using the iron CO cylinder while the other two were performed using the aluminum CO cylinder. The important point is how the conversion and product distribution change with temperature cycling. After the temperature cycle the catalyst is slightly less active (~7%) and the product distribution has shifted to producing a majority of methane. Also the distribution among the C_4 has shifted to the alkanes with isobutane showing about a 50% increase. The third column (Reheat) gives the result for a fresh catalyst subjected to a more extreme temperature cycle (300 K → 673 K → 300 K → 673 K → 300 K → 673 K). Throughout this cycle nitrogen was passed over the catalyst at pretreatment conditions. Again, there was catalyst deactivation (more severe in this case) and a dramatic shift toward methane. The final column (Reheat w/H_2S) is the result for the same catalyst while co-feeding hydrogen sulfide. The conversion is only slightly affected by adding hydrogen sulfide, but the product distribution is significantly changed. Methane and C_2+C_3 are reduced by almost half while C_5+ shows a threefold increase. As found before, this increase is the result of an huge increase in 3-methyl-1-butene production.

The product distribution is extremely sensitive to the temperature to which the catalyst has been subjected. With increasing temperature, the thermodynamically favored products increase regardless of the temperature at which the experiment is performed. In other words, once the catalyst is subjected to a certain (higher) temperature the product distribution achieved at that temperature persists even at lower temperatures. Evidence of this is seen in Table 3.19. Even though the 'reheated' catalyst underwent a more severe temperature cycle it produced less methane than the catalyst that was cycled to 723 K because the highest temperature it was subjected to was only 673 K. Possibly the catalyst active sites are altered with temperature cycling and change more significantly as the temperature is increased.

Hydrogen sulfide somehow overrides the temperature effect on product distribution and the catalyst behaves as if no temperature cycling occurred, except for the loss in activity.

Trickle bed reactor

The commercial zirconia was evaluated in the reactor system, which can be operated as a fixed bed gas phase or as a trickle be reactor. Decalin was determined to be the best oil to use for the trickle bed experiments. Linear hydrocarbons hydrocracked over the zirconia at the temperature of the isosynthesis.

A comparison of the performance of the catalyst when operating the reactor in the fixed and trickle bed modes at 669 K and 51 atm is shown in Figures 3.54 and 3.55. The selectivity for isobutylene and the C_4 components was higher when operating the reactor as a conventional gas phase fixed bed reactor than when operating the reactor as a trickle bed. The CO conversion was approximately the same for both modes of operation. The product distribution obtained with the trickle bed contains more C_3's, less methane, less C_4's, and less C_5+ than the product distribution obtained when operating in the gas phase fixed bed reactor mode.

These experiments indicated that mass transfer resistances were occurring in regard to the propagation of the hydrocarbon chain. A greater amount of propylene is produced in the trickle bed than with the fixed bed gas phase reactor. The separator temperatures and oil flow rates were shown to have minor effects on the product distribution. Figures 3.56 through 3.59 illustrate the effects of the oil flow rate and separator temperature on the product distribution. Figure 3.59 shows that as oil flow rate increases propylene decreases and C_4 and C_5 production increases.

Slurry reactor

All of the previous studies on isosynthesis have been conducted in gas-solid fixed bed reactors. Using a three phase gas-oil-catalyst slurry reactor for isosynthesis can have certain advantages. Primarily, the reaction can be run in the absence of mass transfer limitations. There is evidence in the literature (*12*) that the isosynthesis reaction becomes controlled by external mass transfer at temperatures above 723 K. Continuous circulation of the oil phase may enable separation of light components from the heavy components (C_5+ which are produced by the reaction) at the gas oil separator. The heavy components can be circulated back to the reactor dissolved in the oil and be further converted into light hydrocarbons. In addition, selectivities for the desired products can be increased because of the effect of perfect mixing compared to plug flow. The CO/H_2 ratio in the oil phase may also be quite different than the CO/H_2 ratio in the feed gas because of the differences in Henry's law constants for hydrogen and carbon monoxide which may affect the product distribution.

Both the commercial zirconia and a precipitated zirconia were used in the slurry reactor studies. The commercial and precipitated catalysts had surface areas of 50 and 92 m^2/g, respectively. Experiments with the commercial zirconia used an oil flow rate of 0.04 g/sec while those with the precipitated zirconia used and oil flow rate of 0.08 g/sec. In both cases 10 cm^3 of catalyst and 60 cm^3 of oil were used.

A time on stream study was conducted to determine if there was any catalyst deactivation. Deactivation was not expected because of the stability of the zirconia as found in the fixed bed experiments. As seen in Figure 3.60, a slight increase in conversion was

observed over a period of 17 hours. Figures 3.61 and 3.62 show the comparison of the hydrocarbon and C_4 distributions for the slurry and fixed bed reactor configurations over ZrO_2 (ppt.). Although the CO conversion, at equal inlet flowrates, is lower for the slurry reactor case, the selectivities to C_4 products are higher. Figures 3.63 and 3.64 show the comparison of the hydrocarbon and C_4 distributions for different CO/H_2 ratios over the commercial zirconia. Figure 3.65 shows the change in hydrocarbon distribution with CO/H_2 ratio over ZrO_2 (ppt.).

The mass transfer resistances were calculated based on the data using the procedure outlined by Smith (*58*). Gas bubble to liquid mass transfer coefficients were calculated using the Calderbank and Moo-Young correlation (*59*) and liquid to particle mass transfer coefficients were calculated using the correlation given by Brian *et al.* (*60*). The effectiveness factors were found to be very close to unity. Therefore, it is believed that the reactions were run in the kinetically controlled regime in the absence of any mass transfer limitations.

The experiments with the commercial zirconia were conducted at a slightly higher temperature (679 K instead of 673 K) and lower space velocities (400 hr^{-1} instead of 1050 hr^{-1}) because of the considerably lower activity of this catalyst compared to the zirconia prepared in our laboratory by precipitation. Tables 3.20 through 3.25 give the experimental conditions for run results presented in Figures 3.60 through 3.65.

Equation Development for the Modeling of Carbon Monoxide Conversion (Fixed Bed)

The following equation development is done strictly on an empirical basis. The physical meaning of the parameters obtained from the fit of the data and possible simplified mechanisms that give the final form of the rate equation are discussed in Appendix B.

Alkenes as predominant products with CO_2 inhibition

The reaction to form alkenes may be written as

$$\underset{(A)}{2nCO} + \underset{(B)}{nH_2} \rightleftarrows \underset{(C)}{C_nH_{2n}} + \underset{(D)}{nCO_2}$$

The design equation for a plug flow reactor is

$$-\frac{dn_A}{dW} = r_A = \frac{k_p p_A^a p_B^b}{\left(1 + K_{CO_2} p_D\right)^c} \tag{3.1}$$

The mole balances for the given reaction are written in terms of conversion of carbon monoxide.

$$
\begin{aligned}
n_A &= n_A^o - n_A^o x \\
n_B &= n_B^o - \frac{1}{2} n_A^o x \\
n_C &= n_C^o + \frac{1}{2n} n_A^o x \\
n_D &= n_D^o + \frac{1}{2} n_A^o x \\
\hline
n_T &= n_T^o + n_A^o x \left(\frac{1}{2n} - 1 \right)
\end{aligned}
\tag{3.2}
$$

If k_p is divided out of the design equation then

$$
-\frac{dn_A}{dW} = \frac{p_A^a p_B^b}{(q + s p_D)^c} \tag{3.3}
$$

where

$$
q = \frac{1}{k^{1/c}} \qquad s = \frac{K_{CO_2}}{k^{1/c}} \tag{3.4}
$$

Partial pressures may be written in terms of moles and total pressure as follows

$$
p_i = \frac{n_i}{n_T} P \tag{3.5}
$$

The partial pressures can be written in terms of conversion by substituting the mole balances (3.2) into the above expression and defining β as the feed ratio of hydrogen to carbon monoxide.

$$p_A = \frac{(1-x)}{\left[1+\beta+x\left(\frac{1}{2n}-1\right)\right]}P$$

$$p_B = \frac{\left(\beta-\frac{1}{2}x\right)}{\left[1+\beta+x\left(\frac{1}{2n}-1\right)\right]}P \qquad (3.6)$$

$$p_D = \frac{\frac{1}{2}x}{\left[1+\beta+x\left(\frac{1}{2n}-1\right)\right]}P$$

The left hand side of the design equation (3.3) is written in terms of conversion and space time (τ) according to the following (where ρ_b is bulk density).

$$dn_A = -n_A^o dx \qquad (3.7)$$

$$n_A^o = \frac{p_A^o v_o}{RT_o} \qquad (3.8)$$

$$W = \rho_b V \qquad dW = \rho_b dV \qquad (3.9)$$

$$\tau = \frac{V}{v_o} \qquad (3.10)$$

The left hand side of the design equation can now be expressed as

$$-\frac{dn_A}{dW} = \left[\frac{P}{(1+\beta)\rho_b RT_o}\right]\frac{dx}{d\tau} \qquad (3.11)$$

The complete differential equation describing how conversion changes with space time is written by combining Equations (3.3), (3.6), and (3.11) and is given by

$$\frac{dx}{d\tau} = \frac{\rho_b RT_o P^{a+b-1}(1+\beta)(1-x)^a\left(\beta-\frac{1}{2}x\right)^b}{M^{a+b-c}N^c} \qquad (3.12)$$

where

$$M = \left[1 + \beta + x\left(\frac{1}{2n} - 1\right)\right] \tag{3.13}$$

$$N = \left[q\left(1 + \beta + x\left(\frac{1}{2n} - 1\right)\right) + s\frac{xP}{2}\right] \tag{3.14}$$

Alkenes as predominant products with CO inhibition

The design equation for this case is

$$-\frac{dn_A}{dW} = \frac{p_A^a p_B^b}{(q + s p_A)^c} \tag{3.15}$$

The development of equations for mole balances, partial pressures, and the left side of the design equation is the same as for the case with CO_2 inhibition. Substitution of these equations into the design equation gives

$$\frac{dx}{d\tau} = \frac{\rho_b R T_o P^{a+b-1} (1 + \beta)(1 - x)^a (\beta - \frac{1}{2}x)^b}{M^{a+b-c} N^c} \tag{3.16}$$

where

$$M = \left[1 + \beta + x\left(\frac{1}{2n} - 1\right)\right] \tag{3.17}$$

$$N = \left[q\left(1 + \beta + x\left(\frac{1}{2n} - 1\right)\right) + s(1 - x)P\right] \tag{3.18}$$

Alkanes as predominant products with CO_2 inhibition

The reaction to form alkanes may be written as

$$\underset{\text{(A)}}{2nCO} + \underset{\text{(B)}}{(n+1)H_2} \rightleftarrows \underset{\text{(C)}}{C_nH_{2n+2}} + \underset{\text{(D)}}{nCO_2}$$

The design equation (3.3) is used with the following mole balances

$$
\begin{aligned}
n_A &= n_A^o - n_A^o x \\
n_B &= n_B^o - \left(\frac{n+1}{2n}\right) n_A^o x \\
n_C &= n_C^o + \frac{1}{2n} n_A^o x \\
n_D &= n_D^o + \frac{1}{2} n_A^o x \\
\hline
n_T &= n_T^o - n_A^o x
\end{aligned}
\tag{3.19}
$$

The partial pressures become

$$
\begin{aligned}
p_A &= \frac{(1-x)}{[1+\beta-x]} P \\
p_B &= \frac{\left(\beta - \frac{n+1}{2n} x\right)}{[1+\beta-x]} P \\
p_D &= \frac{\frac{1}{2} x}{[1+\beta-x]} P
\end{aligned}
\tag{3.20}
$$

The complete differential equation describing how conversion changes with space time is written by combining Equations (3.3), (3.11), and (3.20) and is given by

$$
\frac{dx}{d\tau} = \frac{\rho_b R T_o P^{a+b-1} (1+\beta)(1-x)^a (\beta - \frac{n+1}{2n} x)^b}{M^{a+b-c} N^c} \tag{3.21}
$$

where

$$
M = [1 + \beta - x] \tag{3.22}
$$

$$
N = \left[q(1 + \beta + x) + s \frac{xP}{2} \right] \tag{3.23}
$$

Alkanes as primary products with CO inhibition

The design equation (3.15) is used with mole balances (3.19) and partial pressures (3.20) as derived above. The final differential equation for describing how conversion changes with space time is

$$\frac{dx}{d\tau} = \frac{\rho_b R T_o P^{a+b-1} (1+\beta)(1-x)^a (\beta - \frac{n+1}{2n} x)^b}{M^{a+b-c} N^c} \tag{3.24}$$

where

$$M = [1 + \beta - x] \tag{3.25}$$

$$N = [q(1 + \beta + x) + s(1-x)P] \tag{3.26}$$

Results of Modeling of Carbon Monoxide Conversion (Fixed Bed)

The parameters q and s (and thus k_p and K_{CO_2}) were found using the SimuSolv® Modeling and Simulation Software developed by Dow Chemical Company. The routine uses numerical integration to solve the ordinary differential equation and maximizes a log-likelihood function to find the best fit between experimental and predicted data. More details can be found in the *SimuSolv® Reference Guide*.

Model discrimination

Initially, an attempt was made to fit the data using the design equation incorporating olefin formation and CO_2 inhibition (equation 3.1) but with $c=0$ (no CO_2 inhibition). Figure 3.66 illustrates the poor prediction that is achieved when CO_2 inhibition is not included. Also shown in this figure is the CO_2 inhibited fit. In this case an excellent fit of the data is obtained with $a=1$, $b=0.5$, $c=1$, and $n=4$. An equivalent fit of the data was obtained for $a=1$, $b=0.5$, $c=2$, and $n=4$. As mentioned previously, discussion of the parameters is given in Appendix B. The simpler equation ($a=1$, $b=0.5$, $c=1$) was utilized in the remainder of the modeling work. The effect of n on the fit is shown in Figure 3.67. The difference in fit between $n=4$ and $n=1$ is not significant. Thus, a value of $n=4$ (C_4 products predominant) was adopted as the standard. The design equation in which alkanes are the primary products (equation 3.21) was used in preparing Figure 3.67 while that in which alkenes are the primary products (equation 3.12) was used for Figure 3.66. The fit is essentially the same for both cases. Therefore the method involving alkanes was dropped in favor of that involving alkenes (isobutylene). The model involving CO inhibition was investigated because of the effect that CO/H_2 ratio had on conversion. The higher the CO partial pressure was (at same total pressure) the lower the conversion was for the same space time (Figure 3.30). Thus, it was possible that CO was inhibiting the reaction. Figure 3.68 gives the best fit that could be obtained using equation 3.16. The poor fit of the CO inhibition model led to its rejection and the acceptance of the model involving alkenes ($n=4$) as the major products with CO_2 inhibition. The final form used to determine parameters for all of the catalysts tested at more than one space time is given by Equation (3.27).

$$r_{CO} = \frac{k_p p_{CO} p_{H_2}^{0.5}}{\left(1 + K_{CO_2} p_{CO_2}\right)} \qquad (3.27)$$

Fitted parameters for isosynthesis catalysts

Table 3.26 shows the results of SimuSolv® modeling for all catalysts for which conversion data at more than one space time was available at 673 K, 50 atm, and 1/1 CO/H_2 ratio. When the rate constant is multiplied by the catalyst bulk density the agreement in rankings between model and experiment is excellent. Table 3.27 presents the parameters obtained at other reaction conditions. Figure 3.69 illustrates the agreement between predicted and experimental carbon monoxide conversions for the catalysts and conditions given in Tables 3.26 and 3.27.

For those catalysts tested at three temperatures it was possible to calculate an activation energy for the reaction and a heat of adsorption for carbon dioxide. These values were calculated in the traditional manner by plotting $\ln k_p$ (or $\ln K_{CO_2}$) versus $(1/T-1/T_o)$ where T_o is a reference temperature (usually taken as midpoint of temperature range of interest). Examples of these two plots are shown in Figures 3.70 and 3.71. The solid line represents the least-squares fit of the experimental points. The lowest temperature point for k_p was not used in determining the fit. As described in the earlier section on hydrogen sulfide experiments, the data used to determine the rate constant at this temperature were taken after temperature cycling had occurred. Thus, there was some deactivation and the fitted rate constant was lower than what would be expected. The CO_2 adsorption equilibrium constant was not affected by the deactivation.

Table 3.28 gives the results of the least squares fit for those catalysts tested at three or more temperatures. The numbers obtained from the fit are reasonable, though they are lower than those calculated by Maruya *et al.* (*10*) for C_2, C_3, and linear C_4 hydrocarbon formation. The lower activation energy for the cerium catalyst with the iron carbon monoxide cylinder suggests that diffusional limitations are more important in this case.

Equation Development for Modeling of the Product Distribution (Fixed Bed)

Extension of CO rate equation

The product distribution was modeled with a simple extension of the rate equation for predicting carbon monoxide conversion according to

$$\frac{dn_i}{dW} = r_i = \gamma_i r_{CO} = \gamma_i\left(-\frac{dn_{CO}}{dW}\right) \qquad i = 1,2,3,4,5+ \qquad (3.28)$$

which reduces to

$$\frac{df_i}{d\tau} = \gamma_i\left(\frac{dx}{d\tau}\right) \qquad f_i = \frac{n_i}{n_{CO}^o} \tag{3.29}$$

An expression for $dx/d\tau$ has already been found using SimuSolv®. Each of the γ_i's was found by using SimuSolv and the appropriate set of f_i's. A constraint on the γ_i's is found by writing a carbon balance for the reaction on which the rate equation for carbon monoxide conversion is based. This balance is given in the following equation.

$$r_{CO} = \sum r_i \alpha_{ci} + \sum r_{CO_{2,i}} \tag{3.30}$$

The α_{ci} is the number of carbon atoms in the product for the *ith* reaction where $i=1,2,3,4,5+$ (for methane through C_5+ products). The summation term involving carbon dioxide term is the amount of CO_2 formed from the *ith* reaction. From the stoichiometry of the reaction it can be shown that

$$\sum r_{CO_{2,i}} = \frac{1}{2} r_{CO} \tag{3.31}$$

When this equality and the assumed form for r_i are substituted into the carbon balance the result is

$$\sum \alpha_{ci}\gamma_i = \frac{1}{2} \tag{3.32}$$

This constraint was incorporated into the SimuSolv® program. Another approach to γ_i comes from the stoichiometry of the reaction

$$\frac{r_i}{\left(\frac{1}{2\alpha_{ci}}\right)} = r_{CO} \tag{3.33}$$

Now if r_i/r_{CO} is assumed to be constant (as before), a new gamma can be defined based on the number of carbon atoms in the product of the *ith* reaction.

$$\frac{r_i}{r_{CO}} = \frac{1}{2\alpha_{ci}}\gamma_{ci} = \gamma_i \tag{3.34}$$

When this relationship is substituted into Equation (3.32) it can be shown that

$$\sum \gamma_{ci} = 1 \tag{3.35}$$

The γ_{ci} can be taken as a measure of the efficiency of converting carbon monoxide into hydrocarbons with i carbon atoms.

Semi-empirical kinetic model

The distributions of products in Fischer-Tropsch synthesis follow an Anderson-Schulz-Flory scheme:

$$P_{n+1} = \alpha P_n \tag{3.36}$$

where α is the probability of propagation (27). Here, the similarities and differences between F-T synthesis and isosynthesis are presented, and a semi-empirical model is developed by adding an adjustable parameter to the F-T distribution to account for the contribution of condensation reactions to the chain growth.

The following assumptions are made in developing a kinetic model for the correlation of product distributions in isosynthesis.

1. Assume the intermediates on the surface are formed by chain reactions of intermediates on the surface, including initiation, propagation and termination, and assume pseudo-steady state and first order reactions for the intermediates.
2. Assume CO insertions and condensations are the two mechanisms for chain growth, and CO insertions occur on intermediates of any carbon number whereas condensation reactions occur only on C_2 intermediates with a methoxide. The following chain propagation is obtained:

Formation of C_2 intermediates

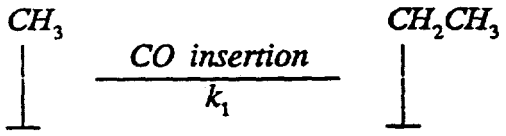

Formation of C_3 intermediates

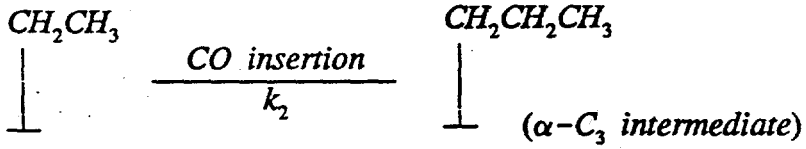

and

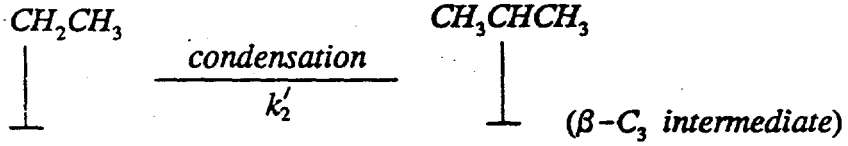

Formation of C_4 intermediates

$$CH_2CH_2CH_3 \xrightarrow[k_3]{CO\ insertion} CH_2(CH_2)_2CH_3$$

and

$$CH_3CHCH_3 \xrightarrow[k_3']{CO\ insertion} CH_3CHCH_2CH_3$$

Formation of $C_{n>4}$ intermediates

$$C_nH_{2n+1} \xrightarrow[k_n]{CO\ insertion} C_{n+1}H_{2n+3}$$

3. Assume that hydrocarbons are formed by the desorption of intermediates.

$$CH_3 \xrightarrow[d_1]{desorption} P_1$$

$$CH_2CH_3 \xrightarrow[d_2]{desorption} P_2$$

$$CH_2CH_2CH_3\ (\alpha\text{-}C_3\ intermediate) \xrightarrow[d_3]{desorption} P_3$$

$$CH_3CHCH_3\ (\beta\text{-}C_3\ intermediate) \xrightarrow[d_3']{desorption} P_3$$

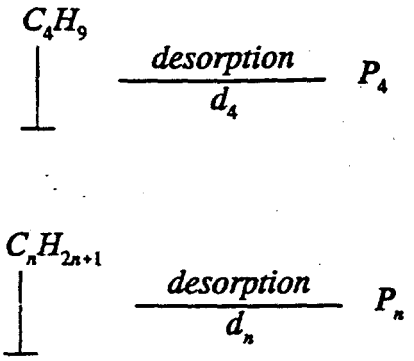

4. Assume the rate of desorption of β-C_3 intermediates is much slower than that of α-C_3 intermediates, i.e., $d_3' \ll d_3$. Assume all the intermediates other than β-C_3 intermediates satisfy the following relation:

$$\frac{k_i}{k_i + d_i} = \alpha \ (a\ constant). \tag{3.37}$$

The following product distributions are obtained:

$$\frac{P_2}{P_1} = \frac{\alpha}{1 + \alpha\kappa} \tag{3.38}$$

$$\frac{P_3}{P_2} = \alpha \tag{3.39}$$

$$\frac{P_4}{P_3} = \alpha + \kappa \tag{3.40}$$

$$\frac{P_{i+1}}{P_i} = \alpha \quad for\ i \geq 4 \quad . \tag{3.41}$$

where P_i is the mole fraction of hydrocarbons with carbon number i, and α and κ are defined as follows.

$$\alpha = \frac{k}{k + d}$$
$$\kappa = \frac{k_2'}{k_2} \tag{3.42}$$

The values of α and κ are obtained by fitting the experimental data to Equations (3.38) through (3.41).

After the distribution of hydrocarbon is correlated by the kinetic model, the production rate of hydrocarbons is further related with the reaction rate of CO by assuming that the reactions are represented as follows.

$$2nCO + \frac{m}{2}H_2 \rightarrow C_nH_m + nCO_2$$

From the stoichiometry, the production rate of hydrocarbons is given by the following.

$$r_{HC} = \frac{-r_{CO}}{\sum_{n=1}^{\infty} 2nP_n} \tag{3.43}$$

By combining with the empirical reaction rate of CO, the production rate of a C_n hydrocarbon is calculated using the following expression.

$$r_{C_n} = P_n r_{HC} = \frac{P_n}{\sum_{n=1}^{\infty} 2nP_n}(-r_{CO}) = \frac{P_n}{\sum_{n=1}^{\infty} 2nP_n} \frac{k_p p_{CO} p_{H_2}^{0.5}}{1+K_{CO_2} p_{CO_2}} \tag{3.44}$$

Results of Modeling of Product Distribution (Fixed Bed)

Extension of CO rate equation

Figure 3.72 shows the fit between experimental and predicted production rates for the C_1-C_5+ hydrocarbons for 7% Ce-ZrO_2. Table 3.29 contains the γ_i's and $\gamma_{\alpha i}$'s obtained using SimuSolv® for each of three catalysts for which sufficient data at one temperature, pressure, and CO/H_2 ratio was available. For all three catalysts the fit is fairly good considering the simplicity of the model. For the 1.6% Na-ZrO_2 and 3.2% Ti, 2% Th, ZrO_2 catalysts the C_5+ fraction was slightly underpredicted. This may be the result of poor oxygenate analysis during these early runs. If oxygenates are lumped in with the C_5+ fraction then the constraint on the gammas is not exactly valid. The intercepts of the C_1-C_5+ production rates with zero space time are given by

$$\lim_{\tau \to 0}\left(\frac{dn_i}{dW}\right) = \lim_{\tau \to 0}(\gamma_i r_{CO}) \tag{3.45}$$

which can be reduced to

$$\lim_{\tau \to 0}\left(\frac{n_i}{W}\right) = \gamma_i k_p p_{CO}^{o} (p_{H_2}^{o})^{0.5} \tag{3.46}$$

The $\gamma_{\alpha i}$'s in Table 3.29 show that the 7% Ce-ZrO_2 and 1.6% Na-ZrO_2 catalysts are more efficient at producing C_4's over methane in terms of carbon. The 1.6% Na-ZrO_2 seems to favor heavier hydrocarbons (possibly oxygenates included) over the C_1-C_4 fraction.

The 3.2% Ti, 2% Th, ZrO_2 catalyst is most efficient in producing methane.

Semi-empirical kinetic model

Figures 3.73 and 3.74 show that this semi-empirical model is capable of simulating the product distribution with two adjustable parameters. The values of α and κ vary with catalysts (Table 3.30). In general, an active isosynthesis catalyst has a large κ value and a catalyst that produces a large amount of heavy hydrocarbons has a large α value. The calculated production rate of C_n hydrocarbon generally agree well with the experimental values (Figure 3.75).

The semi-empirical kinetic model was developed by adding an adjustable parameter γ to the standard polymerization mechanism. This parameter is defined as the ratio of condensation to CO insertion. Several assumptions are made to develop the model, and they are discussed as follows.

The first and third assumptions are directly from the reaction mechanism. The steady state assumption seems to hold for isosynthesis since product distribution does not vary significantly with space velocity.

The second assumption states that condensations occur only for between a methoxide and C_2 intermediates. This can be justified because steric hinderance may occur when the size of the intermediate increases (*15*).

The fourth assumption states that the rate of desorption of β-C_3 intermediates is much slower than that of α-C_3 intermediates, and hence, $k_3/d_3 \gg k_3'/d_3'$. Temperature programmed desorption was conducted to measure the activation energies of desorption for 2-propanol and 1-propanol on a precipitated zirconium oxide, and the values are about 35 and 20 kcal/mol, respectively. The large difference in the activation energies of desorption for 2-propanol and 1-propanol suggests that β-C_3 intermediates adsorbed much stronger than α-C_3 intermediates.

The semi-empirical model calculates the mole fractions of C_1, C_3 and C_4 quite accurately, but tends to underestimate the amount of C_5 hydrocarbons and overestimate C_2 (Figure 3.76). The error comes from the assumptions in the model. First, the reaction mechanism has been drastically simplified: condensations of intermediates other than C_2 are totally neglected and the interchanges between intermediates (such as a bond shift to form branched intermediates) are not taken into consideration. Second, the model completely neglects the desorption of β-C_3 intermediate, and assumes that α is a constant for all the other intermediates. Previous research on F-T synthesis has shown that the probability of propagation (equivalent to the parameter α in this study) might not be a constant for light hydrocarbons (*61*). Since mechanisms for branching were not included when deriving the kinetic model, the distributions of isomers were not calculated. This is a deficiency in the model.

Modeling of Slurry Reactors

To simulate isobutylene synthesis from synthesis gas performed in the slurry reactor in which decalin was used as the oil, it was assumed that there are only five reactions, which involve eight compounds, occurring during the synthesis process. These reactions are written as follows.

$$2CO + 2H_2 \rightarrow CH_4 + CO_2$$

$$2CO + H_2 \rightarrow \frac{1}{2}C_2H_4 + CO_2$$

$$2CO + H_2 \rightarrow \frac{1}{3}C_3H_6 + CO_2$$

$$2CO + H_2 \rightarrow \frac{1}{4}C_4H_8 + CO_2$$

$$2CO + H_2 \rightarrow \frac{1}{5}C_5H_{10} + CO_2$$

It was further assumed that (1) both the gas and liquid phases are perfectly mixed and (2) there is a dynamic equilibrium between the gas and liquid phases. Since the reactor was operated under constant temperature and pressure, only a mass balance is required. Based on the theory developed by Izarraraz *et al.* (*62*) for the vapor-liquid equilibrium involving chemical reactions, the following model equations were derived.

$$\sum_{i=1}^{N} \frac{z_i - \frac{\psi_i(\sigma_j)}{F}}{1 + \frac{V}{F}(K_i - 1) - \frac{1}{F}\sum_{i=1}^{N} \psi_i(\sigma_j)} - 1 = 0 \qquad (3.47)$$

$$\sigma_{CH_4} - r_{CH_4} W_{cat} = 0 \qquad (3.48)$$

$$\sigma_{C_2H_4} - 2r_{C_2H_4} W_{cat} = 0 \qquad (3.49)$$

$$\sigma_{C_3H_6} - 3r_{C_3H_6} W_{cat} = 0 \qquad (3.50)$$

$$\sigma_{C_4H_8} - 4r_{C_4H_8} W_{cat} = 0 \qquad (3.51)$$

$$\sigma_{C_5H_{10}} - 5r_{C_5H_{10}} W_{cat} = 0 \qquad (3.52)$$

where

i=H_2, CO, CO_2, CH_4, C_2H_4, C_3H_6, C_4H_8, C_5H_{10}, and decalin
j=CH_4, C_2H_4, C_3H_6, C_4H_8, and C_5H_{10}

The rate expression for compound j is the same as used for the fixed bed case:

$$r_j=\gamma_j r_{CO} \tag{3.53}$$

The symbols are defined in the notation section. It is noted that ψ_i is the amount of component *i* reacted or produced during the synthesis reactions, which are dictated by the following stoichiometric relationships.

$$\psi_{H_2} = 2\sigma_{CH_4} + \sigma_{C_2H_4} + \sigma_{C_3H_6} + \sigma_{C_4H_8} + \sigma_{C_5H_{10}} \tag{3.54}$$

$$\psi_{CO} = 2\left(\sigma_{CH_4} + \sigma_{C_2H_4} + \sigma_{C_3H_6} + \sigma_{C_4H_8} + \sigma_{C_5H_{10}}\right) \tag{3.55}$$

$$\psi_{CO_2} = -\left(\sigma_{CH_4} + \sigma_{C_2H_4} + \sigma_{C_3H_6} + \sigma_{C_4H_8} + \sigma_{C_5H_{10}}\right) \tag{3.56}$$

$$\psi_{CH_4} = -\sigma_{CH_4} \tag{3.57}$$

$$\psi_{C_2H_4} = -\frac{1}{2}\sigma_{C_2H_4} \tag{3.58}$$

$$\psi_{C_3H_6} = -\frac{1}{3}\sigma_{C_3H_6} \tag{3.59}$$

$$\psi_{C_4H_8} = -\frac{1}{4}\sigma_{C_4H_8} \tag{3.60}$$

$$\psi_{C_5H_{10}} = -\frac{1}{5}\sigma_{C_5H_{10}} \tag{3.61}$$

$$\psi_{decalin} = 0 \tag{3.62}$$

The last term in the denominator of Equation (3.47) is the summation of the contributions from the six reactions, and it is determined by the following.

In the above model equations, there are a total of six unknowns, which are the vapor flow rate V and reaction extent σ_j, and six nonlinear equations. A computer code was developed in which a IMSL subroutine named NEQNF was utilized (uses a modified Powell

$$\sum_{i=1}^{N} \psi_i(\sigma_j) = 2\sigma_{CH_4} + \frac{3}{2}\sigma_{C_2H_4} + \frac{5}{3}\sigma_{C_3H_6} + \frac{7}{4}\sigma_{C_4H_8} + \frac{9}{5}\sigma_{C_5H_{10}} \qquad (3.63)$$

hybrid algorithm and a finite difference approximation to the Jacobian) to solve the nonlinear equations.

The rate expression for CO was derived from the fixed bed experimental data.

$$r_{CO} = \frac{k_p p_{CO} p_{H_2}^{0.5}}{\left(1 + K_{CO_2} p_{CO_2}\right)} \qquad (3.27)$$

Under the operating conditions, it could be further assumed that the gas phase is a perfect gas mixture and the liquid phase is an ideal solution.

The kinetic parameters for the two types of catalysts used in the slurry reactor are listed in Table 3.31.

The phase equilibrium constants K_i for CH_4, C_2H_4, and C_3H_6 were taken from Norris *et al.* (*63*). However, because of lack of information for C_4H_8 and C_5H_{10}, the corresponding K_i values of C_4H_{10} and C_5H_{12}, which were taken from the same reference, were used for C_4H_8 and C_5H_{10} in the modeling. The K_i values for H_2, CO, and CO_2 came from Graaf *et al.* (*64*). The values of K_i are summarized in Table 3.32.

The predicted product distributions at the CO/H_2 feed ratio of 1/1 are summarized in Tables 3.33 and 3.34 for the two different catalysts used, respectively.

It was noted for the model predictions that the feed ratios of hydrogen to carbon monoxide only affected the synthesis conversions but did not change the product distribution. The predicted conversions at different feed ratios are listed in the Table 3.35.

Nomenclature

a,b,c	exponent in empirical rate equation
d_i	rate constant for desorption
F	total molar flow rate in feed stock, mole/h
K_i	phase equilibrium constant for component i
K_{CO_2}	adsorption constant for CO_2, atm^{-1}
k_i	rate constant for CO insertion
k_i'	rate constant for condensation
k_p	rate constant for CO production rate, mole/(kg_{cat} $atm^{1.5}$ s)
n	number of carbon atoms in product
n_i	molar flow rate of component i, mol/hr
n_i°	feed molar flow rate of component i, mol/hr
p_i	partial pressure of component i, atm
P	total pressure, atm
P_i	mole fraction of hydrocarbons with carbon number i
R	gas constant, atm cm^3 mol^{-1} K^{-1}
r_i	reaction rate for component i
r_{CO}	reaction rate for CO, mol/(sec kg_{cat})
T	temperature, K
V	vapor molar flow rate in effluent, mole/hr; catalyst volume, cm^3
W_{cat}	catalyst loading, kg
x	conversion
z_i	molar fraction for component i in the feed

Greek symbols

α	probability of chain propagation
α_{ci}	number of carbon atoms for ith reaction
β	ratio of hydrogen to carbon monoxide in the feed
γ_j	rate constant ratio of component j to that of CO
γ_{ci}	rate constant ratio of component i to that of CO based on carbon
κ	ratio of condensation to propagation
ρ_b	catalyst bulk density, g/cm^3
σ_j	reaction extent for reaction j
τ	space time, sec
v_o	inlet volumetric flow rate, cm^3/sec
ψ_i	amount reacted or produced by reactions for component i

TABLE 3.1. Effect of calcination time on properties of zirconia

Calcination time (min)	N_2 BET surface area (m^2/g)	Crystal phase[a]
5	87	C
30	80	C/M
180	61	M/C

[a] C: cubic, M: monoclinic, predominant phase listed first

TABLE 3.2. d spacings and relative intensities of peaks in zirconia XRD patterns

Monoclinic (#36-420)[a]		Tetragonal (#24-1164)		Cubic (#27-997)	
d (Å)	Intensity	d (Å)	Intensity	d (Å)	Intensity
3.694	18	2.995	100	2.93	100
3.636	12	2.635	10	2.55	25
3.163	100	2.574	13	1.801	50
2.839	64	1.8412	23	1.534	20
2.620	22	1.820	13		
2.605	12	1.5821	8		
2.540	14	1.5553	15		
2.2131	12				
1.8480	16				
1.8186	18				
1.8032	12				
1.6567	12				

[a] The number given is the catalog number in the Powder Diffraction File (*37*).

TABLE 3.3. Effect of calcination temperature on properties of zirconia

Calcination conditions		N_2 BET surface area (m^2/g)	Crystal phase[a]	Bulk density (g/cm^3)
T (K)	Time (hr)			
383	24	270	A	1.64
723	2½	89	C/M	2.14
1273	2½[b]	0.36	M	3.57

[a] A: amorphous, C: cubic, M: monoclinic, predominant phase listed first
[b] 5 K/min heat-up from 348 K and 5 K/min cool-down to 348 K

TABLE 3.4. Changes in catalyst properties with preparation method

Method	Pore volume (cm^3/g)	Pore diameter (Å)	Bulk density (g/cm^3)
Precipitation	0.10	30-40	2.2
Hydrothermal	0.28	150-200	1.0
Calcining	0.20	30-40, 150-200	1.7

TABLE 3.5. Properties of isobutylene synthesis catalysts

Batch #	Precipitated catalysts[a]	N_2 BET Surface area[b] (m^2/g)			Crystal phase[c]	Bulk density (g/cm^3)
		B.R.	A.R.	R.C.		
1	ZrO_2	55	42		M	1.65
2	ZrO_2	52	35	40	M	1.88
3	1.6% Na, ZrO_2	58	45	49	M/C	2.11
4	3.2% Ti, 2% Th, ZrO_2	49	14	46	C/M	2.62
5	2% Mn, ZrO_2	35	0.4		C	2.82
6	7% Ce, ZrO_2	103	49		C	2.28
7	7% Ce, ZrO_2	93	55		C	2.39
8	7% Ce, ZrO_2	98	42	79	C	2.32
9	ZrO_2	89	35	84	C/M	2.14
10	0.22% Li, ZrO_2	98	41	87	C/M	2.18
11	0.34% Li, ZrO_2	99	40	85	C/M	2.10
12	0.67% Li, ZrO_2	101	36	83	C/M	2.13
13	0.79% Mg, ZrO_2	86	29	79	C/M	2.18
14	1.16% Mg, ZrO_2	98	45	86	C/M	2.18
15	1.72% Mg, ZrO_2	85	46	79	C/M	2.19

[a] Catalyst composition is wt%
[b] B.R.-after calcination but before reaction, A.R.-after reaction, R.C.-recalcined
[c] C-cubic, T-tetragonal, M-monoclinic, A-amorphous, predominant phase listed first

TABLE 3.5. Continued

Batch #	Precipitated catalysts[a]	N_2 BET Surface area[b] (m^2/g) B.R.	A.R.	R.C.	Crystal phase[c]	Bulk density (g/cm^3)
16	2.28% Mg, ZrO_2	99	36	84	C/M	2.20
17	0.86% Al, ZrO_2	115	38	100	C	2.00
18	2.50% Al, ZrO_2	133	51	109	C	1.93
19	4.97% Dy, ZrO_2	96	46	80	C	2.32
20	13.39% Dy, ZrO_2	92	33	86	C	2.55
21	5.48% Ta, ZrO_2	35	34		C/M	1.93
22	24.64% Ta, ZrO_2	38	36		M/C	1.60
23	1.30% Y, 4.03% Ba, 2.80% Cu, ZrO_2	85	79	84	C	2.32
24	1.30% Y, 4.03% Ba, 2.80% Cu, ZrO_2	92	70	81	C	2.29
25	ZrO_2	82	55	79	C/M	2.05
26	ZrO_2	93	57	82	C/M	2.14
27	ZrO_2	99	18	83	C/M	2.32
28	7% Ce, ZrO_2	88	71	84	C	2.18
	Hydrothermal catalysts[a]					
29	1.6% Na, 10.3% Ti, ZrO_2	70	68	70	C	0.94

[a] Catalyst composition is wt%
[b] B.R.-after calcination but before reaction, A.R.-after reaction, R.C.-recalcined
[c] C-cubic, T-tetragonal, M-monoclinic, A-amorphous, predominant phase listed first

TABLE 3.5. Continued

Batch #	Hydrothermal catalysts[a]	N_2 BET Surface area[b] (m^2/g) B.R.	A.R.	R.C.	Crystal phase[c]	Bulk density (g/cm^3)
30	0.6% Na, 2% Ti, 2% Th, ZrO_2	53	50	53	C/M	1.08
	Calcination of zirconyl nitrate					
31	ZrO_2	39	36	39	C/M	1.71
	Commercial zirconia					
32	ZrO_2 (H-0304)	35			M	2.4
	Sol gel catalysts[a]					
33	2.2% Al, ZrO_2 (CSG)	13			T/M	0.71
34	ZrO_2 (MSG)	24			T	2.2
35	5.8% Si, ZrO_2 (MSG)	24			A	2.3
36	4.0% Al, ZrO_2 (MSG)	51			T	2.0
37	0.41% Li, ZrO_2 (MSG)	10			M	2.0
38	0.48% Na, ZrO_2 (MSG)	18			T	2.3
39	0.52% K, ZrO_2 (MSG)	32			T	2.3
40	0.44% Rb, ZrO_2 (MSG)	27			M	2.0
41	0.93% Cs, ZrO_2 (MSG)	22			T	2.4

[a] Catalyst composition is wt%

[b] B.R.-after calcination but before reaction, A.R.-after reaction, R.C.-recalcined

[c] C-cubic, T- tetragonal, M-monoclinic, A-amorphous, predominant phase listed first

TABLE 3.5. Continued

Batch #	Sol gel catalysts[a]	N_2 BET Surface area[b] (m^2/g) B.R.	A.R.	R.C.	Crystal phase[c]	Bulk density (g/cm^3)
42	0.46% Mg, ZrO_2 (MSG)	25			T	2.4
43	0.53% Ca, ZrO_2 (MSG)	26			T	2.3
44	1.8% Ca, ZrO_2 (MSG)	34			T	2.3
45	0.54% Ba, ZrO_2 (MSG)	22			T	2.3
46	7.0% Si, ZrO_2 (MSG) (using NaOH)	99			T	1.5

[a] Catalyst composition is wt%

[b] B.R.-after calcination but before reaction, A.R.-after reaction, R.C.-recalcined

[c] C-cubic, T- tetragonal, M-monoclinic, A-amorphous, predominant phase listed first

TABLE 3.6. Ionic radii for 8 coordinated cations

Cation[a]	Ionic Radius (Å)	Cation	Ionic Radius (Å)
Li^{+}	0.700	Ho^{+3}	0.917
Na^{+}	0.979	Lu^{+3}	0.876
Ba^{+2}	1.39	Nd^{+3}	1.03
Ca^{+2}	1.02	Sc^{+3}	0.834
Cu^{+2}	0.989	Sm^{+3}	0.989
Mg^{+2}	0.670	Y^{+3}	0.956
Al^{+3}	0.515	Yb^{+3}	0.886
Dy^{+3}	0.937	Zr^{+4}	0.814
Gd^{+3}	0.968	Ta^{+5}	0.721

[a] Cations used in this study are indicated in outline type.

TABLE 3.7. Details of vacancies created by various dopants

Molar Ratio (M/100 Zr)	Vacancies/100 Zr[a]						Zr defects/100 Zr sites					
	Li	Mg	Al	Dy	Ta	YBaCu[b]	Li	Mg	Al	Dy	Ta	YBaCu
4	6	4	2	2	1	-	4	4	4	4	4	-
6	9	6	-	-	-	-	6	6	-	-	-	-
9	-	9	-	-	-	-	-	9	-	-	-	-
12	18	12	6	6	-	11	12	12	12	12	-	12
24	-	-	-	-	6	-	-	-	-	-	24	-

[a] Refers to oxygen vacancies in the cases of lower valence dopants and zirconium vacancies in the case of higher valence dopants.
[b] Molar ratio refers to total (Y+Ba+Cu)/Zr molar ratio.

TABLE 3.8. Typical coke deposition on catalysts under reaction conditions

Batch #	Precipitated catalysts	Time used[a] (hr)	g_{coke}/g_{cat}
2	ZrO_2	264	0.0374
3	1.6% Na, ZrO_2	1848	0.0378
8	7% Ce, ZrO_2	308	0.0640
11	0.34% Li, ZrO_2	26	0.0740
20	13.39% Dy, ZrO_2	26	0.0395
	Hydrothermal catalyst		
28	1.6% Na, 10.3% Ti, ZrO_2	768	0.0415
	Calcination catalyst		
31	ZrO_2	36	0.0060

[a] Refers to time spent at reaction conditions.

TABLE 3.9. Comparison of hydrocarbon distribution for precipitated, calcination, and hydrothermal catalysts at 673 K, 50 atm, and 1/1 CO/H_2 ratio

	Space time[a]	CO conv.	Hydrocarbon distribution (wt%)					
Precipitated catalysts	(sec)	(%)	C_1	C_2	C_3	C_4	C_5+	$i\text{-}C_4/\Sigma C_4$
ZrO_2[b]	45	12.8	10.2	2.6	2.0	21.2	64.0	70.7
1.6% Na, ZrO_2	30	11.6	6.6	3.0	1.5	18.4	70.5	76.7
3.2% Ti, 2% Th, ZrO_2	30	12.4	31.1	8.5	5.8	27.3	27.3	74.2
7% Ce, ZrO_2	30	13.1	27.8	9.6	8.0	30.7	23.9	63.2
Calcination catalyst								
ZrO_2	60	11.6	27.9	7.5	5.1	33.5	26.0	66.5
Hydrothermal catalysts								
1.6% Na, 10.3% Ti, ZrO_2	90	11.4	35.6	3.4	6.1	29.6	25.4	99.3
0.6% Na, 2% Ti, 2% Th, ZrO_2	90	11.7	27.5	2.8	2.4	14.9	52.4	100

[a] Space time (τ) is defined as V_{bed}/v_o (v_o is inlet volumetric flow rate at reaction P and T).
[b] Reaction pressure is 95 atm in this case.

TABLE 3.10. Comparison of activity and selectivity of commercial, modified sol gel, and precipitated zirconias at 70 atm and 1/1 CO/H_2 ratio

Catalyst	ZrO_2 (H-0304)	ZrO_2 (MSG)	ZrO_2 (ppt.)
Temperature (K)	723	723	673
Space time (sec)	80	80	45
CO conversion (%)	11.8	17.0	13.2
Hydrocarbon distribution (wt%)			
C_1	11.8	22.5	15.3
C_2	3.60	3.71	2.9
C_3	2.91	2.14	2.3
C_4	9.01	15.63	25.3
C_5+	72.68	56.02	54.2
C_4 distribution (wt%)			
isobutane	30.10	25.20	9.1
n-butane	6.14	2.48	2.0
1-butene	3.26	2.98	9.1
isobutylene	47.60	63.90	67.6
trans-2-butene	7.23	2.07	5.5
cis-2-butene	5.66	3.36	6.7

TABLE 3.11. A summary of time on stream experiments over Th-ZrO_2 (HT) at 723 K, 50 atm, 1/1 CO/H_2 ratio, and 40 second space time

Experiment	A	B	C	D
Time on stream, hr	4	20	55	88
CO conversion, %	18.1	17.8	18.7	19.5
CH_4/iso-C_4's, wt/wt	0.827	0.804	0.872	1.36

TABLE 3.12. Comparison of activity and selectivity between iron and aluminum CO cylinders at 673 K, 50 atm, and 1/1 CO/H_2 ratio over 7% $Ce\text{-}ZrO_2$

	Iron cylinder			Aluminum cylinder		
Space time (sec)	60	90	120	60	90	120
CO conversion (%)	20.0	26.7	30.6	23.1	29.2	34.0
Hydrocarbon distribution (wt%)						
C_1	29.5	30.8	32.6	36.1	44.7	47.7
C_2	8.3	7.5	6.6	9.4	8.8	8.5
C_3	7.1	5.3	4.6	8.5	5.0	4.4
C_4	29.0	29.4	28.8	19.8	19.5	20.1
C_5+	26.2	27.0	27.4	26.4	22.0	19.3

TABLE 3.13. Comparison of activity and selectivity at 673 K, 50 atm, and 1/1 CO/H_2 [or $CO/(H_2+H_2S)$] ratio

	without H_2S				with H_2S		
Space time (sec)	60[a]	60	90	120	60	90	120
CO conv (%)	23.56	23.12	29.23	33.96	23.55	27.93	33.07
Hydrocarbon distribution (wt%)							
C_1	29.61	36.05	44.65	47.66	26.46	29.40	32.33
C_2's + C_3's	20.23	17.83	13.81	12.87	10.75	8.26	8.20
C_4's	28.84	19.75	19.54	20.14	22.71	24.51	26.91
C_5+'s	21.23	26.37	22.00	19.33	39.09	37.83	32.57
Oxy/HC[b]	1.6	0.7	1.1	0.8	2.1	2.3	1.6
C_4 distribution (wt%)							
isobutane	10.12	12.30	21.90	29.00	13.97	22.60	30.98
n-butane	3.13	6.03	5.73	6.55	3.03	3.64	4.53
1-butene	8.36	7.75	6.81	6.45	7.26	6.72	6.23
isobutylene	52.11	49.52	43.55	37.29	53.20	46.10	38.70
trans-2-butene	15.82	14.38	13.00	12.26	13.41	12.41	11.57
cis-2-butene	10.47	10.03	9.01	8.44	9.15	8.54	7.99

[a] Run performed as an activity check on second batch of catalyst before feeding H_2S.
[b] Oxygenate produced/hydrocarbon produced (g/100 g)

TABLE 3.14. Effect of hydrogen sulfide on C_5 selectivity at 673 K, 50 atm, and 1/1 CO/H_2 [or $CO/(H_2+H_2S)$] ratio

	without H_2S	with H_2S
Space time (sec)	60	60
CO conversion (%)	23.6	23.6
C_5 distribution (wt%)		
3-m[a]-1-$C_4^=$	4.0	73.0
2-m C_4, 1-$C_5^=$, 2-m-1-$C_4^=$	32.5	8.5
n-C_5, *trans*-2-$C_5^=$, *cis*-2-$C_5^=$, 2-m-2-$C_4^=$	63.5	18.5

[a] m=methyl

TABLE 3.15. Gibbs free energy of formation at 700 K for C_5 alkanes and alkenes

C_5 hydrocarbon	ΔG_f° (kcal/mol)
3-methyl-1-butene	53.96
2-methyl butane	45.18
1-pentene	54.20
2-methyl-1-butene	51.55
n-pentane	46.19
trans-2-pentene	52.60
cis-2-pentene	52.71
2-methyl-2-butene	50.47

TABLE 3.16. Changes in activity and selectivity with temperature at 50 atm, 1/1 $CO/(H_2+H_2S)$ ratio, and 90 second space time

T	CO conv.	Hydrocarbon distribution (wt%)						C_4 distribution (wt%)					
(K)	(%)	C_1	C_{2+3}[a]	C_4	C_5	C_6+	O/HC[b]	*i*-C_4	*n*-C_4	1-$C_4^=$	*i*-$C_4^=$	*t*-2-$C_4^=$	*c*-2-$C_4^=$
648	14.42	33.55	3.56	20.64	22.04	20.21	26.1	18.57	1.64	6.36	59.83	6.78	6.83
673	27.93	29.40	8.26	24.51	16.17	21.66	2.3	22.60	3.64	6.72	46.10	12.41	8.54
698	38.96	37.21	8.57	27.14	12.24	14.84	0.2	45.43	7.38	5.14	26.73	9.09	6.22
723	52.08	50.68	8.97	25.70	7.42	7.22	0.0	66.93	12.2	2.82	10.22	4.75	3.12

		C_5 distribution (wt%)		
		3-m[c]-1-$C_4^=$	2-m C_4, 1-$C_5^=$, 2-m-1-$C_4^=$	*n*-C_5, *t*-2-$C_5^=$, *c*-2-$C_5^=$, 2-m-2-$C_4^=$
648	14.42	93.95	0.55	5.49
673	27.93	67.59	12.26	20.15
698	38.96	50.55	30.30	19.15
723	52.08	25.17	60.47	14.36

[a] C_2 plus C_3 hydrocarbons
[b] Oxygenate produced/hydrocarbon produced (g/100 g)
[c] m=methyl

TABLE 3.17. Comparison of activity and selectivity at 673 K, 50 atm, and 1/1 $CO/(H_2+H_2S)$ ratio over 7% $Ce\text{-}ZrO_2$ without and with presulfiding

	without presulfiding		with presulfiding
Space time (sec)	60	90	90
CO conversion (%)	23.55	27.93	21.22
Hydrocarbon distribution (wt%)			
C_1	26.46	29.40	31.52
C_2	5.93	4.83	5.49
C_3	5.82	3.43	3.18
C_4	22.71	24.51	22.51
C_5	20.46	16.17	23.98
C_6+	18.63	21.66	13.31
C_4 distribution (wt%)			
isobutane	13.97	22.60	11.14
n-butane	3.03	3.64	2.77
1-butene	7.26	6.72	5.55
isobutylene	53.20	46.10	65.75
trans-2-butene	13.41	12.41	8.02
cis-2-butene	9.15	8.54	6.77
C_5 distribution (wt%)			
3-m-1-$C_4^=$	73.1	67.6	82.6
2-m C_4, 1-$C_5^=$, 2-m-1-$C_4^=$	8.5	12.3	4.8
n-C_5, *trans*-2-$C_5^=$, *cis*-2-$C_5^=$, 2-m-2-$C_4^=$	18.4	20.1	12.6
Oxygenate/HC (g/100 g)	2.1	2.3	1.9

TABLE 3.18. Comparison of activity and selectivity for vacancy theory isosynthesis at 673 K, 50 atm, 1/1 CO/H_2 [or $CO/(H_2+H_2S)$] ratio, and 90 second space time

Run	CO conv.	Hydrocarbon distribution (wt%)						C_4 distribution (wt%)					
	(%)	C_1	C_2	C_3	C_4	C_5+	O/HC[a]	*i*-C_4	*n*-C_4	1-$C_4^=$	*i*-$C_4^=$	*t*-2-$C_4^=$	*c*-2-$C_4^=$
PurZ	23.59	32.71	7.65	5.07	23.80	30.77	1.4	19.02	4.08	6.78	49.29	12.31	8.52
LiZ04	25.63	34.09	8.12	5.06	25.36	27.38	1.5	17.99	3.49	6.74	51.63	11.96	8.19
LiZ06	23.47	33.96	8.16	5.09	24.05	28.75	1.5	18.72	3.67	6.30	51.43	11.85	8.03
LiZ12	23.71	33.89	8.23	5.01	24.70	28.17	1.4	17.99	3.84	6.52	51.77	11.75	8.13
MgZ04	22.25	36.13	8.42	5.20	23.64	26.62	1.4	19.96	4.14	6.85	48.37	12.37	8.31
MgZ06	25.55	34.65	8.27	4.99	26.25	25.83	1.4	24.71	2.79	5.97	47.56	11.26	7.71
MgZ09	29.13	31.95	7.95	4.96	29.11	26.02	1.9	18.60	4.52	6.47	51.25	11.33	7.83
MgZ12	25.96	34.21	7.94	5.04	25.49	27.32	1.6	18.05	2.88	6.72	52.82	11.74	7.79
AlZ04	22.89	35.79	8.45	5.50	25.10	25.16	2.2	23.77	3.03	6.52	45.92	12.46	8.31
AlZ12	21.16	38.58	9.17	5.76	24.66	21.84	2.3	17.42	3.73	7.06	49.89	13.15	8.76
DyZ04	24.10	34.50	8.44	6.18	27.53	23.35	2.6	17.52	5.20	7.60	46.77	13.73	9.19
DyZ12	22.44	31.60	8.31	4.99	27.66	27.44	5.5	13.12	5.27	8.01	50.09	13.99	9.50

[a] Oxygenate produced/hydrocarbon produced (g/100 g)

TABLE 3.18. Continued

Run	CO conv.	Hydrocarbon distribution (wt%)						C_4 distribution (wt%)					
	(%)	C_1	C_2	C_3	C_4	C_5+	O/HC[a]	*i*-C_4	*n*-C_4	1-$C_4^=$	*i*-$C_4^=$	*t*-2-$C_4^=$	*c*-2-$C_4^=$
TaZ04	4.55	40.53	16.70	10.89	11.62	20.26	0.0	9.40	0.00	13.78	27.87	29.27	19.68
TaZ24	1.10	46.79	29.37	13.79	3.62	6.43	0.0	24.28	0.00	9.71	18.82	33.52	13.67
YBCZ	33.64	51.77	5.53	3.38	17.78	21.53	0.6	31.52	4.65	6.64	36.04	12.93	8.22
YBCZS	44.85	73.54	3.21	2.36	9.52	11.37	0.0	54.92	4.24	2.55	30.97	4.23	3.09

[a] Oxygenate produced/hydrocarbon produced (g/100 g)

TABLE 3.19. Effect of temperature cycles and H_2S on activity and selectivity over 7% Ce-ZrO_2 at 673 K, 50 atm, and 1/1 CO/H_2 [or $CO/(H_2+H_2S)$] ratio

	Fresh		Cycled	Reheat	Reheat w/H_2S
Space time (sec)	60	90	90	60	60
CO conversion (%)	19.98	26.52	24.77	16.24	15.20
Hydrocarbon distribution (wt%)					
C_1	29.46	30.83	57.96	46.45	24.42
C_2's	8.29	7.48	8.04	15.24	6.43
C_3's	7.05	5.29	4.09	11.41	6.96
C_4's	29.00	29.38	18.40	12.54	17.35
C_5+'s	26.21	27.02	11.51	14.35	44.83
Oxy/HC	1.6	1.6	2.0	0.2	0.5
C_4 distribution (wt%)					
isobutane	13.28	23.35	35.05	11.41	13.24
n-butane	4.66	5.28	7.61	14.94	2.48
1-butene	7.31	6.77	5.33	9.31	8.54
isobutylene	51.66	42.89	35.71	33.24	48.70
trans-2-butene	13.62	12.83	9.40	18.51	16.15
cis-2-butene	9.48	8.88	6.90	12.60	10.90

TABLE 3.20. Variation of CO conversion with time on stream at 673 K, 60 atm, 1050/hr, and 2/1 CO/H_2 over ZrO_2 (ppt.)

Time on stream (hr)	2	11	14	17
CO conversion (%)	12.4	13.2	13.3	13.5

TABLE 3.21. Comparison of fixed bed and slurry reactors at 673 K and 1/1 CO/H_2 over ZrO_2 (ppt.)

	CO conversion (%)	wt% C_1	wt% C_2	wt% C_3	wt% C_4	wt% C_5+
Slurry (60 atm, 1050/hr)	13.0	13.6	15.4	16.5	38.8	15.7
Fixed bed (50 atm, 900/hr)	25.0	31.8	7.9	5.4	28.0	26.8

TABLE 3.22. Comparison of C_4 distribution in slurry and fixed bed reactors at 673 K and 1/1 CO/H_2 over ZrO_2 (ppt.)

weight %	isobutane	*n*-butane	1-butene	isobutylene	*trans*-2-butene	*cis*-2-butene
Slurry (60 atm, 1050/hr)	5.3	6.3	10.2	57.1	12.3	8.9
Fixed bed (50 atm, 900/hr)	14.5	3.4	6.1	58.7	10.2	7.1

TABLE 3.23. Comparison of hydrocarbon distribution at different CO/H_2 ratios in the slurry reactor at 679 K, 60 atm, and 400/hr over commercial zirconia

	CO conversion (%)	wt% C_1	wt% C_2	wt% C_3	wt% C_4	wt% C_5+
2/1 CO/H_2	10.0	28.9	11.8	16.3	22.4	20.6
3/2 CO/H_2	11.0	30.2	12.1	19.1	22.5	16.1
1/1 CO/H_2	11.0	31.8	11.6	28.5	14.0	14.0

TABLE 3.24. Comparison of C_4 distribution at different CO/H_2 ratios in the slurry reactor at 679 K, 60 atm, and 400/hr over commercial zirconia

weight %	isobutane	*n*-butane	1-butene	isobutylene	*trans*-2-butene	*cis*-2-butene
2/1 CO/H_2	7.2	5.6	11.4	59.8	9.0	7.1
3/2 CO/H_2	7.8	4.9	11.0	57.7	10.3	8.9
1/1 CO/H_2	6.7	5.1	13.6	62.8	11.0	8.0

TABLE 3.25. Product distributions for the slurry reactor at 673 K, 60 atm, and 1050/hr over ZrO_2 (ppt.)

	CO conversion (%)	wt% C_1	wt% C_2	wt% C_3	wt% C_4	wt% C_5+
2/1 CO/H_2	13.3	25.7	19.7	12.0	30.1	12.4
1/1 CO/H_2	13.0	13.6	15.4	16.5	38.8	15.7

TABLE 3.26. Rate constants and CO_2 adsorption equilibrium constants obtained from SimuSolv® at 673 K, 50 atm, and 1/1 CO/H_2 ratio

Catalyst	$k_p \times 10^6$ $\left(\frac{mol}{kg_{cat}\, atm^{1.5}\, sec}\right)$	K_{CO_2} (atm^{-1})	$\rho_b k_p \times 10^6$ $\left(\frac{mmol}{cm^3\, atm^{1.5}\, sec}\right)$	Rank	
				Model	Exp.
7% Ce-ZrO_2 (ppt., Al CO cyl.)	11.52	0.504	26.23	1	1
7% Ce-ZrO_2 (ppt., H_2S, Al CO cyl.)	10.97	0.503	25.45	2	2
1.6% Na-ZrO_2 (ppt.)	11.55	1.001	24.37	3	5
7% Ce-ZrO_2 (ppt., Iron CO cyl.)[a]	10.52 ± 0.79	0.596 ± 0.039	23.99	4	3
3.2% Ti, 2% Th -ZrO_2 (ppt.)	8.79	0.641	23.06	5	4
ZrO_2 (ppt.)	6.90	0.330	14.77	6	6
ZrO_2 (CAL.)	5.79	0.643	9.90	7	7
1.6% Na, 10.3% Ti -ZrO_2 (HT)	8.18	0.736	7.65	8	8
0.6% Na, 2% Ti, 2% Th -ZrO_2 (HT)	6.83	0.642	7.36	9	9

[a] Errors given in this case are representative of those obtained for other simulations.

TABLE 3.27. Rate constants and CO_2 adsorption equilibrium constants for other reaction conditions obtained from SimuSolv®

Catalyst	T(K)	P (atm)	CO/H_2 or $[CO/(H_2+H_2S)]$	$k_p \times 10^6$ $\left(\frac{mol}{kg_{cat}\, atm^{1.5}\, sec}\right)$	K_{CO_2} (atm^{-1})
7% Ce-ZrO_2 (ppt., H_2S, Al CO cyl.)	648	50	1/1	4.73	0.804
	698	50	1/1	14.85	0.350
	723	50	1/1	20.55	0.255
1.6% Na-ZrO_2 (ppt.)	673	95	2/1	11.55	0.601
7% Ce-ZrO_2 (ppt., Iron CO cyl.)	698	50	1/1	14.27	0.430
	723	50	1/1	15.38	0.235
ZrO_2 (ppt.)	673	95	2/1	6.12	0.202
	673	95	1/1	6.12	0.306
	673	95	1/3	6.12	0.459
1.6% Na, 10.3% Ti -ZrO_2 (HT)	648	50	1/1	4.55	1.001
	698	50	1/1	12.11	0.508
ZrO_2 (MSG)	723	70	1/1	5.88	0.331

TABLE 3.28. Activation energies and CO_2 heats of adsorption found using SimuSolv® rate parameters

Catalyst	E_a *(kcal/mol)*[a]	ΔH_{ads} CO_2 *(kcal/mol)*
7% Ce-ZrO_2 (ppt.) [H_2S, Al CO cyl.]	12.14 ± 0.50	14.22 ± 0.58
7% Ce-ZrO_2 (ppt.) [Iron CO cyl.]	7.39 ± 2.42	17.91 ± 3.48
1.6% Na, 10.3% Ti, ZrO_2 (HT)	17.64 ± 1.65	12.15 ± 0.92

[a] To convert to *kJ/mol* multiply by 4.184

TABLE 3.29. Gamma values at 673 K, 50 atm, and 1/1 CO/H_2 ratio

	7% Ce, ZrO_2 (ppt.)		1.6% Na, ZrO_2 (ppt.)		3.2% Ti, 2% Th, ZrO_2 (ppt.)	
i	$\gamma_i \times 10^3$	$\gamma_{ci} \times 10^3$	$\gamma_i \times 10^3$	$\gamma_{ci} \times 10^3$	$\gamma_i \times 10^3$	$\gamma_{ci} \times 10^3$
1	137.1 ± 1.4	274.2 ± 2.8	38.30 ± 0.87	76.60 ± 1.7	198.3 ± 3.4	396.6 ± 6.8
2	17.86 ± 1.0	71.44 ± 4.0	8.87 ± 0.25	35.48 ± 1.0	17.99 ± 1.0	71.96 ± 4.0
3	9.33 ± 0.72	55.98 ± 4.3	2.96 ± 0.06	17.76 ± 0.36	8.00 ± 0.46	48.00 ± 2.8
4	39.14 ± 0.38	313.1 ± 3.0	31.27 ± 0.59	250.2 ± 4.7	36.98 ± 1.3	296 ± 10
5+	28.54 ± 0.44	285.4 ± 4.4	62.00 ± 0.58	620.0 ± 5.8	18.77 ± 2.9	188 ± 29

TABLE 3.30. Parameters in the semi-empirical kinetic model

Catalyst	α	κ
ZrO_2 (H-0304)	0.333±0.043	3.80±0.08
ZrO_2 (MSG)	0.508±0.060	2.26±0.34
Li-ZrO_2 (MSG)	0.232	1.76
K-ZrO_2 (MSG)	0.464	3.98
Mg-ZrO_2 (MSG)	0.408	4.49
Ca-ZrO_2 (MSG)	0.480	5.17

TABLE 3.31. Kinetic parameters for the two catalysts used in slurry modeling

	Precipitated catalyst	Commercial catalyst
k_p, $\times 10^6$ mol/(kg_{cat} $atm^{1.5}$ s)	6.12	6.397
K_{CO2}, atm^{-1}	0.306	1.694

TABLE 3.32. Phase equilibrium constants used in the slurry modeling

	CH_4	C_2H_4	C_3H_6	C_4H_8	C_5H_{10}
K_i values	4.0	3.0	2.2	1.5	1.15

TABLE 3.33. Slurry modeling results for the precipitated catalyst at 673 K, 60 atm, 1/1 CO/H_2 ratio, GHSV 1050 1/hr, liquid mass rate 0.08 g/sec, and W_{cat}=20 g

	CH_4	C_2H_4	C_3H_6	C_4H_8	C_5H_{10}
γ_i used in the modeling	0.06167	0.03828	0.02743	0.05115	0.01497
weight percentage, %	13.86	15.05	16.17	40.20	14.71

TABLE 3.34. Slurry modeling results for the commercial catalyst at 679 K, 60 atm, 1/1 CO/H_2 ratio, GHSV 419 1/hr, liquid mass rate 0.04 g/sec, and W_{cat}=15.9 g

	CH_4	C_2H_4	C_3H_6	C_4H_8	C_5H_{10}
γ_i used in the modeling	0.1462	0.03095	0.04838	0.01852	0.01452
weight percentage, %	32.10	11.88	27.86	14.22	13.94

TABLE 3.35. Predicted synthesis conversions for precipitated and commercial catalyst

H_2/CO	Conversion, %			
	Precipitated catalyst		Commercial catalyst	
	CO	H_2	CO	H_2
1.0	12.30	6.91	13.53	8.74
1.5			12.11	11.74
2.0	10.41	11.69	11.16	14.43

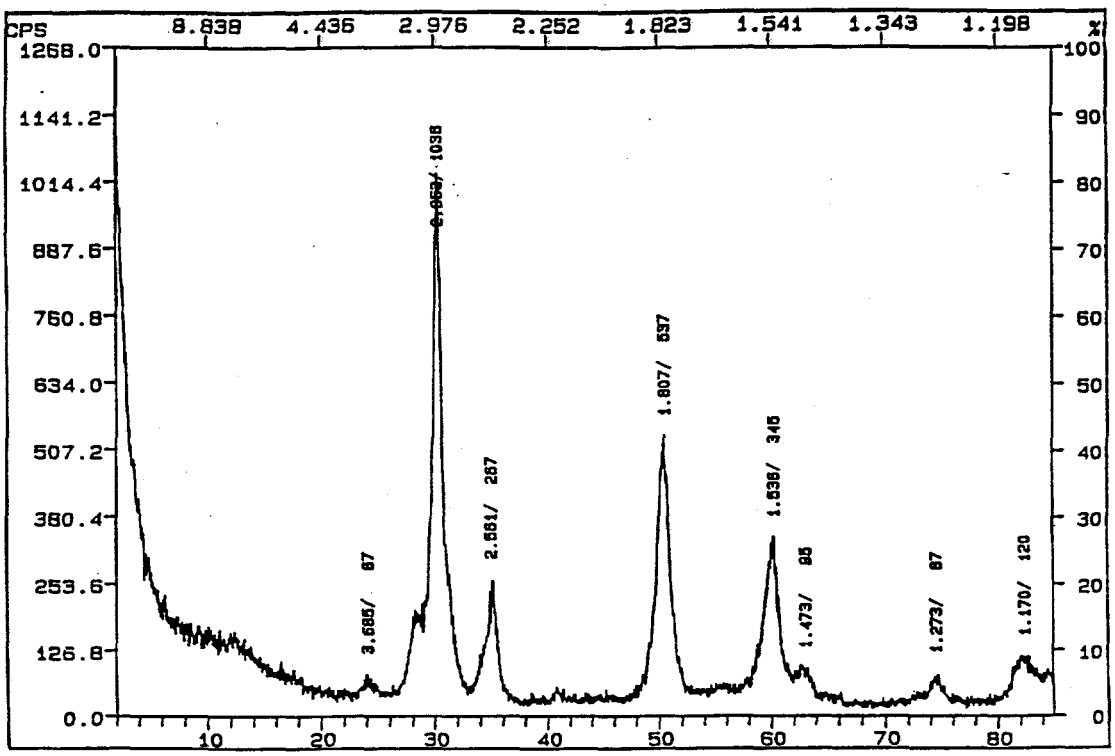

Figure 3.1. XRD pattern for ZrO_2 (ppt.) calcined at 773 K for 5 minutes.

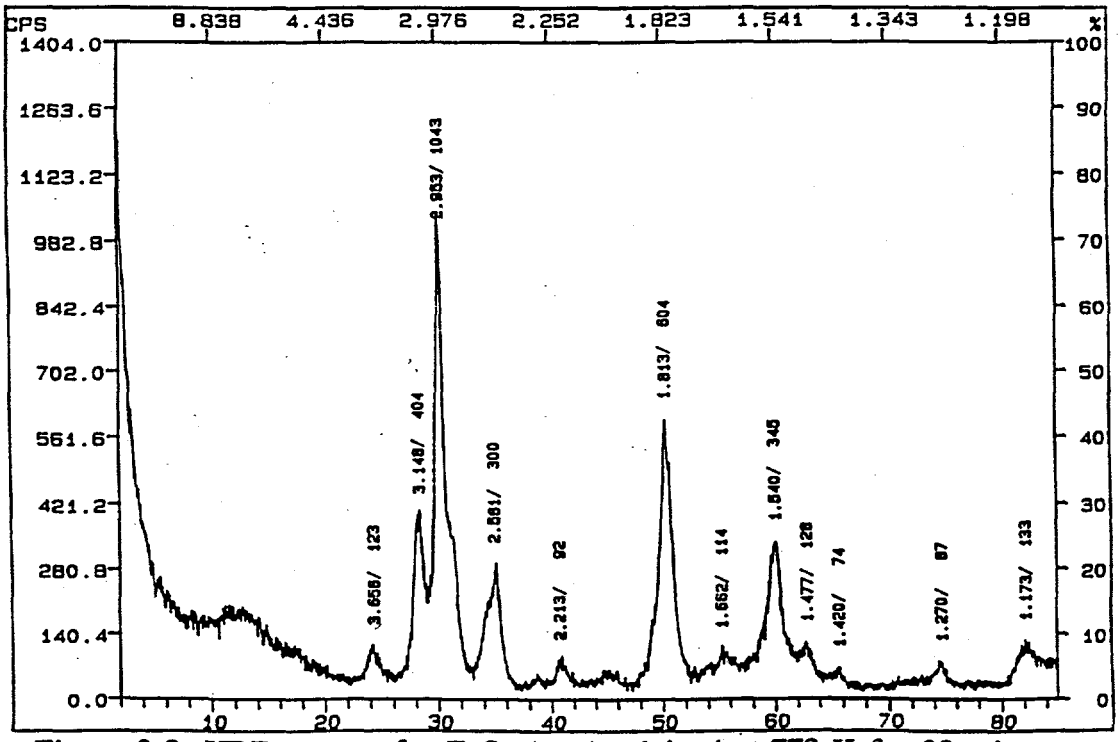

Figure 3.2. XRD pattern for ZrO_2 (ppt.) calcined at 773 K for 30 minutes.

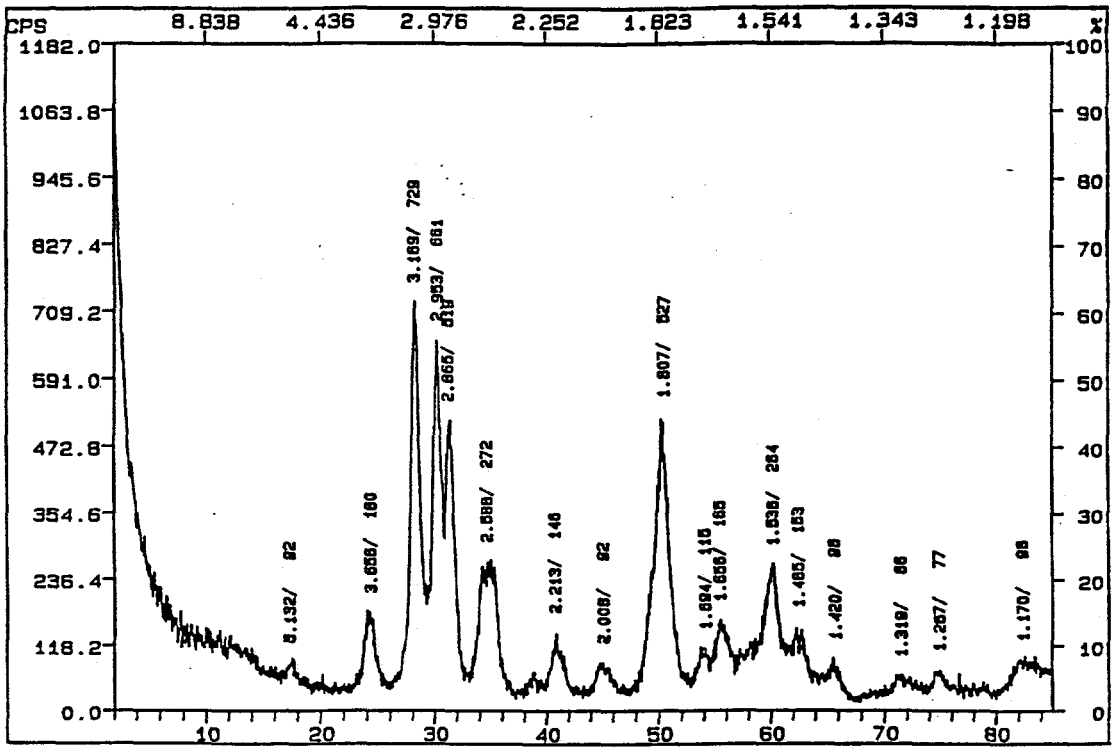

Figure 3.3. XRD pattern for ZrO_2 (ppt.) calcined at 773 K for 3 hours.

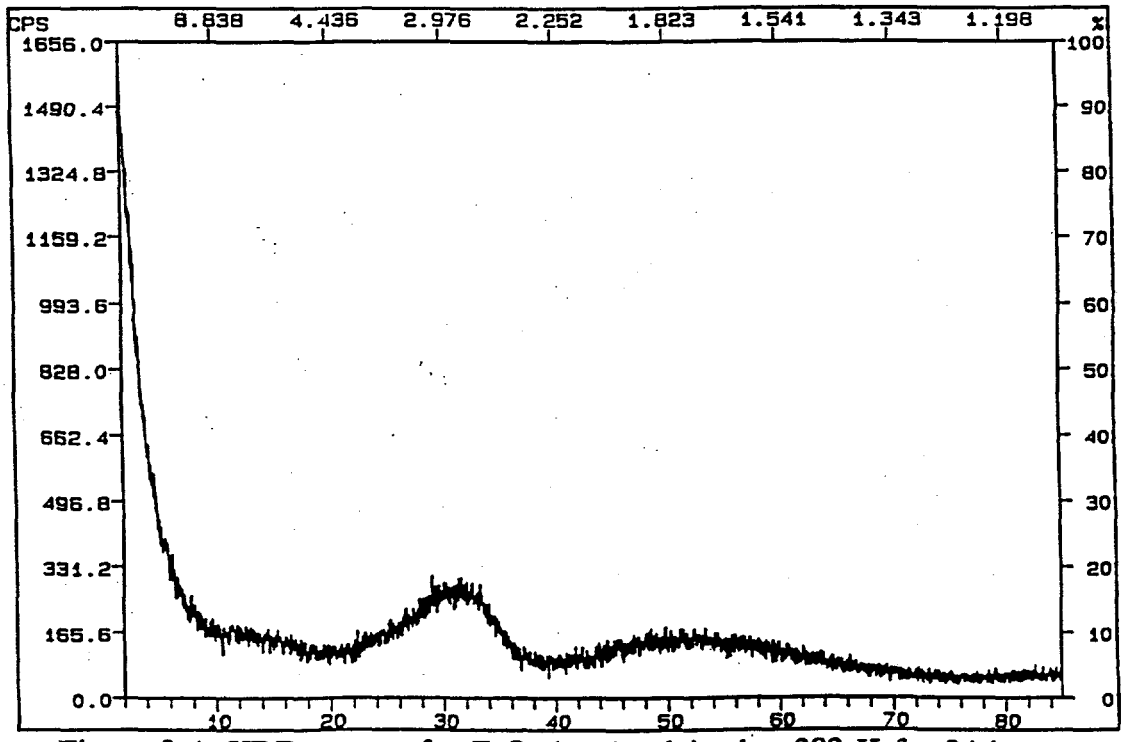

Figure 3.4. XRD pattern for ZrO_2 (ppt.) calcined at 383 K for 24 hours.

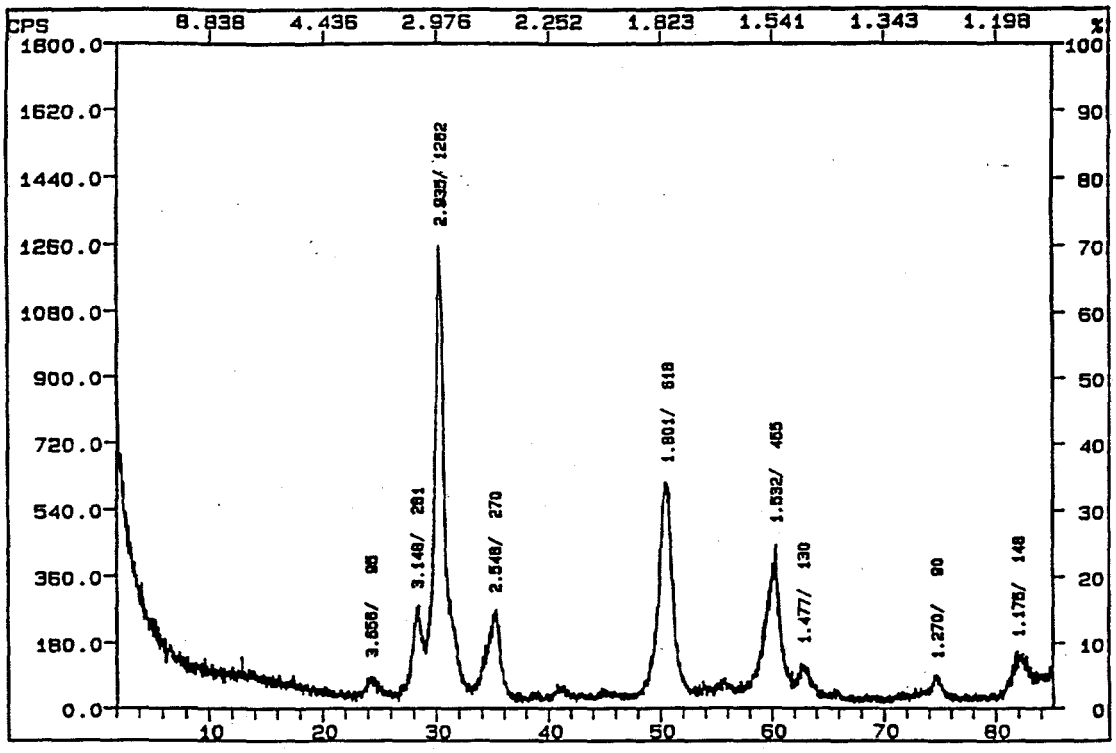

Figure 3.5. XRD pattern for ZrO_2 (ppt.) calcined at 723 K for 2½ hours.

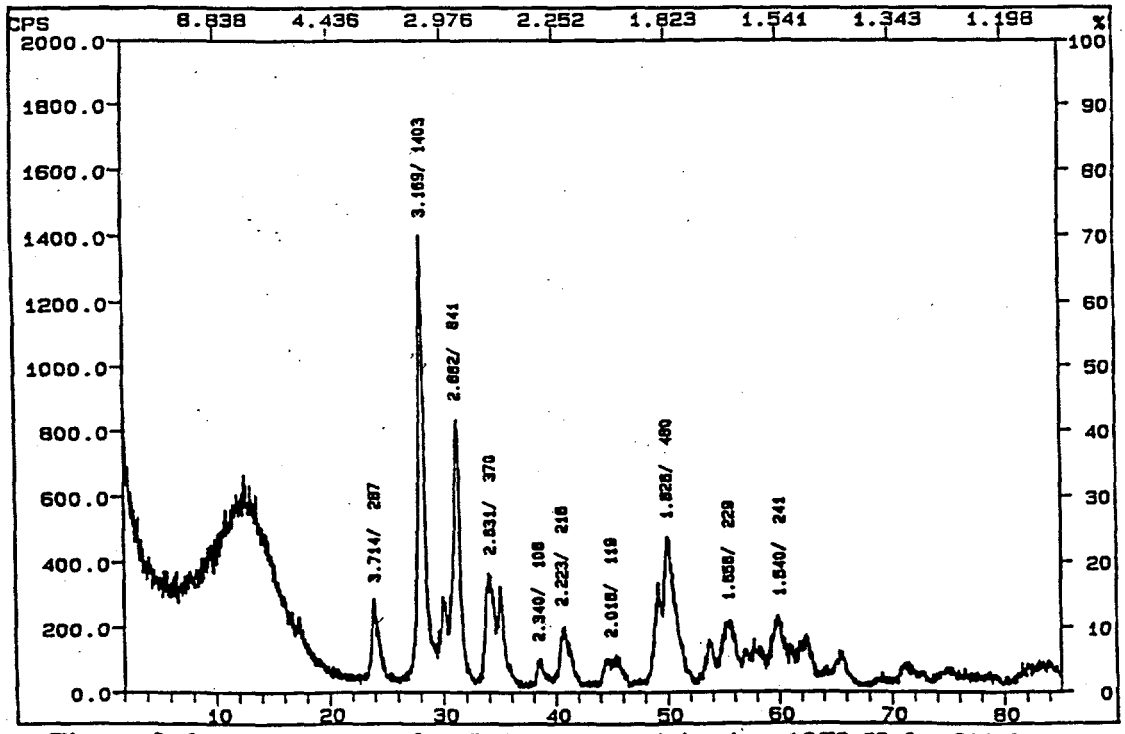

Figure 3.6. XRD pattern for ZrO_2 (ppt.) calcined at 1273 K for 2½ hours.

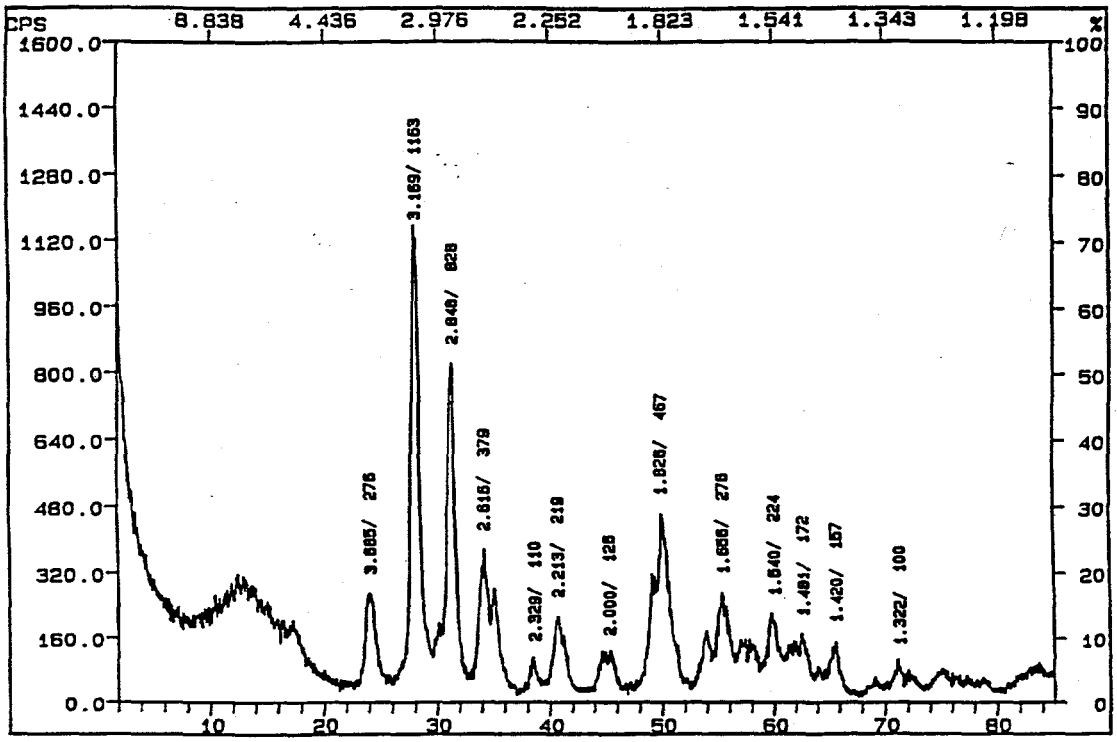

Figure 3.7. XRD pattern for ZrO_2 (ppt.) calcined at 773 K for 2½ hours.

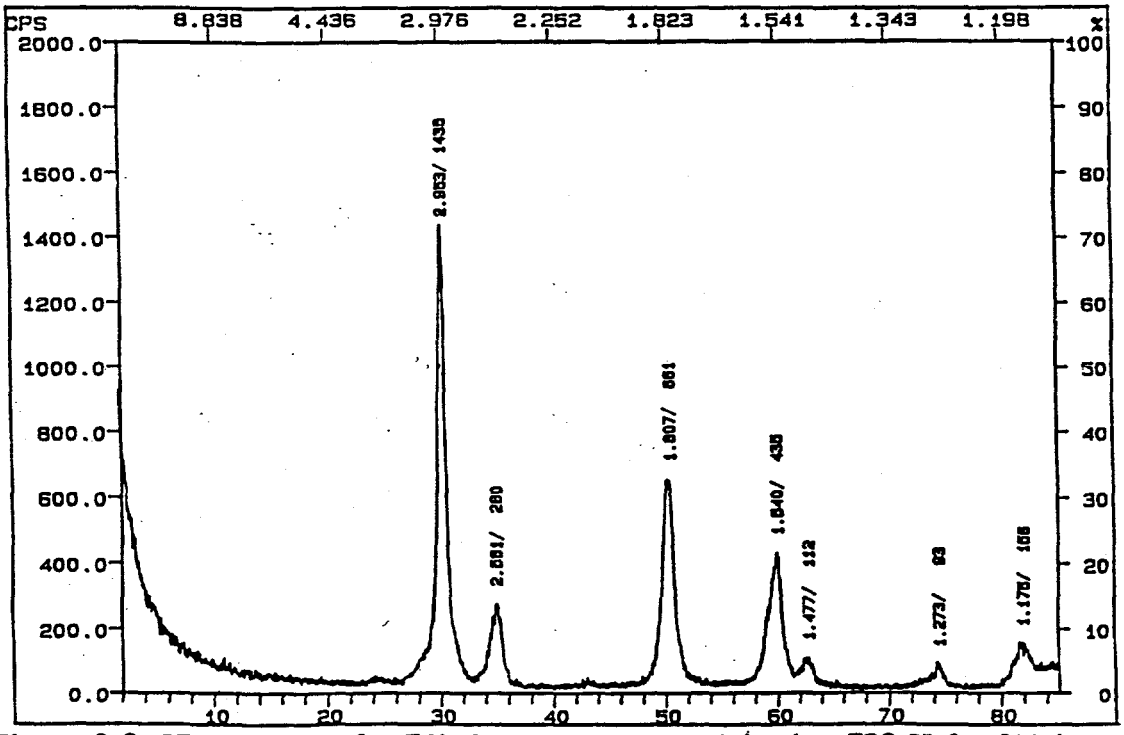

Figure 3.8. XRD pattern for 7% Ce, ZrO_2 (ppt.) calcined at 723 K for 2½ hours.

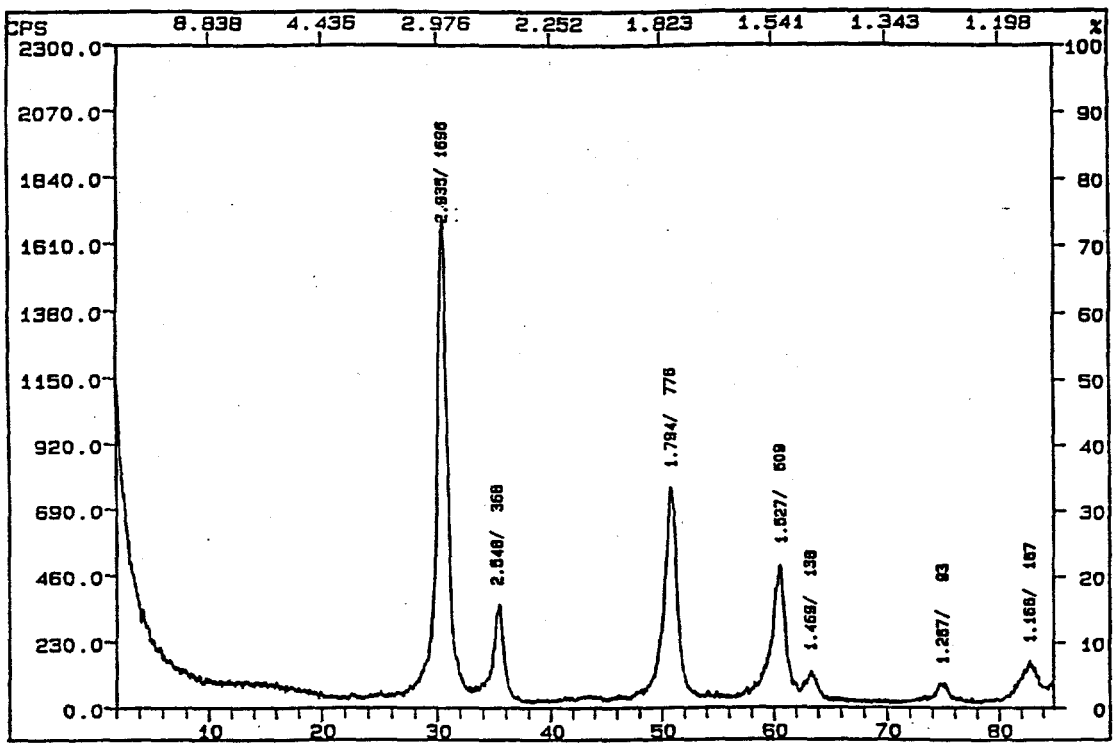

Figure 3.9. XRD pattern for 1.6% Na, 10.3% Ti, ZrO_2 (HT) calcined at 773 K for 2½ hours.

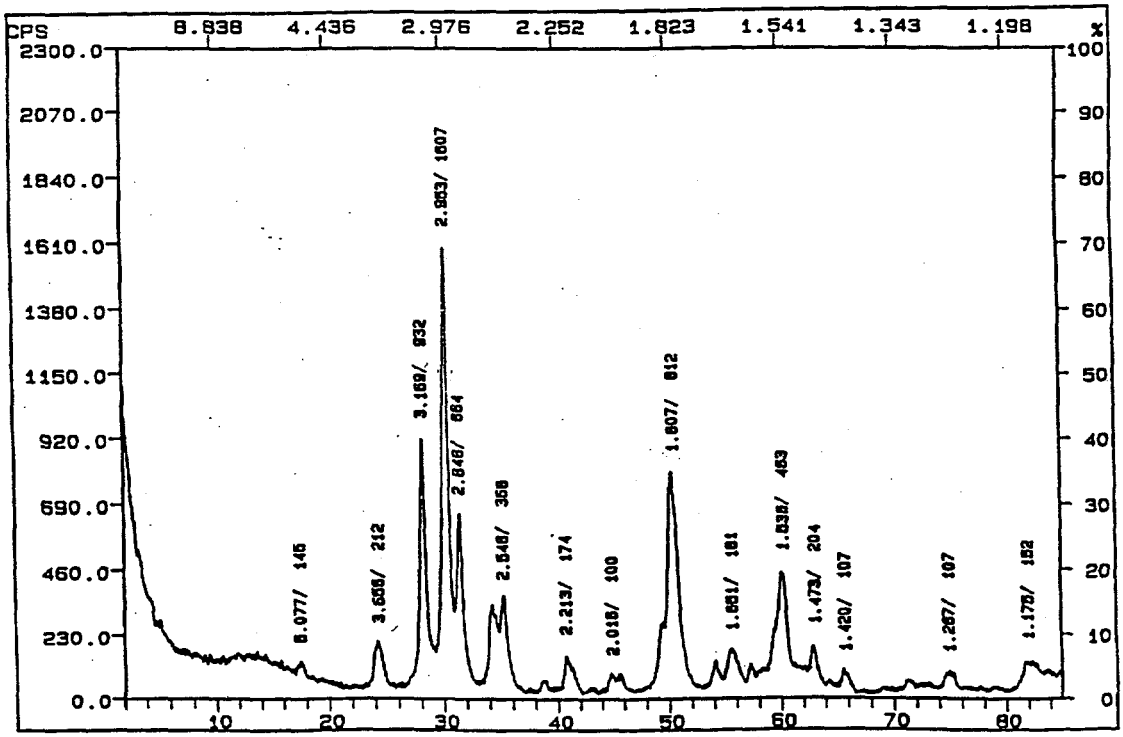

Figure 3.10. XRD pattern for ZrO_2 (CAL) calcined at 773 K for 4 hours.

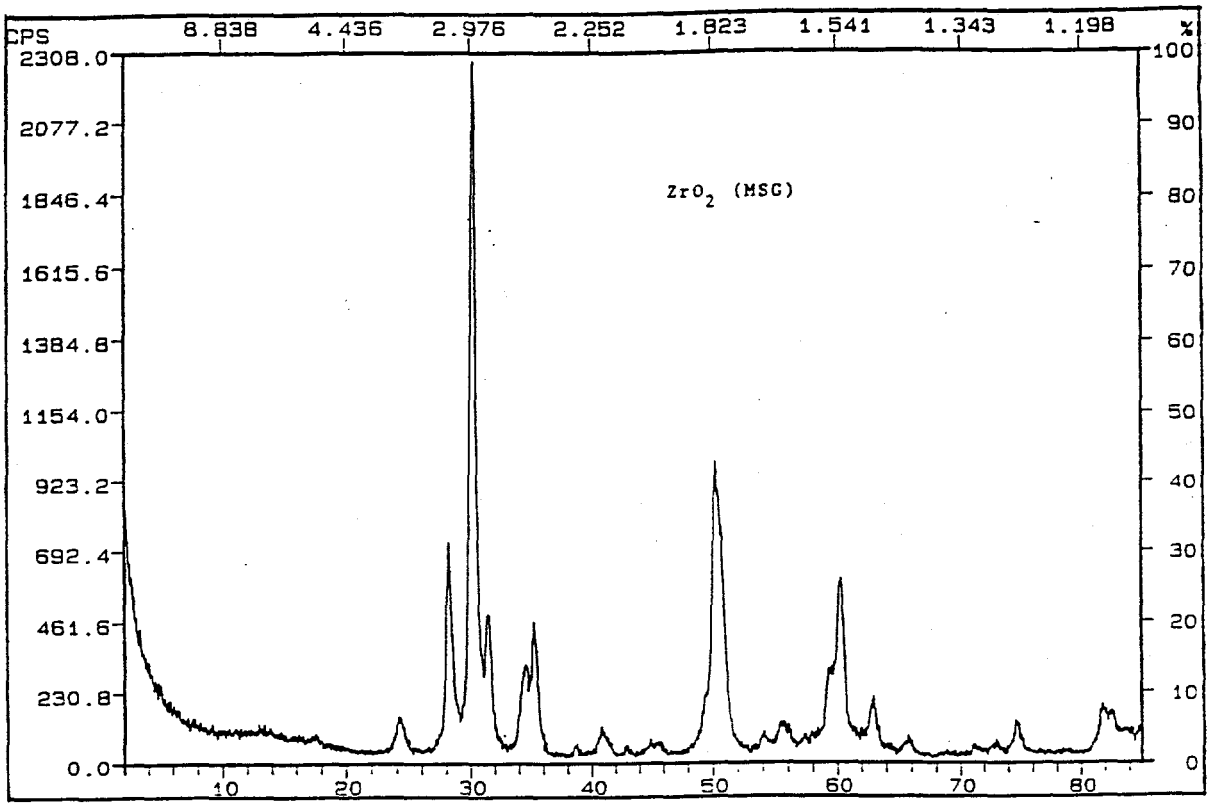

Figure 3.11. XRD pattern for ZrO_2 (MSG) calcined at 773 K for 3 hours.

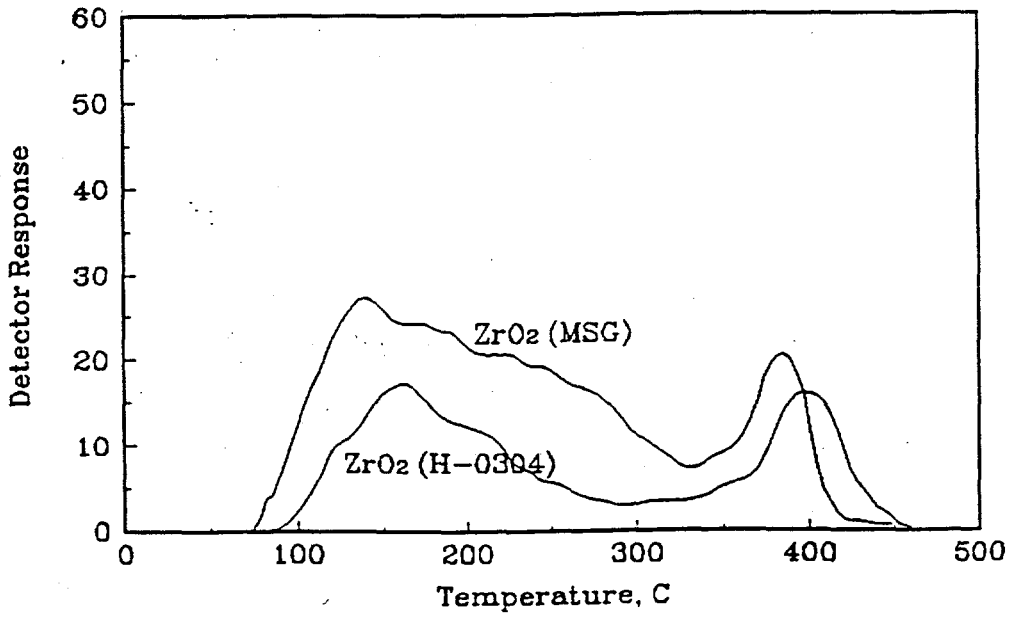

Figure 3.12. A comparison of basicity for catalysts prepared by different methods. TPD of CO_2, 0.2 g catalyst. ZrO_2 (MSG) has more basic sites.

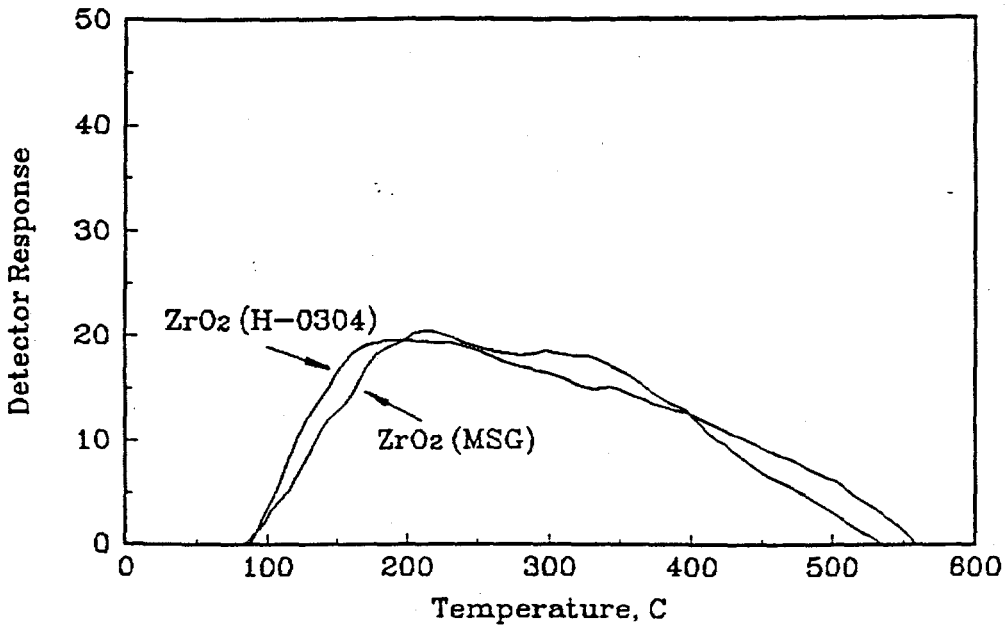

Figure 3.13. A comparison of acidity for catalysts prepared by different methods. TPD of NH_3, 0.2 g catalyst. Catalysts have similar acidity.

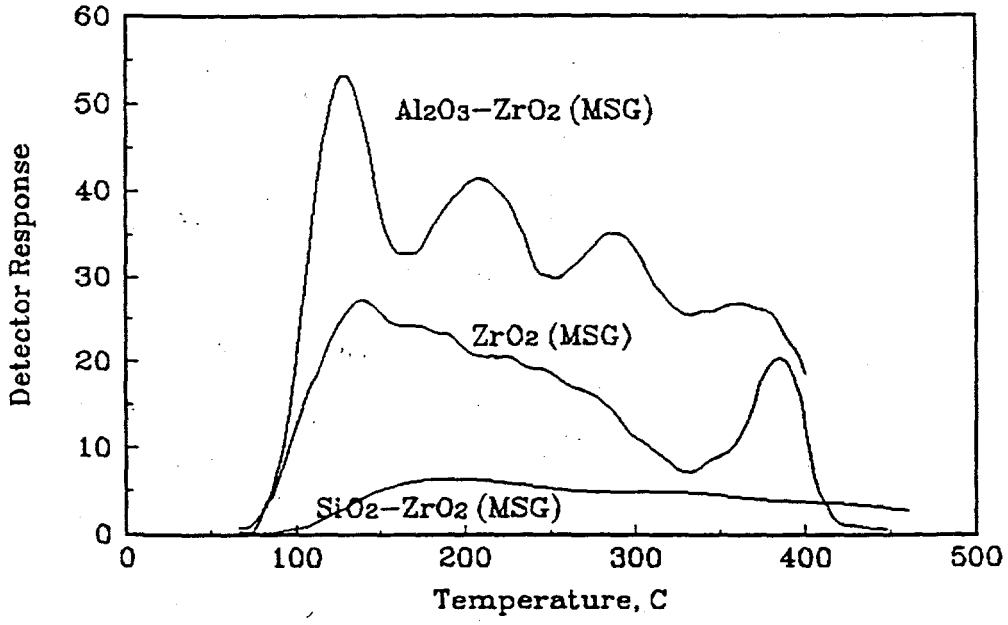

Figure 3.14. Basicity of the catalysts prepared by the modified sol gel method. TPD of CO_2, 0.2 g catalyst.

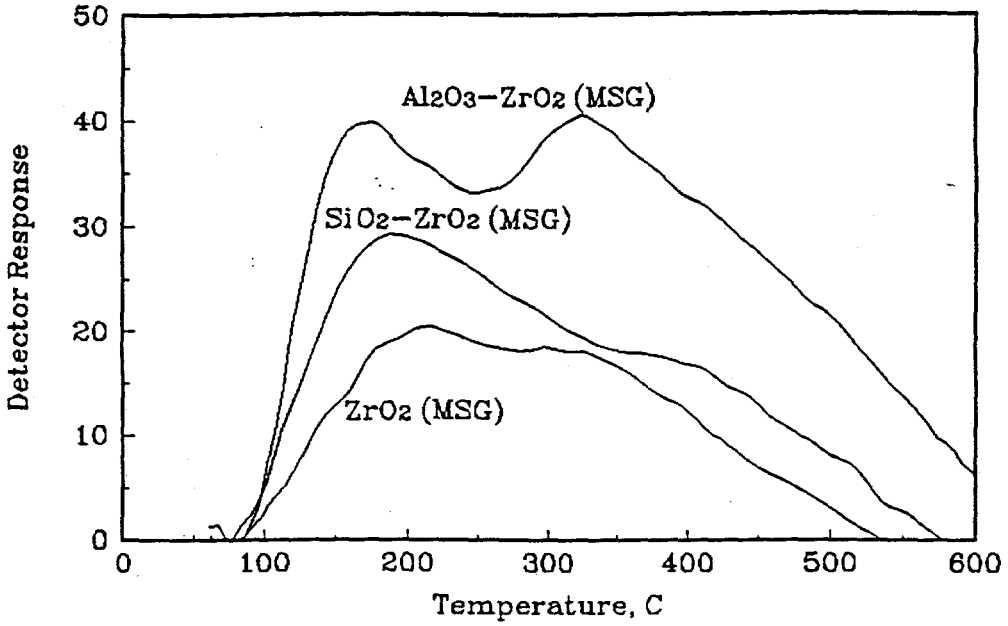

Figure 3.15. Acidity of the catalysts prepared by the modified sol gel method. TPD of NH_3, 0.2 g catalyst.

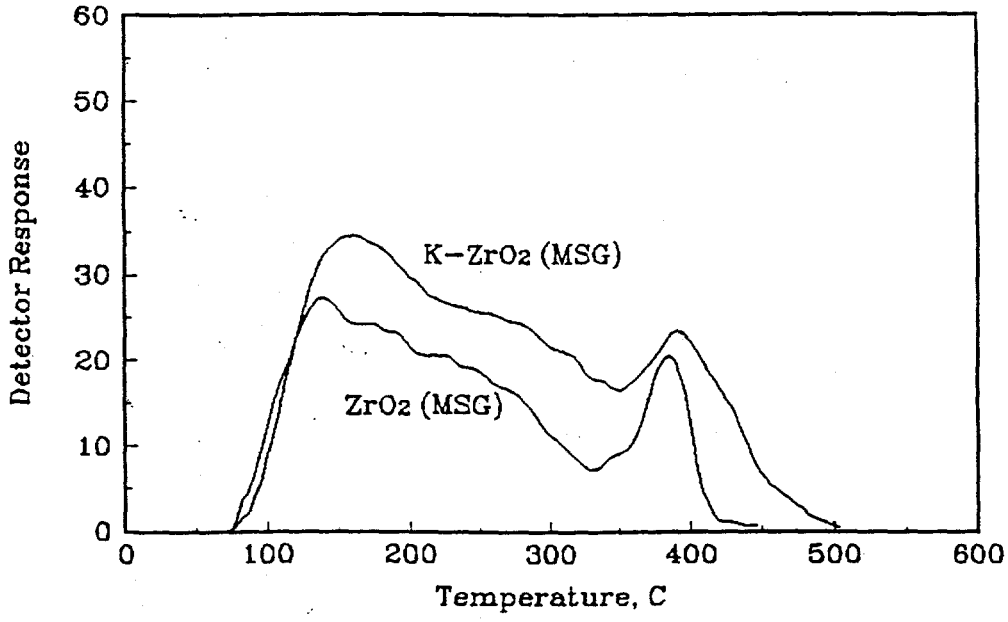

Figure 3.16. Modification of basicity by potassium. TPD of CO_2, 0.2 g catalyst.

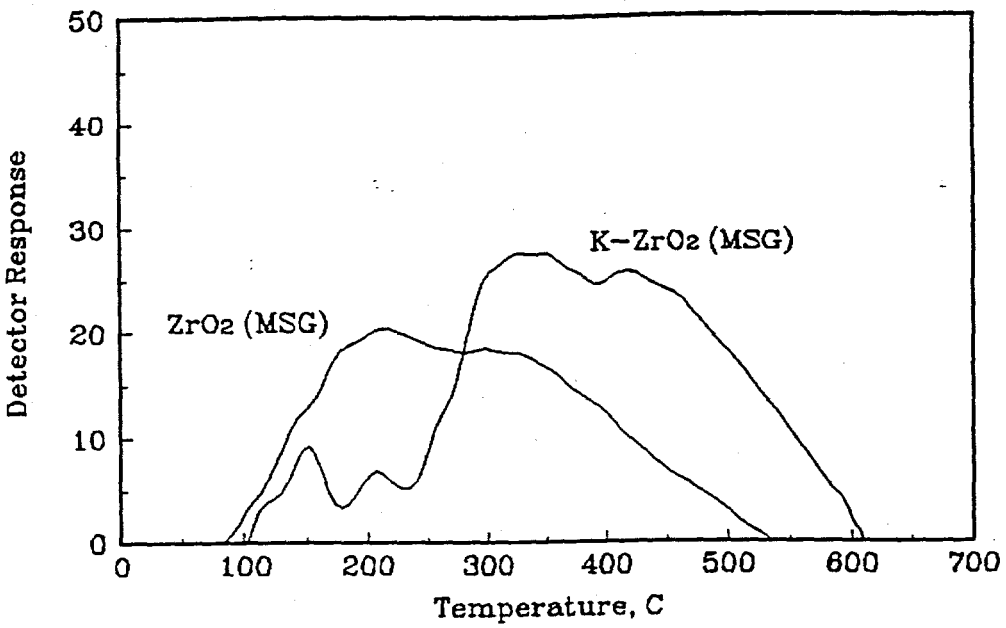

Figure 3.17. Modification of acidity by potassium. TPD of NH_3, 0.2 g catalyst.

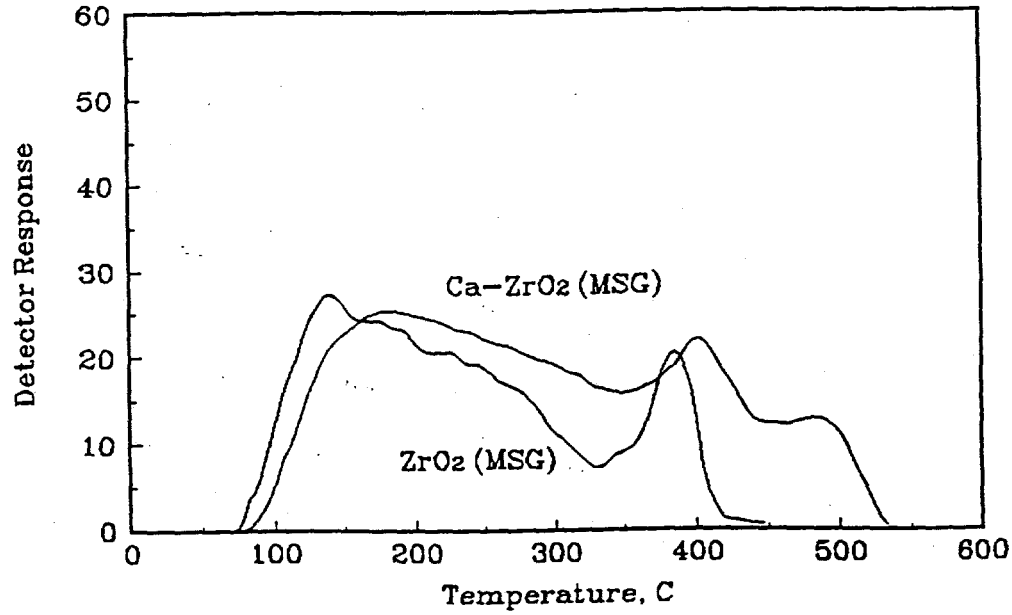

Figure 3.18. Modification of basicity by calcium. TPD of CO_2, 0.2 g catalyst.

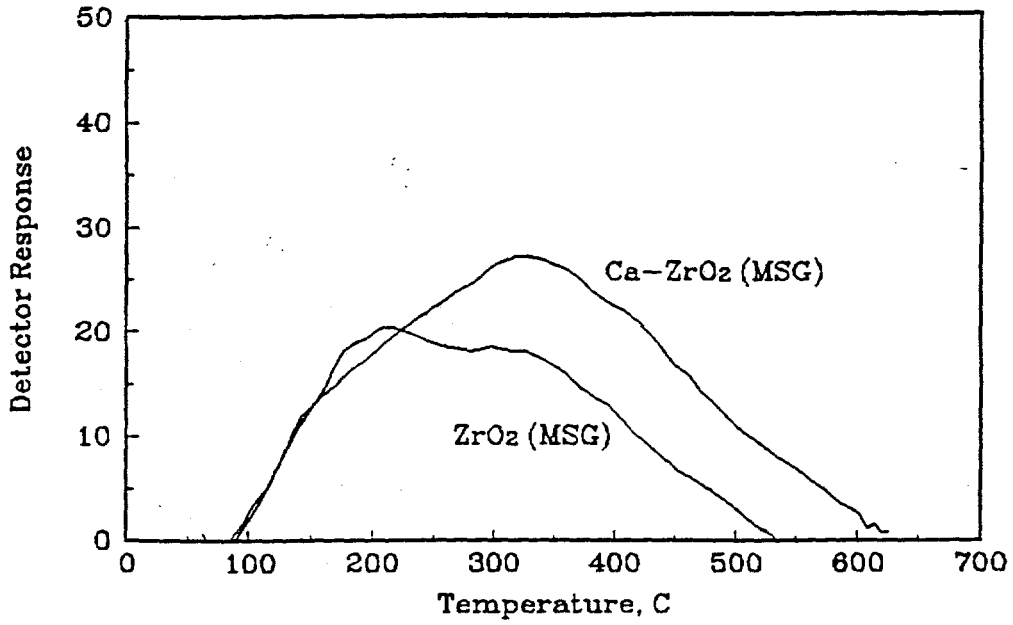

Figure 3.19. Modification of acidity by calcium. TPD of NH_3, 0.2 g catalyst.

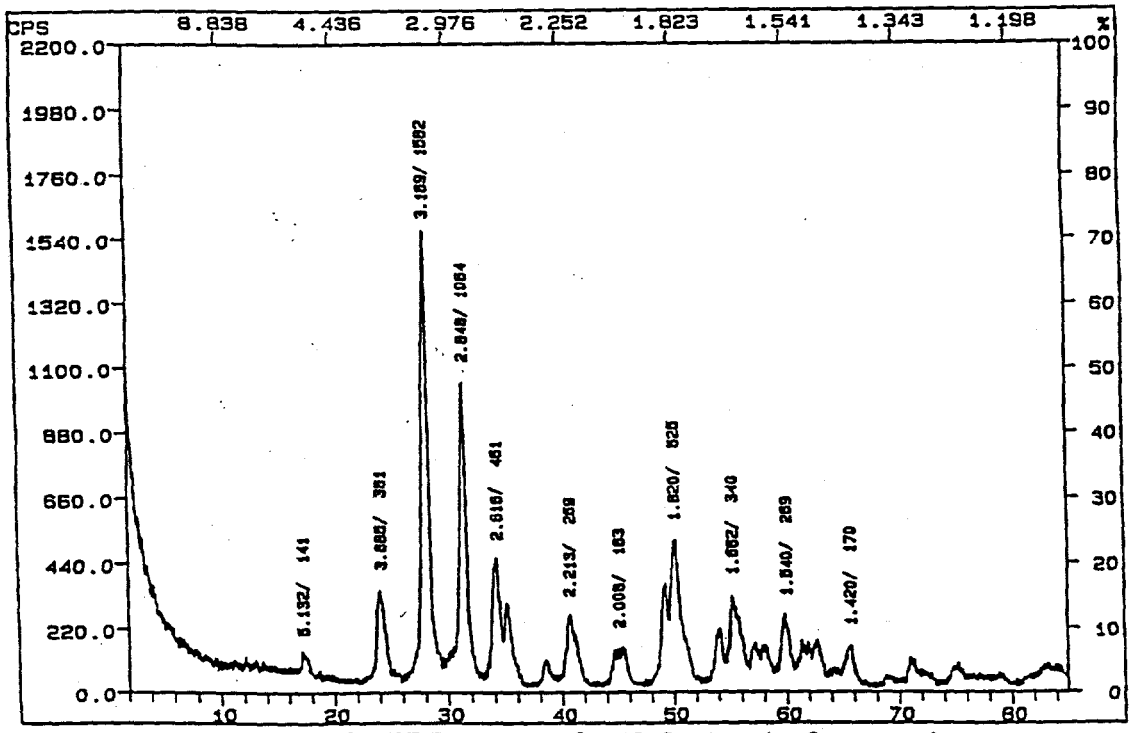

Figure 3.20. XRD pattern for ZrO_2 (ppt.) after reaction.

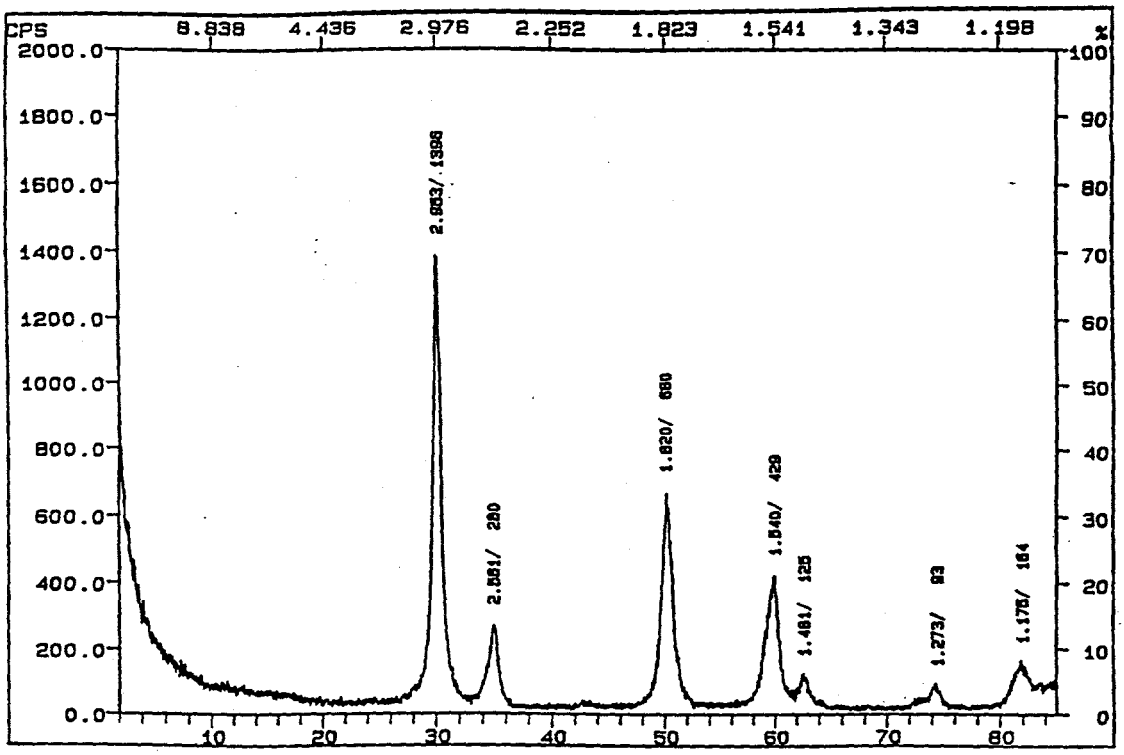

Figure 3.21. XRD pattern for 7% Ce, ZrO_2 (ppt.) after reaction.

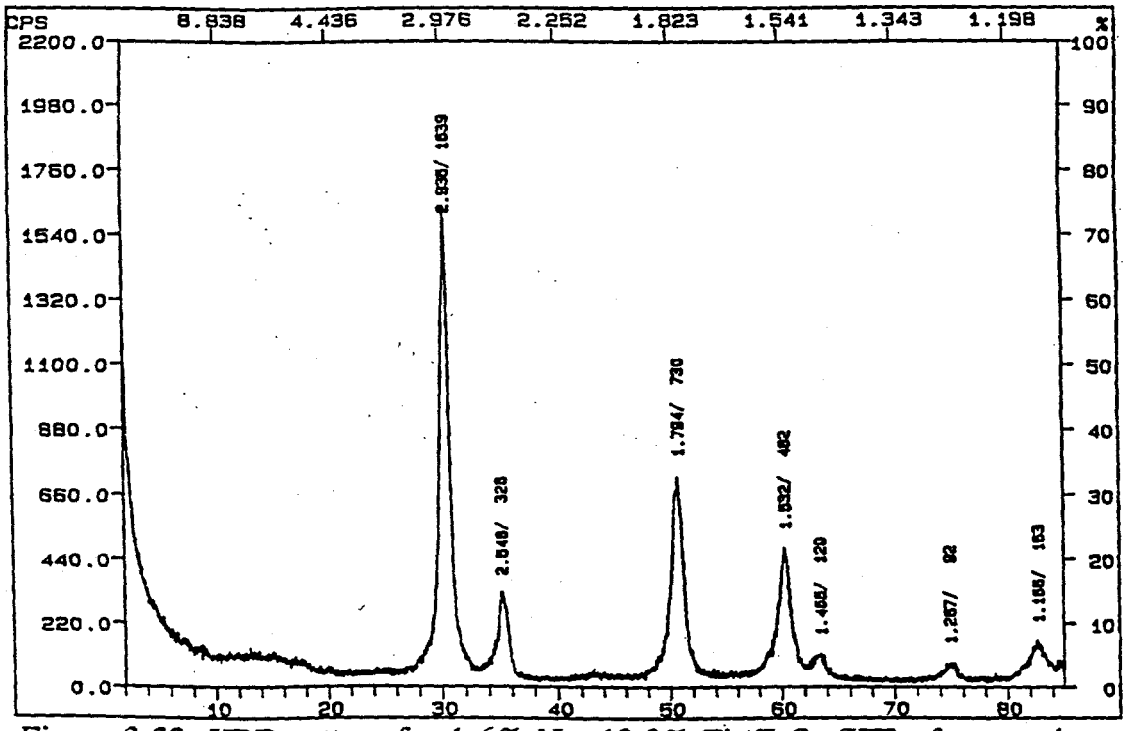

Figure 3.22. XRD pattern for 1.6% Na, 10.3% Ti, ZrO_2 (HT) after reaction.

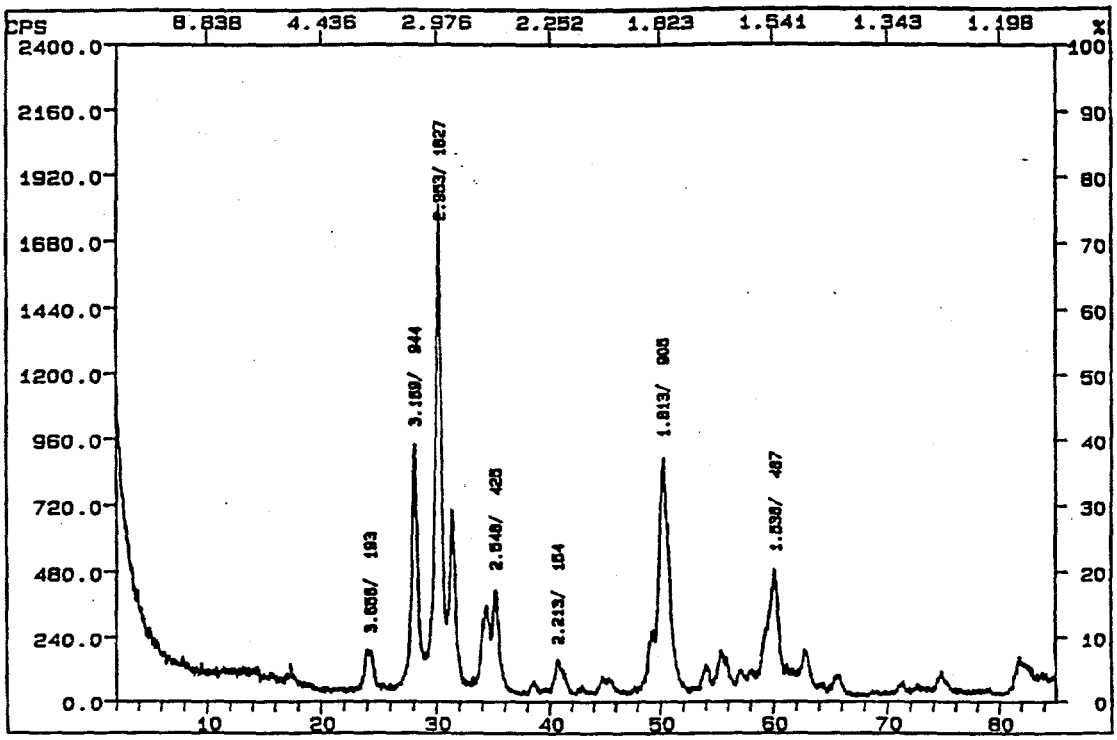

Figure 3.23. XRD pattern for ZrO_2 (CAL) after reaction.

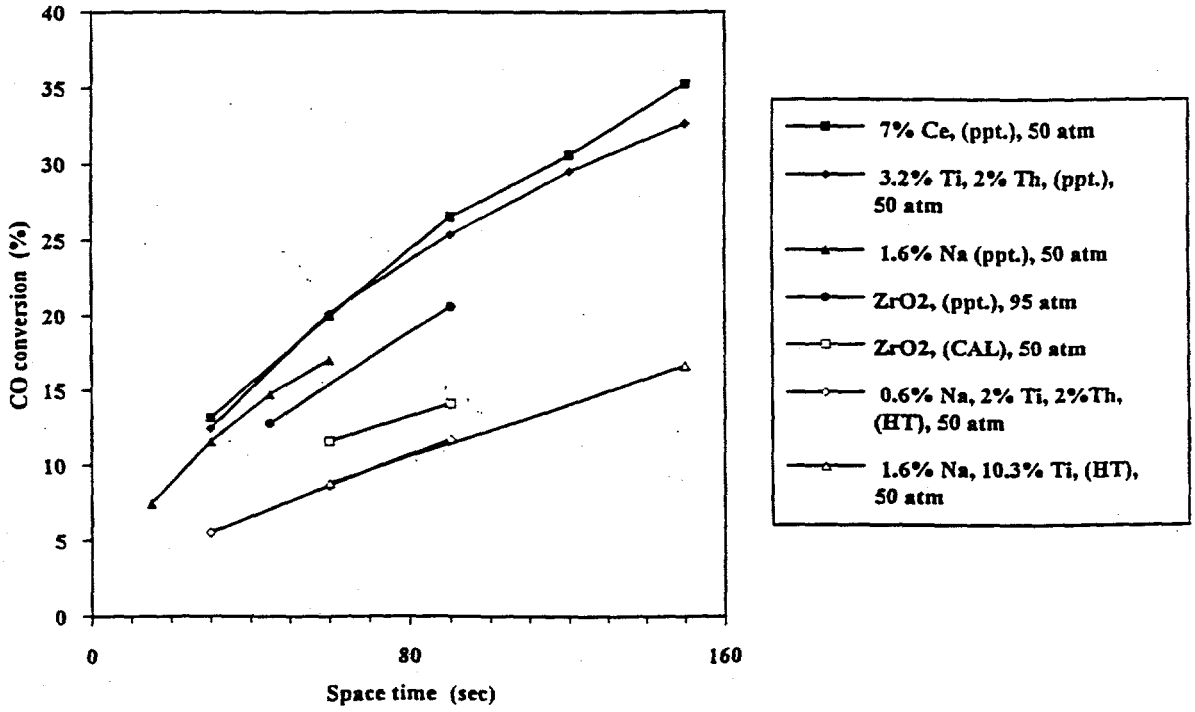

Figure 3.24. Comparison of catalytic activity for precipitated (ppt.), calcination (CAL), and hydrothermally (HT) prepared zirconias at 673 K and 1/1 CO/H_2 ratio.

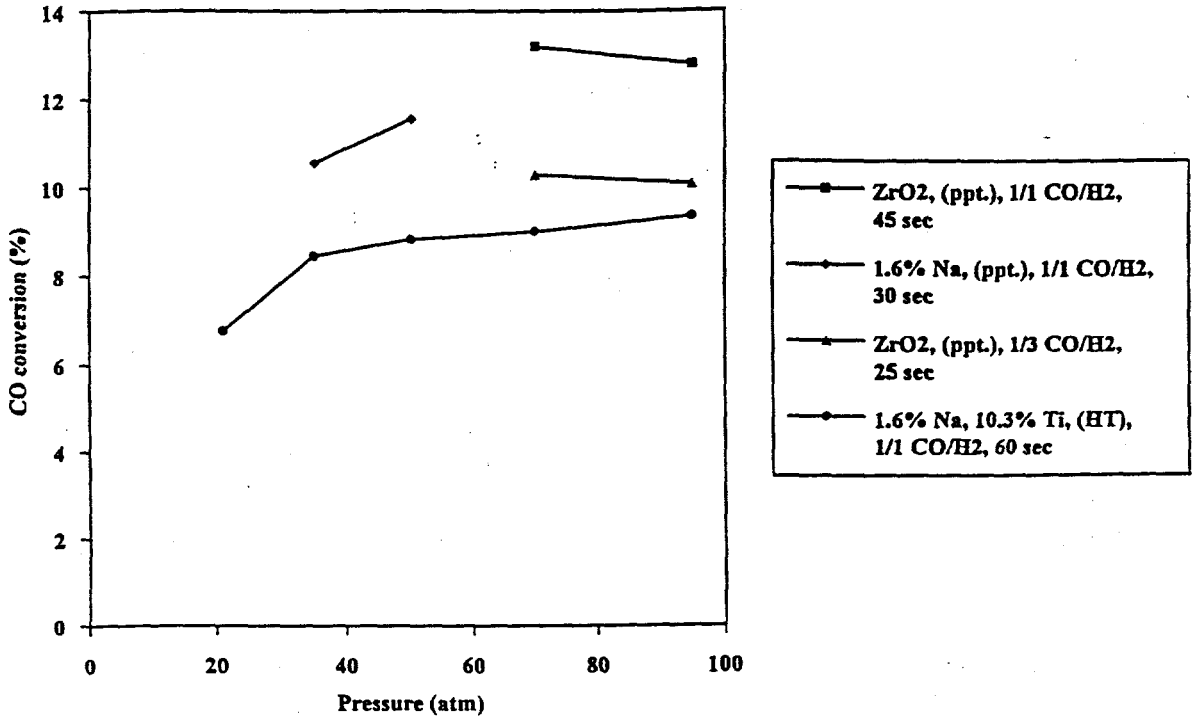

Figure 3.25. Effect of pressure on CO conversion at 673 K.

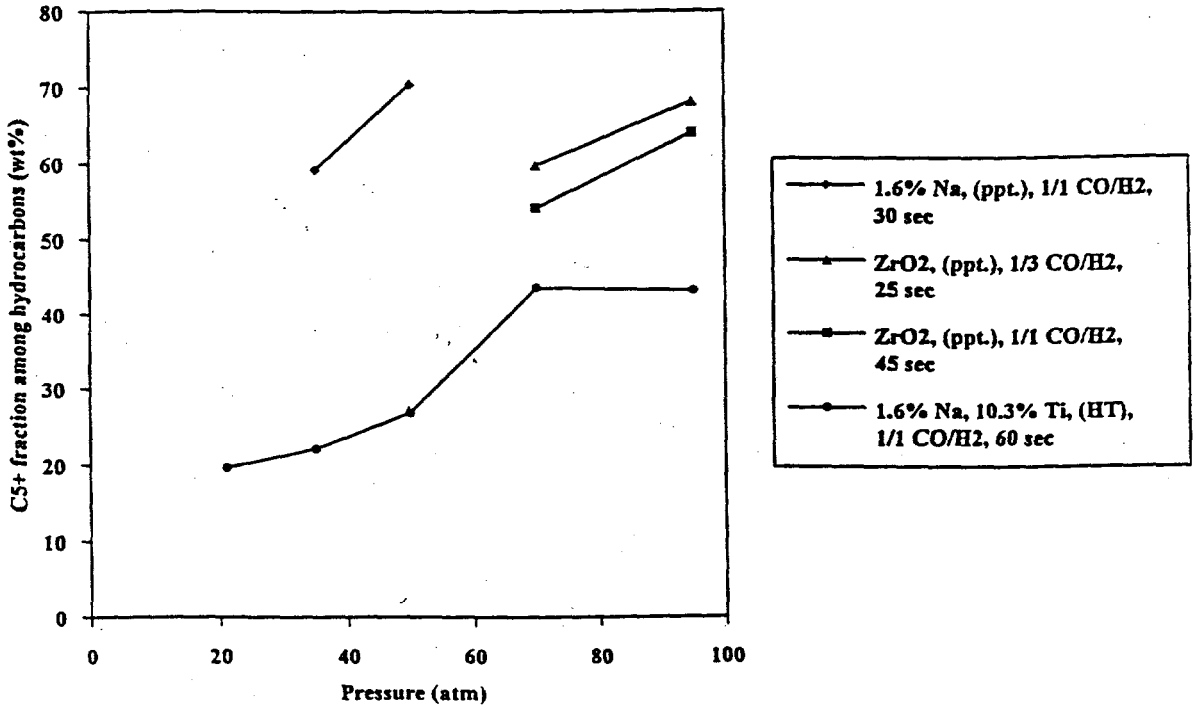

Figure 3.26. Effect of pressure on C_5+ fraction at 673 K.

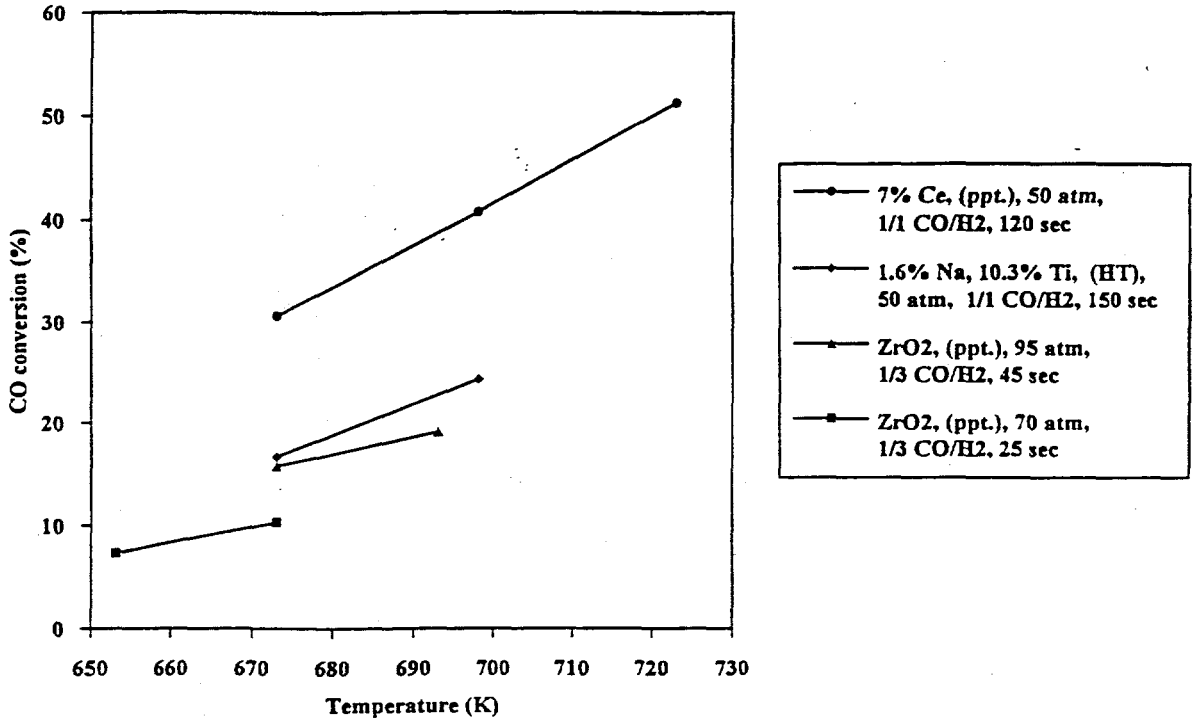

Figure 3.27. Effect of temperature on CO conversion.

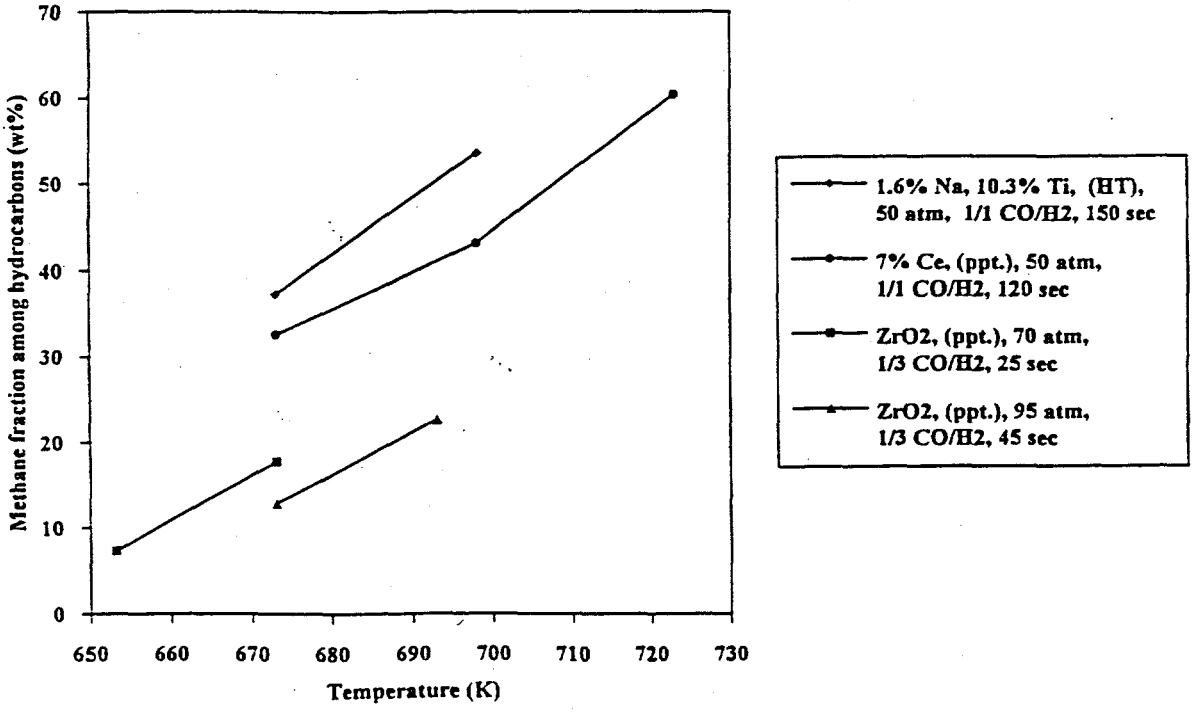

Figure 3.28. Effect of temperature on methane fraction.

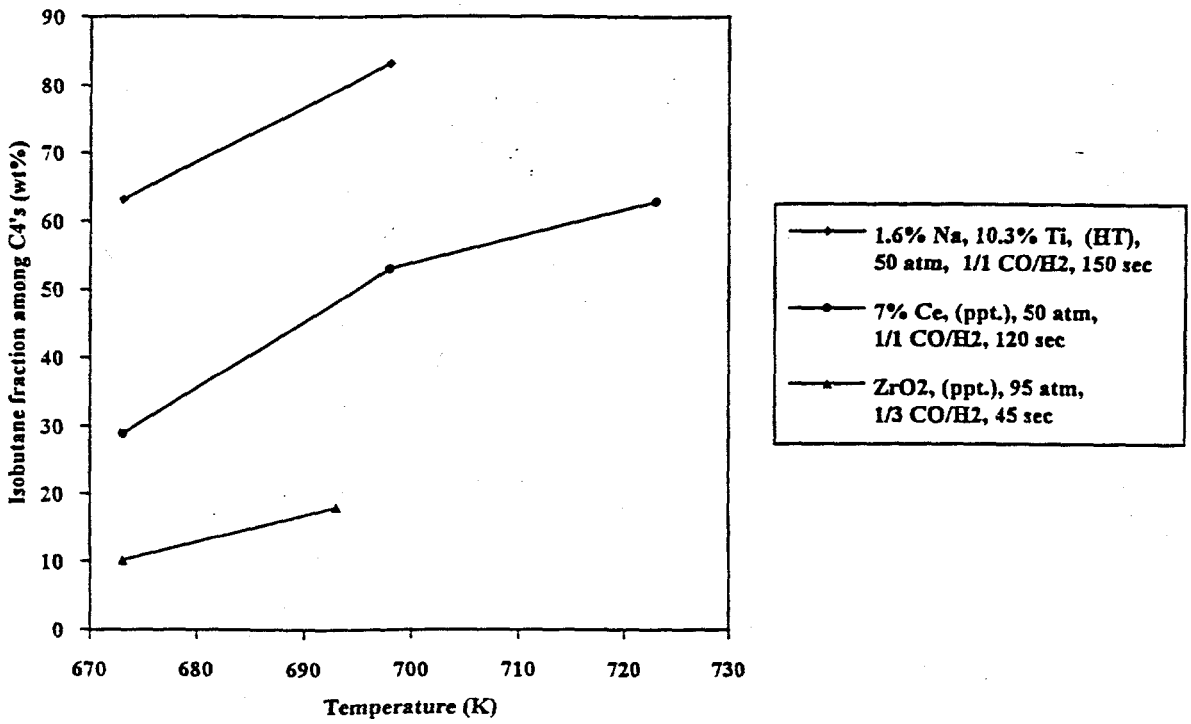

Figure 3.29. Effect of temperature on isobutane fraction among C_4's.

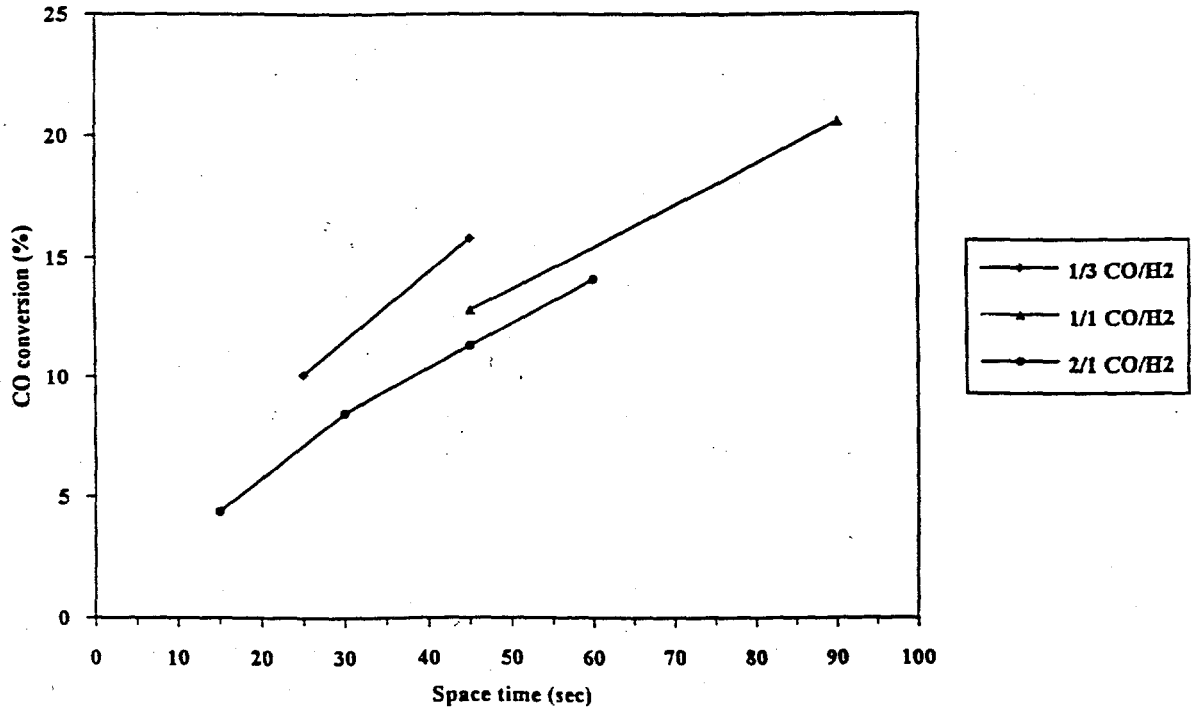

Figure 3.30. Effect of CO/H_2 ratio on CO conversion at 673 K and 95 atm over ZrO_2 (ppt.).

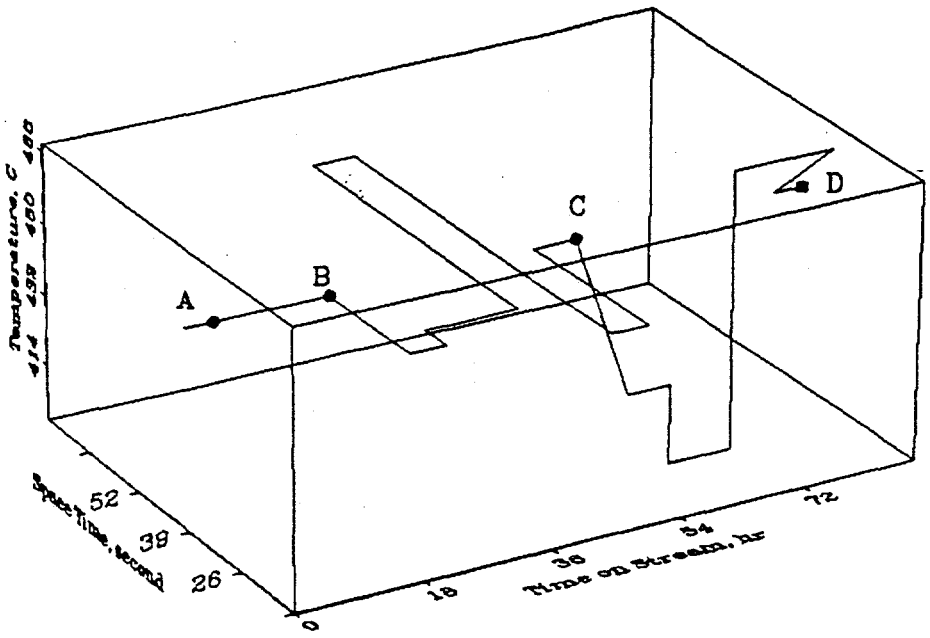

Figure 3.31. Procedure of the study of time on stream.

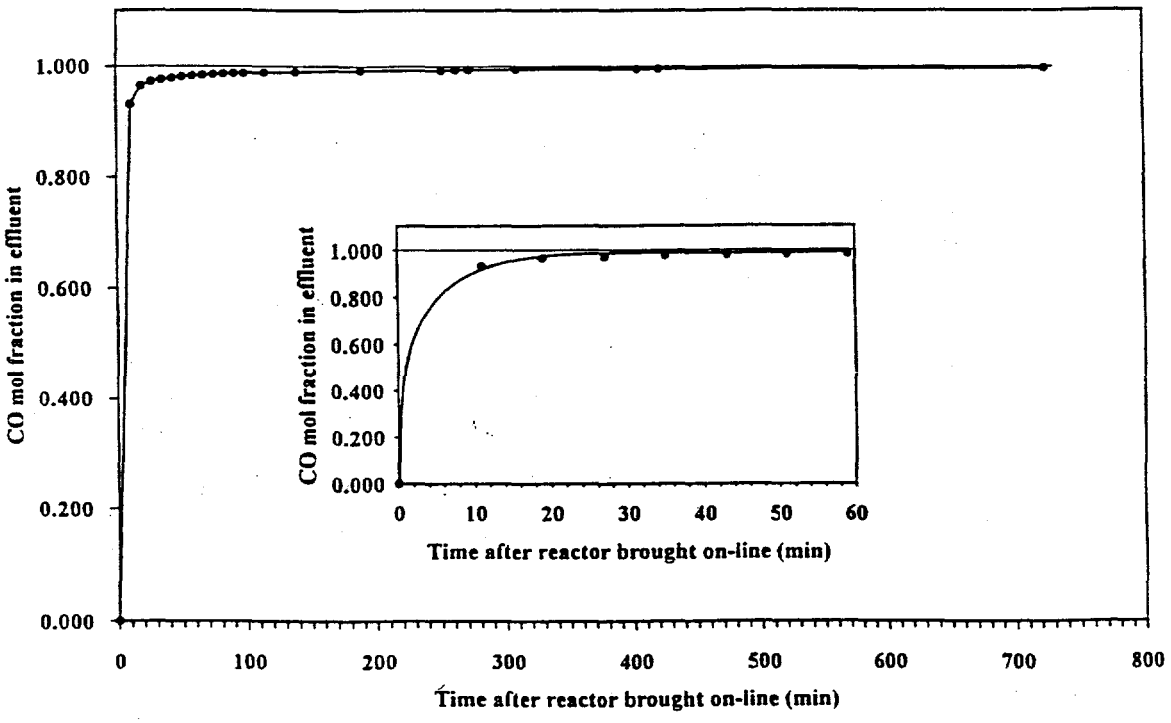

Figure 3.32. Breakthrough curve for CO over 7% Ce-ZrO_2 at 673 K, 25 atm, and 90 second space time.

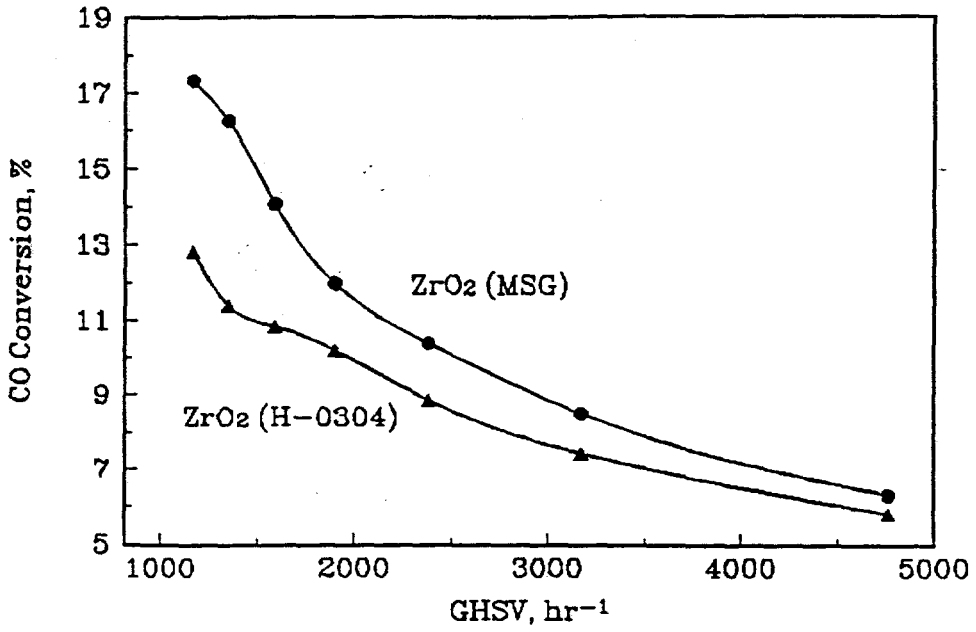

Figure 3.33. Activities of ZrO_2 (MSG) and ZrO_2 (H-0304) at 723 K, 70 atm, and 1/1 CO/H_2 ratio.

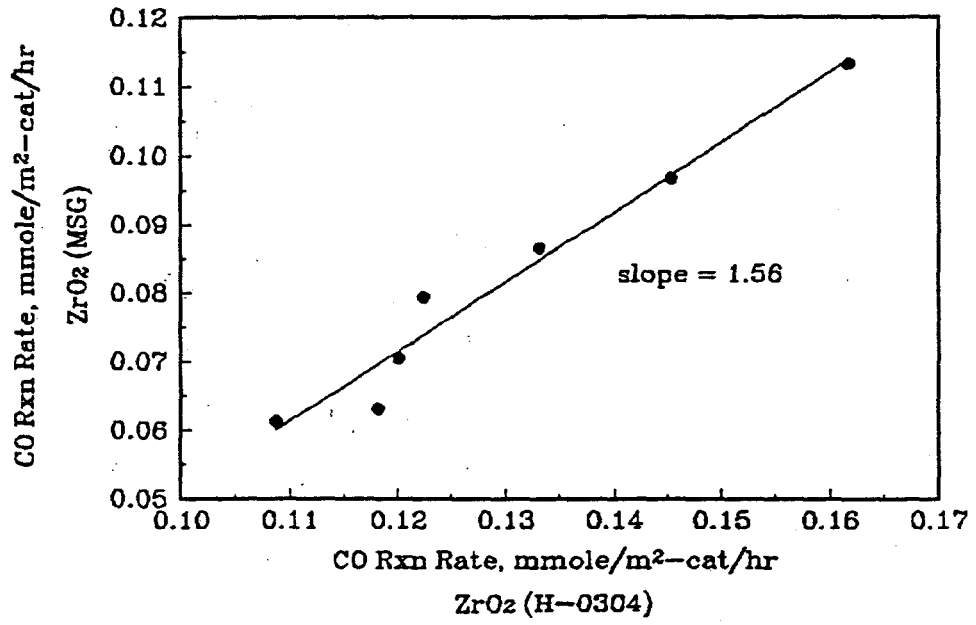

Figure 3.34. Reaction rates of CO over ZrO_2 (H-0304) and ZrO_2 (MSG) at 723 K, 70 atm, and 1/1 CO/H_2 ratio. CO reaction rates were calculated from Figure 3.33 and each scatter point corresponds to a space velocity.

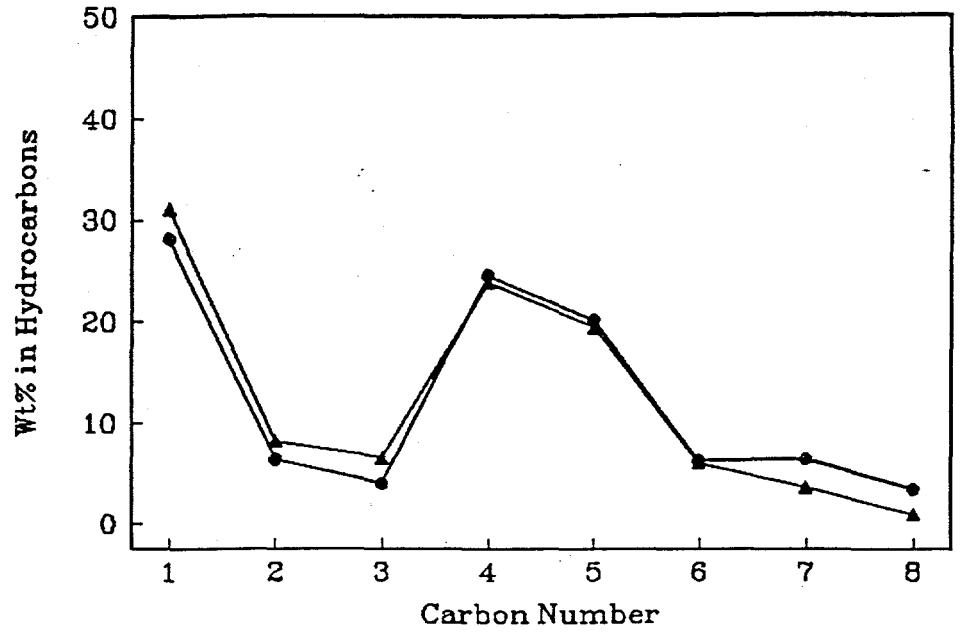

Figure 3.35. Distribution of hydrocarbons at 723 K, 70 atm, 1/1 CO/H_2 ratio, and CO conversion 11 to 12%: ▲-ZrO_2 (H-0304); ●-ZrO_2 (MSG).

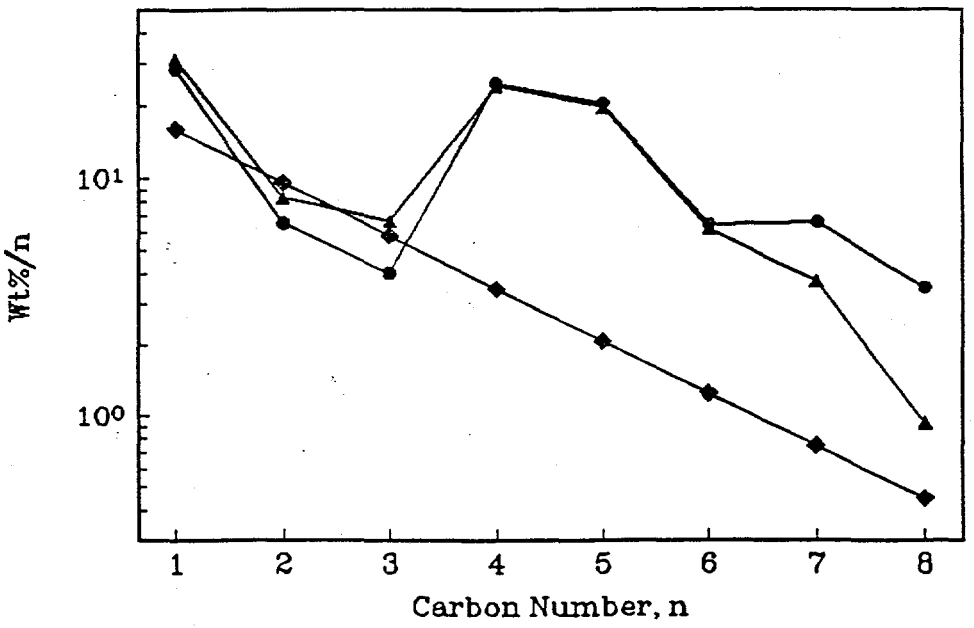

Figure 3.36. The Anderson-Schulz-Flory plots of hydrocarbon distributions for isosynthesis and Fischer-Tropsch synthesis. Isosynthesis: ▲-ZrO_2 (H-0304), ●-ZrO_2 (MSG); F-T synthesis: ◆-adapted from Dry (*27*).

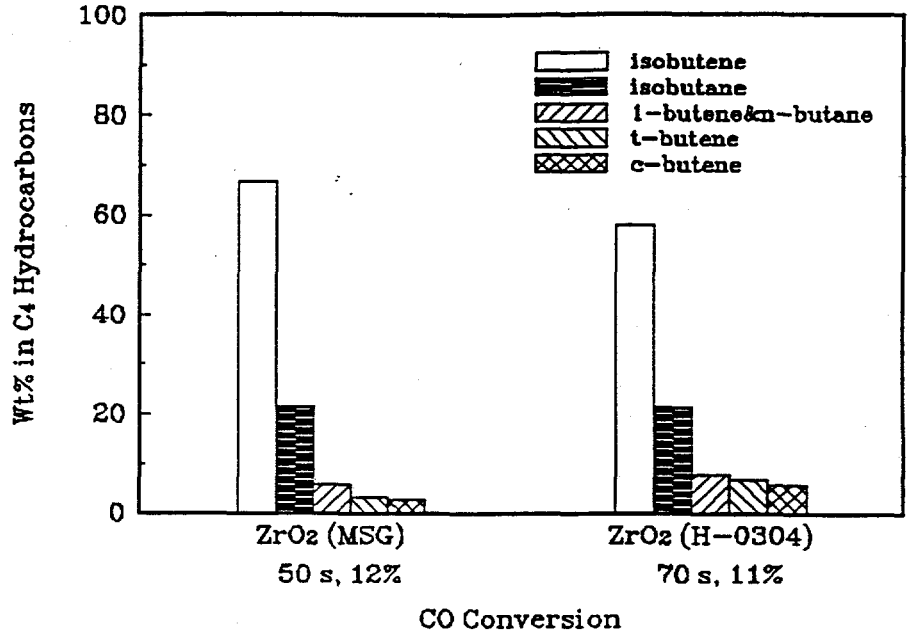

Figure 3.37. Distribution of C_4 hydrocarbons over ZrO_2 (MSG) and ZrO_2 (H-0304) at 723 K, 70 atm, and 1/1 CO/H_2 ratio.

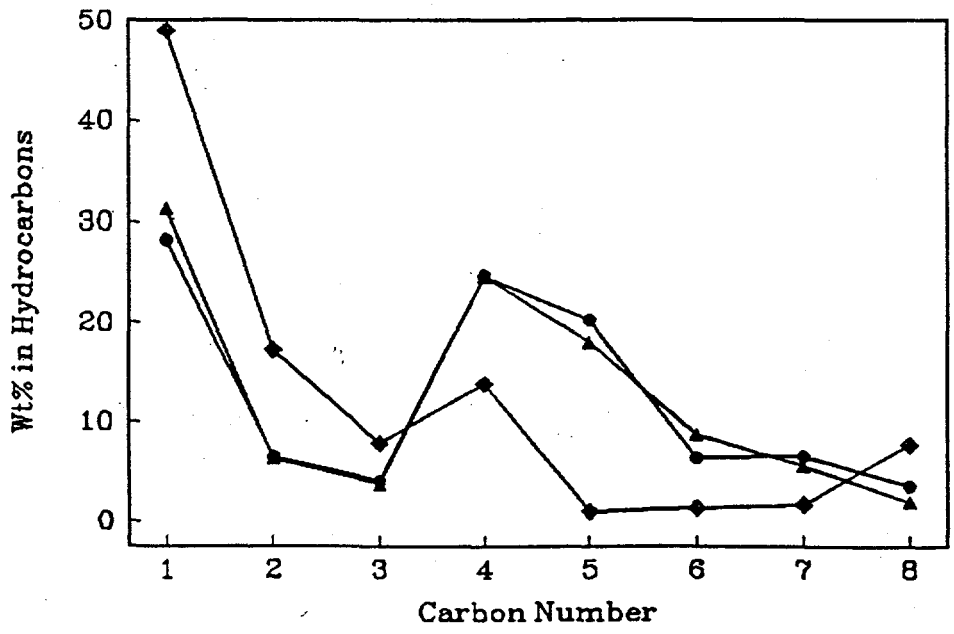

Figure 3.38. Distribution of hydrocarbons at 723 K, 70 atm, 1/1 CO/H_2 ratio, and 80 second space time: ▲-Al_2O_3-ZrO_2 (MSG), ◆-SiO_2-ZrO_2 (MSG), ●-ZrO_2 (MSG).

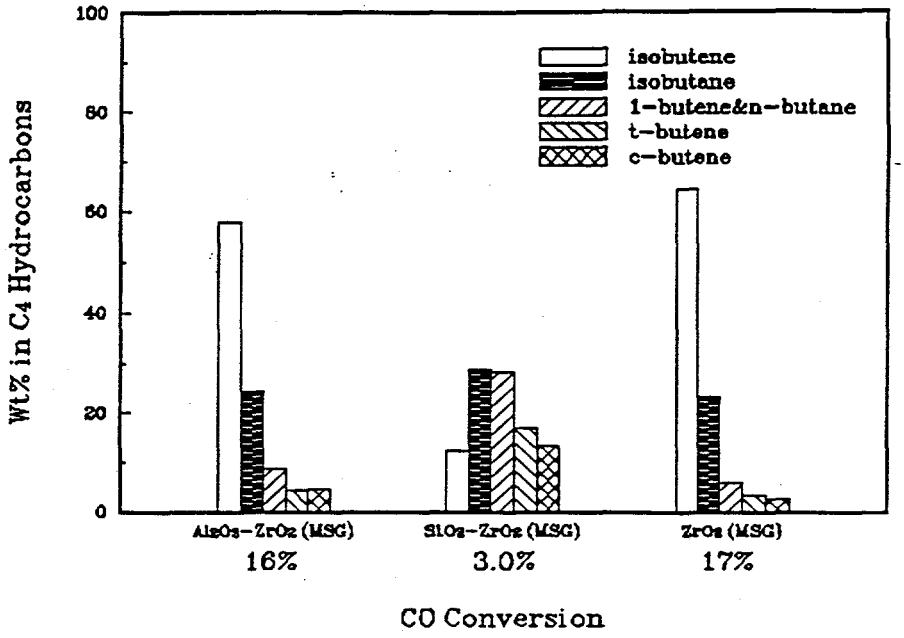

Figure 3.39. Distribution of C_4 hydrocarbons at 723 K, 70 atm, 1/1 CO/H_2 ratio, and 80 second space time.

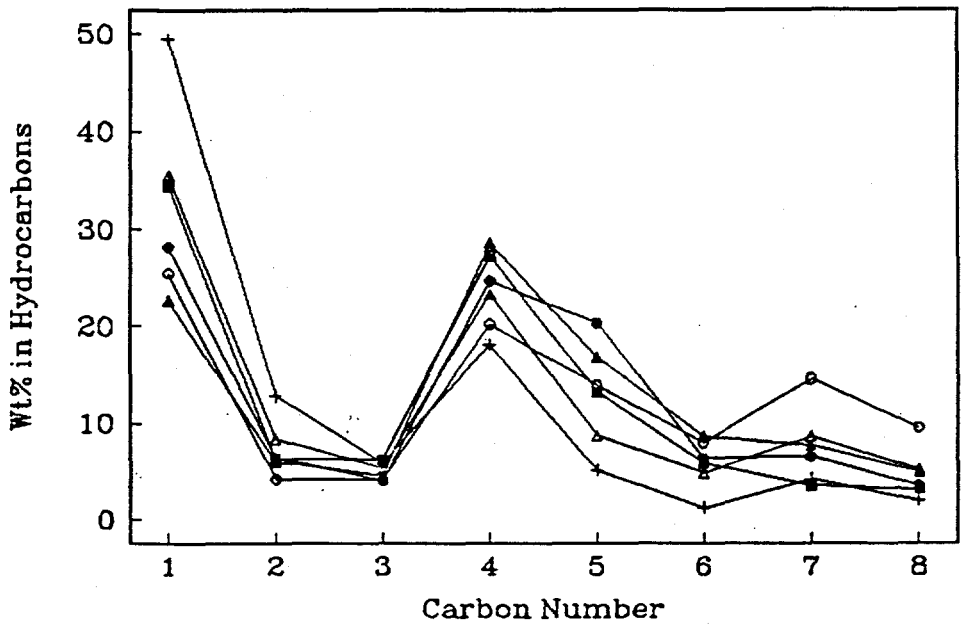

Figure 3.40. Effect of alkali metals on hydrocarbon distribution at 723 K, 70 atm, 1/1 CO/H_2 ratio, and 80 second space time: +-Li-ZrO_2 (MSG), ▵-Na-ZrO_2 (MSG), ▲-K-ZrO_2 (MSG), ○-Rb-ZrO_2 (MSG), ■-Cs-ZrO_2 (MSG), ●-ZrO_2 (MSG).

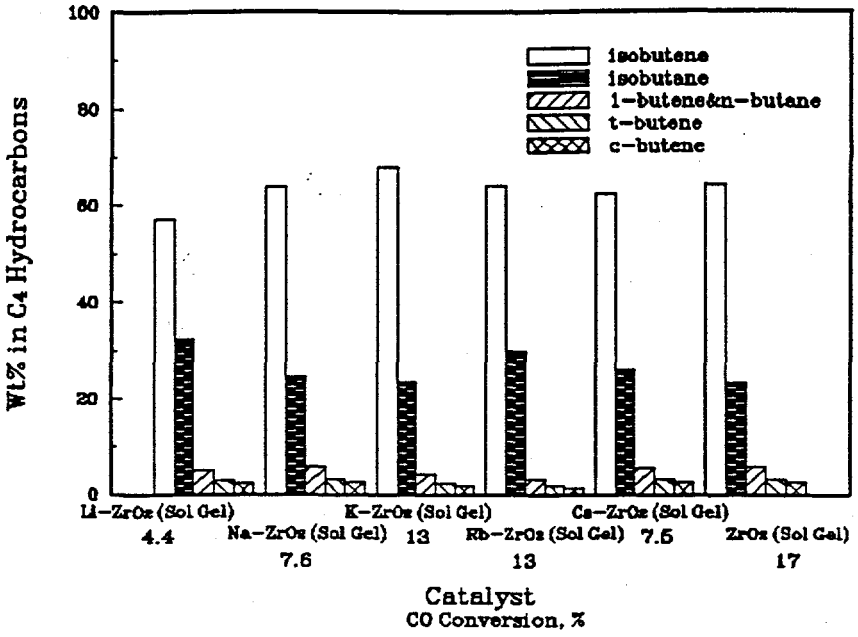

Figure 3.41. C_4 hydrocarbon distribution and CO conversion over alkali promoted catalysts at 723 K, 70 atm, 1/1 CO/H_2 ratio, and 80 second space time.

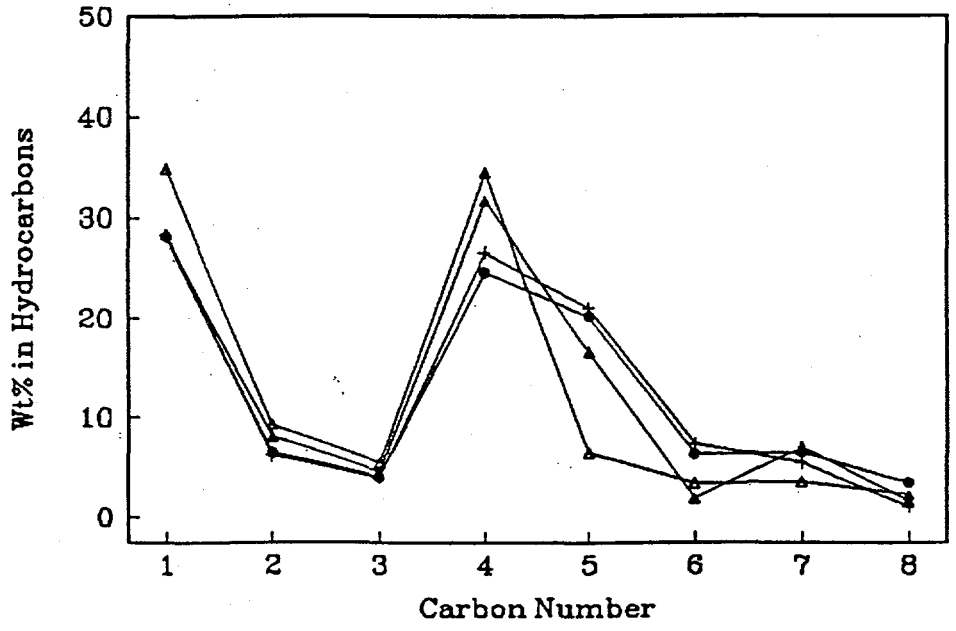

Figure 3.42. Effect of alkaline earth metals on hydrocarbon distribution at 723 K, 70 atm, 1/1 CO/H_2 ratio, and 80 second space time: +-Mg-ZrO_2 (MSG), ▲-Ca-ZrO_2 (MSG), △-Ba-ZrO_2 (MSG), ●-ZrO_2 (MSG).

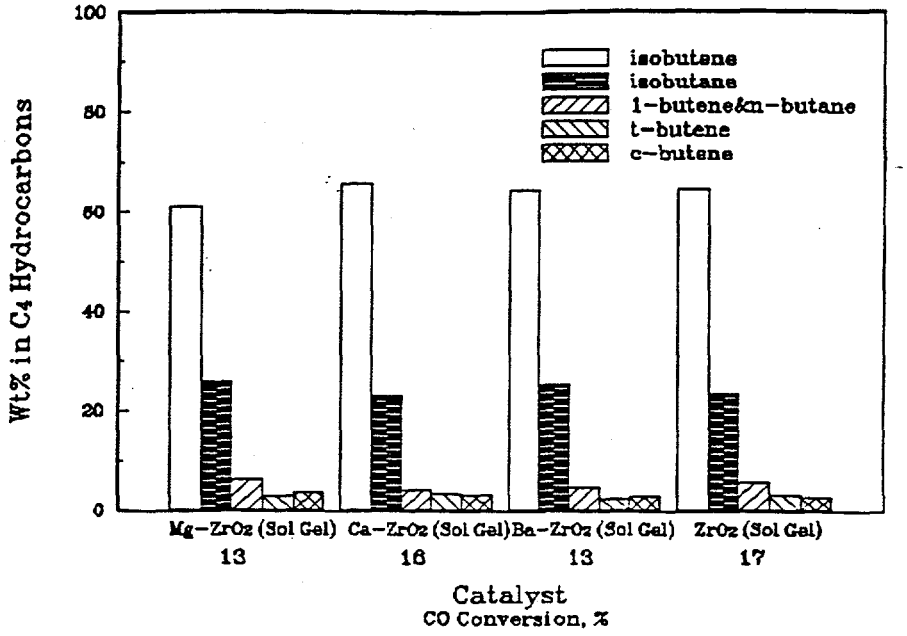

Figure 3.43. C_4 hydrocarbon distribution and CO conversion over alkaline promoted catalysts at 723 K, 70 atm, 1/1 CO/H_2 ratio, and 80 second space time.

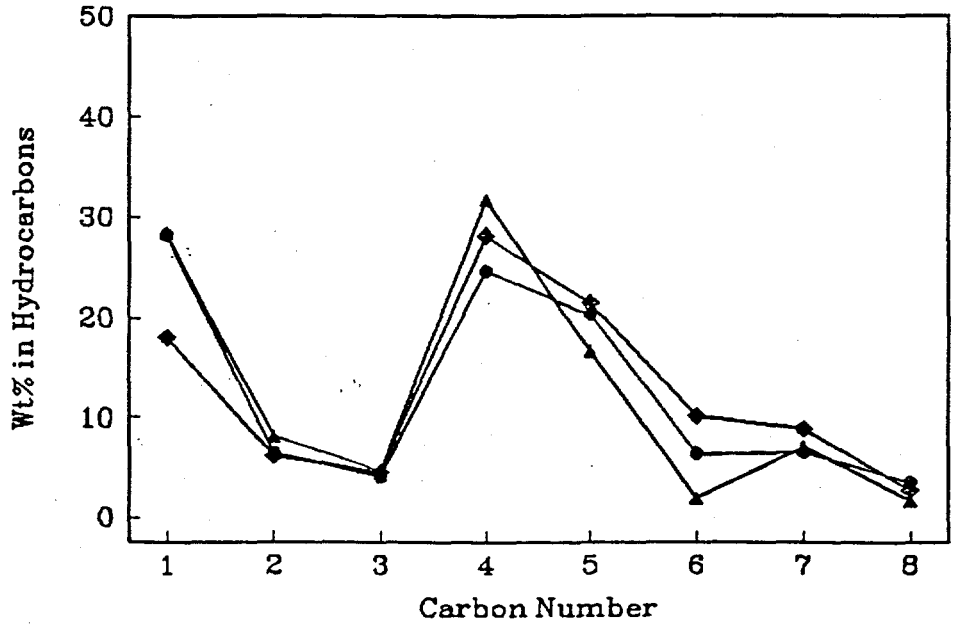

Figure 3.44. Effect of calcium loading on hydrocarbon distribution at 723 K, 70 atm, 1/1 CO/H_2 ratio, and 80 second space time: ◆-Ca(2%)-ZrO_2 (MSG), ▲-Ca-ZrO_2 (MSG), ●-ZrO_2 (MSG).

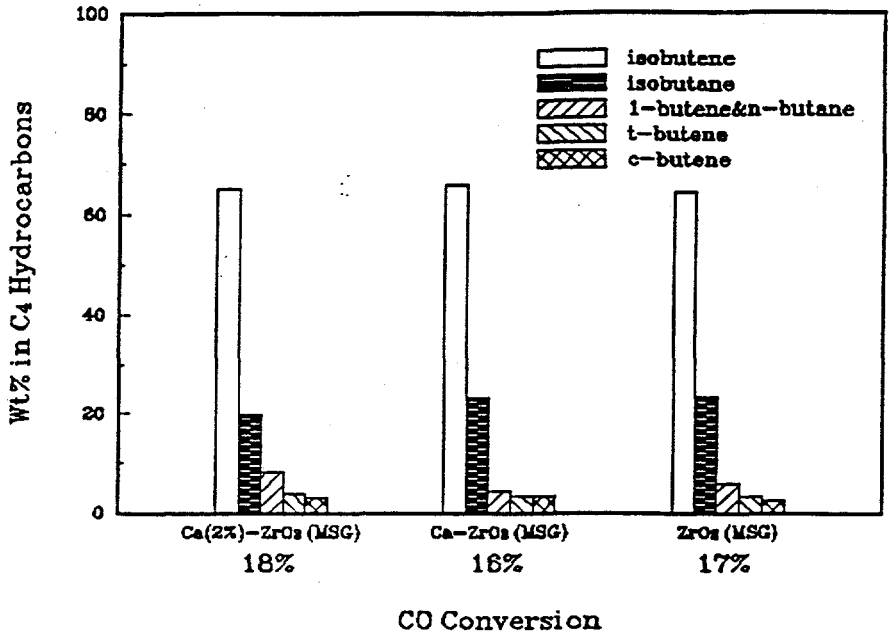

Figure 3.45. Effect of calcium loading on C_4 hydrocarbon distribution at 723 K, 70 atm, 1/1 CO/H_2 ratio, and 80 second space time.

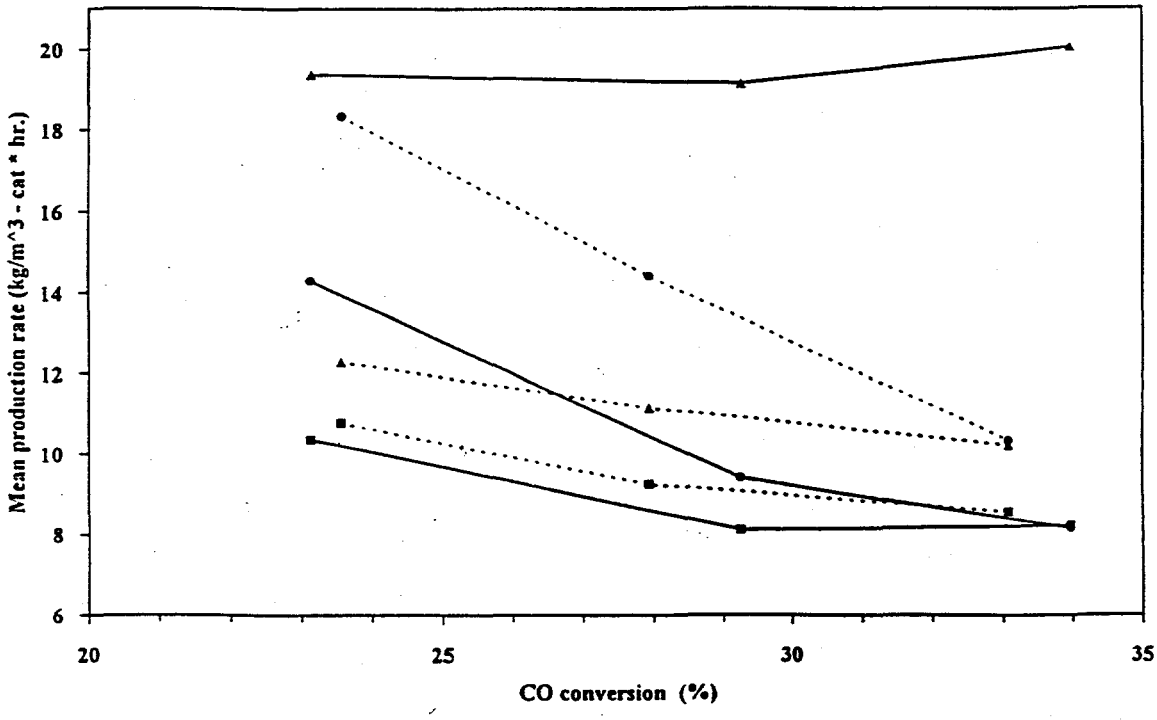

Figure 3.46. Comparison of mean production rates for non-H_2S (solid line) and H_2S (dashed line) runs for methane (▲), total C_4 (■), and C_5+ (●) at 673 K, 50 atm, and 1/1 CO/H_2 [or $CO/(H_2+H_2S)$] ratio.

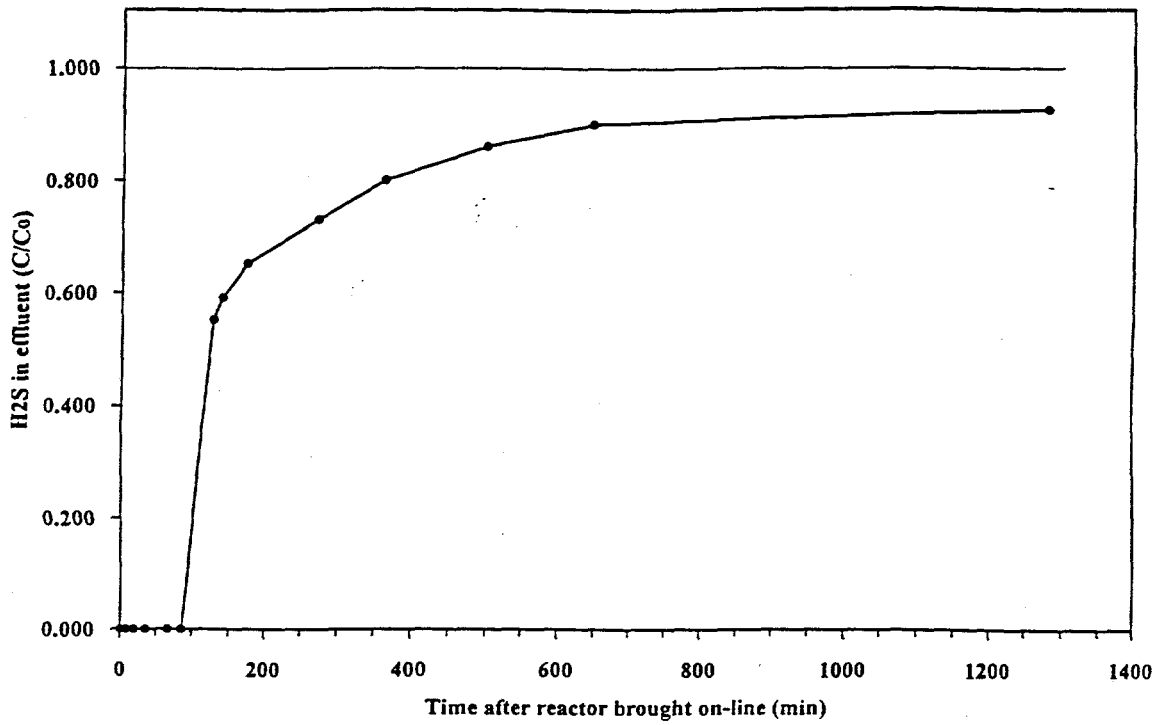

Figure 3.47. Breakthrough curve for H_2S over 7% Ce-ZrO_2 at 673 K, 25 atm, and 90 second space time.

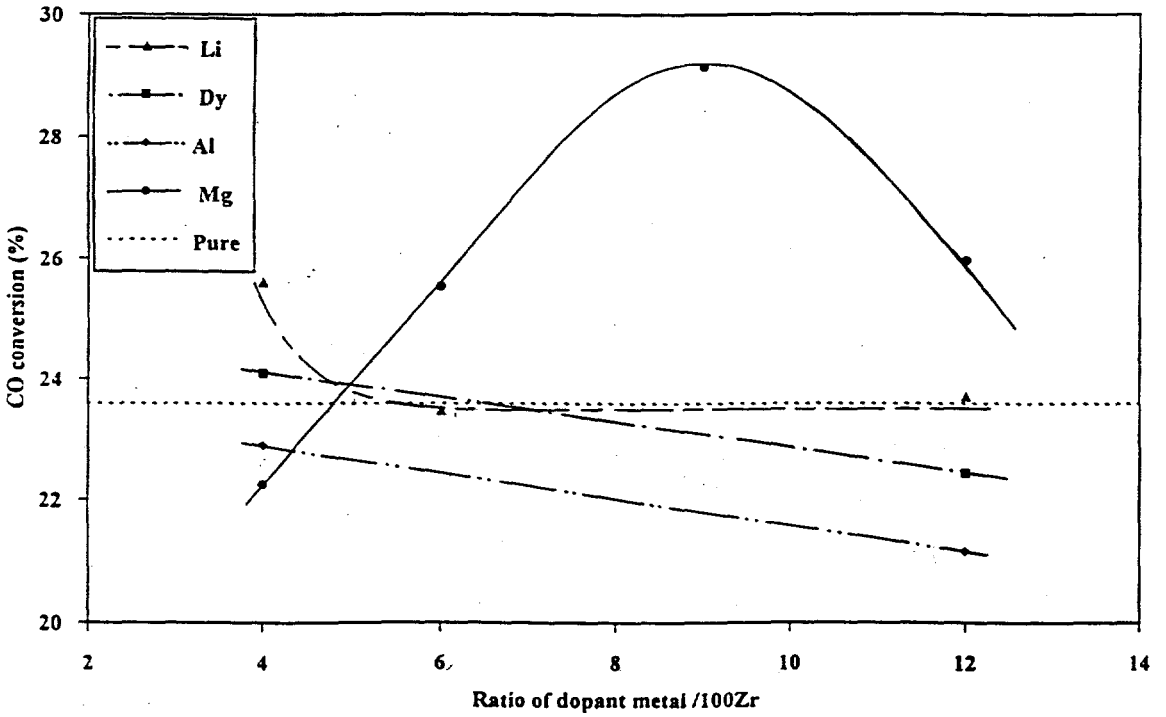

Figure 3.48. Changes in CO conversion with dopant level at 673 K, 50 atm, 1/1 CO/H_2 ratio, and 90 second space time.

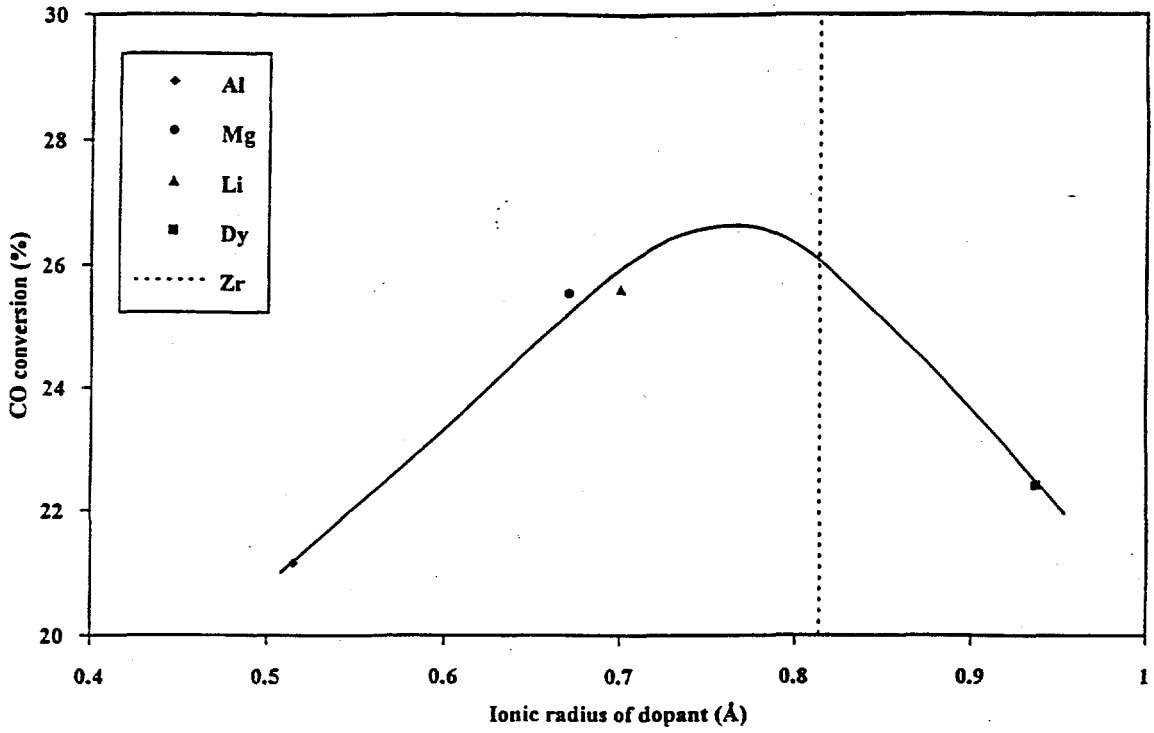

Figure 3.49. Changes in CO conversion with ionic radius of the dopant cation at an oxygen vacancy to zirconium ratio of 0.06 at 673 K, 50 atm, 1/1 CO/H_2 ratio, and 90 second space time.

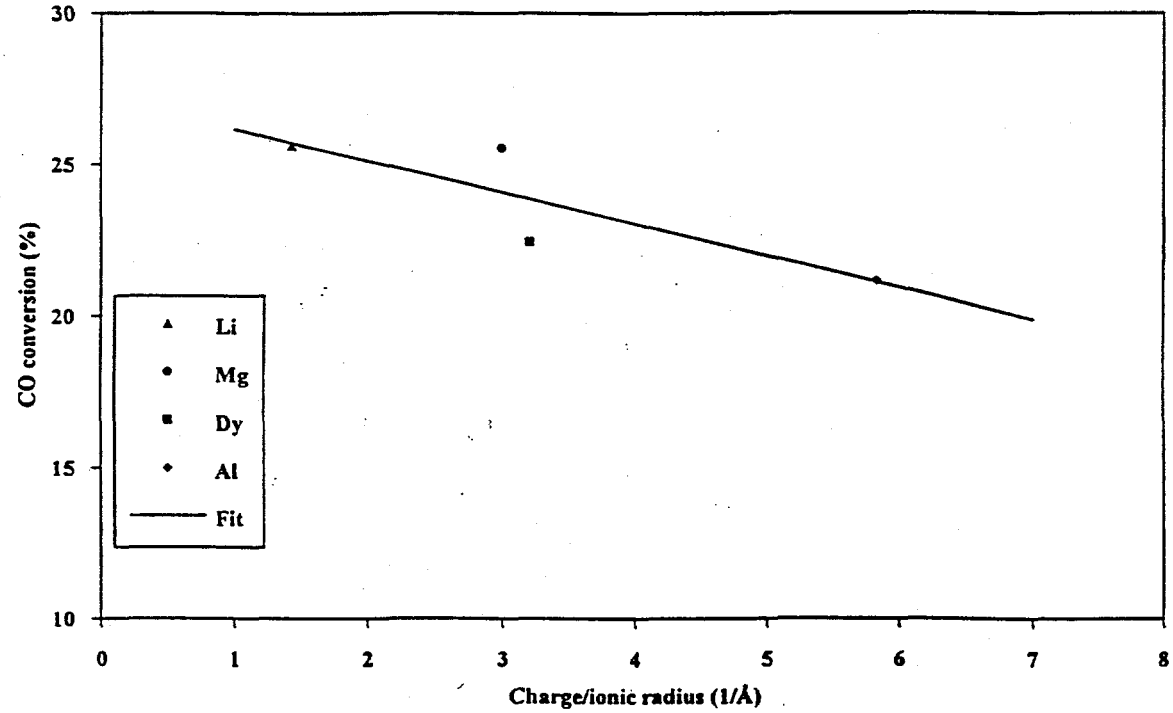

Figure 3.50. Changes in CO conversion with dopant charge to ionic radius ratio at an oxygen vacancy to zirconium ratio of 0.06 at 673 K, 50 atm, 1/1 CO/H_2 ratio, and 90 second space time.

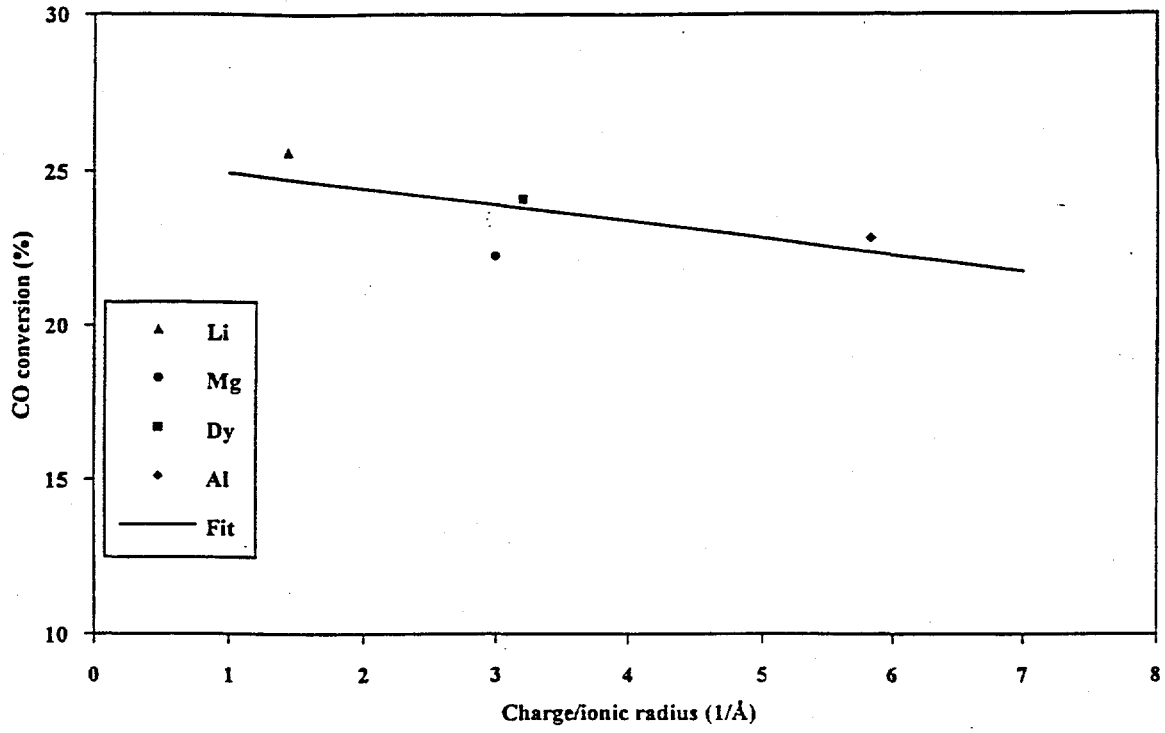

Figure 3.51. Changes in CO conversion with dopant charge to ionic radius ratio at a dopant metal to zirconium ratio of 0.04 at 673 K, 50 atm, 1/1 CO/H_2 ratio, and 90 second space time.

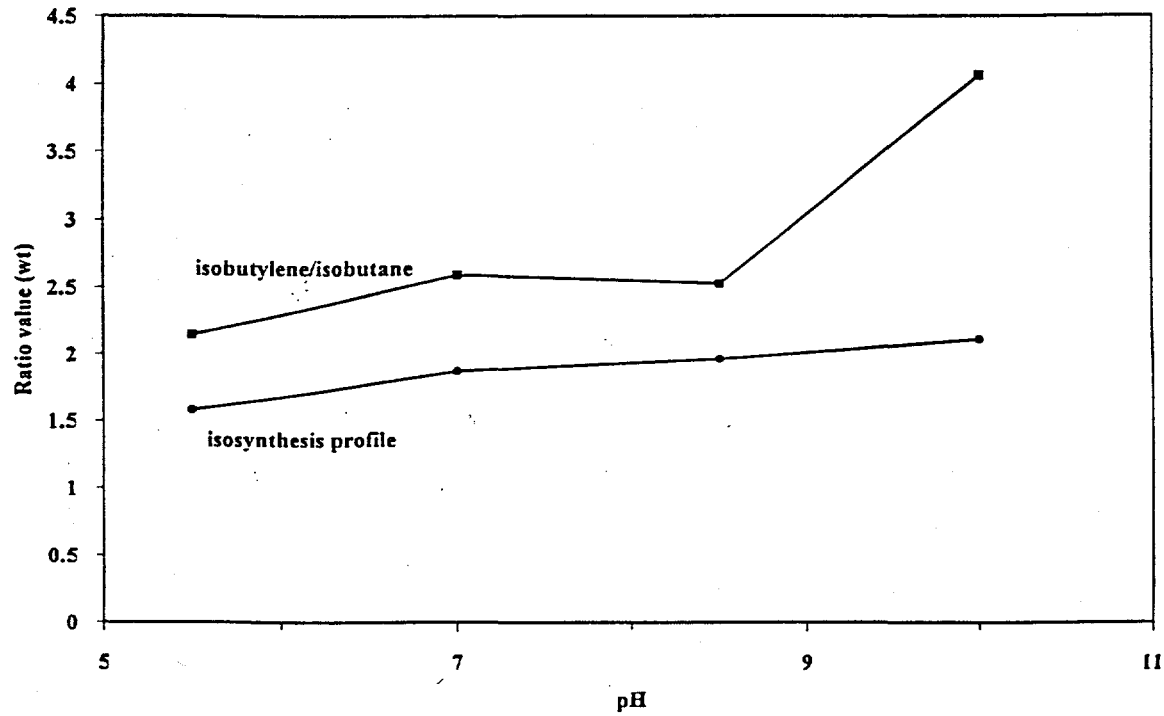

Figure 3.52. Changes in isobutylene/isobutane ratio and isosynthesis profile with *p*H at 673 K, 50 atm, 1/1 CO/H_2 ratio, and 90 second space time.

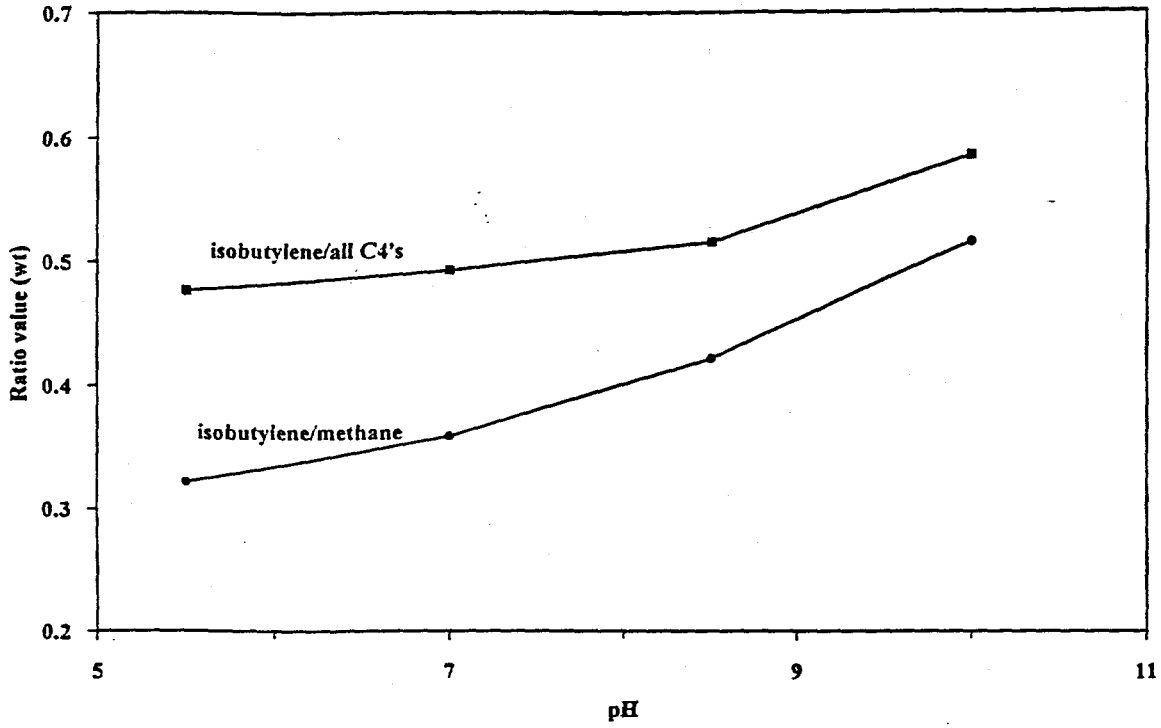

Figure 3.53. Changes in isobutylene fraction among C_4's and isobutylene/methane ratio with *p*H at 673 K, 50 atm, 1/1 CO/H_2 ratio, and 90 second space time.

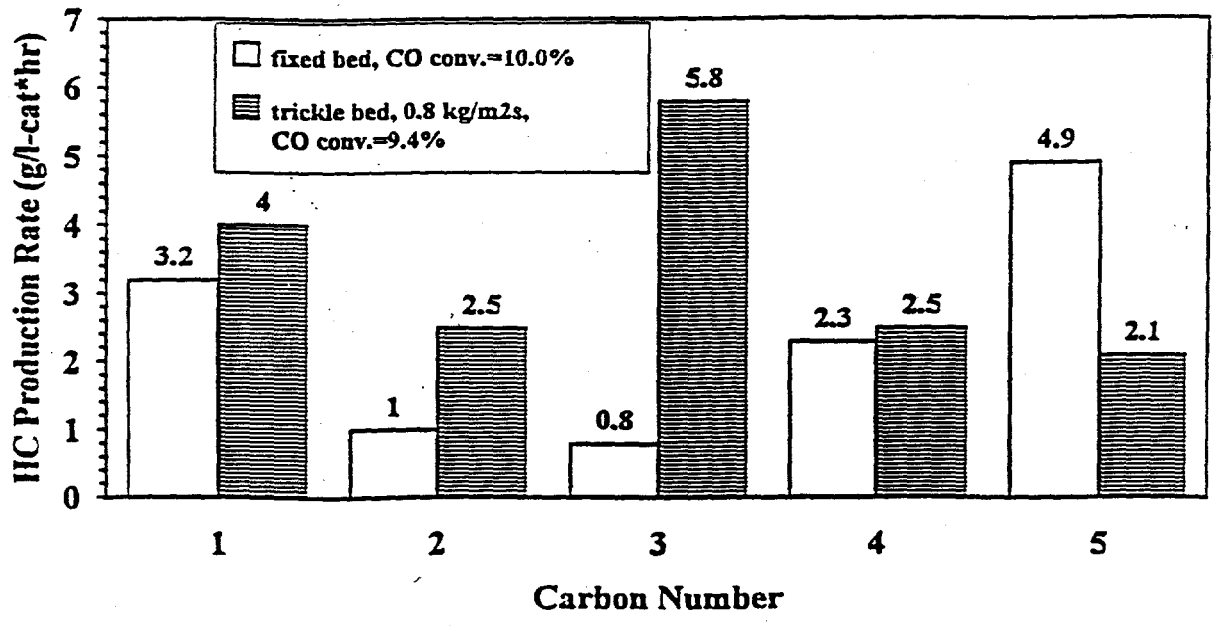

Figure 3.54. Comparison of the hydrocarbon distribution for fixed and trickle bed reactors at 669 K, 51 atm, 1/1 CO/H_2 ratio and 89 second space time.

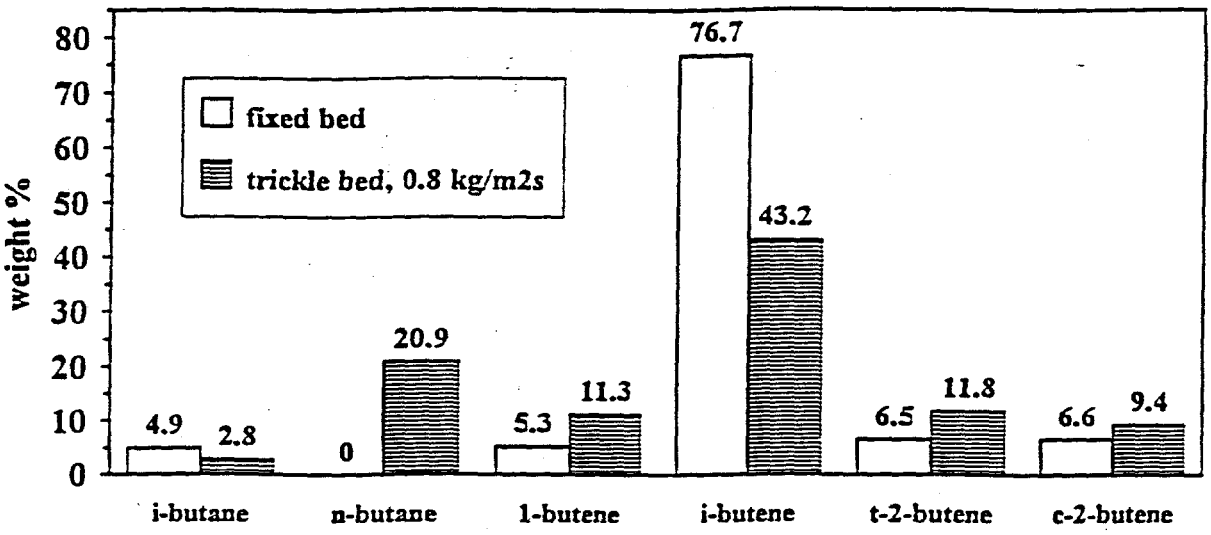

Figure 3.55. Comparison of C_4 distribution for fixed and trickle bed reactors at 669 K, 51 atm, 1/1 CO/H_2 ratio, and 89 second space time.

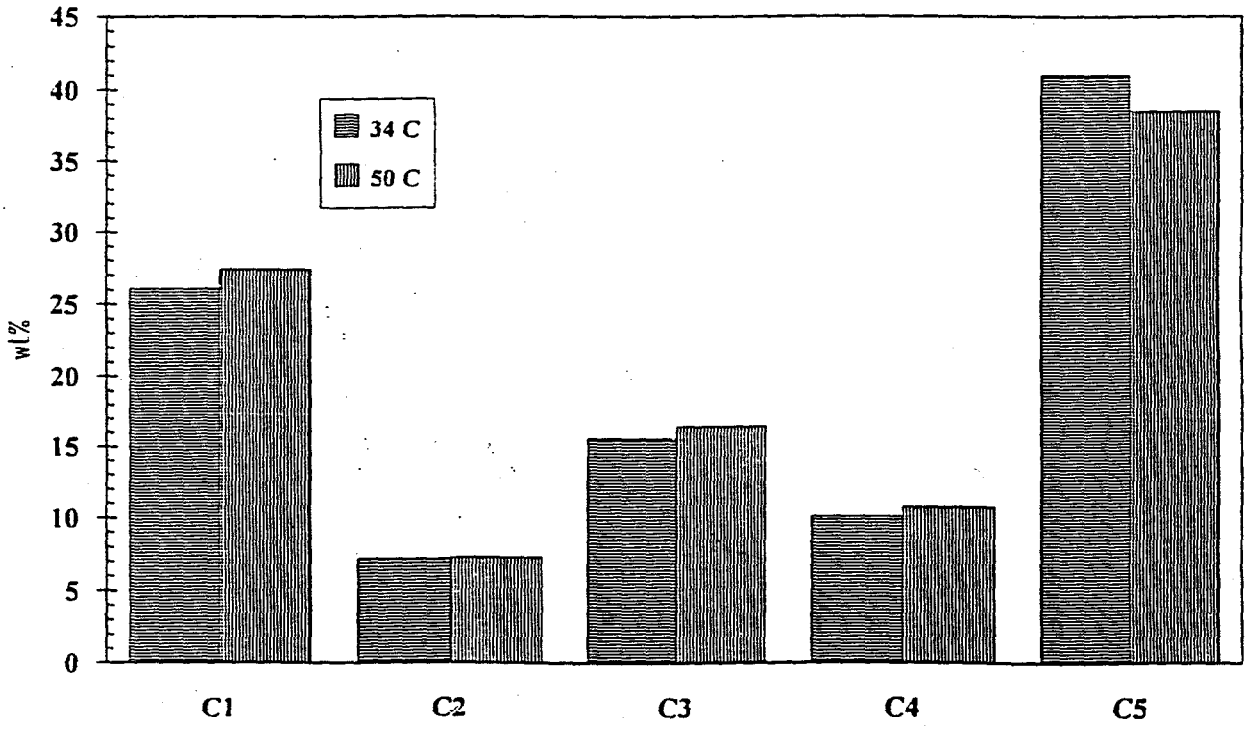

Figure 3.56. Effect of gas oil separator temperature on hydrocarbon distribution in the trickle bed reactor at 10% CO conversion, 669 K, 51 atm, 1/1 CO/H_2, and 89 second space time.

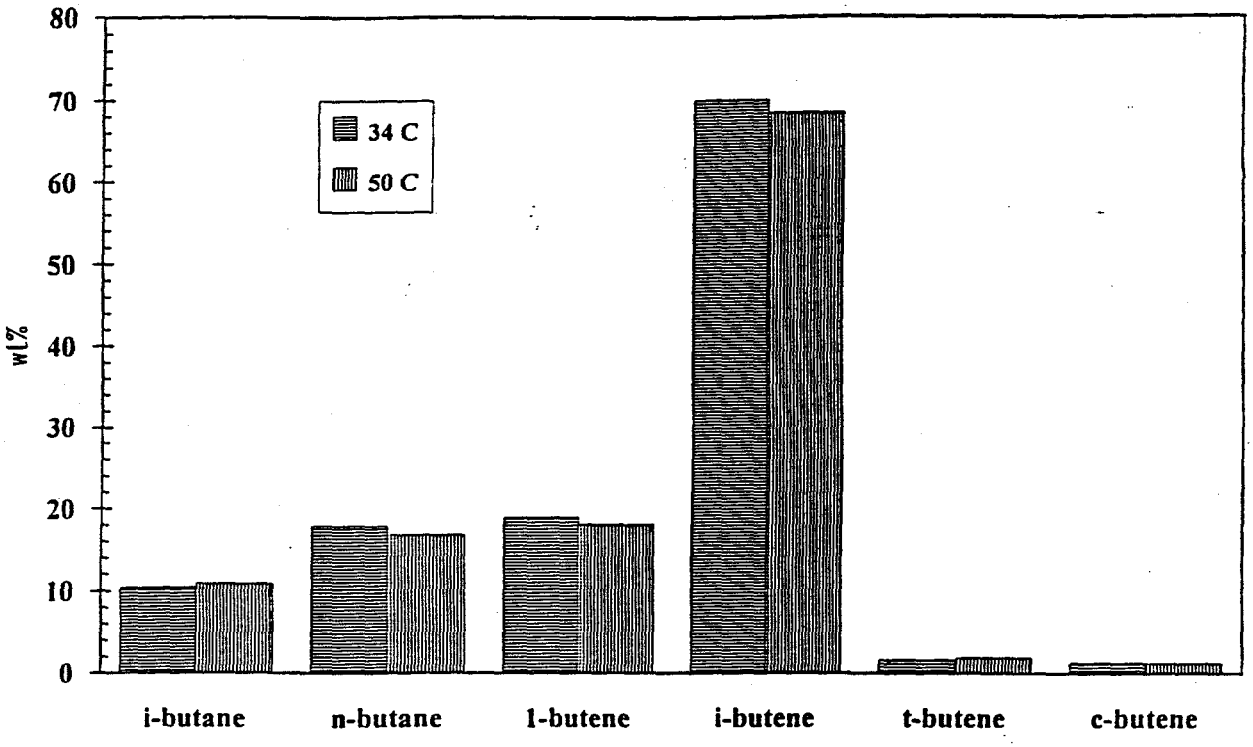

Figure 3.57. Effect of gas oil separator temperature on C_4 distribution in the trickle bed reactor at 10% CO conversion, 669 K, 51 atm, 1/1 CO/H_2 ratio, and 89 second space time.

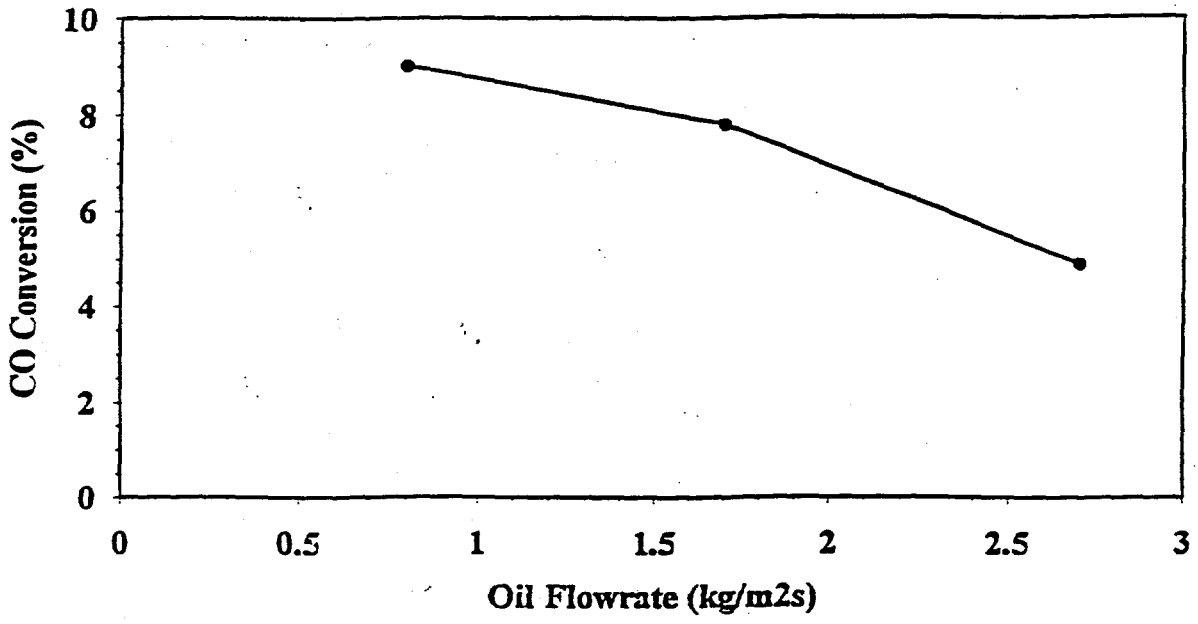

Figure 3.58. Variation of CO conversion with oil flow rate in the trickle bed reactor at 669 K, 51 atm, 1/1 CO/H_2 ratio, and 668 (1/hr) space velocity.

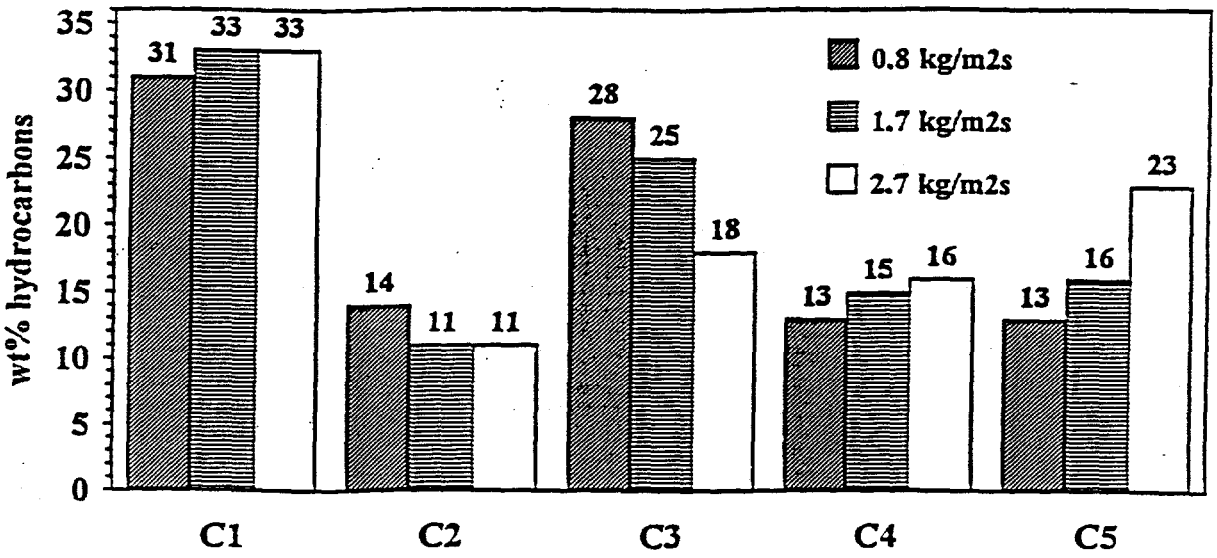

Figure 3.59. Change in hydrocarbon distribution with oil flow rate in the trickle bed reactor at 669 K, 51 atm, 1/1 CO/H_2 ratio, and 668 (1/hr) space velocity.

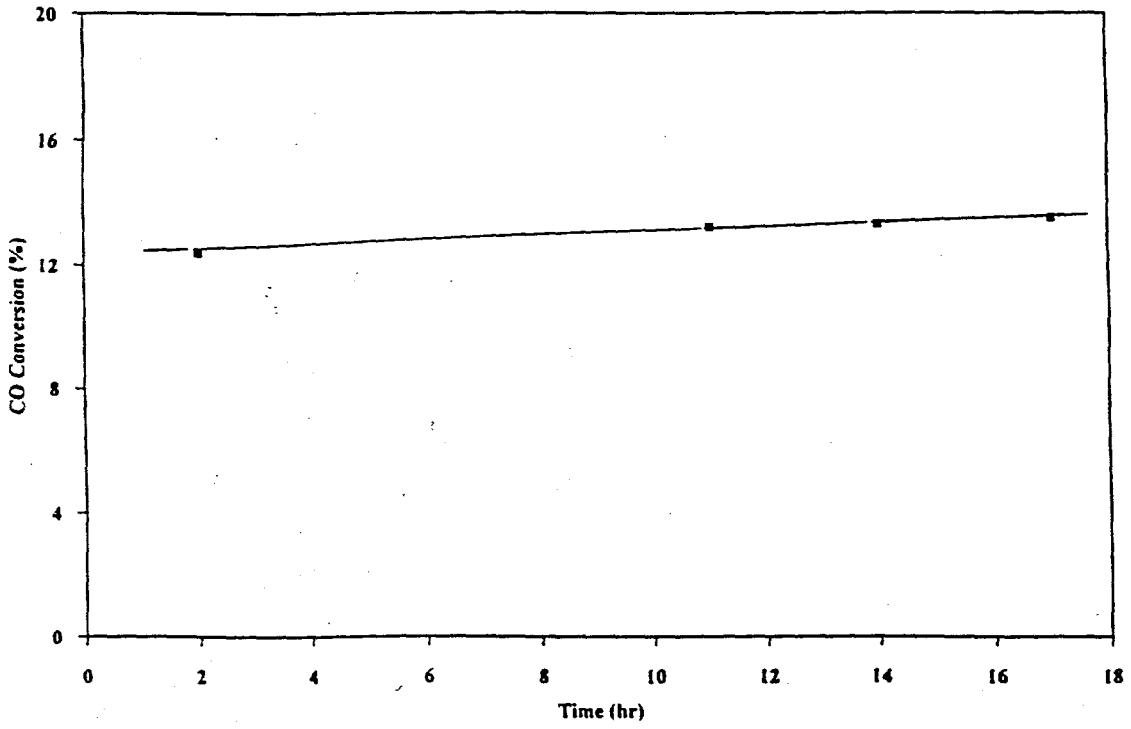

Figure 3.60. Changes in CO conversion level with time on stream in the slurry reactor over ZrO_2 (ppt.).

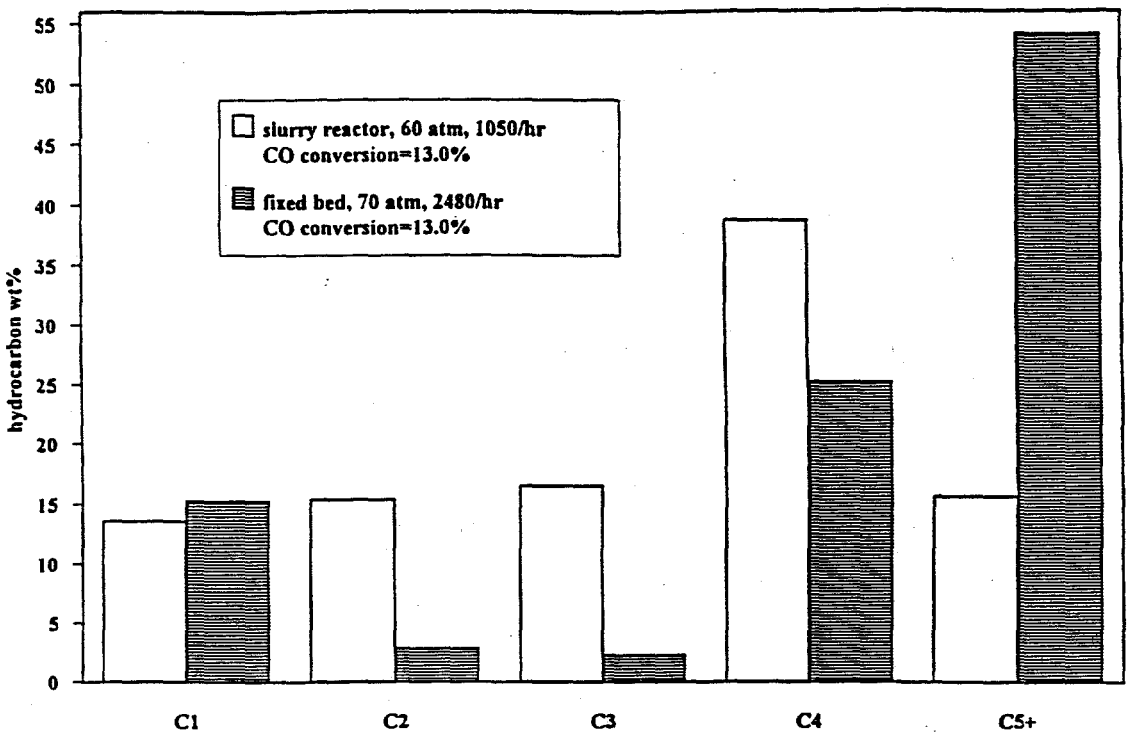

Figure 3.61. Comparison of hydrocarbon distribution between slurry and fixed bed reactors over ZrO_2 (ppt.).

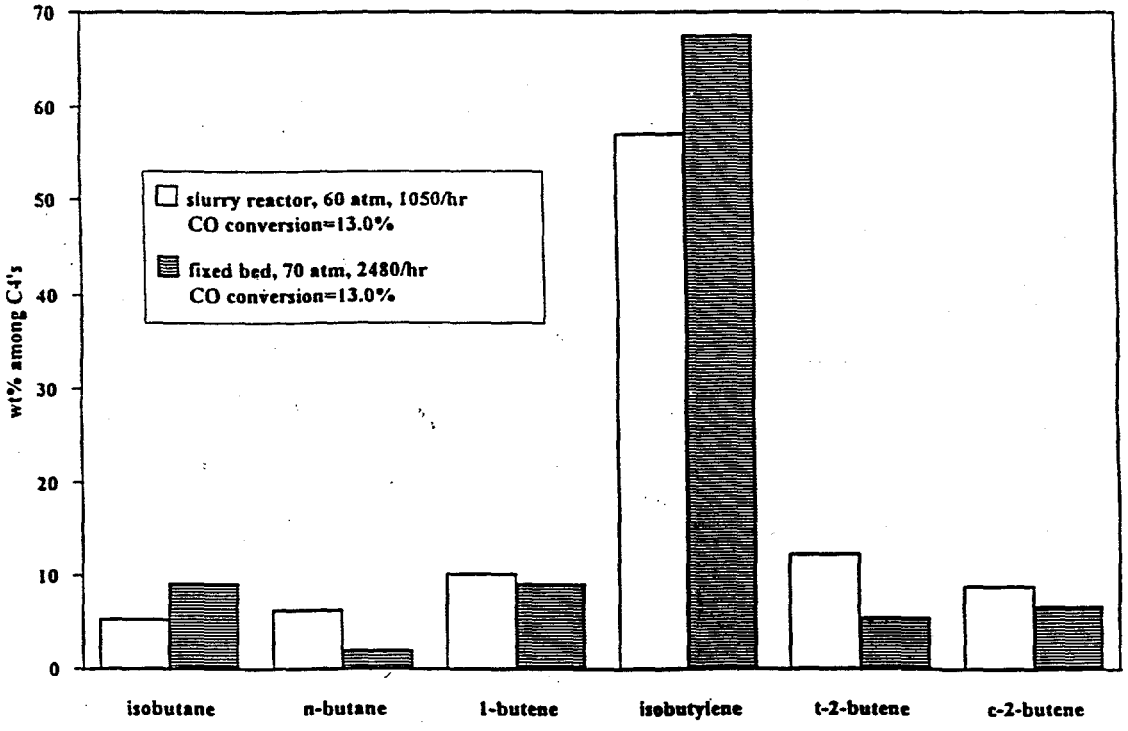

Figure 3.62. Comparison of C_4 distribution between slurry and fixed bed reactors over ZrO_2 (ppt.).

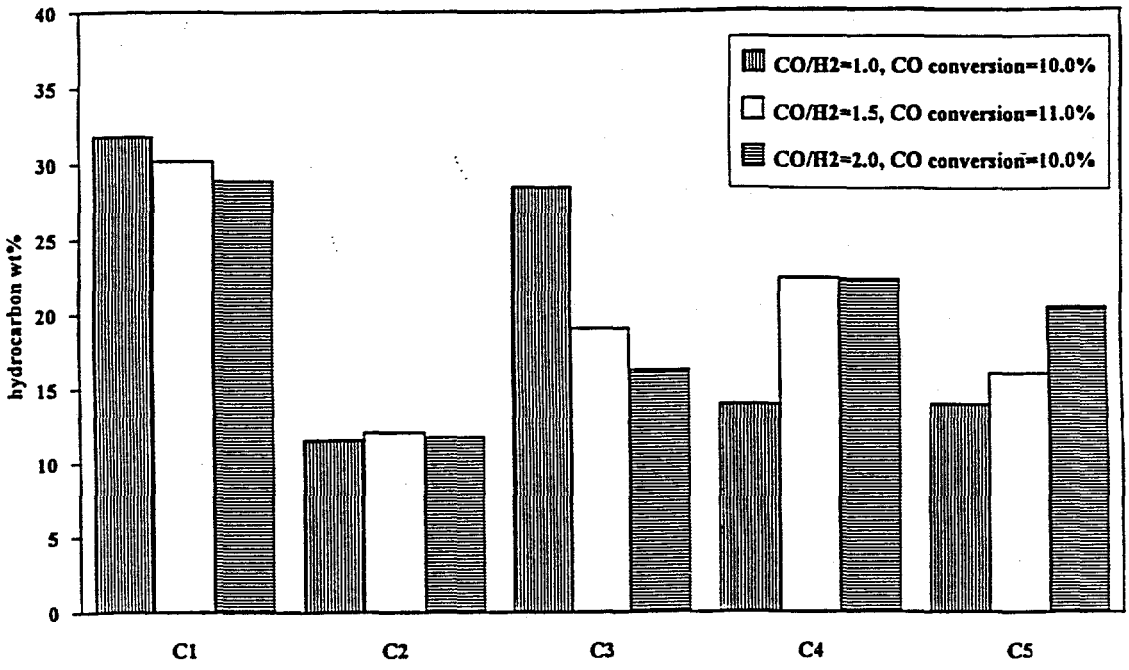

Figure 3.63. Changes in hydrocarbon distribution with CO/H_2 ratio in the slurry reactor over commercial ZrO_2.

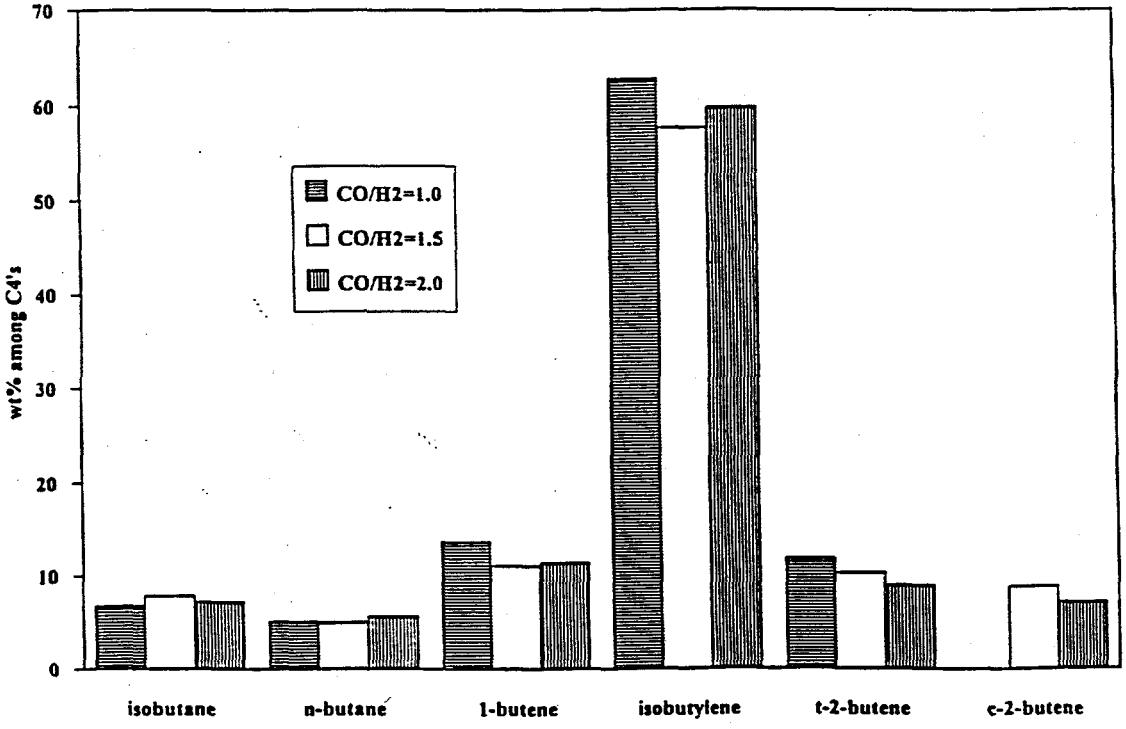

Figure 3.64. Changes in C_4 distribution with CO/H_2 ratio in the slurry reactor over commercial ZrO_2.

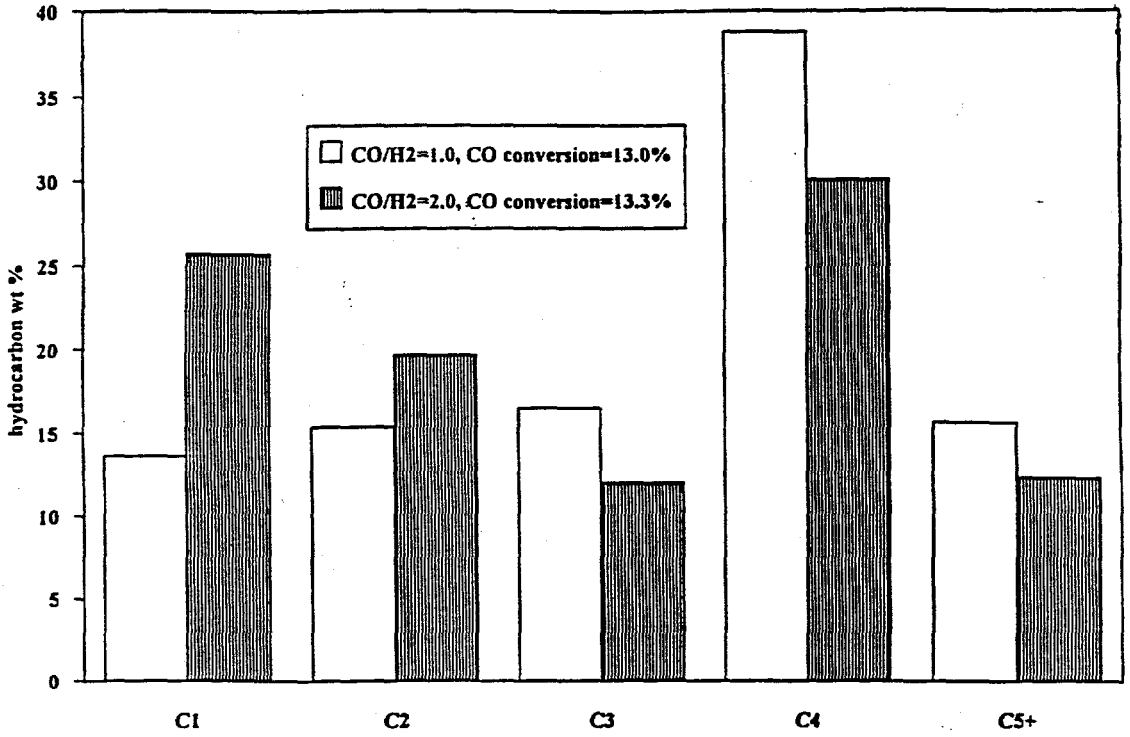

Figure 3.65. Changes in Hydrocarbon distribution with CO/H_2 ratio in the slurry reactor over ZrO_2 (ppt.).

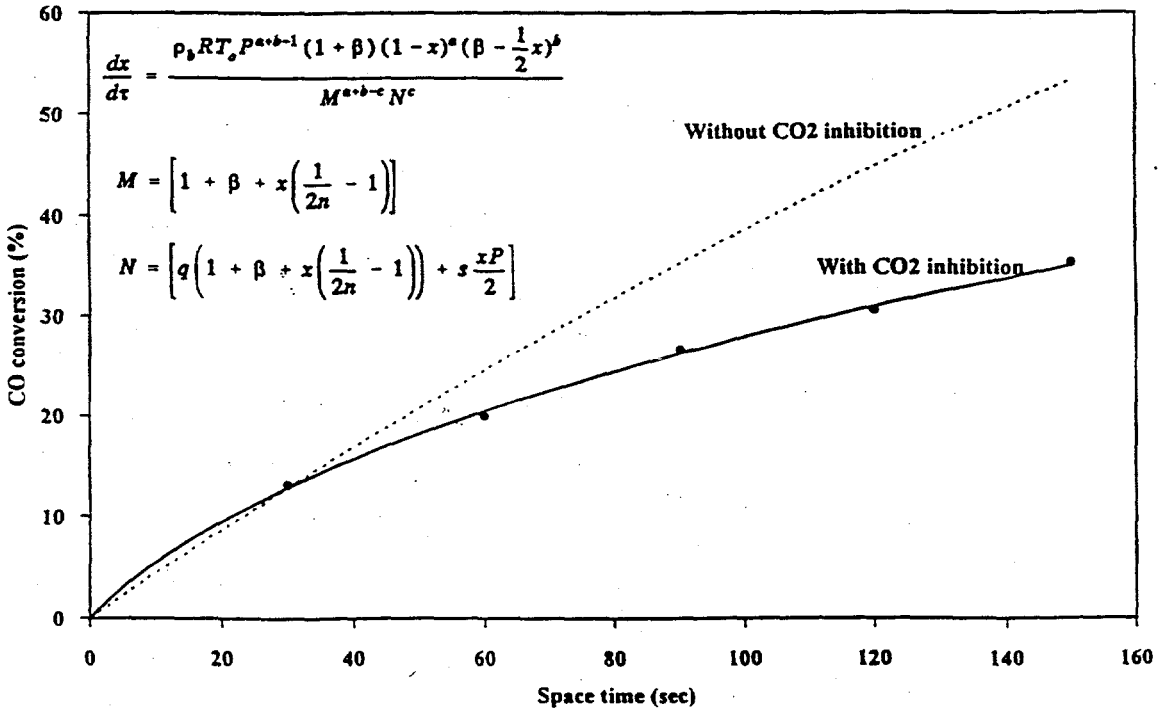

Figure 3.66. Predicted conversion over 7% Ce-ZrO_2 at 673 K, 50 atm, and 1/1 CO/H_2 ratio, with and without CO_2 inhibition.

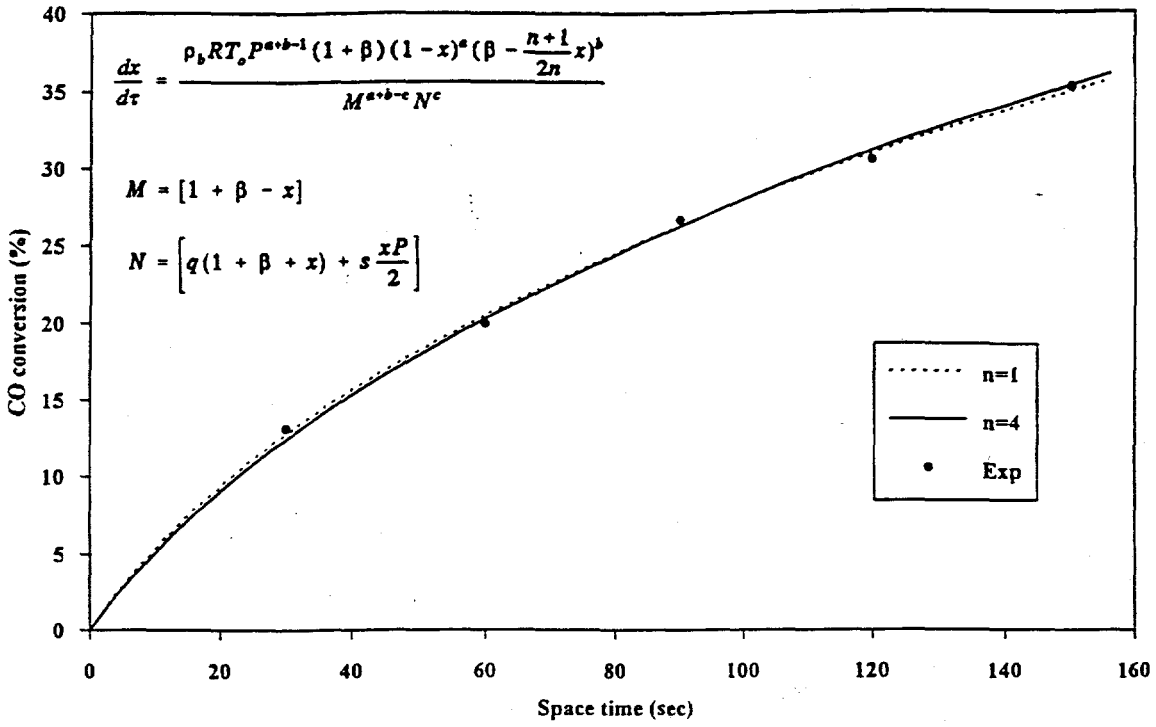

Figure 3.67. Changes in predicted conversion over 7% Ce-ZrO_2 at 673 K, 50 atm, and 1/1 CO/H_2 ratio with *n*.

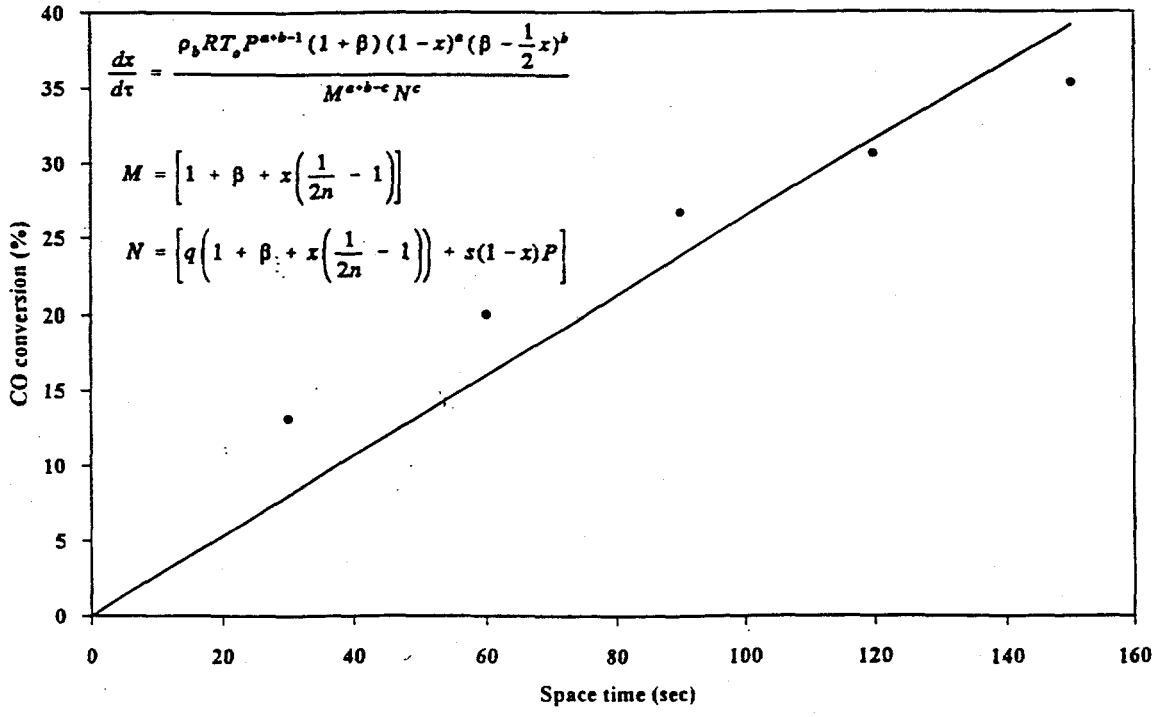

Figure 3.68. Predicted conversion over 7% Ce-ZrO_2 at 673 K, 50 atm, and 1/1 CO/H_2 ratio with CO inhibition.

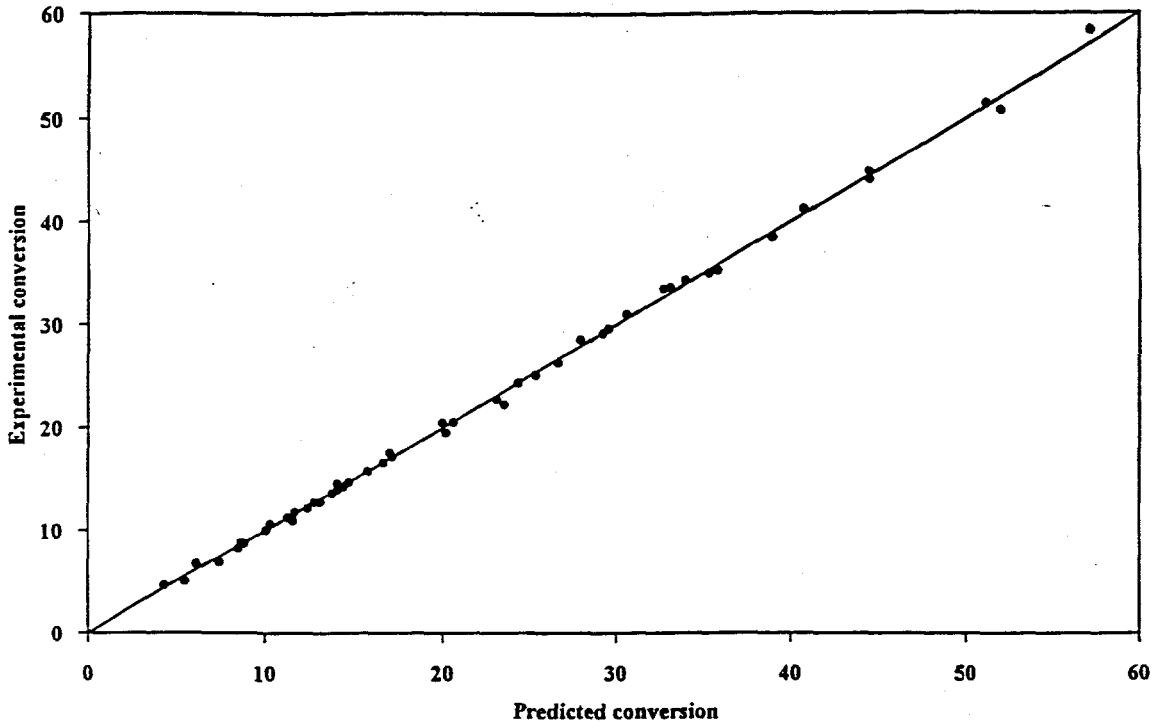

Figure 3.69. Comparison of experimental and predicted carbon monoxide conversion for all catalysts.

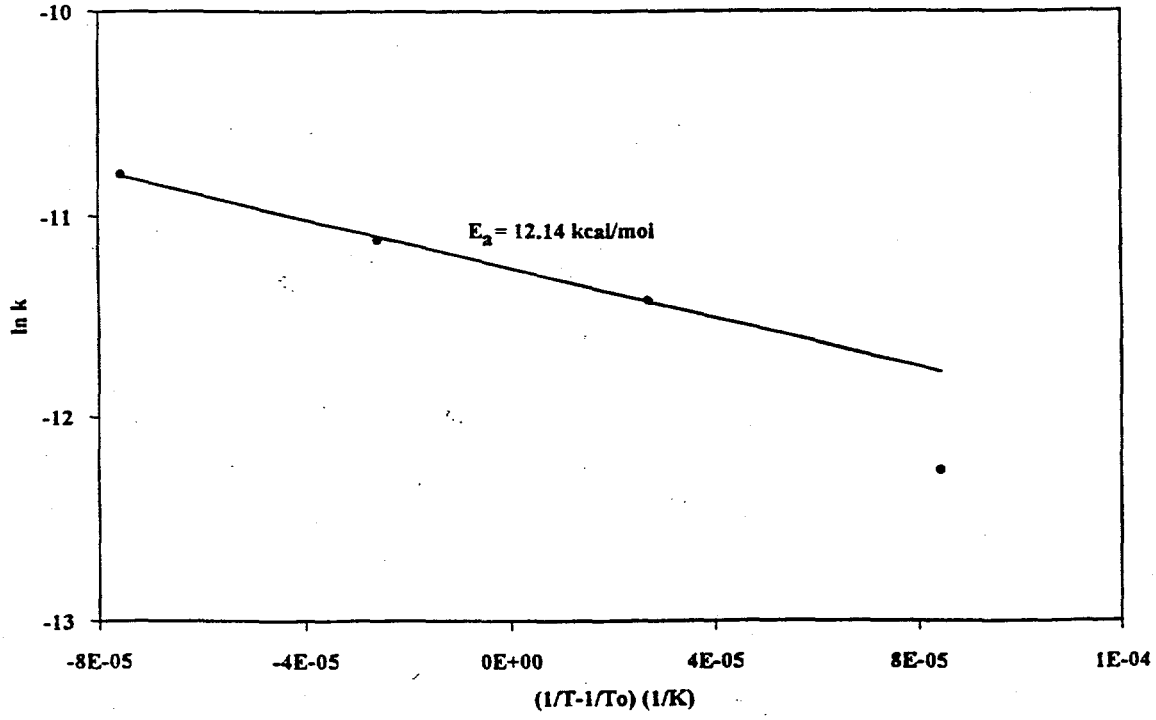

Figure 3.70. Determination of activation energy over 7% Ce-ZrO_2 (ppt.) with aluminum CO cylinder at 50 atm and 1/1 CO/(H_2+H_2S) ratio.

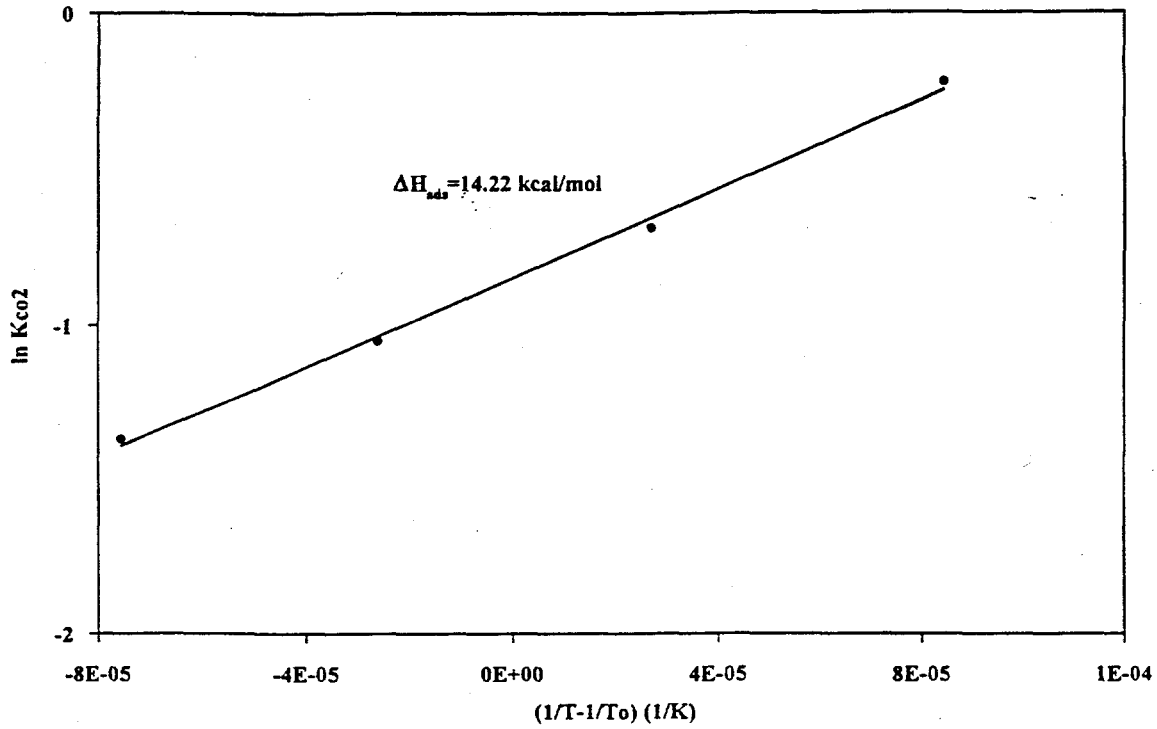

Figure 3.71. Determination of the heat of adsorption for CO_2 over 7% Ce-ZrO_2 (ppt.) with aluminum CO cylinder at 50 atm and 1/1 CO/(H_2+H_2S) ratio.

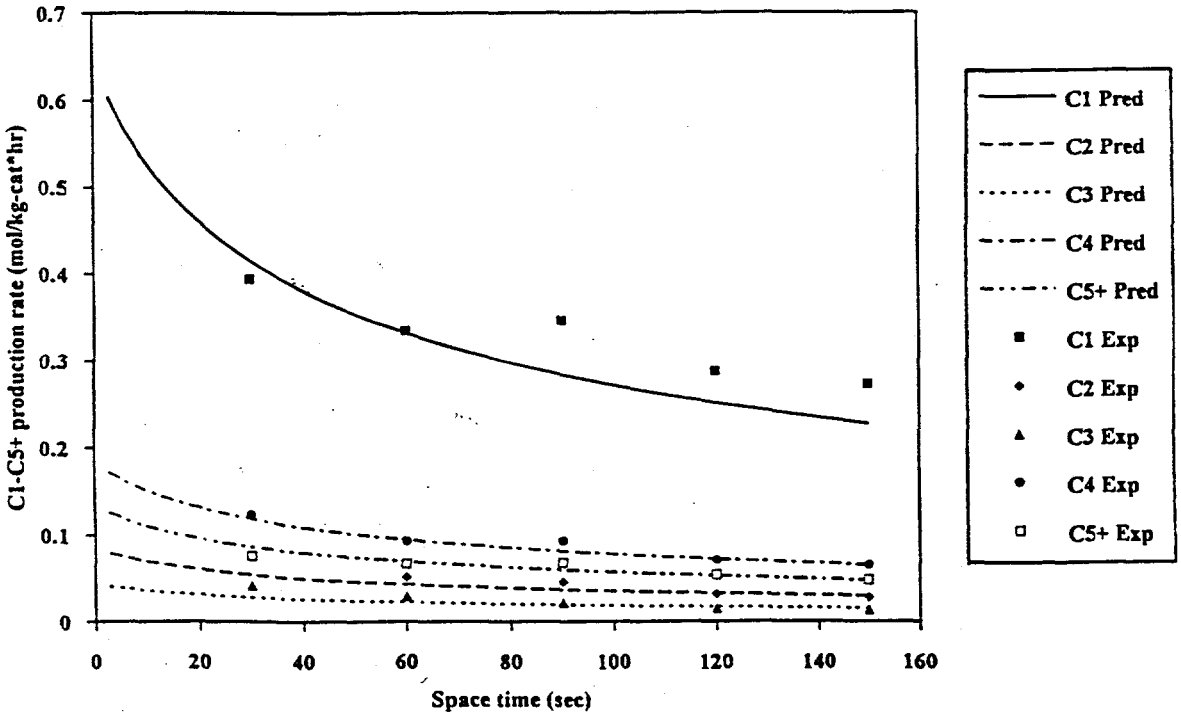

Figure 3.72. Comparison of experimental and predicted C_1-C_5+ production rates over 7% Ce-ZrO_2 at 673 K, 50 atm, and 1/1 CO/H_2 ratio.

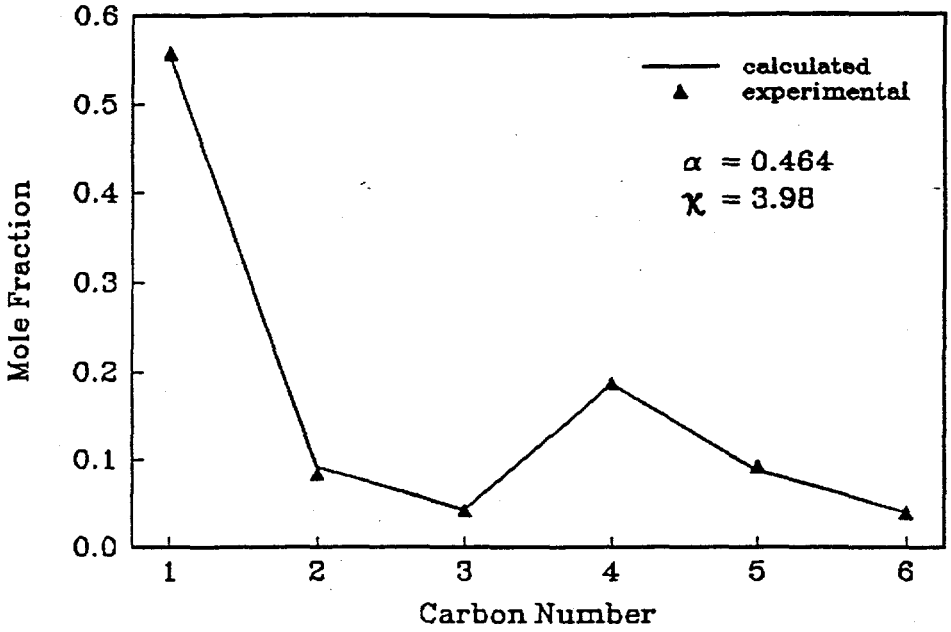

Figure 3.73. Product distribution generated by the semi-empirical model over K-ZrO_2 (MSG), at 723 K, 70 atm, 1/1 CO/H_2 ratio, and 80 second space time.

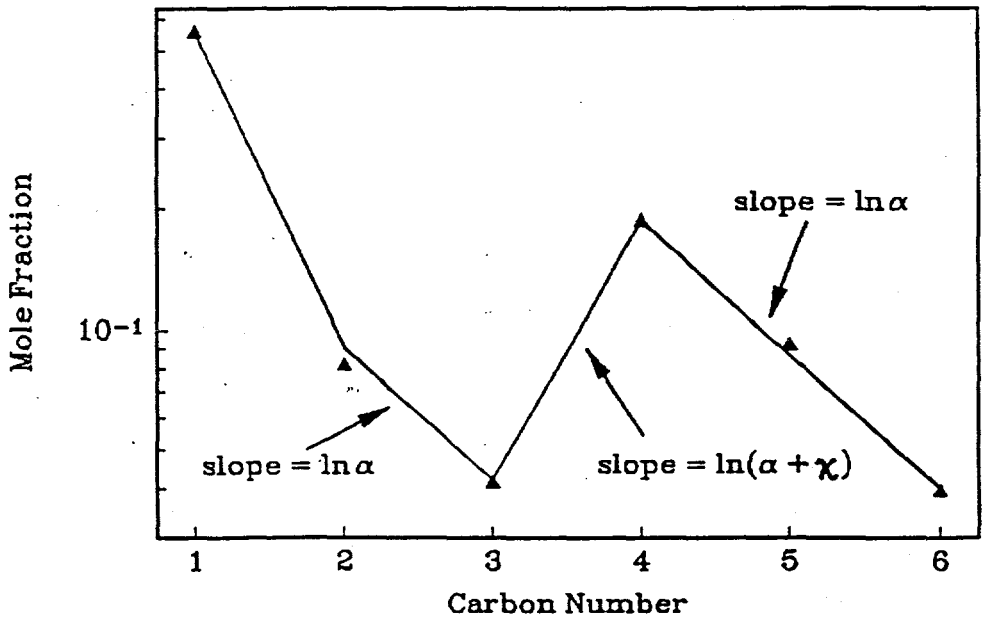

Figure 3.74. Parameters in the semi-empirical model. The distribution in Figure 3.73 is plotted on a semi-log scale, and α and κ are related to the slopes of the line segments.

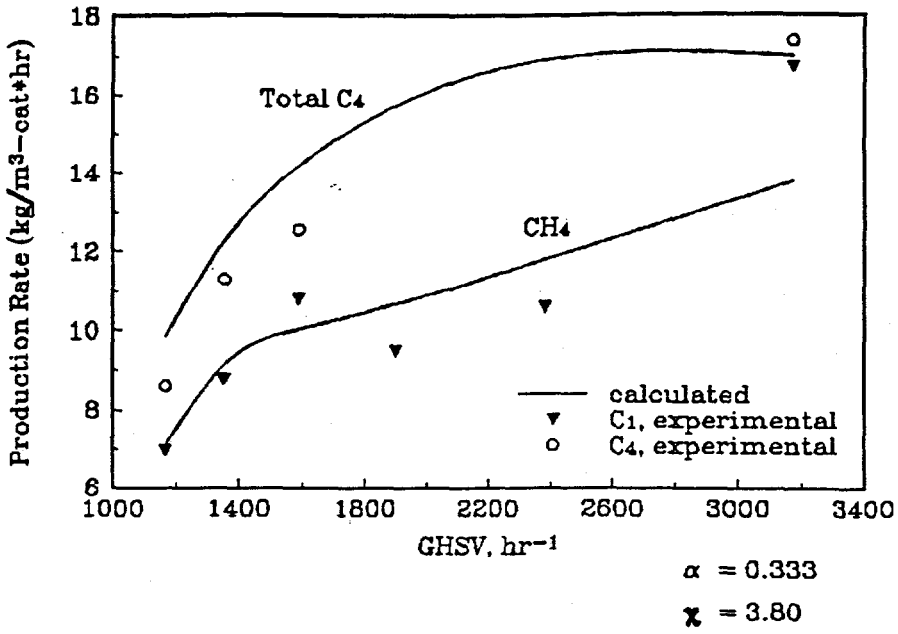

Figure 3.75. Production rates of CH_4 and C_4 hydrocarbons. Calculated by combining the semi-empirical model for hydrocarbon distribution with the empirical CO reaction rate. ZrO_2 (H-0304), 723 K, 70 atm, 1/1 CO/H_2 ratio.

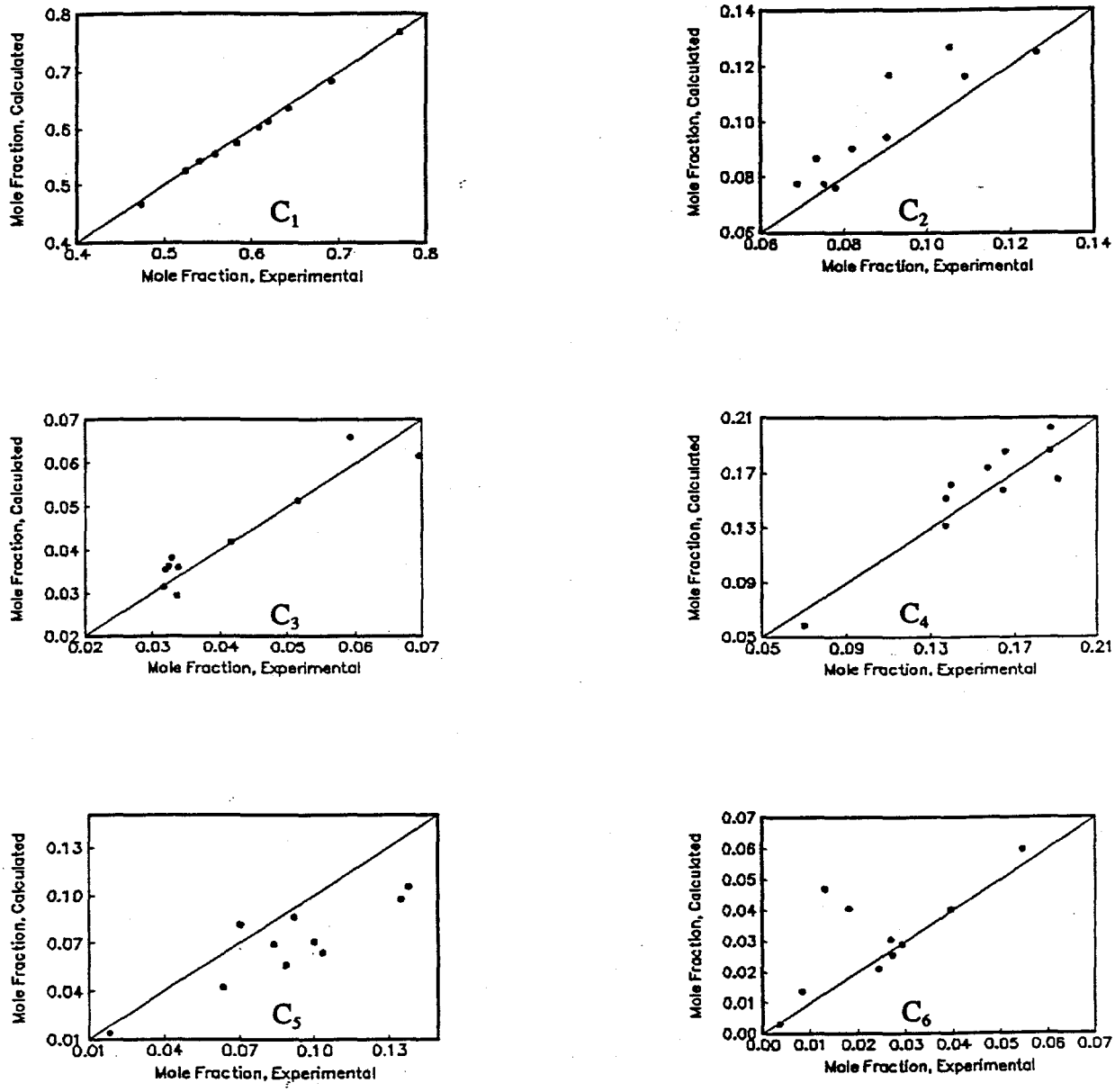

Figure 3.76. Residual plots for hydrocarbon distributions. For all the catalysts in Table 3.30 at 723 K, 70 atm, and 20 to 80 second space times.

REFERENCES

1. Hoffman, H., *Hydrocarbon Process.* **69,** 15 (1990).

2. Piel, W.J., and Thomas, R.X., *Hydrocarbon Processs.* **69,** 68 (1990).

3. Ainsworth, S.J., *Chem. Engr. News* **69,** 13 (1991).

4. Sofianos, A., *Catal. Today* **15,** 149 (1992).

5. Johnson, J.E., and Peterson, F.M., *CHEMTECH* **21,** 296 (1991).

6. Nakamura, D.W., *Hydrocarbon Process.* **72,** 21 (1993).

7. Pichler, H., and Ziesecke, K., *Brennst. Chem.* **30,** 1 (1949).

8. Kieffer, R., Varela, J., and Deluzarche, A., *J. Chem. Soc. Chem. Commun.* 763 (1983).

9. Maehashi, T., Maruya, K., Domen, K., Aika, K., and Onishi, T., *Chem. Lett.* 747 (1984).

10. Maruya, K., Maehashi, T., Haraoka, T., Narui, S., Asakawa, Y., Domen, K., and Onishi, T., *Bull. Chem. Soc. Jpn.* **61,** 667 (1988).

11. Maruya, K., Fujisawa, T., Takasawa, A., Domen, K, and Onishi, T., *Bull. Chem. Soc. Jpn.* **68,** 11 (1989).

12. Tseng, S.C., Jackson, N.B., and Ekerdt, J.G., *J. Catal.* **109,** 284 (1988).

13. Jackson, N.B., and Ekerdt, J.G., *J. Catal.* **126,** 31 (1990).

14. Jackson, N.B., and Ekerdt, J.G., *J. Catal.* **126,** 46 (1990).

15. Mazanec, T.J., *J. Catal.* **98,** 115 (1986).

16. Davis, B., *J. Am. Ceram. Soc. Comm.* **67,** C-168 (1984).

17. Srinivasan, R., De Angelis, R., and Davis, B.H., *J. Mater. Res.* **1,** 583 (1986).

18. Li-Min, T., Srinivasan, R., De Angelis, R.J., Pinder, T., and Davis, B.H., *J. Mater. Res.* **3,** 561 (1988).

19. Benedetti, A., Fagherazzi, G., and Pinna, F., *J. Am. Ceram. Soc.* **72,** 467 (1989).

20. Benedetti, A., Fagherazzi, G., Pinna, F., and Polizzi, S., *J. Mater. Sci.* **25,** 1473

(1990).

21. Smith, D.K., and Newkirk, H.W., *Acta. Cryst.* **18,** 983 (1965).

22. Jansen, H.J.F., *Phys. Rev. B* **43,** 7267 (1991).

23. Bragg, L., and Claringbull, G.F., *in*"The Crystalline State" (L. Bragg, Ed.), Vol. IV-Crystal Structures of Minerals, p. 239. Cornell University Press, New York, 1965.

24. Stull, D.R., Westrum, E.F. Jr., and Sinke, G.C., "The Chemical Thermodynamics of Organic Compounds," Wiley & Sons, New York, 1969.

25. Fajula, F., Anthony, R.G., and Lunsford, J.H., *J. Catal.* **73,** 237 (1982).

26. Gadalla, A.M., Chan, T., and Anthony, R.G., *Inter. J. Chem. Kinet.* **15,** 759 (1983).

27. Dry, M.E., *in* "Catalysis. Science and Technology" (J.R. Anderson and M. Boudart, Eds.), Vol. I, Springer-Verlag, New York, New York, 1980.

28. Anderson, R.B., *in* "Catalysis" (P.H. Emmett, Ed.), Vol. IV, Reinhold, New York, New York, 1956.

29. Hofer, L.J.E., *in* "Catalysis" (P.H. Emmett, Ed.), Vol. IV, Reinhold, New York, New York, 1956.

30. Snel, R., *Catal. Rev.-Sci. Eng.* **29,** 361 (1987).

31. Aris, R., "Elementary Chemical Reactor Analysis," Prentice Hall, Englewood Cliffs, New Jersey, 1969.

32. Holland, C.D., and Anthony, R.G., "Fundamentals of Chemical Reaction Engineering," Prentice Hall, Englewood Cliffs, New Jersey, 1989.

33. Rabo, J.A., Risch, A.P., and Poutsma, M.L., *J. Catal.* **53,** 295 (1978).

34. Karles, G.D., and Ekerdt, J.G., Preprint Paper-*Amer. Chem. Soc., Div. Petr. Chem., Inc.* **37,** 239 (1992).

35. Evans, P.A., Stevens, R., and Binner, J.G.P., *Br. Ceram Trans. J.* **83,** 39 (1984).

36. Dosch, R.G., Stephens, H.P., and Stohl, F.V., U.S. Patent 4,511,455 (1985).

37. "Powder Diffraction File," Alphabetical Index, Compiled by the JCPDS - International Centre for Diffraction Data, Swarthmore, PA, 1987.

38. Jackson, N.B., Ph.D. Dissertation, Department of Chemical Engineering, University of Texas, Austin, Texas, 1990.

39. Kieffer, E.P., and Van Der Baan, H.S., *in* "Chemical Reaction Engineering" (M.J. Comstock, Ed.), ACS Symposium Series No. 196, 1981.

40. Henderson, A.W., and Higbie, K.B., *J. Am. Chem. Soc.* **76,** 5878 (1954).

41. Barker, M.A., M.S. Thesis, Department of Chemical Engineering, University of Texas, Austin, Texas, 1987.

42. Saryp, B., and Wojciechowski, B.W., *Can. J. Chem. Eng.* **66,** 831 (1988).

43. Dean, J.A. Ed., "Lange's Handbook of Chemistry" 13th edition, McGraw-Hill Book Company, New York, p.3-121 - 3-126 (1985).

44. Mackrodt, W.C., and Woodrow, P.M., *J. Am. Ceram. Soc.* **69,** 277 (1986).

45. Rajendran, S., Swain, M.V., and Rossell, H.J., *J. Mater. Sci.* **23,** 1805 (1988).

46. Rajendran, S., Drennan, J., and Badwal, S.P.S., *J. Mater. Sci. Lett.* **6,** 1431 (1987).

47. Silver, R.G., Hou, C.J., and Ekerdt, J.G., *J. Catal.* **118,** 400 (1989).

48. Platero, E.E., and Mentruit, M.P., *Mater. Lett.* **14,** 318 (1992).

49. Nakajo, T., Arakawa, H., Sano, K.-I., and Matsuhira, S., *Chem. Lett.* 593 (1987).

50. Etsell, T.H., and Flengas, S.N., *Chem. Rev.* **70,** 339 (1970).

51. Jackson, N.B., and Ekerdt, J.G., *J. Catal.* **101,** 90 (1986).

52. Uehara, T., Koto, K., Emura, S., and Kanamaru, F., *Solid State Ionics* **23,** 331 (1987).

53. Strickler, D.W., and Carlson, W.G., *J. Am. Ceram. Soc.* **48,** 286 (1965).

54. Badwal, S.P.S., and Drennan, J., *Solid State Ionics* **53-56,** 769 (1992).

55. Gur, T.M., Raistrick, I.D., and Huggins, R.A., *Mater. Sci. Engr.* **46,** 53 (1980).

56. Kaneko, H., Jin, F., Taimatsu, H., and Kusakabe, H., *J. Am. Ceram. Soc.* **76,** 793 (1993).

57. Stafford, R.J., Rothman, S.J., and Routbort, J.L., *Solid State Ionics* **37,** 67 (1989).

58. Smith, J.M., "Chemical Engineering Kinetics," 3rd ed., McGraw-Hill, New York 1981.

59. Calderbank, P.H., and Moo-Young, M.B., *Chem. Engr. Sci.* **16,** 39 (1961).

60. Brian, P.L.T., Hales, H.B., and Sherwood, T.K., *AIChE J.* **15,** 419 (1969).

61. Yokoyama, A., Komiyama, H., Inoue, H., Masumoto, T., and Kimura, H., *in* "Chemical Reaction Engineering" (M.J. Comstock, Ed.), ACS Symposium Series No. 196, 1981.

62. Izarraraz, A.G., Benzen, G.W., Anthony, R.G., and Holland, C.D., *Hydrocarbon Process.* **April,** (1980).

63. Graaf, H., Smit, H.J., Stamhuls, E.J., and Beenackers, A.A.C.M., *J. Chem. Eng. Data* **37,** 146 (1992).

64. Norris, J.C., "Engineering Data Book," 9th ed., Gas Processors Association, Tulsa, OK, 1972.

65. Lee, H.H., "Heterogeneous Reactor Design," Butterworth Publishers, Boston, 1985.

66. Saryp, B., and Wojciechowski, B.W., *Can. J. Chem. Eng.* **67,** 62 (1989).

67. Lamotte, J., Lavalley, J.C., Druett, E., and Freund, E., *J. Chem. Soc. Faraday Trans. 1* **79,** 2219 (1983).

68. He, M.Y., and Ekerdt, J.G., *J. Catal.* **87,** 381 (1984).

69. Frolich, P.K, and Cryder, D.S., *I & EC Chem.* **22,** 1051 (1930).

70. Smith, K.J., and Anderson, R.B., *J. Catal.* **85,** 428 (1984).

71. Boudart, M., *AIChE J.* **18,** 465 (1972).

APPENDIX A - Relationship Between wt% and Carbon Conversion

Relationship Between wt% and Carbon Conversion

The total carbon conversion is equivalent to the total carbon monoxide conversion. From the stoichiometry of the reactions to produce alkanes and alkenes it can be shown that half of the carbon monoxide reacted is converted to carbon dioxide. The carbon converted to each of the hydrocarbon groups C_i is given by

$$x_{C\text{-}C_i} = \frac{\textit{moles of carbon in } C_i}{\textit{total moles of carbon converted to hydrocarbons}} \tag{A.1}$$

this becomes

$$x_{C\text{-}C_i} = \frac{2\alpha_{ci} y_{ci} n_T}{y_{CO}^o n_T^o - y_{CO} n_T} \tag{A.2}$$

The α_{ci}'s are the number of carbons in each product. The relationship between $y_{ci}n_T$ and weight fraction, w_i, (wt fraction equals wt percent divided by 100) is given by

$$y_{ci} n_T = \frac{w_i TG_{HC}}{MW_i} \tag{A.3}$$

TG_{HC} is the total grams of hydrocarbons produced per hour (when molar flow rate is mol/hr). When this is substituted into equation (A.2) the result is

$$x_{C\text{-}C_i} = \frac{2\alpha_{ci} TG_{HC} w_i}{MW_i\left(y_{CO}^o n_T^o - y_{CO} n_T\right)} \tag{A.4}$$

The results for carbon conversion are normalized if the total is not exactly 100. The error introduced by assuming an average molecular weight for C_2, C_3, C_4, and C_5+ fractions is small since usually the difference is only two hydrogen atoms. An example of this calculation is given in Table A.1 for a run over the 7% Ce-ZrO_2 catalyst.

TABLE A.1. Comparison of wt% with carbon conversion to that hydrocarbon group for run C7B (673K, 50 atm, 1/1 CO/H_2 ratio, and 60 second space time)

Hydrocarbon group	wt%	Carbon conversion (%)
C_1	29.46	27.18
C_2	8.29	8.44
C_3	7.05	7.26
C_4	29.00	30.24
C_5+	26.21	26.88

APPENDIX B - Rate Equation Parameters, Surface Intermediates, and Simplified Mechanisms

This appendix contains some discussion about the physical meaning of the parameters obtained for the carbon monoxide rate equation, mechanisms describing the surface intermediates involved in the isosynthesis, and some possible simplified mechanisms that could account for the final form of the rate equation.

Parameters in the Carbon Monoxide Rate Equation

Recall that an equivalent fit of the data was obtained using the following equation with $a=1$, $b=0.5$, and $c=1$ or 2. The expression with $c=1$ was used for modeling in this study because it was the simpler equation.

$$r_{CO} = \frac{k_p p_{CO}^{a} p_{H_2}^{b}}{\left(1 + K_{CO_2} p_{CO_2}\right)^{c}} \tag{B.1}$$

The values obtained for a and b indicate that carbon monoxide was adsorbed as a molecule, while hydrogen was dissociatively adsorbed. Table B.1 shows the comparison of fitted parameters for the cases where c either equals 1 or 2. This example is for the 7% Ce-ZrO_2 while co-feeding hydrogen sulfide and using the aluminum carbon monoxide cylinder. Both the rate constant and adsorption equilibrium constant are affected by the change in c value, though the effect is more significant for the adsorption equilibrium constant. Table B.2 shows the change in calculated activation energy and CO_2 heat of adsorption for the two models using the SimuSolv® parameters in Table B.1.

The change in activation energy is within the experimental error, while the change in CO_2 heat of adsorption is about 12%. Lee (*65*) gave two rules that can be used to test the significance of adsorption equilibrium constants that appear in Langmuir-Hinshelwood expressions. These rules are given by the following equations.

$$10 < (-\Delta S_a)^o < 12.2 - 0.0014(\Delta H_a)^o \tag{B.2}$$

$$0 < (-\Delta S_a)^o < (S_g)^o \tag{B.3}$$

Where $(\Delta S_a)^o$ *(cal/mol K)* is the entropy change referred to a standard state of 1 atm at the temperature of adsorption, $(\Delta H_a)^o$ *(cal/mol)* is the corresponding enthalpy change, and $(S_g)^o$ is the standard state entropy of the gas phase. Stull *et al.* (*24*) give $(S_g)^o$ as 59.9 *cal/mol K* for CO_2 at 700 K. The entropy change and enthalpy change can be found from the following equation.

$$K_{CO_2} = e^{(\Delta S_a)^o/R} e^{-(\Delta H_a)^o/RT} = A e^{\lambda/RT} \tag{B.4}$$

The value of $(\Delta S_a)^o$ is found from the y-intercept of the plot to find $(\Delta H_a)^o$. Using the two $-(\Delta H_a)^o$ values calculated for c equal to either 1 or 2, Equation (B.2) can be reduced to

$$10 < (-\Delta S_a)^o < 32 \qquad (cal/mol\,K) \tag{B.5}$$

and

$$10 < (-\Delta S_a)^o < 30 \qquad (cal/mol\ K) \tag{B.6}$$

for the cases of $c=1$ and $c=2$ respectively. The calculated $(\Delta S_a)^o$ values are -22.43 *cal/mol K* and -21.35 *cal/mol K* respectively. These entropy values satisfy Equations (B.5) and (B.6) respectively and also satisfy the requirement of Equation (B.3). This result, combined with the fact that the adsorption equilibrium constant for CO_2 (found in this study) decreases with increasing temperature indicates that this is a true equilibrium constant and not a ratio of rate constants. Similar results are obtained for the other catalysts for which activation energies and heats of adsorption for CO_2 were calculated. In this study, the difference in fit between $c=1$ and $c=2$ was not significant enough to reject one of the models. Therefore the simpler equation ($c=1$) was utilized.

Surface Intermediates

Modification of catalyst properties affects the isosynthesis activity, as shown in the previous sections. There are similarities between the mechanism of isosynthesis and that of Fischer-Tropsch synthesis. Hydrocarbons are formed in both processes by chain reactions starting with C_1 intermediates (*15,27-29,42,66*), and the chain reactions include chain initiation, chain growth, and chain termination. However, the products from isosynthesis are rich in branched hydrocarbons, whereas F-T synthesis yields primarily linear products. Furthermore, the product distribution of isosynthesis does not resemble an Anderson-Schulz-Flory distribution. Therefore, a different mechanism is needed for isosynthesis. The mechanisms of isosynthesis and the interactions between surface intermediates and acidic and basic sites are discussed in the following sections.

Chain initiation

The first step of isosynthesis, as in any other synthesis gas reactions, is the activation of CO and H_2 on the surface. Hydrogen has been shown to undergo heterolytic cleavage on ThO_2 (*67*), which is an active isosynthesis catalyst. The adsorption of CO on an isosynthesis metal oxide is non-dissociative, which is different with that on the F-T catalyst in which CO is dissociatively adsorbed (*15*).

Coadsorption of carbon monoxide and hydrogen produces adsorbed formaldehyde (I) and methoxide (II) species on the surface (*8,11,15,38,68*), as shown in Figure B.1. Anion vacancies (i.e., oxygen vacancies for zirconia) are believed to be active sites for the formation of methoxide (*15,38,47,51*). The C_1 species will undergo a series of reaction to form hydrocarbons.

Chain propagation

CO insertion is the primary carbon-carbon bond-forming step (*15*). The first step in the CO insertion is the formation of a cyclic acyl (III). Then, the cyclic acyl is hydrogenated to form a coordinated diol (IV), which can be rearranged to an enol (V) and dehydrated to an adsorbed aldehyde (VI), as shown in Figure B.2. CO insertion is similar to the chain growth in F-T synthesis.

The condensation reaction is another mechanism for chain-propagation. The name

was first proposed by Frolich and Cryder (*69*) to describe the formation of higher alcohols from lower alcohols, such as :

$$2CH_3CH_2OH \rightarrow n\text{-}Butanol + H_2O \ .$$

More recently, Smith and Anderson (*70*) studied the distribution of higher alcohols over promoted methanol synthesis catalyst, and proposed a scheme in which one- or two-carbon species can add to the growing intermediates to give higher products. The chain growth can be at the α or β carbon atom, and β addition accounts for the selectivity to branched products.

In isosynthesis, condensation is faster for the C_2 species than for the C_3 and C_4 species (*8,12,15*). The reaction involves alkylation by a nearby alkoxide (primarily methoxide because of its large surface concentration) of an η^3-enolate (VII) at the terminal carbon atom to form an adsorbed aldehyde (VIII in Figure B.3). The condensation reactions are slow compared with CO insertion reactions, but are kinetically significant due to the large surface concentration of methoxide groups on the surface (*15*).

The condensation reaction as a unique chain growth mechanism for isosynthesis, provides an additional route for chain propagation other than CO insertion, and is the primary factor that causes the deviation of product distribution of isosynthesis from the Anderson-Schulz-Flory distribution for a standard polymerization reaction.

Formation of branched products

Unlike Fischer-Tropsch synthesis, isosynthesis produces branched hydrocarbons. Mazanec (*15*) contributed the formation of branched products to two different enols (X and XIII in Figure B.4) from a coordinated 1,2-propanediolate (IX). These two routes lead to two different types of η^3-enolates (XI and XIV), and eventually to linear (XII) and branched (XV) adsorbed aldehydes. Both η^3-enolates are stabilized on oxides such as ZrO_2 and ThO_2 (*15*), which contributes to the selectivity of branched products on these metal oxides.

The mechanism described herein provides information on how the intermediates are formed and reacted. The nature of the catalyst surface has a strong impact on the relative stability of these intermediates and precursors, which ultimately determines the distribution of products.

Simplified Mechanisms

In this section three mechanisms will be discussed that, with simplifying assumptions, lead to the final form of the rate equation found by the empirical fit. Boudart (*71*) used two simplifying assumptions to reduce complex Langmuir-Hinshelwood expressions. These assumptions were: (1) one step is the rate-determining step, and (2) one surface intermediate is dominant and thus all the other intermediates are present in relatively insignificant amounts. Using these assumptions it is not necessary to assume details of the overall mechanism.

CO and H_2 adsorbed, single catalyst site

In this mechanism CO is molecularly adsorbed and H_2 is dissociatively adsorbed on

the same type of catalyst site and react to form intermediates on the surface according to the following eight steps.

$$CO + S \rightleftharpoons COS$$

$$H_2 + 2S \rightleftharpoons 2HS$$

$$COS + HS \rightarrow CHOS + S$$

$$CHOS + HS \rightleftharpoons CH_2OS + S$$

$$CH_2OS + HS + COS \rightleftharpoons I_iS + 2S$$

$$I_iS + HS + COS \rightleftharpoons I_i'S + CO_2S + S$$

$$I_i'S + HS + COS \rightleftharpoons I_{i+1}S + 2S$$

$$I_{i+1}S + HS + COS \rightleftharpoons I_{i+1}'S + CO_2S + S$$

In this notation S is a surface catalyst site, I_i ($i \geq 2$) is a surface intermediate with the structure $C_iH_{2i-1}O_2$, and I_i' ($i \geq 2$) is a surface intermediate with the structure $C_iH_{2i}O$. These propagation steps can continue on the surface, or the intermediates can desorb to form products as shown in the following two steps.

$$I_i'S + COS \rightleftharpoons P_i + CO_2S + S$$

$$CO_2S \rightleftharpoons CO_2 + S$$

This mechanism is written so alkenes are formed, therefore P_i ($i \geq 2$) has the structure C_iH_{2i}; however, similar steps could be written for alkane formation. If the third step is taken to be rate controlling and essentially irreversible then the carbon monoxide rate equation can be written as follows.

$$r_{CO} = k_3 c_{COS} c_{HS} \tag{B.7}$$

The concentrations of molecular carbon monoxide and atomic hydrogen on the catalyst surface can be solved for using the first two steps of the mechanism.

$$c_{COS} = K_{CO} p_{CO} c_S \tag{B.8}$$

$$c_{HS} = \sqrt{K_{H_2} p_{H_2}}\, c_S \tag{B.9}$$

The adsorption equilibrium constant for CO and H_2 are defined as the ratio of the rate constant for adsorption divided by the rate constant for desorption. When Equations (B.8) and (B.9) are substituted into Equation (B.7) the following equation results.

$$r_{CO} = k_3 K_{CO} \sqrt{K_{H_2}} p_{CO} p_{H_2}^{0.5} c_S^2 \tag{B.10}$$

The concentration of surface sites (c_S) can be solved for by using a total site balance.

$$c_T = c_S + c_{COS} + c_{HS} + c_{CHOS} + c_{CH_2OS} + \sum_{i=2}^{n} c_{I_iS} + \sum_{i=2}^{n} c_{I_i'S} + c_{CO_2S} \tag{B.11}$$

If carbon dioxide is assumed to be the most abundant surface intermediate, since more of this specie is formed than any other intermediate, then the total site balance can be reduced to the following expression.

$$c_T = c_S + K_{CO_2} p_{CO_2} c_S \tag{B.12}$$

The adsorption equilibrium constant for carbon dioxide is defined in the same manner as those for carbon monoxide and hydrogen. When Equation (B.12) is solved for c_S and substituted into Equation (B.10) the result is

$$r_{CO} = \frac{k_p p_{CO} p_{H_2}^{0.5}}{\left(1 + K_{CO_2} p_{CO_2}\right)^2} \tag{B.13}$$

where

$$k_p = k_3 K_{CO} \sqrt{K_{H_2}} c_T^2 \tag{B.14}$$

This mechanism leads to a final expression in which the denominator is squared (c=2 from empirical fit).

CO and H_2 adsorbed, dual catalyst sites

In this mechanism CO is molecularly adsorbed and H_2 is dissociatively adsorbed on different types of catalyst sites and react to form intermediates on the surface according to the following eight steps.

$$CO + S_1 \rightleftharpoons COS_1$$

$$H_2 + 2S_2 \rightleftharpoons 2HS_2$$

$$COS_1 + HS_2 \rightarrow CHOS_1 + S_2$$

$$CHOS_1 + HS_2 \rightleftharpoons CH_2OS_1 + S_2$$

$$CH_2OS_1 + HS_2 + COS_1 \rightleftharpoons I_iS_1 + S_1 + S_2$$

$$I_iS_1 + HS_2 + COS_1 \rightleftharpoons I_i'S_1 + CO_2S_1 + S_2$$

$$I_i'S_1 + HS_2 + COS_1 \rightleftharpoons I_{i+1}S_1 + S_1 + S_2$$

$$I_{i+1}S_1 + HS_2 + COS_1 \rightleftharpoons I_{i+1}'S_1 + CO_2S_1 + S_2$$

In this case, S_1 and S_2 are the two types of surface catalyst sites. The other notation is the same as previously given. The desorption to form products are now given by the following two steps.

$$I_i'S_1 + COS_1 \rightleftharpoons P_i + CO_2S_1 + S_1$$

$$CO_2S_1 \rightleftharpoons CO_2 + S_1$$

Again, step three is taken to be rate controlling and essentially irreversible. The rate equation for carbon monoxide becomes

$$r_{CO} = k_3 c_{COS_1} c_{HS_2} \tag{B.15}$$

The concentrations of molecular carbon monoxide and atomic hydrogen on the catalyst surface are again solved for using the first two steps of the mechanism.

$$c_{COS_1} = K_{CO} p_{CO} c_{S_1} \tag{B.16}$$

$$c_{HS_2} = \sqrt{K_{H_2} p_{H_2}}\, c_{S_2} \tag{B.17}$$

When Equations (B.16) and (B.17) are substituted into Equation (B.15) the following expression results.

$$r_{CO} = k_3 K_{CO} \sqrt{K_{H_2}}\, p_{CO} p_{H_2}^{0.5} c_{S_1} c_{S_2} \tag{B.18}$$

The concentration of surface sites are again solved for by using total site balances.

$$c_{T_1} = c_{S_1} + c_{COS_1} + c_{CHOS_1} + c_{CH_2OS_1} + \sum_{i=2}^{n} c_{I_iS_1} + \sum_{i=2}^{n} c_{I_i'S_1} + c_{CO_2S_1} \tag{B.19}$$

$$c_{T_2} = c_{S_2} + c_{HS_2} \tag{B.20}$$

Again, carbon dioxide is assumed to be the most abundant surface intermediate. The total site balances can be reduced to the following expressions.

$$c_{T_1} = c_{S_1} + K_{CO_2} p_{CO_2} c_{S_1} \tag{B.21}$$

$$c_{T_2} = c_{S_2} \tag{B.22}$$

When Equations (B.21) and (B.22) are solved for their respective free surface site concentrations and substituted into Equation (B.18) the result is

$$r_{CO} = \frac{k_p p_{CO} p_{H_2}^{0.5}}{\left(1 + K_{CO_2} p_{CO_2}\right)} \tag{B.23}$$

where

$$k_p = k_3 K_{CO} \sqrt{K_{H_2}}\, c_{T_1} c_{T_2} \tag{B.24}$$

This mechanism leads to a final expression in which the denominator is first order ($c=1$ from empirical fit).

Rideal mechanism, H_2 adsorbed

In this mechanism H_2 is dissociatively adsorbed and carbon monoxide reacts with the adsorbed hydrogen from the gas phase. The reaction can be represented by the following seven steps.

$$H_2 + 2S \rightleftharpoons 2HS$$

$$CO + HS \rightarrow CHOS$$

$$CHOS + HS \rightleftharpoons CH_2OS + S$$

$$CH_2OS + HS + CO \rightleftharpoons I_iS + S$$

$$I_iS + HS + CO \rightleftharpoons I_i'S + CO_2S$$

$$I_i'S + HS + CO \rightleftharpoons I_{i+1}S + S$$

$$I_{i+1}S + HS + CO \rightleftharpoons I_{i+1}'S + CO_2S$$

For the Rideal mechanism, the desorption to form products are given by the following two steps.

$$I_i'S + CO \rightleftharpoons P_i + CO_2S$$

$$CO_2S \rightleftharpoons CO_2 + S$$

The reaction between adsorbed hydrogen and gas phase carbon monoxide is assumed to be the rate-determining and essentially irreversible step. Using this assumption, the rate equation is written as follows.

$$r_{CO} = k_2 p_{CO} c_{HS} \tag{B.25}$$

When c_{HS} is solved for using the first step of the Rideal mechanism and CO_2 is assumed to be the most abundant surface intermediate (for the site balance), the rate equation for carbon monoxide becomes

$$r_{CO} = \frac{k_p p_{CO} p_{H_2}^{0.5}}{\left(1 + K_{CO_2} p_{CO_2}\right)} \tag{B.26}$$

where

$$k_p = k_2 \sqrt{K_{H_2}}\, c_T \tag{B.27}$$

The Rideal mechanism also leads to a final expression in which the denominator is first order.

Discrimination Between Mechanisms

As shown in the previous section, mechanisms can be written that result in a final

form of the carbon monoxide rate equation with c equal to either 1 or 2. Carbon monoxide is either molecularly adsorbed or reacts from the gas phase. Hydrogen is dissociatively adsorbed in all cases. The rate-determining step in all three mechanisms assumes that initiation is the slow step, while propagation occurs fairly rapidly. This would lead to a product distribution that is constant with CO conversion. In this study, the product distribution did remain fairly constant with CO conversion. Runs over the 7% Ce-ZrO_2 catalyst covered the CO conversion range from 13-35% while the product distribution (wt%) remained at approximately 30% C_1, 8% C_2, 6% C_3, 29% C_4, and 27% C_5+.

The assumption that carbon dioxide is the most abundant (most strongly adsorbed) surface species is reasonable. The poor fit found when CO inhibition was used supports the assumption that CO was not a major surface specie. As mentioned earlier, however, rejection of the c=1 or c=2 model was not possible with the data collected in this study. Perhaps data at higher conversions or conversion data when carbon dioxide is included in the feed would help in the model selection process.

TABLE B.1. Comparison of fitted parameters obtained from SimuSolv® for different c values for 7% Ce-ZrO_2 at 50 atm and 1/1 CO/(H_2+H_2S) ratio

T(K)	c=1		c=2	
	$k_p \times 10^6$ $\left(\frac{mol}{kg_{cat}\, atm^{1.5}\, sec}\right)$	K_{CO_2} (atm^{-1})	$k_p \times 10^6$ $\left(\frac{mol}{kg_{cat}\, atm^{1.5}\, sec}\right)$	K_{CO_2} (atm^{-1})
648	4.73	0.804	4.80	0.335
673	10.97	0.503	12.85	0.252
698	14.85	0.350	17.38	0.170
723	20.55	0.255	24.23	0.125

TABLE B.2. Changes in activation energy and CO_2 heat of adsorption with c for 7% Ce-ZrO_2 at 50 atm and 1/1 CO/(H_2+H_2S) ratio

c	E_a *(kcal/mol)*[a]	ΔH_{ads} CO_2 *(kcal/mol)*
1	12.14 ± 0.50	14.22 ± 0.58
2	12.25 ± 0.59	12.50 ± 0.67

[a] To convert to *kJ/mol* multiply by 4.184

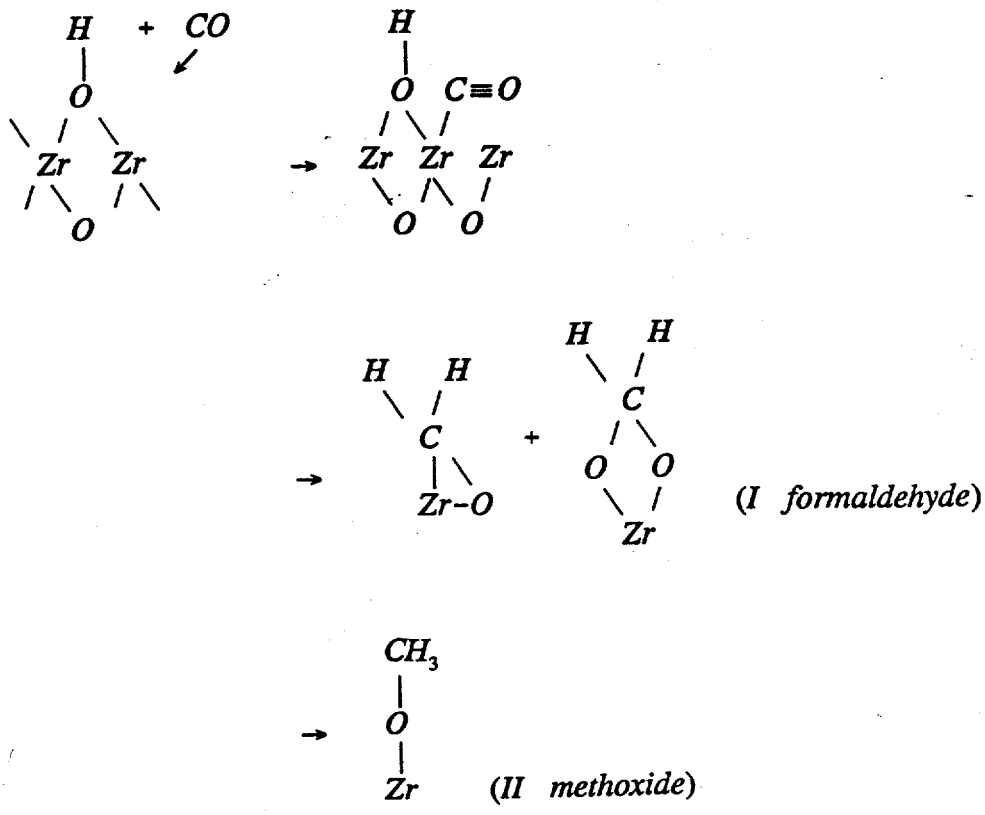

Figure B.1. Formation of adsorbed formaldehyde and methoxide species. Adapted from ref. (*15,51*).

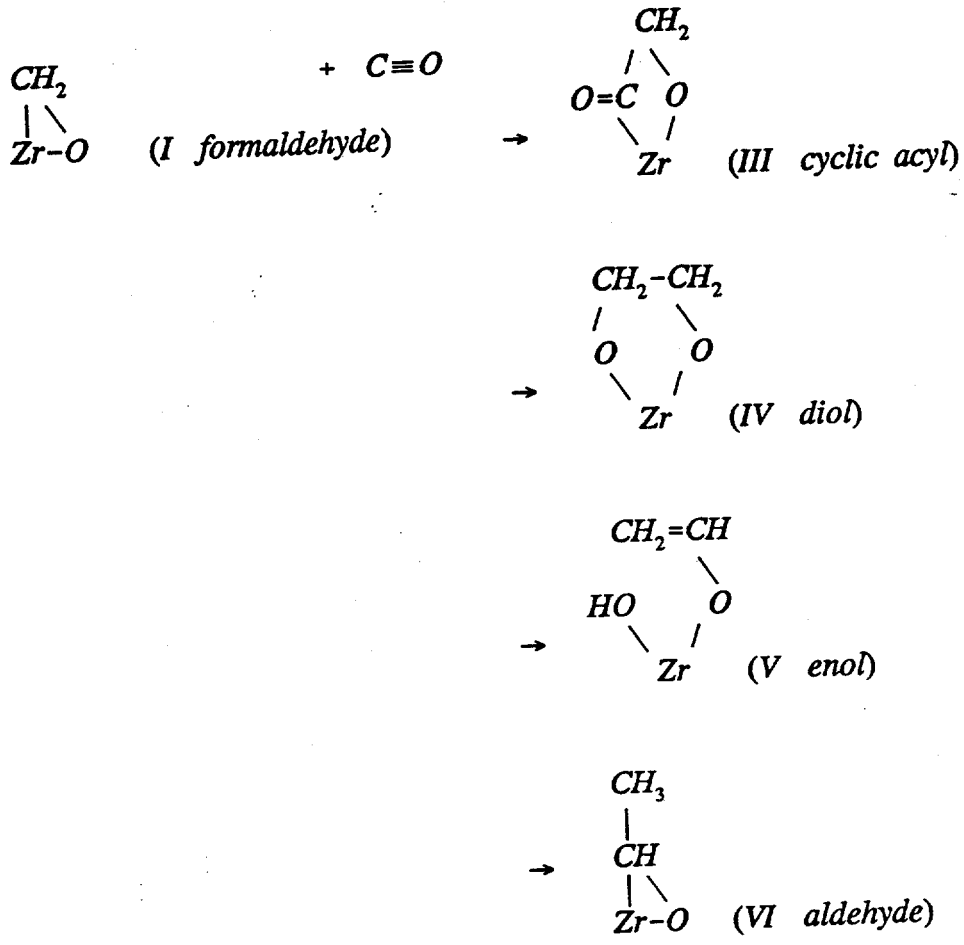

Figure B.2. Mechanism of chain propagation via CO insertion. Adapted from ref. (*15*).

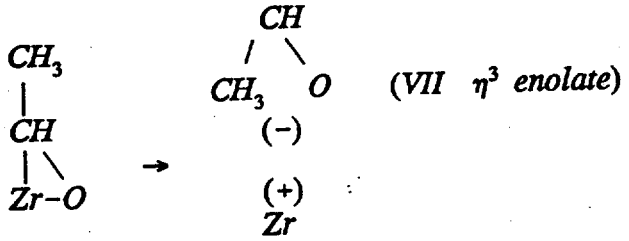

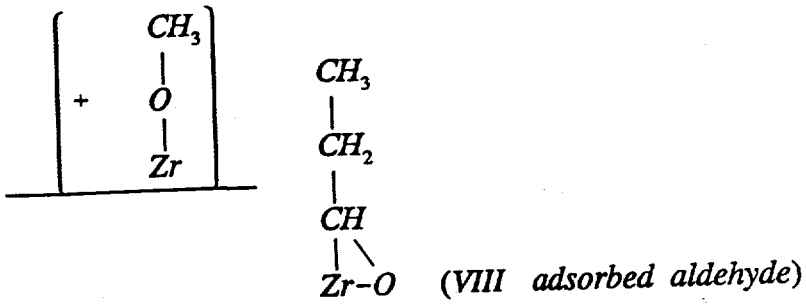

Figure B.3. Mechanism of chain propagation via condensation reaction. Adapted from ref. (*15*,*38*)

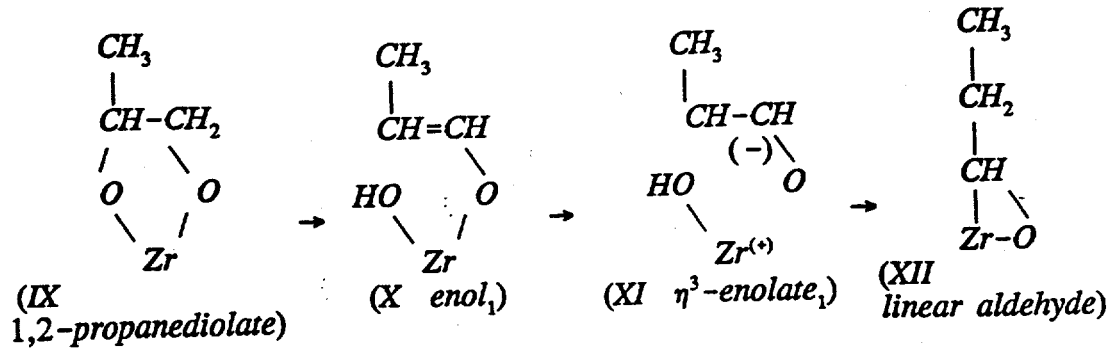

or:

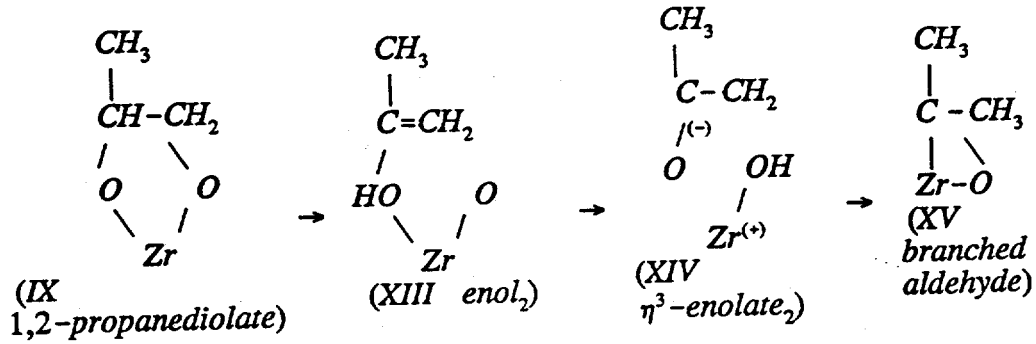

Figure B.4. Formation of linear and branched intermediates. Adapted from ref (*15*).

APPENDIX C - Publications, Conference Papers, and Presentations based on this work

Publications

Refereed

Postula, W.S., Z. Feng, C.V. Philip, A. Akgerman, and R.G. Anthony, "Conversion of Synthesis Gas to Isobutylene over Zirconium Dioxide Based Catalysts," *J. Catal.* **145**, 126 1994.

Postula, W.S., A. Akgerman, and R.G. Anthony, "The Effect of Hydrogen Sulfide on Isosynthesis over 7% (wt) Cerium Zirconia Catalyst," accepted for publication in *Appl. Catal. A*, January 29, 1994.

Feng, Z., W.S. Postula, C. Erkey, C.V. Philip, A. Akgerman, and R.G. Anthony, "Selective Formation of Isobutane and Isobutene from Synthesis Gas over Zirconia Catalysts Prepared by a Modified Sol Gel Method," accepted for publication in *J. Catal.*, February 14, 1994.

Postula, W.S., A. Akgerman, and R.G. Anthony, "The Effect of Oxygen Vacancies on Isosynthesis over Zirconia Based Catalysts," currently under revision for publication in *J. Catal.*.

Feng, Z., W.S. Postula, A. Akgerman, and R.G. Anthony, "Synthesis and Characterization of Zirconia Based Catalysts Prepared by Precipitation, Calcination, and Modified Sol-Gel Methods," to be sibmitted to *I&EC Research (Kinetics and Catalysis)*.

Feng, Z., A. Akgerman, and R.G. Anthony, "Selective Formation of Isobutane and Isobutene from Synthesis over Calcium Promoted Zirconias," to be submitted to *Appl. Catal. A*.

Erkey, C., J. Wang, W.S. Postula, Z. Feng, C.V. Philip, A. Akgerman, and R.G. Anthony, "Isobutylene Production from Synthesis Gas over Zirconia in a Slurry Reactor," to be submitted to *I&EC Research (Kinetics and Catalysis)*.

Papers for Technical Conferences

Anthony, R.G., A. Akgerman, C. Erkey, Z. Feng, W. Postula, and C.V. Philip, "Catalyst and Process Development for Synthesis Gas Conversion to Isobutylene," *Proceedings of DOE Liquefaction Contractors' Review Meeting*, Pittsburgh, PA, September 3-5, 1991.

Anthony, R.G., W. Postula, Z. Feng, and A. Akgerman, "Use of Zirconia in the Conversion of Hydrogen Lean Synthesis Gas to Isobutylene," Preprint Paper-*Am. Chem. Soc., Div. Fuel Chem.*, 37, 247-53 (1992). Preprints of Symposium on Coal Liquefaction at the Spring ACS National Meeting in San Francisco, CA, April 1992.

Anthony, R.G., A. Akgerman, W.S. Postula, Z. Feng, C.V. Philip, and C. Erkey, "Catalyst and Process Development for Synthesis Gas Conversion to Isobutylene," *Proceedings of DOE Liquefaction Contractors' Review Meeting*, Pittsburgh, PA, September 22-24, 1992.

Anthony, R.G., W.S. Postula, Z. Feng, C.V. Philip, and A. Akgerman, "Isobutylene Synthesis Using Zirconia and Modified Zirconia," *Proceedings of the Ninth Annual International Pittsburgh Coal Conference*, Pittsburgh, PA, October 12-16, 1992.

Anthony, R.G., A. Akgerman, W.S. Postula, Z. Feng, C.V. Philip, and C. Erkey, "Catalyst and Process Development for Synthesis Gas Conversion to Isobutylene," *Proceedings of DOE Liquefaction Contractors' Review Meeting*, Pittsburgh, PA, September 27-29, 1993.

Also, monthly and quarterly reports were filed at the appropriate times with DOE.

Presentations

Anthony, R.G., "Catalyst and Process Development for Synthesis Gas Conversion to Isobutylene," DOE Liquefaction Contractors' Review Meeting, Pittsburgh, PA, September 3-5, 1991.

Postula, W.S., "Conversion of SynGas to Isobutylene over Zirconium Dioxide Catalyst," Second Annual Chemical Engineering Graduate Research Symposium, Texas A&M University, College Station, Texas, January 9, 1992.

Anthony, R.G., "Use of Zirconia in the Conversion of Hydrogen Lean Synthesis Gas to Isobutylene," Symposium on Coal Liquefaction at the Spring ACS National Meeting in San Francisco, CA, April 1992.

Anthony, R.G., "Catalyst and Process Development for Synthesis Gas Conversion to Isobutylene," DOE Liquefaction Contractors' Review Meeting, Pittsburgh, PA, September 22-24, 1992.

Anthony, R.G., "Isobutylene Synthesis Using Zirconia and Modified Zirconia," Ninth Annual International Pittsburgh Coal Conference, Pittsburgh, PA, October 12-16, 1992.

Anthony, R.G., "Catalyst and Process Development for Synthesis Gas Conversion to Isobutylene," DOE Liquefaction Contractors' Review Meeting, Pittsburgh, PA, September 27-29, 1993.

Postula, W.S., "Isobutylene Synthesis Over Zirconia-Based Catalysts," 49th American Chemical Society Southwest Regional Meeting, Hyatt Regency Hotel, Austin, Texas, October 27, 1993.